

CHARACTERIZATION OF YisK, A CELL SHAPE MODIFIER AND ENZYME IN

Bacillus subtilis

A Dissertation

by

ANTHONY MICHAEL SPERBER

Submitted to the Office of Graduate and Professional Studies of
Texas A&M University
in partial fulfillment of the requirements for the degree of

DOCTOR OF PHILOSOPHY

Chair of Committee,	Jennifer Herman
Co-Chair of Committee,	Ryland Young
Committee Members,	Jason Gill
	Junjie Zhang
Head of Department,	Gregory D. Reinhart

December 2017

Major Subject: Biochemistry

Copyright 2017 Anthony Michael Sperber

ABSTRACT

Bacterial growth and division requires the careful coordination of peptidoglycan (PG) synthesis and PG hydrolysis, allowing the insertion of new cell wall material at sites of active growth. In many rod-shaped bacteria, the bacterial actin homolog MreB is thought to coordinate this balance of synthesis and hydrolysis, particularly during cell elongation, and the current model is that MreB-like proteins act as a scaffold, directing the PG synthesis machinery to sites of active growth. Despite their importance, very little is known about how MreB-like proteins in prokaryotes are regulated. Using a *Bacillus subtilis* misexpression screen, we identified *yisK* and *yodL*, which cause a loss of cell shape and viability when misexpressed. Suppressors resistant to YisK's killing activity primarily occur in *mbl* (the structural gene for an MreB paralog in *B. subtilis*), while suppressors resistant to YodL's activity primarily occur in MreB. Consistent with the idea that YisK targets Mbl activity and YodL targets MreB activity, deletion of *mbl* confers resistance to YisK, while deletion of MreB confers resistance to YodL. In an *mbl* deletion background, YisK expressing cells also become 20% shorter, suggesting that YisK activity affects at least one other target integral to cell shape. Using a bacterial 2-hybrid assay, we detected an interaction between YisK and FtsE (the ATPase of the ABC Transporter FtsEX). Interestingly, published data indicates that FtsEX, which is important for regulating the activity of the D,L-endopeptidase CwlO, appears to act in the same pathway as Mbl, and both *ftsE* and *cwlO* mutants exhibit short-cell phenotypes. Our data suggest that *ftsE* is required for YisK-dependent cell shortening, but not cell

widening. YisK shows ~40% amino acid identity to an FAH from *Mycobacterium abscessus*, and we have obtained a preliminary crystal structure for YisK, with a dicarboxylic acid, most likely L-tartrate, bound in the active site. Surprisingly, introducing mutations in YisK's active site has no effect on its ability to perturb cell shape. Our current model is that YisK is an enzyme, possibly involved in the dicarboxylate pathway, that utilizes interactions with Mbl and possibly FtsE to localize its enzymatic activity to specific regions within the cell.

DEDICATION

This work is dedicated to my mother, who could not be with me today. In these pages, I fulfill one of the promises I made to her before she passed away.

ACKNOWLEDGEMENTS

I would like to thank my father (Jerry) and two brothers (Daniel and Nathan), for their support throughout my graduate career. They are proud to say I am the nerd of the family, and so am I. I would like to thank my mother, who although passed away at the start of my graduate career, was the reason I made it to the end.

I would like to thank my friends and fellow band members of “Jane and the Apes”, which includes Alyssa Cahill, Jesse Cahill, and Benjamin Kaster. It has been an absolute blast playing music with you guys throughout the years of graduate school, and I wouldn’t trade it for the world.

I would like to thank my committee members Dr. Jason Gill and Dr. Junjie Zhang for their support and guidance throughout my graduate career.

I would like to thank all of the labs comprising the Center for Phage Technology (Herman Lab, Zeng Lab, Zhang Lab, Gill Lab, Young Lab) for their support and guidance throughout my graduate career. Particularly, I would like to thank Yi Duan. Your mentorship and friendship throughout my graduate career was appreciated. It is privilege and honor to call you my friend.

I would like to thank my Co-advisor Dr. Ryland Young. I can say definitively that your aggressive, tough-love style mentorship forges students into thinkers that will change the world in whatever profession they choose.

I would like to thank my previous mentor during my undergraduate education at the University of Missouri, Dr. Linda Randall. I remember her teaching me biochemistry

in her office after work on the weekdays. Her mentorship and guidance lay the foundation for my success in graduate school.

Last but not least, I would like to thank my advisor Dr. Jennifer Herman. I could not have picked a better advisor. I don't think I have ever seen the combination of brilliance, compassion, and perseverance that is Jen. I would never have become the scientist I am today without her.

CONTRIBUTORS AND FUNDING SOURCES

Contributors

This work was supervised and guided by a dissertation committee consisting of Dr. Jennifer Herman [Graduate Advisor and Chair of Committee], Dr. Ryland Young [Graduate Advisor and Co-Chair of Committee], and Dr. Junjie Zhang [Committee Member] from the Department of Biochemistry and Biophysics and Dr. Jason Gill [Committee Member] from the Department of Animal Sciences.

The crystal structure for YisK shown in Chapter III was solved in collaboration with Dr. Inna Krieger and Dr. Jim Sacchettini of the Department of Biochemistry and Biophysics. The metabolomics data acquisition in Chapter III was done in collaboration with Dr. Cory Klemashevich of the Integrated Metabolomics Analysis Core at Texas A&M University. Experiments shown in Chapter II were done in part by Dr. Yi Duan of the Department of Biochemistry and Biophysics and were published in 2016. Strains for Chapters II and III were made in part by Yi Duan. Assistance in assays and strain construction for Chapter II was from Ashley Marchand of the Department of Genetics. Assistance in Strain Construction, Lysis Curves, and plating shown in Chapter IV was done by Matthew Theodore for the Center for Phage Technology at Texas A&M University. Fluorescent labeling of PBSX shown in Chapter IV was done in part by Laith Harb during his graduate rotation in the Center for Phage Technology. Sequencing of the PBSX packaged DNA and subsequent analysis of the sequences shown in Chapter

IV was done by Shr-Hau Hung and his advisor Dr. Anca Segall at San Diego State University. All other work conducted for the dissertation was completed by the student independently.

Funding Sources

The work in Chapters II and III of this dissertation was funded by the Start-up fund as well as a NSF Grant (award #1514629) to Dr. Jennifer Herman. The work in Chapter IV was funded by the Center for Phage Technology as well as a Bill and Melinda Gates Foundation Grant (award #1601961) to Dr. Jennifer Herman and Dr. Ryland Young. The authors are responsible for the contents of this dissertation, and information within this dissertation does not represent the official views of the Department of Biochemistry and Biophysics or the Texas A&M University.

TABLE OF CONTENTS

	Page
ABSTRACT	ii
DEDICATION	iv
ACKNOWLEDGEMENTS	v
CONTRIBUTORS AND FUNDING SOURCES.....	vii
TABLE OF CONTENTS	ix
LIST OF FIGURES.....	xi
LIST OF TABLES	xiv
CHAPTER I INTRODUCTION.....	1
<i>B. subtilis</i> sporulation.....	3
Cell elongation and division machinery.....	6
Uncharacterized gene function.....	12
Metabolism shapes the cell	15
Bacteriophages	31
CHAPTER II YodL AND YisK POSSESS SHAPE-MODIFYING ACTIVITIES THAT ARE SUPPRESSED BY MUTATIONS IN MreB AND Mbl.....	41
Introduction	41
Materials and methods	45
Results	57
Discussion	86
CHAPTER III CHARACTERIZATION OF YisK, AN ENZYME IN THE FUMARYLACETOACETATE HYDROLASE SUPERFAMILY	95
Introduction	95
Materials and methods	96
Results	113
Discussion	169

	Page
CHAPTER IV CHARACTERIZATION AND MANIPULATION OF PBSX, A DEFECTIVE PROPHAGE IN <i>B. subtilis</i>	175
Introduction	175
Materials and methods	176
Results	187
Discussion	205
 CHAPTER V SUMMARY AND FUTURE DIRECTIONS	 209
Summary of chapters II and III	209
Summary of chapter IV	211
Future directions for YisK.....	214
PBSX future directions.....	216
 REFERENCES.....	 218
 APPENDIX	 249

LIST OF FIGURES

FIGURE	Page
1.1 Metabolic pathways implicated in the regulation of cell shape and size ...	30
2.1 Misexpression of YodL and YisK prevents cell growth on solid media and causes loss of cell shape in liquid media	58
2.2 Growth curves in LB following misexpression of YodL and/or YisK	59
2.3 Misexpression of YodL and YisK on PAB media	61
2.4 DNA sequence upstream of <i>yodL</i> and <i>yisK</i>	63
2.5 Expression from <i>yodL</i> and <i>yisK</i> promoters during a CH timecourse.....	65
2.6 Expression from <i>yodL</i> and <i>yisK</i> promoters following sporulation by resuspension	66
2.7 A strain harboring a GFP reporter without a promoter during a sporulation timecourse	67
2.8 Strains lacking <i>yodL</i> and/or <i>yisK</i> appear morphologically similar to wildtype during a sporulation timecourse	72
2.9 Location of MreB residues conferring resistance to YodL.....	77
2.10 Location of Mbl residues conferring resistance to YisK.....	80
2.11 YodL and YisK co-misexpression causes cell lysis.....	81
2.12 YodL and YisK's cell-widening activities require MreB and Mbl, respectively.....	84
2.13 YisK expression results in cell shortening	87
3.1 YisK perturbs Mbl-GFP localization and MreB-GFP localization during misexpression.....	116
3.2 YisK and YodL perturb LytE-GFP localization	117

FIGURE	Page
3.3 YisK expression profile during sporulation	120
3.4 Bacterial 2-hybrid of YisK and FtsE.....	123
3.5 YisK does not require FtsEX or CwlO for cell shape modifying activity .	125
3.6 Model of interaction with components of the PG synthesis machinery.....	127
3.7 YodL misexpression in cells lacking RodZ	130
3.8 Bacterial 2-hybrid of MreB variants and RodZ	132
3.9 Purification of YisK-His using nickel affinity chromatography.....	134
3.10 Preliminary crystal structure of YisK.....	136
3.11 Bacterial 2-hybrid of YisK self-interaction.....	137
3.12 Illustration of YisK catalytic divalent cation within putative active site ...	138
3.13 YisK Compound Screening using Differential Scanning Fluorimetry	141
3.14 Specificity of YisK binding.....	142
3.15 Images of cells expressing a YisK catalytic mutant.....	145
3.16 Characterization of YisK variants	147
3.17 Phase-contrast microscopy of spore germination.....	149
3.18 Phenotype of the Tn insertion between <i>gapA</i> and <i>pgk</i>	151
3.19 Overview of relevant metabolic pathways	152
3.20 Phase-contrast microscopy of samples.....	156
3.21 Total ion concentration of LC/MS/MS of metabolite extractions using optimized LC method and bead breaking lysis	157
3.22 Optimized LC/MS/MS parameters.....	159

FIGURE	Page
3.23 Metabolites decreased more than two-fold in the $\Delta yisK$ mutant compared to wild-type in the Arginine and Proline metabolism pathway.....	163
3.24 Metabolites decreased more than two-fold in the $\Delta yisK$ mutant compared to wild-type in Valine, Leucine, and Isoleucine biosynthesis pathway	164
3.25 Metabolites decreased more than two-fold in the $\Delta yisK$ mutant compared to wild-type in the Nicotinate and Nicotinamide metabolism pathway	166
3.26 YisK pull-down assay using α -YisK and dynabeads protein A.....	168
3.27 Current model of YisK <i>in vivo</i> function.....	173
4.1 PBSX is successfully induced and assembled from thermosensitive <i>xre</i> . .	189
4.2 PBSX adsorbs to <i>B. subtilis</i> W23 but not <i>B. subtilis</i> strain 168WT	190
4.3 Genetic construct of hybrid PBSX-PBSZ phagocin	191
4.4 DNA gel confirmation of tape measure proteins	192
4.5 DNA gel confirmation of tail fiber proteins.....	193
4.6 The tail fiber of PBSZ is sufficient to switch host specificity from <i>B. subtilis</i> W23 to <i>B. subtilis</i> 168.....	197
4.7 Lysis curve of PBSX lysis gene knockouts.....	198
4.8 Lysate spotting of WT, <i>xhIA</i> , <i>xhIB</i> , and <i>xhIAB</i> knockouts.....	199
4.9 Single cell membrane potential assay using Alexa Fluor 488 labeled PBSX and Thioflavin T (ThT) stained <i>B. subtilis</i> W23	201
4.10 PBSX single cell adsorption assay with redox dye CTC	203

LIST OF TABLES

TABLE	Page
2.1 Strains used in Chapter II.....	46
2.2 Plasmids used in Chapter II.....	50
2.3 Oligonucleotides used in Chapter II.....	51
2.4 Sporulation efficiency of <i>yodL</i> and <i>yisK</i> mutants	71
2.5 Whole-genome sequencing analysis of genomic DNA from six YodL-resistant suppressors	74
2.6 Analysis of suppressor strains resistant to YodL and/or YisK.....	76
3.1 Strains used in Chapter III.....	98
3.2 Plasmids used in Chapter III	101
3.3 Oligonucleotides used in Chapter III	102
3.4 <i>ftsEX</i> mutant resistant to YisK mediated cell shortening.....	126
3.5 Summary of compounds screened by differential scanning fluorimetry for binding to YisK	143
3.6 Redundant factor screen for YisK during sporulation conditions.....	150
3.7 MZ cloud summary of identified compounds	161
4.1 Strains used in Chapter IV	177
4.2 Plasmids used in Chapter IV	178
4.3 Oligonucleotides used in Chapter III	179
4.4 PBSX-Z requires glucosylated teichoic acids and minor teichoic acids for killing activity.....	204

CHAPTER I

INTRODUCTION*

This introduction covers two disparate projects: one project covers the characterization of a previously uncharacterized protein in *Bacillus subtilis*, and the other project centers on the defective prophage-like element PBSX. As such, the introduction covers a broad range of topics ranging from subcellular organization of *Bacillus* to the the phage lysis paradigm, and is organized accordingly.

Bacillus subtilis is a rod-shaped, Gram-positive, soil-dwelling facultative anaerobe (1) of the phylum Firmicutes. The phylum Firmicutes includes a diverse assortment of organisms ranging from *Lactobacillus* (which is utilized in cheese and yogurt production) to pathogenic bacteria such as *Clostridia*, *Staphylococcus*, *Listeria*, and *Streptococcus*. *B. subtilis* has been used for industrial production of enzymes as well as polyglutamic acid, which is used as an additive in food. *B. subtilis* is capable of cell differentiation, allowing for diverse cell processes including swarming motility, sliding motility, surfactin production, cannibalism, biofilm formation, natural competence, and sporulation (2). In addition, *B. subtilis* as the best characterized Gram-positive model system, is genetically tractable, with powerful tools to allow precise manipulation of the genome. *B. subtilis* strain 168, the strain utilized in this study, is an auxotroph that was created by Paul Burkholder and Norman Giles at Yale University in the 1947 by exposing *B. subtilis* Marburg to sublethal doses of X-Rays and then isolating

*Adapted with permission from “Metabolism Shapes the Cell” by Sperber, A.M. and Herman, J.K., 2017. *Journal of Bacteriology*, 199(11) pii:e00039-17. Copyright 2017 by American Society for Microbiology.

auxotrophic mutants (3, 4); *B. subtilis* strain 168 *trpC2* is a tryptophan auxotroph, which cannot become a prototroph through reversion (5). *B. subtilis* strain 168 shows natural competence in a growth phase and media dependent manner; competence is primarily turned on by the master regulator of competence ComK during stationary phase in glucose minimal media (maximally about 2-10% of the cells in the culture) (6, 7). *B. subtilis* 3610 is not naturally competent unless the plasmid containing ComI, the competence repressor, is cured (8). *B. subtilis* can uptake a maximum of fifty pieces of DNA per cell (50 binding sites) (3, 9) and the transformation machinery colocalizes together at the cell poles (10). The transformation efficiency varies based on the size of DNA used, with the best transformation efficiency centering around 12kb-14kb. Of the DNA that *B. subtilis* binds, over 50% will eventually integrate into the chromosome through homologous recombination (3, 11). Furthermore, under saturating conditions of DNA uptake, congression can occur, whereas two unlinked genetic markers can be integrated into the chromosome, even when one of the genetic markers is not selected against; this happens at a frequency of about 1-5% (3). In *Streptococcus pneumoniae*, DNA is taken up as a single strand in the 3'-5' direction, with the non-transforming strand being subsequently degraded; this process is thought to be similar in *B. subtilis* (12-14). DNA uptake was shown to occur at around 80bp/s, and the process is processive (15). Genetic approaches to answer questions are relatively simple in this organism, as point mutations, insertions, and deletions can be made in the chromosome with little trouble. Furthermore, integrations into the chromosome through double crossover homologous recombination do not require selective pressure for maintenance

in the chromosome. The *cre lox* system functions in *B. subtilis*, allowing for easy excision of chromosomal segments, leaving only a 34 basepair scar (16).

***B. subtilis* sporulation**

Chromosome organization during sporulation

B. subtilis undergoes the process of sporulation under nutrient starvation conditions. During this process, the bacteria stops further DNA replication (via halting additional rounds of initiation through SirA) (17, 18), and has only two full copies of the chromosome present. The *B. subtilis* chromosome then extends into an elongated structure called the axial filament, followed by asymmetric division/polar septation. During axial filament formation, the protein RacA binds the *B. subtilis* DNA at several sites around the chromosome that are more concentrated around the *oriC* (origin of replication), facilitating chromosome collapsing/compacting, especially around *oriC* (19). RacA also binds the protein DivIVA, which is anchored at the cell poles through an amphipathic helix (20-22). This process anchors the two chromosomal *oriC* regions to opposite poles of the cell (23, 24).

Cell division during sporulation

FtsZ initially forms a Z ring at the midcell, followed by a spiral FtsZ intermediate and subsequent reassembly of the Z ring at the cell poles (25); Spo0A-P and σ^H transcriptionally drive this Z ring reassembly at the poles (25, 26). One or two FtsZ rings are formed at the poles of the cell (quarter cell position), followed by maturation of one

ring into a division septum at the quarter cell (27, 28). It was shown that increasing levels of FtsZ at the beginning of sporulation (driven by a σ^H promoter) alongside *spoIIE* expression (driven by Spo0A-P) is responsible for the shift of FtsZ from midcell to the quarter cell (25). The protein RefZ (Regulator of FtsZ) binds regions of the chromosome at this quarter cell region, promoting trapping of precise regions of the chromosome within the forespore compartment (29) (unpublished, E. Brown and J. Herman). The establishment of the septum at the quarter cell traps different portions of the bacterial chromosome in the two compartments (known as the forespore and mother cell), and allows for differential gene expression within the two compartments via forespore and mother cell specific sigma factors. Afterwards, the rest of the chromosome which was partially trapped in the forespore is pumped completely into the forespore via a DNA translocase called SpoIIIE, which is located within the polar septum and whose pumping is driven by ATP hydrolysis (30); this ensures that the spore will have a complete copy of the chromosome at the end of sporulation.

Maturation of the forespore

Following the polar septation, the single layer of peptidoglycan (PG) is synthesized towards the pole of the forespore during a process known as engulfment (31); eventually, the mother cell envelope surrounds the forespore, and PG hydrolysis and membrane fission leads to the release of a separate mother cell and endospore, each with a full chromosome (30). The forespore chromosome is then remodeled into a toroidal structure that is resistant to radiation damage (30). The spore outer layer called

the cortex is then formed as a thick layer of peptidoglycan (PG), followed by a crystalline array of spore coat proteins. Heat and desiccation resistance in the mature spore is the result of the replacement of water with dipicolinic acid (DPA) (32). Lastly, the mother cell, driven by activation of σ^K , lyses and frees the spore into the environment (33).

Entry into sporulation is driven by the sporulation master regulator Spo0A. Transcription of Spo0A is σ^H and Spo0A-P dependent. When Spo0A is phosphorylated (Spo0A-P), it binds a conserved motif known as the 0A box, and is known to regulate more than 200 genes (34). Different genes respond to different levels of Spo0A-P, and thus Spo0A-P regulation is classified as low threshold activated, low threshold repressed, high threshold activated, or high threshold repressed (35). The entire process of sporulation is carefully regulated by specific sigma factors that are activated at sequential stages in the developmental program. After Spo0A-P initiates the process of sporulation, and a polar septum is formed, σ^F is activated in the forespore, followed by σ^E being activated in the mother cell (30, 33). After the engulfment stage of sporulation, σ^G is turned on in the forespore, and replaces σ^F as the forespore specific sigma factor (33). Lastly, σ^K is activated in the mother cell and allows programmed mother cell lysis (33).

The cellular programming behind the differentiation of *B. subtilis* into spores is complex. For instance, the σ^F is actually present in the cytoplasm of *B. subtilis* cell prior to the step of polar septation; however, it is held in an inactive form by the anti-sigma factor AB (33). The anti-sigma factor AB is inhibited by the active (dephosphorylated)

anti anti sigma factor AA in the forespore after polar septation, which allows σ^F to be active (33). The phosphatase that activates AA is called E, and it is localized at the polar septum only in the forespore (33). The differential gene expression in mother cell and forespore are linked to each other. The order of activation is σ^F , σ^E , σ^G , σ^K . Furthermore, it was recently shown that activation of σ^E is the critical decision point or point of no return during the sporulation process (36).

Cell elongation and division machinery

Peptidoglycan synthesis

Bacteria are surrounded by a complex polymer meshwork called peptidoglycan (PG). PG is a polymer consisting of GlcNAc-MurNAc-pentapeptide in which the sugars are incorporated via transglycosylation and the peptides are crosslinked to each other via transpeptidation. The proteins that carry out transglycosylation and transpeptidation reactions are called Penicillin Binding Proteins (PBPs). PBPs can be bifunctional (transglycosylase and transpeptidase activity) or monofunctional (transpeptidase activity). Recently, it was shown that certain Shape, Elongation, Division proteins (SEDs) have transglycosylase activity and work alongside monofunctional PBPs during the process of cell elongation (37). The composition of the pentapeptide side chain is organism dependent, but in *B. subtilis* is comprised of L-Ala-D-Glu-mDAP-D-Ala-D-Ala. Furthermore, the crosslinking in PG varies based on the organism, but typically 4-3 crosslinking (where mDAP is crosslinked to D-Ala) is observed. 3-3 crosslinking in older PG has been observed in other organisms and may be important for structural

integrity under specific conditions (38). PG allows the cell to maintain structural integrity, even under several atmospheres of turgor pressure, and thus protects against osmotic lysis. Due to turgor pressure, actively growing cells must be capable of coordinating the activity of autolysins, which are required to open the PG meshwork for growth, with the insertion of new PG into the cell wall (39).

Bacterial elongation and division in rod-shaped bacteria is facilitated by the actin homolog MreB and the tubulin homolog FtsZ, respectively, although their roles can overlap (40-43), or even be completely reversed (44-46). FtsZ polymerizes into a ring-like structure at the midcell in a GTP dependent manner and acts as a scaffold for other cell division proteins. It has also been proposed that constriction of the FtsZ ring generates the force necessary for cytokinesis during cell division (47). Recent data suggests that the FtsZ ring is actually composed of smaller FtsZ protofilaments that exhibit treadmilling activity (48). Proper placement of FtsZ at the midcell is facilitated by the Min system, which in *Escherichia coli*, consists of MinCDE. In *E. coli*, MinC's concentration oscillates across the entire cell length, with the greatest concentration of MinC being at the poles; MinC prevents polymerization of FtsZ at the poles. In *B. subtilis*, the Min system consists of MinCD, and MinC is localized to the poles by the actions of MinD, thus preventing FtsZ localization at the poles. Deletion of the Min system results in improper Z-ring formation at the poles and the formation of mini-cells. Furthermore, the Min system is also responsible for proper *oriC* capture during sporulation; failure to capture the *oriC* during sporulation results in cell death. Another system that contributes to Z-ring positioning is Nucleoid Occlusion, in which a DNA-

binding protein (SlmA in *E. coli* and Noc in *B. subtilis*), binds to motifs enriched all around the chromosome, but relatively absent from the *ter* region. SlmA and Noc are also inhibitors of FtsZ, thus preventing FtsZ assembly around the chromosome except for near the *ter* region, which is at the midcell at the time of division (49-54).

MreB and the bacterial actin cytoskeleton

MreB is a member of the actin superfamily, which contains such diverse members as hexokinase, Hsp70, and actin (55, 56). MreB is widely conserved among rod shaped bacteria, and is involved in the peptidoglycan elongation machinery (PGEM). The current favored model is that MreB acts as a scaffold, directing sites of new PG synthesis and old PG degradation/recycling during active growth along the lateral cell wall. Rod shaped bacteria lacking an MreB protein such as *Corynebacter* undergo polar growth, inserting new PG at the poles (56, 57); this is a DivIVA based mechanism of growth. There are spherical bacteria that contain an MreB protein, but it is thought that MreB is used in processes of cell differentiation (i.e. sporulation) (56, 58). Gram-positive bacteria contain several MreB proteins. *B. subtilis* contains three MreB paralogs, MreB, Mbl, and MreBH; MreB is discerned from the other two paralogs by its presence in the MreBCD operon. MreC is a bitopic membrane protein with N in C out topology, whereas MreD is a polytopic membrane protein; both of these proteins are known to play a role in cell shape, as a deletion results in a loss of rod-shape (59); however, their exact role in cell-shape has not been elucidated.

MreB, Mbl, and MreBH share more than fifty percent sequence identity and more than eighty percent sequence similarity with each other, and are known to have significant functional redundancy with regard to their cell shape functions; overexpression of any one of the paralogs in trans can compensate for the deletion of any of the other two (60). MreB and Mbl are conditionally essential, and can be deleted in a *ponA* (encoding PBP1a) deletion background as long as cells are supplemented with excess Mg^{2+} (61). MreBH is only essential under extremely low Mg^{2+} concentration, experimentally determined to be under $100\mu M$ (62). Depleting each of the paralogs under non-permissive conditions results in a loss of rod shape and eventually cell lysis (56, 60-64).

The three paralogs also have distinct, non-overlapping functions. MreBH directly interacts with the cell wall autolysin LytE, and is responsible for proper localization of LytE along the lateral cell wall (65). There is genetic evidence that MreB controls LytE activity, but it was never shown to be responsible for its localization (66). Furthermore, the paralogs show differential regulation, hinting at non-identical functions. MreBH, like LytE, is regulated by a SigI promoter (heat shock sigma factor) (67). Mbl is under a sporulation promoter (SigE) in addition to its vegetative promoter, although its role in sporulation has not been determined (68). MreB, which is constitutively expressed during vegetative growth, is also subject to regulation by the competence transcriptional regulator ComK. More specifically, *mreB* expression is upregulated during competence, whereas *mbl* and *mreBH* were not (68). Furthermore, MreB was shown to be responsible for proper localization of the ComGA machinery at the poles (68).

Besides differential regulation of the MreB-like proteins in *B. subtilis*, the MreB like proteins are known to be responsible for activating the cell wall hydrolases. Mbl interacts with the ABC Transporter FtsEX, which is responsible for the activity of the D-L endopeptidase CwlO. CwlO cleaves the peptide bond between D-Glu and mDAP in the peptide bridge of PG, and thus is thought to be important for opening the PG meshwork for insertion of new PG (66, 69). MreB and MreBH are responsible for the activity of the D-L endopeptidase LytE (66, 69), which is proposed to carry out a similar role to CwlO, but is most active under heat shock conditions (70, 71).

MreB, Mbl, and MreBH colocalize together at the membrane in patches and move circumferentially around the cell perpendicular to the longitudinal axis of growth (72-74). Their dynamic movement requires PG synthesis, as inhibition of PG synthesis, depletion of PG synthesis machinery or depletion of PG precursors stops the rotation of the MreB patches around the cell (72-74). Although previously thought to organize as helices around the bacterial cell membrane, TIRF Microscopy experiments as well as Cryo Electron Microscopy supports the evidence that MreB proteins localize as patches.

In *E. coli*, an amphipathic helix at the N-terminal of MreB (as well as a hydrophobic insertion loop) is responsible for direct interaction with the membrane (75). In Gram-positive organisms like *B. subtilis*, interaction with the membrane is facilitated by the membrane insertion loop (F97 and A98 in *B. subtilis*) (75). MreB has been shown to prefer and interact with regions of negative curvature of the membrane, and that this behavior allows the maintenance of uniform cell width and rod-shape in actively growing cells (76). Furthermore, work with L-form *B. subtilis* revealed that PG synthesis

does not require a preexisting template (64). Together, this suggests that MreB like proteins can direct sites of PG synthesis and create rod shape *de novo*.

MreB and RodZ

MreB colocalizes with the bitopic membrane protein RodZ at all stages of growth, and MreB is responsible for the proper localization of RodZ. RodZ is a bitopic membrane protein with an N-in C-out topology, and while previously thought to be essential for rod-shape, its inactivation can be compensated for by mutations in MreB (77-79). RodZ may also facilitate the interaction between MreB on the cytoplasmic side of the membrane and PG synthesis on the periplasmic side of the membrane (in *E. coli*) (80); RodZ couples MreB to PBP2 and RodA, and in the absence of RodZ (in an MreB suppressor mutant) MreB no longer moves circumferentially around the cell, even though PG synthesis is ongoing (80). Furthermore, cells lacking RodZ produce a less robust PG sacculus that is more sensitive to osmotic stress (80).

RodZ typically interacts with MreB through its N-terminal helix-turn-helix motif that extends into a conserved pocket in Domain IIA of MreB; this has been shown via a *Thermotoga maritima* crystal structure of the cytoplasmic portion of RodZ with MreB (78). Furthermore, it was suggested that RodZ is making use of a pocket in MreB that was conserved for proper protein folding, as this fold is still found in MreB proteins in organisms that lack RodZ (78). MreB was shown previously to polymerize in the presence of nucleotide triphosphate (ATP or GTP), regardless of the presence of Mg²⁺ (81, 82). In *Caulobacter crescentus*, *in vitro* experiments showed that MreB lacks

polarity and formed antiparallel filaments that facilitated direct membrane binding; this is unlike actin or actin homologs like ParM, which do exhibit polarity (83, 84). MreB forms stable filaments *in vitro*, and the mechanism of depolymerization is unknown at this time (83).

Uncharacterized gene function

Gene discovery and its implication on the microbiome

In the last several decades, the discovery of cytoskeletal-like elements in bacteria and improvements in live cell imaging techniques have led to a reinvigoration of bacterial cell biology. In more recent years, researchers armed with comprehensive gene knockout libraries of all non-essential genes (16, 85), and CRISPRi knock-downs of essential genes (86) have used forward genetic approaches to visually screen for mutants with morphological defects to identify new factors contributing to cellular organization. These approaches have identified only a handful of significant new players (87). Extensions of the brute-force screening approach have also been used to screen for defects in growth under specific conditions including heat, alkaline, and osmotic, following antibiotic treatments that target different cellular processes, as well as under different nutrient conditions (88), revealing networks that allow uncharacterized genes to be tentatively associated with specific pathways (i.e PG synthesis).

Although revealing, there are several significant limitations to using gene knockout approaches to identify gene products involved in cellular organization. Functional redundancy, homeostatic regulation, and context specific expression often

mask easily observable phenotypes. This problem is exacerbated when working with domesticated strains, as genes that confer a fitness advantage in the wild are easily dispensable under laboratory growth conditions (89, 90). Relatedly, the expression context that would be needed to reveal phenotypes is often unknown.

Some of these obstacles have been addressed by the development of lethal screening methodologies (91, 92), including Tn-seq (93). However, given that as many as 50% of genes remain to be experimentally characterized even in model organisms (94), considerable barriers remain.

The human microbiome

Although the focus of this thesis is on gene products that affect morphological processes, uncharacterized genes pose a significant problem for all fields of biology. For example, in recent years there has been an intensified focus on the role of microbiota in human health and disease. The human microbiota in the gut plays a role in processing nutrients that are later absorbable by intestinal tissue (95-97), immune system crosstalk via signaling pathways (96, 98), production of metabolites that are beneficial to human health (such as short chain fatty acids, bile acids, and choline) (99), and production of metabolites that are linked to disease such as trimethylamine N-oxide (TMAO) (100, 101). Short chain fatty acids (SCFA) are among compounds produced and excreted by bacteria in the human gut microbiota, and SCFAs have been associated with reducing inflammation (98, 102), as well as having anti-tumorigenic properties (99).

The human gut microbiome has also been shown to metabolize certain xenobiotics (particularly, pharmaceuticals) into non-functional forms. For example, the drug digoxin (a drug used to treat cardiac arrhythmias) is reduced (and becomes less effective) through the activity of a pair of glycoside reductase enzymes produced in certain strains of the gut bacteria *Eggerthella lenta* (103).

Uncharacterized enzymes and orphan reactions

The major role of the microbiota in human health, particularly its metabolic role, demands a better understanding of metabolism itself, yet we have experimental data for only a fraction of the open reading frames that have been sequenced. As of August 2017, there were 88,032,926 protein coding sequences deposited in UniProt or SwissProt, and of this only 555,110 were associated with annotation based on experimental evidence (0.63%). In the Human Microbiome Project, about 50% of genes cannot be given any annotation, and 78-86% of genes cannot be given a metabolic function (95, 104, 105).

Misannotation is also a significant problem in protein sequence databanks (UniProtKB/Swiss-Prot, GenBank NR, UniProtKB/TrEMBL, and KEGG). In one study using a model set of 37 enzyme families that were experimentally characterized, as many as 80% were misannotated in at least one database for 10 of the 37 enzyme families (106). Even the ability to class a protein into a superfamily (usually based on sequence identity) does not always give sufficient information to make testable hypothesis regarding function, as the diversity of both substrates and catalysis mechanisms can vary greatly between two enzymes within the same superfamily (95,

107, 108). Structural genomics approaches coupled with small molecule docking has been a subsequent approach to address enzyme function, as this provides an optimized set of ligands to test as well as a catalytic activity to be looking for (107).

The large number of putative enzymes without characterized activities is just one facet of a two-sided problem. On the flip side, it is estimated that 22% of enzymatic reactions are orphans (109). That is, the reactions are known to occur in nature, yet lack even a single associated enzyme or protein superfamily (107-109). Furthermore, it is clear that we are missing key pieces of metabolic pathways. For instance, metabolites within a biochemical pathway are typically linked to at least two enzymes, once as a product, and once as a substrate. Metabolites that are only linked to one enzyme are termed dead-end metabolites and represent the gap in our knowledge base. As of 2013, there were 127 dead-end metabolites in the extensively studied model organism *E. coli* K12 (110).

Metabolism shapes the cell

To accurately partition chromosomes and other cell contents during reproduction, cells must possess mechanisms to organize repeated cycles of cell growth, chromosome replication, and division. Eukaryotes orchestrate this coordination using the cell cycle and separate growth, DNA synthesis, and cytokinesis into distinct, temporally sequestered phases. Bacteria, by contrast, simultaneously increase in cell size and replicate DNA before (or concurrent with) cell division. Elucidating the molecular mechanisms prokaryotes employ to achieve spatiotemporal organization of these

intertwined yet functionally disparate processes is of considerable interest to scientists seeking to understand bacterial reproduction, and many outstanding questions remain to be answered. For example, how is DNA replication kept in sync with changing growth and division rates? How are cell dimensions maintained or actively rearranged in response to environmental or developmental cues? What signals do cells sense to switch between increasing in cell size and dividing during the cell cycle? Relatedly, how are these signals transduced to activate/deactivate the distinct machineries required for each process?

Perhaps one of the biggest mysteries remaining in bacterial cell biology relates to understanding the regulatory crosstalk that must occur to integrate central metabolism with macromolecular biosynthesis. Nutrients are converted into the stored energy and precursors used to synthesize macromolecules like DNA and peptidoglycan (PG), so it is no surprise that nutrient availability has a profound impact on growth capacity. However, a growing body of evidence also suggests that metabolites and metabolic enzymes may play a more direct role in regulating critical aspects of cell growth and division than previously appreciated. These findings raise the intriguing possibility that metabolism itself may be the major determinant in shaping the underlying organization of the bacterial cell.

Actively growing bacteria respond rapidly to changing conditions by adjusting their overall shape and size. When nutrients are unrestricted, bacteria often capitalize on the available resources by increasing in cell size and reproducing more often. For rod-shaped bacteria including *Escherichia coli* and *Bacillus subtilis*, cell size is determined

by both the length and width of the cell envelope. During steady-state growth, rapidly growing cells are generally longer and sometimes wider than their slower growing counterparts (111-114), at least when nutrients are unrestricted (113). The positive correlation between cell size and growth rate is likely due to nutrient availability rather than the growth rate itself, because the relationship can be broken under conditions where growth rate is controlled by restricting nutrients. For example, in minimal media with different tryptophan concentrations, *E. coli* cells growing at steady-state are largest (by volume) at concentrations of tryptophan that result in $\sim 1/2$ the maximal growth rate achieved with non-limiting tryptophan (115).

During balanced growth, cell size is remarkably homogenous across a population, suggesting that the signals cuing growth and division cycles are regulated and not random. Single cell experiments performed on *E. coli* and *Caulobacter crescentus* show that cells achieve cell size homeostasis not by triggering cell division when a specific cell volume is achieved, rather by elongating a constant amount (and thus adding a constant volume) before dividing (116-119). Precise division at mid-cell allows for a homogenous population size to be maintained over time (117). A more recent study demonstrates that when bacteria grow, surface area and cell volume scale together across a variety of bacteria (120). The authors of this study also provide data implicating levels of a limiting PG precursor as the likely signal for cuing cell division, thus providing a possible mechanistic basis to describe how bacteria may integrate central metabolism with growth and division (120).

Gluconeogenic growth factor YvcK

The enzyme of unknown function YvcK is essential under gluconeogenic growth regimes (growth using Krebs Cycle intermediates or Pentose Phosphate Pathway sugars) (121). YvcK is a member of the CofD family of proteins, which are enzymes involved in coenzyme F420 synthesis in archaea and high G+C content Gram-positive bacteria (121). YvcK, as well as many of its homologs, are found in bacteria that do not synthesize coenzyme F420, suggesting another role for YvcK; out of all its homologs, YvcK has been best studied in *B. subtilis* (121-124). YvcK essentiality under gluconeogenic growth regimes can be overcome by deletion of *zwf*, *cggR*, and *mfd*. Zwf is Glucose-6-Phosphate 1-Dehydrogenase, and is involved in shuttling glucose-6-phosphate into the Pentose Phosphate Pathway (121). CggR represses genes in central carbon metabolism, specifically those in the bottom half of gluconeogenesis, and so a deletion could result in increased flux of metabolites through gluconeogenesis and thus increased precursors for cell wall synthesis (121, 125). Mfd is involved in the synthesis of poly- γ -glutamic acid (PGA), and so inactivation of *mfd* via the transposon insertion could result in increasing the metabolic flux through other pathways which utilize glutamate (121, 125). YvcK essentiality under gluconeogenic growth regimes can be overcome via overexpression of MreB, and MreB conditional essentiality (needed additional Mg^{2+} and typically a *ponA* deletion) can be overcome with YvcK overexpression (122). YvcK localizes in a patchy “helical” pattern reminiscent of the localization of MreB like proteins in *B. subtilis*; however, YvcK does not co-localize with MreB and does not require MreB for its localization (122). MreB does not require YvcK for its localization either (122). YvcK

does not require the other MreB isoforms (Mbl and MreBH) for its localization (122), and overexpression of Mbl or MreBH does not rescue a *yvcK* deletion strain under gluconeogenic growth regimes (122).

In *B. subtilis*, *ponA* encodes the class A (high molecular weight) penicillin binding protein 1, which is bifunctional (having both transglycosylase and transpeptidase activity) (61). PBP1 has dynamic localization, and shuttles between the axial wall and the septum; this shuttling is dependent on MreB. *mreB* deletion results in mislocalization of PBP1 at the cell pole and subsequent loss in cell shape and death. *ponA* is not essential, and its deletion makes knockouts of the MreB-like proteins stable (along with added Mg^{2+}) (61). Similarly, loss of YvcK under gluconeogenic growth regimes results in a loss of PBP1 localization, and subsequent loss of cell shape and lysis; the loss of PBP1 localization and the subsequent effects on cell-shape can be prevented by addition of glucose to the media (no longer gluconeogenic regime), added Mg^{2+} , or overexpression of MreB (122). It is important to note that YvcK is found in both rod-shaped and spherical bacteria (and are essential in those as well) (122, 126), suggesting an important role in the cell-envelope synthesis machinery.

Posttranslational modifications of proteins has been shown to affect activity and/or localization of many proteins (123, 127-129). YvcK has been shown to be phosphorylated at Thr304 by the Ser/Thr kinase PrkC, but this phosphorylation does not affect its ability to allow growth under gluconeogenic growth regimes or its localization (123). However, YvcK phosphorylation does play a role in its cell shape activity (123). The phosphorylated state of YvcK (when overexpressed) is the only state that can

compensate for a loss of MreB and a return of the proper localization of PBP1, at least under the gluconeogenic growth regime tested (LB media) (123). It is a possibility that phosphorylation affects the interaction partners for YvcK, thereby regulating the pathway that its product is partitioned into. This makes sense, given that PrkC has been shown to respond to PG fragments (130), possibly through its extracellular PASTA domains (131); PrkC activation by a need for PG synthesis would trigger phosphorylation of YvcK, changing its interaction partners and thereby partitioning the product of its enzymatic reaction towards cell envelope synthesis. PknB, the homolog of PrkC in *Staphylococcus aureus*, requires its PASTA domains for proper localization (132). PknB also interacts with and has its kinase activity stimulated by Lipid II (132). PknB phosphorylates WalR (of the WalRK stress response regulator) and FtsZ, resulting in expression of autolysins, amidases, and hydrolases due to WalR and decreased GTPase activity in FtsZ (about 60% of normal activity was detected in the phosphomimic) (132). Essentially, PknB is coordinated the PG machinery with all of the division machinery (132).

Phosphomannose isomerase (ManA) (B. subtilis)

ManA, a phosphomannose isomerase in *B. subtilis*, is another example of a protein involved in carbon metabolism which affects cell shape when it is nonfunctional (catalytic mutant) or deleted (133). ManA is an enzyme that is responsible for converting mannose-6-phosphate to fructose-6-phosphate; this isomerization is reversible (133, 134). The *manA* mutant, when grown under gluconeogenic growth regimes (such as LB),

causes a loss of cell shape and subsequent death, even though there is no mannose present and it is not needed as a carbon source (133). Despite a growth condition where mannose is not present, there is high expression of ManA in LB (133, 135). Furthermore, *B. subtilis* contains a *manA* homolog (*pmi*), which shares over 56% sequence identity, yet has no cell morphological effect when knocked out under gluconeogenic growth regimes and is not expressed during cell growth in LB (133). ManA homologs in other organisms (archaea and bacteria) have been shown to have phosphoglucose isomerase activity, facilitating the isomerization between glucose-6-phosphate and fructose-6-phosphate (136). In *B. subtilis* and most other bacteria, *pgi* is the characterized phosphoglucose isomerase. Research into utilizing *B. subtilis* ManA in the industrial production of L-Ribose has revealed that *in vitro*, ManA shows promiscuity in its isomerization activity (137). It is therefore speculated that ManA can act as a phosphoglucose isomerase *in vivo* as well.

When the cell walls of a *manA* deletion and wild type were isolated and hydrolyzed and HPAEC neutral monosaccharide analysis was performed, the *manA* mutant showed ~five fold decrease in N-acetylgalactosamine (GalNAc) and ~four fold decrease in Glucose (Glc) compared to wild type, while GlcNAc levels remained the same (133). These sugars are used in/found in Teichoic Acids; this evidence links the cell shape defect in the *manA* mutant to its possible enzymatic activity. UDP-GalNAc is typically generated through epimerization of UDP-GlcNAc (138), which could suggest that the *manA* mutant is compromised in its ability to produce UDP-GlcNAc, and that the PG pathway takes priority in using this metabolite over the Teichoic Acid pathway.

The *manA* mutant showed polyploidy, with multiple rounds of replication completed, and an altered chromosome structure in addition to loss of cell shape/cell wall defects (133). *E. coli* actually shows a similar phenotype when the pools of pyrimidine precursors are limited (139); being that PG synthesis and DNA synthesis share UTP as precursor (for the synthesis of UDP-GlcNAc and dCTP/dTTP respectively), it makes sense that during steady state growth, DNA replication and cell growth are linked (125). Unlike YvcK, ManA localization is diffuse in the cell, making it difficult to speculate if there could be a moonlighting function to cell envelope morphogenesis (133). It was possible that ManA's true role in the cell is as a phosphoglucose isomerase, favoring fructose-6-phosphate to glucose-6-phosphate conversion under gluconeogenic growth regimes; this hypothesis is in agreement with the defect in cell shape, nucleoid morphology, and teichoic acid composition, as these phenotypes can result from lack of fructose-6-phosphate and glucose-6-phosphate (125).

It has been established that other enzymes involved in carbon metabolism are essential under conditions where the products of their enzymatic activity are not needed, such as glycolytic enzymes in LB + Glucose media (140). It has also been shown that trigger enzymes have a moonlighting role of regulating gene expression in various bacteria including *B. subtilis* (141-143). In *E. coli*, the glycolytic protein Enolase (eno) has been shown to interact with the RNA degradosome (RNase E, RhlB, PnpA), and that it plays a role in the regulation of glucose transporter *ptsG* mRNA stability (144). In *B. subtilis*, enzymes involved in glycolysis also interact with the RNA degradosome; Phosphofructokinase (PFK), Enolase (ENO), PnpA, Rny, RNase J1, RNase J2 form a

complex *in vivo* (140). The physiological reason for this interaction is still unclear. This same study also shows a complex of several glycolytic enzymes together (PFK, Phosphoglycerate mutase PGM, ENO, and possibly Glyceraldehyde phosphate dehydrogenase GAPDH) (140), and supports the theory of substrate channeling among enzymes in a given pathway (140). There have been numerous other studies suggesting substrate channeling in various pathways in both prokaryotes (140, 145-151) and eukaryotes, and research on eukaryotes (human cells) had shown compartmentalization of the enzymes involved in branched chain amino acid catabolism (152) and purine biosynthesis (153).

UDP-Glucose and UgtP (B. subtilis)

Evidence for genetic interactions between carbon and nitrogen metabolism and cell division are also abundant, and many are summarized in recent reviews (154, 155). UgtP, an enzyme in the non-essential glucolipid biosynthesis pathway in *Bacillus subtilis*, was shown to localize to FtsZ as well as inhibit polymerization of FtsZ in a UDP-Glucose (UDP-Glc) dependent manner (156, 157). Glucose-6-Phosphate may go through the glycolysis pathway, or can be converted to UDP-Glucose (through Glucose-1-Phosphate), where it can be used for glucolipid biosynthesis or major and minor wall teichoic acid synthesis (156, 158). According to the model, nutrient rich conditions should result in excess Glc-6-P, which results in an increased flux towards and amount of UDP-Glc. This results in the transient inhibition of FtsZ by UgtP, an enzyme in the glucolipid biosynthesis pathway, and continued cell growth, and allows the time

necessary to successfully segregate the bacterial chromosomes (156). UgtP expression is nutrient/media dependent; there are about 400 copies of UgtP per cell in minimal media with sorbitol, vs. ~2400 copies of UgtP per cell when grown in LB (156). Under nutrient rich conditions, UgtP colocalizes with FtsZ, while under nutrient poor conditions, UgtP localizes in punctate foci randomly around the cell (156, 157); this localization is dynamic, as UgtP foci relocate under conditions where nutrient availability is altered but protein synthesis is inhibited (157). Based on *in vivo* as well as *in vitro* assays, UgtP appears to be in an oligomeric state; UgtP's affinity for itself is fourfold higher in the absence of UDP-Glc than in the presence (157). UgtP was shown to inhibit FtsZ single-filament formation *in vitro* (157). Regulation of FtsZ assembly by metabolic enzymes (linking cell division with growth) was shown in *E. coli* by OpgH (159) and in *C. crescentus* by KidO and GdhZ (160).

UDP-Glucose and OpgH (E. coli)

OpgH is a glucosyltransferase involved in the synthesis of osmoregulated periplasmic glucans (OPG): OpgH does not show structural homology to UgtP in *B. subtilis*, but it is a functional homologue of UgtP in the sense that it inhibits FtsZ polymerization in a UDP-Glucose dependent manner (156, 157, 159). OpgH inhibition of FtsZ polymerization is independent of its role in synthesis of OPGs, or secondary upregulation of FtsZ in response to OPG pathway knockouts i.e. activation of the Rcs phosphorelay (159). Unlike UgtP in *B. subtilis*, OpgH appears to localize to FtsZ in a UDP-Glc independent manner; however, OpgH still localizes to FtsZ in a growth rate

dependent manner, as OpgH localizes at midcell only in the presence of FtsZ and only when grown in rich media (growth rate dependent) (159). Based on an *opgH* deletion analysis, it was concluded that the N terminal 138 amino acids were necessary and sufficient for FtsZ inhibition *in vivo* (159). Furthermore, it was also determined that the N-terminal portion of OpgH is sufficient to allow for medial localization, but that it was not necessary, as N terminal deletions of OpgH still colocalized with FtsZ (159). In vitro assays showed that OpgH inhibits FtsZ polymerization by binding FtsZ monomers, thereby increasing FtsZ's apparent critical concentration (CcApp) for GTP hydrolysis (159).

Nitrogen metabolism, GdhZ and KidO (Caulobacter crescentus)

In *C. crescentus*, GdhZ is responsible for conversion of glutamate to α -ketoglutarate, and its inhibition of FtsZ is substrate dependent (Glutamate or NAD⁺) (160). GdhZ colocalizes with FtsZ and acts to stimulate FtsZ GTPase activity, thereby promoting disassembly of the FtsZ filament, while KidO acts to disrupt FtsZ lateral interactions/bundling (160). GdhZ and KidO act to prevent premature Z ring formation early in the cell cycle while also promoting disassembly of the Z ring during cytokinesis (160, 161). Both of these mechanisms of regulating FtsZ are distinct from the glucosyltransferases UgtP in *B. subtilis* and OpgH in *E. coli* (157, 159, 160). GdhZ localizes to the midcell in an FtsZ dependent and nutrient dependent manner; when growth media is supplemented with sugars that allow avoidance of the glutamate metabolism pathway (and complement a *gdhZ* knockout), GdhZ does not localize at the

midcell (160). Furthermore, GdhZ catalytic activity is necessary for stimulation of FtsZ GTPase activity, but not essential for GdhZ interaction with FtsZ (160). KidO shows NADH dependent inhibition of FtsZ through inhibiting lateral interactions/bundling (160), and shows FtsZ dependent localization to the division site (161). GdhZ and KidO copy number both oscillate together over the course of the cell cycle, and both appear to be ClpXP degraded; GdhZ and KidO also appear to be in a complex, according to *in vitro* pulldown data (160, 161). The current model for GdhZ and KidO is that they work synergistically together to regulate FtsZ by affecting both polymerization and lateral bundling (155, 160). *E. coli* and *B. subtilis* using UDP-Glc while *C. crescentus* using Glutamate as a proxy for cellular energy or nutrient level to regulate division has raised the conjecture that perhaps different organisms regulate division based on their preferred carbon source (155).

While nutrient availability has been shown to regulate Z ring formation temporally, it has also been shown to regulate Z ring formation spatially. In *B. subtilis*, a deletion of *pyk* (pyruvate kinase) resulted in rescuing a temperature sensitive allele of FtsZ at non-permissive temperatures, and it was determined that this rescuing was not stress response dependent (162); furthermore, a *pyk* deletion in a Wild type background resulted in the formation of polar Z rings as well as multiple Z rings in ~32% and ~6% of the population, respectively (162). These results strongly suggested that the deletion of *pyk* affects FtsZ assembly, as it is a similar phenotype to knockouts of the nucleoid occlusion system in *B. subtilis* (163-165). It was shown that pyruvate itself was enough to complement the aberrant Z ring assembly in a *pyk* deletion (162), and further

investigation linked this pyruvate dependent defect in FtsZ assembly to PDH E1 α (pyruvate dehydrogenase E1 α subunit) (162). PDH E1 α localizes over the nucleoid in a pyruvate dependent fashion, and appears to stimulate Z ring formation over the midcell under nutrient rich conditions (155, 162). Taken together, it appears metabolic enzymes in *B. subtilis* assist in correctly positioning the Z ring as well as allowing division only when the critical cell-size is attained.

UndP availability as a regulator of growth and division

While the rapid fine-tuning of metabolic activity and cell division allows the cell to quickly adapt to its environment, it does not compensate for a growing problem, limited resources. A growing body of evidence suggests that critical substrates are bottlenecks on metabolic flux (166, 167). For instance, current research suggests that the lipid carrier undecaprenyl phosphate (Und-P) exists in a common pool, shared between peptidoglycan (PG) synthesis, enterobacterial common antigen (ECA) synthesis, O antigen synthesis, and colonic acid synthesis in *Escherichia coli* (166, 167). Genetic knockouts that block the non-essential pathways of ECA or O antigen synthesis cause deleterious effects on PG synthesis, which can be overcome through increasing Und-P levels, increasing Und-P recycling, or preventing Und-P from being sequestered for the pathway initially (166, 167). Although it was previously shown that ECA plays a role in outer membrane integrity and sensitivity to bile salts (168), knocking out the entire pathway at the first step (*wecA*) does not cause a loss of rod-shape (167); only when the gene that is further downstream of the pathway, *wecE*, was knocked out does a loss of

rod-shape and an accumulation of ECA-Lipid II occur (167). Since increased expression of Und-P rescued the cell-shape defect of a *wecE* mutant, it suggested that depletion of Und-P pools and not accumulation of ECA-Lipid II were the cause of the cell-shape defect (167); furthermore, overexpression of genes that redirected Und-P to competing pathways such as PG synthesis (*murA*) or O-antigen synthesis (*wbbL*) rescued cell shape defects of the *wecE* mutant, supporting the hypothesis that the depletion of Und-P was resulting in the cell-shape defect (167). Additional deletions of genes in the ECA pathway that would result in Und-PP-linked intermediates also had similar cell-shape defects, again suggesting depletion of the Und-P pool as the cause of the cell-shape defect (167). Similarly, it has been shown in the Gram-positive organisms *Bacillus subtilis* and *Staphylococcus aureus* that the teichoic acid pathway is dispensible, as long as *tagO* or *tarO* is knocked out, respectively (169, 170). *tagO* and *tarO* encode a UDP-N-acetylglucosamine-undecaprenyl-phosphate N-acetylglucosaminephosphotransferase (UDP-GlcNAc-Und-P Glc-NAc phosphotransferase), which links UDP-GlcNAc to Und-P, drawing from the common pool of Und-P; this is the first synthetic step of teichoic acid synthesis (171). As it appears that this Und-P pool is limiting, and that the cell does not produce more Und-P under conditions where Und-P is committed to a biosynthetic pathway that cannot be completed (due to gene deletion), the cell experiences cell-shape defects and dies (166, 167, 169, 170).

This illustrates another important and overarching concept in bacterial cell growth, sharing of metabolites. Certain key substrates in the cell are positioned at metabolic hubs, and substrate availability can dynamically shift the flow of metabolites

(i.e carbon or nitrogen) down different pathways. This phenomenon is utilized frequently in biotechnology to increase yield of desired products and/or decrease unwanted biproducts (172, 173). Pathway perturbation has also been investigated as a mechanism to sensitize pathogens to specific antibiotics (86).

Metabolic tuning based on nutrient conditions

It has been known for decades that bacteria can grow up to twice as large in rich media as minimal media (112, 113, 174), and that they can adapt their size and metabolism dynamically in response to nutrient availability (175). Along those lines, a cell's metabolic flux is fine-tuned based on nutrient conditions, and the tuning can occur at the transcriptional and post-transcriptional level. For example, enzymes involved in the utilization of alternative sugars are generally repressed in the presence of glucose (176-179). Examples of post-translational regulation are also numerous. For example, many key metabolic enzymes are regulated allosterically by metabolites as well as through acetylation, phosphorylation, pupylation, and addition of 3-phosphoglyceryl-lysine (pgK) modifications (175).

A summary of the previous discussion is depicted in Fig 1.1.

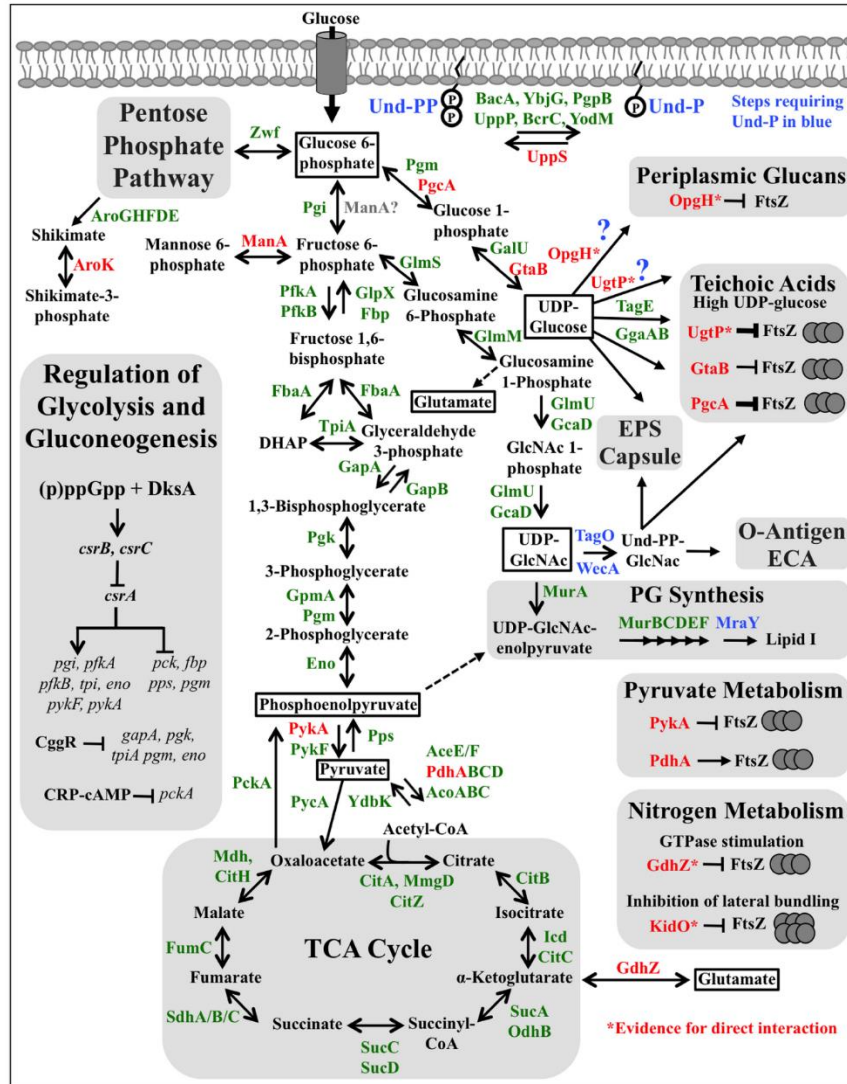


Figure 1.1 Metabolic pathways implicated in the regulation of cell shape and size. Enzymes are indicated by green, red, or blue text. Enzymes discussed in the text are indicated in red or blue. Enzymes shown in blue denote steps dedicating Und-P (also in blue) to one or more pathways. Enzymes predicted to coincide with or precede Und-P dedication to one or more pathways are followed by blue question marks. In most cases, the relevant enzyme(s) for both *E. coli* and *B. subtilis* is given; however, not all organisms possess every enzyme shown. Enzymes that are less studied or have not been tested experimentally are generally excluded. Enzymes shown to interact directly with FtsZ are denoted with an asterisk. Only regulators of glycolysis and gluconeogenesis discussed in the text are shown in the left-hand block.

Bacteriophages

Historical perspective on phage

Phages (or Bacteriophage) are viruses that specifically target bacteria; the translation of bacteriophage literally means “bacteria eater”. Phage were discovered in the early 20th century by the British pathologist Frederick Twort and by the French-Canadian microbiologist Felix d’Herelle (in 1915 and 1917 respectively) (180-182). Felix d’herelle worked at the Pasteur Institute during World War I, and noticed that the fecal material of patients who had recovered from *Shigella dysenteriae* contained a component that killed *S. dysenteriae* and conferred protection when given to patients who were suffering from *S. dysenteriae* (181-184). Felix d’Herelle did the early characterization of phage, noting that the phage was far smaller than bacteria, as it passed through a filter that trapped bacteria (185); he also developed the plaque formation assay for determining the amount of phage particles in a given lysate/solution (185).

The use of phages for treatment of bacterial infections (Phage Therapy) continued throughout the 1920’s and 1930’s, with mixed success, attributable to a lack of understanding of phage, bacterial evolution, and quality control/standardization of phage production (some of the preservatives used actually inactivated the phages) (184). In the 1930s, the first antibiotics were introduced and phage therapy in the US rapidly declined. Antibiotics were broad spectrum, easily produced, better understood, and more stable than the phage products of the time (184). Phage therapy continued throughout

Eastern Europe, particularly the Soviet Bloc country of Georgia where Felix D'Herelle and Geoge Eliava established a phage institute at Tbilisi (184).

There are double stranded DNA phages, single stranded DNA phages, and RNA phages; however, only the dsDNA phages are discussed here, as they are germane to the dissertation. dsDNA phages are members of the *Caudovirales* Order, which is comprised of three families: *Myoviridae*, *Siphoviridae*, and *Podoviridae*; classification into these families is based on morphology on the phage, and not on genetic homology. It is not uncommon to have a Myophage that shares greater homology to a Podophage than to another Myophage (185). Myophages have long, rigid contractile tales, Siphophages have long, flexible non-contractile tales, and Podophages have short non-contractile tails.

Phage infection cycles

During phage infection, the tail fibers of the phage recognize a cognate receptor on the surface of the target bacterium. The phage then ejects its DNA into the bacterial host, at which point the infection cycle begins. There are two types of phage infection cycles, lytic and lysogenic, and phage may be obligately lytic (virulent) or both lytic and lysogenic (temperate). The phage infection cycle is divided into early, middle, and late designations for genes; early designates genes that are transcribed prior to viral DNA replication, middle designates genes transcribed during viral DNA replication, and late genes are genes transcribed after viral DNA replication. During lytic cycles, the phage DNA is replicated and all of the phage structural machinery is synthesized, and the

components assemble with the genome to form a complete phage. This is followed by lysis of the host cell, releasing newly formed phage particles into the environment. During lysogenic cycles, the phage DNA either circularizes and is maintained as an autonomously replicating plasmid, as occurs with Phage P1, or integrates into the host chromosome. Chromosomal insertion may occur through site-specific recombination, such as integration of Lambda DNA at the att locus on the *E. coli* chromosome, or randomly as occurs with phage Mu. The decision of temperate phages to go lytic or lysogenic following DNA ejection has been the focus of much research (186-189). Environmental factors such as multiplicity of infection (MOI- the number of phages infecting each cell) (190), nutrient status (191, 192), and temperature (193, 194), have been shown to influence the lysis/lysogeny decision. For example, higher MOI shifts phage toward a lysogenic decision (188). More recently, single cell assays using the model phage Lambda have given us insight into the decision making process in real time (186-189). These studies have revealed that when multiple phage infect the same cell, the decision to lysogenize must be unanimous (186); furthermore, during a mixed decision where one phage votes to lysogenize and another votes for the lytic cycle, lysogeny occur, whereas integration of a phage genome into the *E. coli* chromosome occurs, followed by phage lysis (188).

Phages that go through the lysogenic cycle can later excise from the host chromosome and initiate the lytic cycle when conditions in the host become unfavorable. Excision requires a stimulus, such as a signal that DNA damage is occurring (195). Temperate phages have been the focus of clinical research because they can often

encode virulence factors, as is the situation for *E. coli* O157:H7, where the prophage encodes Shiga toxin (196).

Phage lysis

If a phage is obligately lytic, chooses the lytic cycle, or undergoes excision from the chromosome, new infectious particles are generated and phage lysis occurs. Phage lysis in Gram-negative bacteria occurs through the expression of the lysis genes, which are under the control of a late promoter. Typically the lysis genes are found in clusters together called “cassettes”. The lysis genes include a holin (and cognate antiholin), an endolysin, and spanin(s) (197). The holin acts as an allelic specific molecular timer for phage lysis. In phage Lambda, for example, the holin is S105 and the antiholin is S107 (197). The holin and antiholin have three transmembrane domains, but S107 contains an N-terminal positively charged residue which keeps the S107 inactive by preventing the TMD1 from entering the membrane. Heterodimers of S105:S107 are inactive, and only when enough S105 homodimers have accumulated does holin raft formation and the subsequent dissipation of the proton motive force (which turns S105:S107 heterodimers into an active holin conformation as the TMD1 of S107 can now enter the membrane) as well as release of the endolysin (the PG degrading enzyme) into the periplasm. The holin rafts are on the micron scale in size (average is 340nm but can be over 1µm), but few in number (average is 1-3 per cell) (198, 199). Following endolysin release, cells lyse with the aid of membrane fusing spanins.

Another variation of the typical holin endolysin paradigm is pinholins and SAR endolysins (197, 200). Phage 21 has the best characterized pinholin Signal Anchor Release (SAR) endolysin system, and so will be used as the model. Phage 21 contains a pinholin, S68. When the critical concentration of S68 is reached, S68 assembles into heptameric channels with a very small lumen size, estimated to be ~2nm (201); furthermore, instead of making only a few holes like phage Lambda S105 holin makes, S68 forms about 10^3 channels that dissipate the proton motive force (200). The loss of proton motive force activates the SAR endolysin, which degrades the PG (200). Before activation by the pinholin, the SAR endolysin is produced and exported using the host *sec* system (200, 202, 203) and remains tethered to the membrane, catalytically inactive (200) activation by the pinholin S68 dissipating the proton motive force releases SAR endolysin from the membrane and it adopts its catalytically active form (203, 204). It is important to note that in SAR endolysin systems, there is a spontaneous rate for release of SAR endolysins from the membrane, and so pinholins are not absolutely necessary for host lysis, rather they function to concertedly instigate lysis (197, 200). Spanin(s) function by facilitating membrane fusion of the inner and outer membranes of Gram-negative bacteria (205). Spanins can be in a pair (i-spanin and o-spanin) or be a single, unimolecular spanin (u-spanin) (197, 200, 205, 206). Obviously, phages with Gram-positive hosts do not encode a spanin.

Endolysins encoded in phage that have a Gram-positive host typically have a cell wall binding domain. Since Gram-positive bacteria lack an outer membrane and true periplasm, it is thought this prevents release of the endolysin into the environment,

which might lead to the destruction of nearby phage host (207). Endolysins are not necessarily true lysozymes, which function by breaking the glycosidic bond between GlcNAc-MurNAc (200).

PBSX in B. subtilis strain 168

PBSX is a prophage present in *B. subtilis* 168 that is capable of selectively killing a closely related subspecies, *B. subtilis* W23, when excision is activated and phage particles are formed (195). In the domesticated lab strain, *B. subtilis* 168, PBSX is defective. More specifically, it fails to package its own DNA and form a functional (replicating) phage particle. PBSX has a genome size of around 33kb (208), and it packages about 13kb of random DNA from the host *B. subtilis* chromosome (195, 209-213), although because it is defective, that DNA is not thought to eject into the sensitive W23 strain upon phage adsorption (195, 213).

PBSX like phagocins are found in *B. subtilis* strains as well some strains of *B. pumilis* and *B. licheniformis* (214, 215). Each phagocin is capable of selectively killing another subspecies or species of *Bacillus*, but not their host. The ability to kill other strains of *Bacillus subtilis* would confer an evolutionary advantage to having PBSX like phagocins, and it has been hypothesized that this is why they have been conserved in the genome's of their hosts (214, 215); furthermore, since some cannot be deleted from the host genome without loss of viability, it is speculated that some phagocins may confer an advantage to the host beyond their bacteriocidal activity (213). However, PBSX can be cured from *B. subtilis* strain 168, so if this is accurate, there are exceptions (216). PBSX

can be induced from the *B. subtilis* chromosome similarly to temperate phages, by inducing the SOS response with UV irradiation, mitomycin C treatment, or Carbadox treatment (195, 210-212) As with other temperate phage induction, PBSX induction results in chromosomal replication around the prophage DNA region (209, 217), the production of phage proteins, and the assembly of PBSX particles. It is estimated that the burst size (number of particles of a phage produced per host per infection cycle) is 550 (218). However, this estimate may not be particularly accurate, as it is technically difficult to ascertain burst size with non-replicating particles such as phagocins, because particle number cannot be determined using serial dilutions and plaque assays. Instead, burst size is estimated by mixing phagocin lysates with known concentrations of cells, plating, and determining survival from a Poisson distribution (218).

The physical dimensions of PBSX were well characterized in 1968 by Marmurs group (195). The head, tail, and sedimentation coefficient are as follows: 410A head, 1920A long tail with 52 or 53 striations, 185A wide tail, 160s sedimentation coefficient, a density of $1.375\text{g}\cdot\text{cm}^{-3}$ in CsCl (195). The physical dimensions and characteristics of PBSX assist in identification of it when comparing to other defective prophages, as they are highly similar in structure.

Maintenance of PBSX lysogeny

Maintenance of PBSX as a prophage element is regulated by the CI-like repressor Xre, a 113 amino acid protein with an N-terminal helix-turn helix DNA-binding domain (219). Xre has homology (in the N-terminal region) to both the Φ 105

repressor and C2 repressor from phage P22 (219, 220). Xre possesses a SigA promoter (vegetative sigma factor), and overlapping this promoter are four highly similar palindromic 15bp repeats (denoted O1-O4) (beginning with the site farthest upstream of the promoter is O1 and the site closest to the promoter is O4), with the consensus sequence of 5'-GATACAAAATGTATC-3'; these consensus sequences are directly bound by Xre (219, 220). Xre has a higher affinity for O1 and O2, and when bound at these sites represses a divergent SigA promoter controlling the PBSX late gene (lytic) operon (220). At higher concentrations Xre also binds to O3 and O4, leading to repression of *xre* itself (220). This paradigm of gene expression, where a repressor is autoregulated and expressed divergently from a repressor controlled operon, is well characterized in lambdoid phages (Lambda and Φ 105) (220-222). This autoregulation ensures that enough of the repressor is made to maintain lysogeny during normal growth, but also does not allow repressor levels to get so high that the prophage cannot excise when a signal such as DNA damage induces the SOS response (219, 220). It was later determined that *pcf*, which resembled a transcription factor but was only 20.1kDa (hypothetically), was required for late gene expression of PBSX (P_L) (223).

Isolation of a thermoinducible allele of Xre

A thermoinducible Xre was first isolated and designated as the xhi-1479 mutation by Buxton in 1976 (224); temperature shift from 37°C to 48°C would result in phagocin induction, production of PBSX particles, and subsequent host lysis. It was later found that this xhi-1479 mutant of Xre was thermolabile, and therefore recessive to a

wild-type copy of the allele (219). This allowed Wood et. al to isolate the fragment that complemented the xhi-1479 mutant (abolished thermosensitivity), and to subsequently identify the associated point mutations (219). Three Xre substitutions were identified: G4S, A19V, and L78V (219). Since A19V resided within the predicted helix-turn-helix domain of the protein (predicted DNA-binding region), it was hypothesized that the A19V substitution alone conferred temperature sensitivity to Xre (219). Codon usage analysis was performed on *xre* to estimate its expression level, and the estimation was that it is poorly expressed or expressed at low levels (219, 225, 226).

Phage receptors

Bacteriophages require receptors for the ability to infect their subsequent host; phage tail fibers recognize molecules present on the surface of the host. In Gram-negative bacteria, host-cell recognition is much better understood, and receptors include lipopolysaccharide (LPS), exopolysaccharides/capsule, and channel-forming β -barrel proteins present in the outer membrane (227-229). Once contact is made with the host receptor(s), they are stably adsorbed and the phage DNA is ejected into the host.

The primary receptor for *E. coli* phage Lambda is the outer membrane protein LamB (the maltose porin). The proteins ManY and ManZ, which are part of the PTS, are believed to play a role in Lambda DNA transport across the inner membrane (230-232). LamB is essential for Lambda infection, while *manYZ* deletion results in several orders of magnitude decreased efficiency of plating, suggesting an important but not essential role for ManYZ during the infection process (230-232). Other examples of phage

receptors in Gram-negative bacteria include the ferrichrome transporter FhuA (TonA) of phage T1, and LPS for phage P1 and numerous other phages (233-236).

The process of phage infection, particularly the binding of phage to its receptor, is less studied in Gram-positive hosts. The well-characterized siphophage SPP1 binds to glucosylated teichoic acids and the inner membrane protein YueB (237-239). Teichoic acids (TA) are important for phage recognition/adsorption for a variety of phages, with specificity conferred by TA composition (239-243). *B. subtilis* strain 168 and *B. subtilis* W23 differ in their teichoic acid compositions, the former having polyglycerol phosphate teichoic acids while the latter have polyribitol phosphate teichoic acid (171, 242, 244). It was suggested that PBSX, the *B. subtilis* 168 phagocin that targets *B. subtilis* W23, and PBSZ, the *B. subtilis* W23 phagocin that targets *B. subtilis* 168, possess changes in their tail fibers that confer specificity of the phagocin, while allowing the host strain to avoid sensitivity (death) (241)

CHAPTER II

YodL AND YisK POSSESS SHAPE-MODIFYING ACTIVITIES THAT ARE SUPPRESSED BY MUTATIONS IN *Bacillus subtilis* MreB AND Mbl*

Introduction

Bacterial cell growth requires that the machineries directing enlargement and division of the bacterial cell envelope be coordinated in both time and space (245). The cell envelope is comprised of membranes and a macromolecular mesh of peptidoglycan (PG) that possesses both rigid and elastic properties (246, 247). PG is highly cross-linked, allowing bacteria to maintain shapes and avoid lysis, even in the presence of several atmospheres of internal turgor pressure. PG rearrangements are required during the inward redirection of growth that occurs at the time of cell division, but are also necessary when cells insert new PG and dynamically modify their morphologies in response to developmental or environmental signals (248, 249). To avoid lysis during PG rearrangements, bacteria must carefully regulate the making and breaking of glycan strands and peptide crosslinks (247). In rod-shaped bacteria, PG enlargement during steady-state growth is constrained in one dimension along the cell's long-axis and can either occur through polar growth, as is the case in *Agrobacterium tumefaciens* and *Streptomyces coelicolor*, or through incorporation of new cell wall material along the length of the cell cylinder, as observed in *Escherichia coli*, *Bacillus subtilis*, and *Caulobacter crescentus* (250).

*Reprinted with permission from "YodL and YisK possess shape-modifying activities that are suppressed by mutations in *Bacillus subtilis* MreB and Mbl" by Duan, Y., Sperber, A.M. and Herman, J.K., 2016. *Journal of Bacteriology*, 198(15):2074-2088. Copyright 2016 by American Society for Microbiology.

To control cell diameter and create osmotically stable PG, bacteria that exhibit non-polar growth require the activity of the highly conserved actin-like protein MreB. Biochemical, genetic, and cell biological data suggest that MreB likely directs PG synthesis during cell elongation and in some bacteria, MreB may also function during cell division (41, 45, 251). MreB possesses ATPase activity, and polymerizes at sites along the cytoplasmic side of the inner membrane (75). ATP binding and hydrolysis is required for MreB polymerization and activity (252) and two S-benzylisothiourea derivatives, A22 and MP265, target the ATPase domain of MreB in Gram negative organisms, possibly preventing nucleotide hydrolysis and/or release (253-256). Depletion or inactivation of MreB is lethal except in some conditional backgrounds (257, 258), so organisms sensitive to A22 and/or MP265 lose shape and eventually lyse (253-256).

MreB has been found to interact with several other proteins involved in PG synthesis, including the bitopic membrane protein RodZ (61, 78, 251, 257, 259). RodZ interacts directly with MreB through a cytoplasmic helix-turn-helix motif located at its N-terminus (78). A co-crystal structure of RodZ and MreB shows the N-terminus of RodZ extending into a conserved hydrophobic pocket located in subdomain IIA of MreB (78). Depletion of RodZ also leads to loss of cell shape and cell death (79, 260, 261). However, in various mutant backgrounds, *rodZ* can be deleted without loss of rod shape or viability, indicating that RodZ is not absolutely required for MreB's function in maintaining shape (77, 80, 262). Based on these observations and others, it has been

proposed that MreB-RodZ interactions may regulate some aspect of MreB activity (75, 80).

Gram-positives often encode multiple paralogs (263). *B. subtilis* possesses three *mreB* family genes: *mreB*, *mbl*, and *mreBH*. *mreB* is distinguished from *mbl* and *mreBH* by its location within the highly conserved *mreBCD* operon. Although *mreB*, *mbl*, and *mreBH* are essential, it has been reported that each can be deleted under conditions in which cells are provided sufficient magnesium (62, 65, 264), or in strain backgrounds lacking *ponA*, the gene encoding penicillin binding protein 1 (PBP1) (61). In addition, all three genes can be deleted in a single background with only minor effects on cell shape if any one of the paralogs is artificially overexpressed in *trans* from an inducible promoter (60). The ability of any one of the paralogs to compensate for the loss of the others, at least under some growth conditions, strongly suggests that MreB, Mbl, and MreBH share significant functional redundancy (60, 265).

At the same time, several lines of evidence suggest that the paralogs possess non-overlapping functions. The genes themselves exhibit different patterns of transcriptional regulation, suggesting that each likely possesses specialized activities that are important in different growth contexts. For example, *mreB* and *mbl* are maximally expressed at the end of exponential growth, but expression falls off sharply during stationary phase (68), whereas *mreBH* is part of the SigI heat-shock regulon (266). There is also evidence suggesting that each protein may possess specialized activities. For example, MreBH interacts with the lytic transglycosylase LytE, and is required for LytE localization (69), whereas the lytic transglycosylase CwlO, depends on Mbl for wildtype function (69).

More recently MreB (but not Mbl or MreBH) was shown to aid in escape from the competent cell state (68).

Aside from RodZ (75, 80), only a handful of proteins targeting MreB activity in vivo have been identified. In *E. coli*, the YeeU-YeeV prophage toxin-antitoxin system is comprised of a negative regulator of MreB polymerization, CbtA (267), and a positive regulator of MreB bundling, CbeA (268). Another *E. coli* prophage toxin, CptA, is also reported to inhibit MreB polymerization (269). The MbiA protein of *C. crescentus* appears to regulate MreB in vivo, however, its physiological role is unknown (270). Given the importance of PG synthesis to cell viability and in cell shape control, it is likely that many undiscovered factors exist that modulate the activity of MreB and its paralogs.

In the present work we describe the identification of YodL and YisK, modulators of MreB and Mbl activity that are expressed during early stages of *B. subtilis* sporulation. Misexpression of either *yodL* or *yisK* during vegetative growth results in loss of cell width control and cell death. Genetic evidence indicates that YodL targets and inhibits MreB activity, whereas YisK targets and inhibits Mbl. Our data also show that YisK activity affects cell length control through an Mbl and MreBH-independent pathway.

Materials and methods

General methods

All *B. subtilis* strains were derived from *B. subtilis* 168. *E. coli* and *B. subtilis* strains utilized in this study are listed in Table 2.1. Plasmids are listed in Table 2.2. Oligonucleotide primers are listed in Table 2.3. Details on plasmid and strain construction can be found in the Supplementary text. *Escherichia coli* DH5 α was used for cloning. All *E. coli* strains were grown in LB-Lennox medium supplemented with 100 $\mu\text{g/ml}$ ampicillin. The following concentrations of antibiotics were used for generating *B. subtilis* strains: 100 $\mu\text{g/ml}$ spectinomycin, 7.5 $\mu\text{g/ml}$ chloramphenicol, 0.8 mg/ml phleomycin, 10 $\mu\text{g/ml}$ tetracycline, 10 $\mu\text{g/ml}$ kanamycin. To select for erythromycin resistance, plates were supplemented with 1 $\mu\text{g/ml}$ erythromycin (erm) and 25 $\mu\text{g/ml}$ lincomycin. *B. subtilis* transformations were carried out as described previously (271). When indicated, the LB in the *B. subtilis* microscopy experiments was LB-Lennox broth. Sporulation by resuspension was carried out at 37°C according to the Sterlini-Mandelstam method (272). Penassay broth (PAB) is composed of 5 g peptone, 1.5 g beef extract, 1.5 g yeast extract, 1.0 g D-glucose (dextrose), 3.5 g NaCl, 3.68 g dipotassium phosphate, and 1.32 g monopotassium phosphate per liter of distilled water. To make solid media, the relevant media was supplemented with 1.5% (w/v) bacto-agar.

Table 2.1. Strains used in Chapter II.

Strain	Description	Reference
Parental		
<i>B. subtilis</i> 168	<i>Bacillus subtilis</i> laboratory strain 168 <i>trpC2</i>	BGSC (1A866)
<i>B. subtilis</i> 3610	<i>spo0H::cat (sigH::cat)</i>	(273)
<i>B. subtilis</i> PY79	<i>Bacillus subtilis</i> laboratory strain	(274)
<i>E. coli</i> DH5 α	<i>F⁻ endA1 glnV44 thi-1 recA1 relA1 gyrA96 deoR nupG Φ80dlacZΔM15 Δ(lacZYA-argF)U169, hsdR17(rK^- mK^+), λ^-</i>	
<i>B. subtilis</i> 168		
BAS040	<i>amyE::P_{hy}-yodL (spec)</i>	This study
BAS041	<i>amyE::P_{hy}-yisK (spec)</i>	This study
BAS146	<i>ponA::erm, kan$\Omega$$\Delta$mreB</i>	This study
BAS147	<i>ponA::erm, kan$\Omega$$\Delta$mbl</i>	This study
BAS170	<i>amyE::P_{yodL}-lacZ (spec)</i>	This study
BAS171	<i>amyE::P_{yodL}-gfp (spec)</i>	This study
BAS191	<i>amyE::P_{hy}-yodL (spec), yhdG::P_{hy}-yodL (phleo)</i>	This study
BAS192	<i>amyE::P_{yisK}-lacZ (spec)</i>	This study
BAS193	<i>amyE::P_{yisK}-gfp (spec)</i>	This study
BAS205	<i>amyE::P_{empty}-gfp (spec)</i>	This study
BAS248	<i>ponA::erm, kan$\Omega$$\Deltambl, cat\Omega$$\Delta$mreBH, amyE::P_{hy}-yisK (spec), yhdG::P_{hy}-yisK (phleo)</i>	This study
BAS249	<i>ponA::erm, kan$\Omega$$\Deltambl, cat\Omega$$\Delta$mreBH, amyE::P_{hy}-yodL (spec), yhdG::P_{hy}-yodL (phleo)</i>	This study
BAS265	<i>spo0A::erm</i>	This study
BAS266	<i>amyE::P_{yodL}-gfp (spec), spo0A::erm</i>	This study
BAS267	<i>amyE::P_{yisK}-gfp (spec), spo0A::erm</i>	This study
BAS282	<i>sigH::cat</i>	This study
BAS301	<i>amyE::P_{yodL}-lacZ (spec), spo0A::erm</i>	This study
BAS302	<i>amyE::P_{yisK}-lacZ (spec), spo0A::erm</i>	This study
BAS303	<i>amyE::P_{yodL}-lacZ (spec), sigH::cat</i>	This study
BAS304	<i>amyE::P_{yisK}-lacZ (spec), sigH::cat</i>	This study
BAS305	<i>amyE::P_{yodL}-lacZ (spec), spo0A::erm, sigH::cat</i>	This study
BAS306	<i>amyE::P_{yisK}-lacZ (spec), spo0A::erm, sigH::cat</i>	This study
BDR992	<i>amyE::P_{hy}-lacZ (spec)</i>	David Z. Rudner
BKE10750	<i>yisK::erm</i>	BGSC

Table 2.1. Continued.

Strain	Description	Reference
BKE19640	<i>yodL::erm</i>	BGSC
BKE22320	<i>ponA::erm</i>	BGSC
BYD048	<i>amyE::P_{hy}-yodL (spec)</i> , <i>ycgO::P_{hy}-yodL (tet)</i> , <i>yhdG::P_{hy}-yodL (phleo)</i> , <i>sacA::P_{hy}-lacZ (erm)</i>	This study
BYD074	<i>amyE::P_{hy}-yisK (spec)</i> , <i>yhdG::P_{hy}-yisK (phleo)</i>	This study
BYD076	<i>amyE::P_{hy}-yisK (spec)</i> , <i>yhdG::P_{hy}-yisK (phleo)</i> , <i>yycR::P_{hy}-yisK (cat)</i> , <i>sacA::P_{hy}-lacZ (erm)</i>	This study
BYD175	<i>ponA::erm</i> , <i>amyE::P_{hy}-yisK (spec)</i> , <i>yhdG::P_{hy}-yisK (phleo)</i>	This study
BYD176	<i>ponA::erm</i> , <i>amyE::P_{hy}-yodL (spec)</i> , <i>yhdG::P_{hy}-yodL (phleo)</i>	This study
BYD177	<i>kanΩmreB_{G323E}</i> , <i>amyE::P_{hy}-yisK (spec)</i> , <i>yhdG::P_{hy}-yisK (phleo)</i> , <i>yycR::P_{hy}-yisK (cat)</i>	This study
BYD178	<i>kanΩmreB_{P147R}</i> , <i>amyE::P_{hy}-yisK (spec)</i> , <i>yhdG::P_{hy}-yisK (phleo)</i> , <i>yycR::P_{hy}-yisK (cat)</i>	This study
BYD179	<i>kanΩmreB_{R282S}</i> , <i>amyE::P_{hy}-yisK (spec)</i> , <i>yhdG::P_{hy}-yisK (phleo)</i> , <i>yycR::P_{hy}-yisK (cat)</i>	This study
BYD180	<i>kanΩmreB_{G143A}</i> , <i>amyE::P_{hy}-yisK (spec)</i> , <i>yhdG::P_{hy}-yisK (phleo)</i> , <i>yycR::P_{hy}-yisK (cat)</i>	This study
BYD184	<i>kanΩmreB_{R117G}</i> , <i>amyE::P_{hy}-yisK (spec)</i> , <i>yhdG::P_{hy}-yisK (phleo)</i> , <i>yycR::P_{hy}-yisK (cat)</i>	This study
BYD258	<i>ponA::erm</i> , <i>kanΩΔmbl</i> , <i>amyE::P_{hy}-yisK (spec)</i> , <i>yhdG::P_{hy}-yisK (phleo)</i>	This study
BYD259	<i>ponA::erm</i> , <i>kanΩΔmbl</i> , <i>amyE::P_{hy}-yodL (spec)</i> , <i>yhdG::P_{hy}-yodL (phleo)</i>	This study
BYD262	<i>ponA::erm</i> , <i>kanΩΔmreB</i> , <i>amyE::P_{hy}-yisK (spec)</i> , <i>yhdG::P_{hy}-yisK (phleo)</i>	This study
BYD263	<i>ponA::erm</i> , <i>kanΩΔmreB</i> , <i>amyE::P_{hy}-yodL (spec)</i> , <i>yhdG::P_{hy}-yodL (phleo)</i>	This study
BYD276	<i>ΔyodL</i>	This study
BYD278	<i>ΔyisK</i>	This study
BYD279	<i>ΔyodL</i> , <i>ΔyisK</i>	This study
BYD281	<i>amyE::P_{hy}-yisK (spec)</i> , <i>ycgO::P_{hy}-yisK (tet)</i> , <i>yhdG::P_{hy}-yodL (phleo)</i> , <i>yycR::P_{hy}-yodL (cat)</i>	This study
BYD327	<i>kanΩmreB_{G323E}</i> , <i>amyE::P_{hy}-yodL (spec)</i> , <i>yhdG::P_{hy}-yodL (phleo)</i> , <i>yycR::P_{hy}-yodL (cat)</i>	This study
BYD328	<i>kanΩmreB_{R117G}</i> , <i>amyE::P_{hy}-yodL (spec)</i> , <i>yhdG::P_{hy}-yodL (phleo)</i> , <i>yycR::P_{hy}-yodL (cat)</i>	This study
BYD329	<i>kanΩmreB_{N145D}</i> , <i>amyE::P_{hy}-yodL (spec)</i> , <i>yhdG::P_{hy}-yodL (phleo)</i> , <i>yycR::P_{hy}-yodL (cat)</i>	This study

Table 2.1. Continued.

Strain	Description	Reference
BYD330	<i>kanΩmre</i> _{B_{P147R}} , <i>amyE</i> :: <i>P_{hy}-yodL</i> (<i>spec</i>), <i>yhdG</i> :: <i>P_{hy}-yodL</i> (<i>phleo</i>), <i>yycR</i> :: <i>P_{hy}-yodL</i> (<i>cat</i>)	This study
BYD332	<i>kanΩmre</i> _{B_{S154R,R230C}} , <i>amyE</i> :: <i>P_{hy}-yodL</i> (<i>spec</i>), <i>yhdG</i> :: <i>P_{hy}-yodL</i> (<i>phleo</i>), <i>yycR</i> :: <i>P_{hy}-yodL</i> (<i>cat</i>)	This study
BYD333	<i>kanΩmre</i> _{B_{G143A}} , <i>amyE</i> :: <i>P_{hy}-yodL</i> (<i>spec</i>), <i>yhdG</i> :: <i>P_{hy}-yodL</i> (<i>phleo</i>), <i>yycR</i> :: <i>P_{hy}-yodL</i> (<i>cat</i>)	This study
BYD334	<i>kanΩmbl</i> _{E_{250K}} , <i>amyE</i> :: <i>P_{hy}-yisK</i> (<i>spec</i>), <i>yhdG</i> :: <i>P_{hy}-yisK</i> (<i>phleo</i>), <i>yycR</i> :: <i>P_{hy}-yisK</i> (<i>cat</i>)	This study
BYD335	<i>kanΩmbl</i> _{T_{317L}} , <i>amyE</i> :: <i>P_{hy}-yodL</i> (<i>spec</i>), <i>yhdG</i> :: <i>P_{hy}-yodL</i> (<i>phleo</i>), <i>yycR</i> :: <i>P_{hy}-yodL</i> (<i>cat</i>)	This study
BYD336	<i>kanΩmbl</i> _{T_{158M}} , <i>amyE</i> :: <i>P_{hy}-yodL</i> (<i>spec</i>), <i>yhdG</i> :: <i>P_{hy}-yodL</i> (<i>phleo</i>), <i>yycR</i> :: <i>P_{hy}-yodL</i> (<i>cat</i>)	This study
BYD337	<i>kanΩmbl</i> _{Δ_{S251}} , <i>amyE</i> :: <i>P_{hy}-yisK</i> (<i>spec</i>), <i>yhdG</i> :: <i>P_{hy}-yisK</i> (<i>phleo</i>), <i>yycR</i> :: <i>P_{hy}-yisK</i> (<i>cat</i>)	This study
BYD338	<i>kanΩmbl</i> _{P_{309L}} , <i>amyE</i> :: <i>P_{hy}-yisK</i> (<i>spec</i>), <i>yhdG</i> :: <i>P_{hy}-yisK</i> (<i>phleo</i>), <i>yycR</i> :: <i>P_{hy}-yisK</i> (<i>cat</i>)	This study
BYD339	<i>kanΩmbl</i> _{G_{156D}} , <i>amyE</i> :: <i>P_{hy}-yisK</i> (<i>spec</i>), <i>yhdG</i> :: <i>P_{hy}-yisK</i> (<i>phleo</i>), <i>yycR</i> :: <i>P_{hy}-yisK</i> (<i>cat</i>)	This study
BYD340	<i>kanΩmbl</i> _{T_{158A}} , <i>amyE</i> :: <i>P_{hy}-yisK</i> (<i>spec</i>), <i>yhdG</i> :: <i>P_{hy}-yisK</i> (<i>phleo</i>), <i>yycR</i> :: <i>P_{hy}-yisK</i> (<i>cat</i>)	This study
BYD341	<i>kanΩmbl</i> _{D_{153N}} , <i>amyE</i> :: <i>P_{hy}-yisK</i> (<i>spec</i>), <i>yhdG</i> :: <i>P_{hy}-yisK</i> (<i>phleo</i>), <i>yycR</i> :: <i>P_{hy}-yisK</i> (<i>cat</i>)	This study
BYD342	<i>kanΩmbl</i> _{R_{63C}} , <i>amyE</i> :: <i>P_{hy}-yisK</i> (<i>spec</i>), <i>yhdG</i> :: <i>P_{hy}-yisK</i> (<i>phleo</i>), <i>yycR</i> :: <i>P_{hy}-yisK</i> (<i>cat</i>)	This study
BYD343	<i>kanΩmbl</i> _{M_{51L}} , <i>amyE</i> :: <i>P_{hy}-yisK</i> (<i>spec</i>), <i>yhdG</i> :: <i>P_{hy}-yisK</i> (<i>phleo</i>), <i>yycR</i> :: <i>P_{hy}-yisK</i> (<i>cat</i>)	This study
BYD344	<i>kanΩmbl</i> _{A_{314T}} , <i>amyE</i> :: <i>P_{hy}-yisK</i> (<i>spec</i>), <i>yhdG</i> :: <i>P_{hy}-yisK</i> (<i>phleo</i>), <i>yycR</i> :: <i>P_{hy}-yisK</i> (<i>cat</i>)	This study
BYD345	<i>kanΩmbl</i> _{E_{204G}} , <i>amyE</i> :: <i>P_{hy}-yisK</i> (<i>spec</i>), <i>yhdG</i> :: <i>P_{hy}-yisK</i> (<i>phleo</i>), <i>yycR</i> :: <i>P_{hy}-yisK</i> (<i>cat</i>)	This study
BYD346	<i>kanΩmbl</i> _{E_{250K}} , <i>amyE</i> :: <i>P_{hy}-yodL</i> (<i>spec</i>), <i>yhdG</i> :: <i>P_{hy}-yodL</i> (<i>phleo</i>), <i>yycR</i> :: <i>P_{hy}-yodL</i> (<i>cat</i>)	This study
BYD348	<i>kanΩmbl</i> _{T_{158A}} , <i>amyE</i> :: <i>P_{hy}-yodL</i> (<i>spec</i>), <i>yhdG</i> :: <i>P_{hy}-yodL</i> (<i>phleo</i>), <i>yycR</i> :: <i>P_{hy}-yodL</i> (<i>cat</i>)	This study
BYD349	<i>kanΩmbl</i> _{G_{156D}} , <i>amyE</i> :: <i>P_{hy}-yodL</i> (<i>spec</i>), <i>yhdG</i> :: <i>P_{hy}-yodL</i> (<i>phleo</i>), <i>yycR</i> :: <i>P_{hy}-yodL</i> (<i>cat</i>)	This study
BYD351	<i>kanΩmbl</i> _{D_{153N}} , <i>amyE</i> :: <i>P_{hy}-yodL</i> (<i>spec</i>), <i>yhdG</i> :: <i>P_{hy}-yodL</i> (<i>phleo</i>), <i>yycR</i> :: <i>P_{hy}-yodL</i> (<i>cat</i>)	This study
BYD352	<i>kanΩmbl</i> _{M_{51L}} , <i>amyE</i> :: <i>P_{hy}-yodL</i> (<i>spec</i>), <i>yhdG</i> :: <i>P_{hy}-yodL</i> (<i>phleo</i>), <i>yycR</i> :: <i>P_{hy}-yodL</i> (<i>cat</i>)	This study

Table 2.1. Continued.

Strain	Description	Reference
BYD353	<i>kanQmbl</i> _{A314T} , <i>amyE</i> :: <i>P</i> _{hy-yodL} (<i>spec</i>), <i>yhdG</i> :: <i>P</i> _{hy-yodL} (<i>phleo</i>), <i>yycR</i> :: <i>P</i> _{hy-yodL} (<i>cat</i>)	This study
BYD354	<i>kanQmbl</i> _{E204G} , <i>amyE</i> :: <i>P</i> _{hy-yodL} (<i>spec</i>), <i>yhdG</i> :: <i>P</i> _{hy-yodL} (<i>phleo</i>), <i>yycR</i> :: <i>P</i> _{hy-yodL} (<i>cat</i>)	This study
BYD361	<i>amyE</i> :: <i>P</i> _{hy-yisK} (<i>spec</i>), <i>yhdG</i> :: <i>P</i> _{hy-yodL} (<i>phleo</i>)	This study
BYD363	<i>kanQmreB</i> _{S154R,R230C} , <i>amyE</i> :: <i>P</i> _{hy-yisK} (<i>spec</i>), <i>yhdG</i> :: <i>P</i> _{hy-yisK} (<i>phleo</i>), <i>yycR</i> :: <i>P</i> _{hy-yisK} (<i>cat</i>)	This study
BYD365	<i>kanQmreB</i> _{R282S} , <i>amyE</i> :: <i>P</i> _{hy-yodL} (<i>spec</i>), <i>yhdG</i> :: <i>P</i> _{hy-yodL} (<i>phleo</i>), <i>yycR</i> :: <i>P</i> _{hy-yodL} (<i>cat</i>)	This study
BYD404	<i>kanQmreB</i> _{N145D} , <i>amyE</i> :: <i>P</i> _{hy-yisK} (<i>spec</i>), <i>yhdG</i> :: <i>P</i> _{hy-yisK} (<i>phleo</i>), <i>yycR</i> :: <i>P</i> _{hy-yisK} (<i>cat</i>)	This study
BYD405	<i>kanQmbl</i> _{R63C} , <i>amyE</i> :: <i>P</i> _{hy-yodL} (<i>spec</i>), <i>yhdG</i> :: <i>P</i> _{hy-yodL} (<i>phleo</i>), <i>yycR</i> :: <i>P</i> _{hy-yodL} (<i>cat</i>)	This study
BYD406	<i>kanQmbl</i> _{ΔS251} , <i>amyE</i> :: <i>P</i> _{hy-yodL} (<i>spec</i>), <i>yhdG</i> :: <i>P</i> _{hy-yodL} (<i>phleo</i>), <i>yycR</i> :: <i>P</i> _{hy-yodL} (<i>cat</i>)	This study
BYD407	<i>kanQmbl</i> _{P309L} , <i>amyE</i> :: <i>P</i> _{hy-yodL} (<i>spec</i>), <i>yhdG</i> :: <i>P</i> _{hy-yodL} (<i>phleo</i>), <i>yycR</i> :: <i>P</i> _{hy-yodL} (<i>cat</i>)	This study
BYD510	<i>ΔyodL</i> , <i>ΔyisK</i> , <i>amyE</i> :: <i>P</i> _{yisK-yisK} (<i>spec</i>)	This study

Table 2.2. Plasmids used in Chapter II.

Plasmid	Description	Reference
pAS015	<i>yhdG::P_{hy}-yisK (amp)</i>	This study
pAS040	<i>amyE::P_{yodL}-lacZ (amp)</i>	This study
pAS041	<i>amyE::P_{yodL}-gfp (amp)</i>	This study
pAS044	<i>amyE::P_{yisK}-lacZ (amp)</i>	This study
pAS045	<i>amyE::P_{yisK}-gfp (amp)</i>	This study
pAS047	<i>amyE::gfp (amp)</i>	This study
pAS067	<i>amyE::P_{yisK}-yisK (amp)</i>	This study
pDR111	<i>amyE::P_{hy} (amp)</i>	David Z. Rudner
pDR244	Temperature sensitive Cre recombinase plasmid (<i>amp</i>)(<i>spec</i>)	David Z. Rudner
pJH036	<i>sacA::P_{hy}-lacZ (amp)</i>	This study
pJW004	<i>yhdG::P_{hy} (amp)</i>	This study
pJW006	<i>amyE::P_{hy}-sirA-gfp (amp)</i>	(275)
pJW033	<i>ycgO::P_{hy} (amp)</i>	This study
pJW034	<i>yycR::P_{hy} (amp)(cat)</i>	This study
pKM062	<i>sacA::erm (amp)</i>	David Z. Rudner
pWX114	<i>yrvN::P_{hy} (amp)(kan)</i>	David Z. Rudner
pYD073	<i>yhdG::P_{hy}-yodL (amp)</i>	This study
pYD155	<i>yycR::P_{hy}-yodL (amp)</i>	This study
pYD156	<i>ycgO::P_{hy}-yisK (amp)</i>	This study

Table 2.3. Oligonucleotides used in Chapter II.

Oligo	Sequence 5' to 3'
OAM001	AGAAGCGTTAGCGGCAGCAAGTGAT
OAM002	CCATGTCTGCCCCGTATTTTCGCGTAAGGAAATCCATTATGTACT ATTTTCGATCAGACCAG
OAM009	GAAAACAATAAACCTTGCATAGGGGGATCGGGCAAGGCTAG ACGGGACTTACC
OAM010	ATGGACACAACAACAGCAAAAACAGGC
OAM011	TAATGGATTTCCCTTACGCGAAATA
OAM013	AGTAGTTCCTCCTTATGTAAGC
OAS064	TCCTCCTTTTCAAAGAAAAAAC
OAS067	TGTTACATATTGCTGCTTTTTGGT
OAS078	GGATCCCAGCGAACCATTTGA
OAS079	GTCGACAAATTCCTCGTAGGC
OAS080	CCTATCACCTCAAATGGTTCGCTGGGATCCAAAGCAAAAATA CCCTAAAGGGAA
OAS081	GTCCCGAGCGCCTACGAGGAATTTGTCGACACACTTTTTTTTT CGTCGAATTAAG
OAS086	CGAATACATACGATCCTACAGC
OAS087	CCTATCACCTCAAATGGTTCGCTGGGATCCAAAAGTTGGAA GCACAATAAGTT
OAS088	GTCCCGAGCGCCTACGAGGAATTTGTCGACATCACCTGGCATT GCCTTCTT
OAS089	ATTAATGGTGATATTCTTCATTGA
OAS091	AGATGGATGTGCTCCAGTGCTCCAAGATCTATACCAAGGTCT
OAS092	AGACCTTGGTATAGATCTTGGAGCACTGGAGCACATCCATCT
OAS095	GGAAGCTTGTCCATATTATCAAGATTTGCAGTACCGAGGTCAA TA
OAS096	TATTGACCTCGGTACTGCAAATCTTGATAATATGGACAAGCTT CC
OAS114	TCTAAGGAATTCCTGTTTTAGTCGGCATAAGCAG
OAS116	GTAATCTTACGTCAGTAACTTCCACCAAGATCCCCTCCCTTTT ATTT
OAS117	AAGAAATAAAAGGGAGGGGATCTTGGTGGAAGTTACTGACGT AAGAT
OAS118	ACTTAGGGATCCTTATTTTTGACACCAGACCAACT
OAS119	TGAAAAGTTCTTCTCCTTTACTCATCAAGATCCCCTCCCTTTTA TTT
OAS120	AAGAAATAAAAGGGAGGGGATCTTGATGAGTAAAGGAGAAG AACTTTTC
OAS121	ACTTAGGGATCCTTATTTGTATAGTTCATCCATGCCAT
OAS134	TCTAAGGAATTCCTTTTCAGCTGCTCCCGAT

Table 2.3. Continued.

Oligo	Sequence 5' to 3'
OAS135	GTAATCTTACGTCAGTAACTTCCACGTTATTCCTCCATCATCTT TTAAA
OAS136	ATTTAAAAGATGATGGAGGAATAACGTGGAAGTTACTGACGT AAGAT
OAS137	TGAAAAGTTCTTCTCCTTTACTCATGTTATTCCTCCATCATCTT TTAAA
OAS138	ATTTAAAAGATGATGGAGGAATAACATGAGTAAAGGAGAAG AACTTTTC
OAS148	TCTAAGGAATTCATGAGTAAAGGAGAAGAACTTTTC
OAS149	ACTTAGGGATCCTTATTTGTATAGTTCATCCATGCC
OAS274	TCTAAGGAATTCCTTTTCAGCTGCTCCCGA
OAS275	ACTTAGGGATCCTCAGCCAATTTGGTTTGACAG
OEA035	GGATAACAATTAAGCTTACATAAGGAGGAACTACTATGAAAT TTGCGACAGGGGAACTT
OEA036	TTCCACCGAATTAGCTTGCATGCGGCTAGCCCAGTTTTATTCA GCCAATTTGGT
OEA275	GGATAACAATTAAGCTTACATAAGGAGGAACTACTATGATGT TATCCGTGTTAAAAAAG
OEA276	TTCCACCGAATTAGCTTGCATGCGGCTAGCTTTCTTTTCATTAT GTCGTTTGTA
OJH159	CTGCAGGAATTCGACTCTCTA
OJH160	TAGCTTGCATGCGGCTAGC
OJH185	CAGGAATTCGACTCTCTAGC
OJH186	CTCAGCTAGCTAACTCACATTAATTGCGTTGC

Microscopy

For microscopy experiments, all strains were grown in the indicated medium in volumes of 25 ml in 250 ml baffled flasks, and placed in a shaking waterbath set at 37°C and 280 rpm. Unless stated otherwise, misexpression was performed by inducing samples with 1.0 mM isopropyl-beta-D-thiogalactopyranoside (IPTG) and imaging samples 90 min post-induction. Fluorescence microscopy was performed with a Nikon Ti-E microscope equipped with a CFI Plan Apo lambda DM 100X objective, Prior Scientific Lumen 200 Illumination system, C-FL UV-2E/C DAPI and C-FL GFP HC HISN Zero Shift filter cubes, and a CoolSNAP HQ2 monochrome camera. Membranes were stained with TMA-DPH [1-(4-trimethylammoniumphenyl)-6-phenyl-1,3,5-hexatriene *p*-toluenesulfonate] (0.02 mM) and imaged with exposure times of 1 sec with a neutral density filter in place to reduce cytoplasmic background. All GFP images were captured with a 1 sec exposure time. All images were captured with NIS Elements Advanced Research (version 4.10), and processed with NIS Elements Advanced Research (version 4.10) and ImageJ64 (276). Cells were mounted on glass slides with 1% agarose pads or polylysine-treated coverslips prior to imaging. To quantitate cell lengths for Fig 2.11, the cell lengths for 500 cells were determined for each population. The statistical significance of cell length differences between populations was determined using an unpaired student's t-test.

Plate growth assay

B. subtilis strains were streaked on LB-Lennox plates containing 100 µg/ml spectinomycin and 1 mM IPTG. The plates were supplemented with the indicated concentrations of MgCl₂ when indicated. Plates were incubated at 37°C overnight and images were captured on a ScanJet G4050 flatbed scanner (Hewlett Packard).

Heat kill

Spore formation was quantified by growing cells in Difco sporulation medium (DSM)(277). A freshly grown single colony of each strain was inoculated into 2 mL of DSM media and placed in a roller drum at 37°C, 60 rpm for 36 hrs. To determine colony forming units/ml, an aliquot of each culture was serially diluted and plated on DSM agar plates. To enumerate heat resistant spores/ml, the serial diluted cultures were subjected to a 20 min heat treatment at 80°C and plated on DSM agar plates. The plates were incubated at 37°C overnight and the next day colony counts were determined. The relative sporulation frequency compared to wildtype was determined by calculating the spores/CFU of each experimental and dividing it by the spores/CFU of wildtype. The reported statistical significance was determined using an unpaired student's t-test.

Transcription fusions

Transcriptional fusions were constructed by fusing a ~200 bp region up to the start codon of either *yodL* or *yisK* to *gfp* or *lacZ* and integrating the fusions into the *B. subtilis* chromosome at the *amyE* locus (for more details, see strain construction in the supplemental text). Microscopy was conducted on each strain over a timecourse in sporulation by resuspension media (see general methods) or in a nutrient exhaustion timecourse in CH (272). Beta-galactosidase assays were performed as described (278), except all samples were frozen at -80°C before processing. All experiments were performed on at least three independent biological replicates.

Suppressor selections

Single colonies of BYD048 (3X P_{hy}-*yodL*, P_{hy}-*lacZ*) or BYD076 (3X P_{hy}-*yisK*, P_{hy}-*lacZ*) were used to inoculate independent 5 ml LB-Lennox cultures. Six independent

cultures were grown for each strain. The cultures were grown for 6 hrs at 37°C and 0.3 µl of each culture was diluted in 100 µl LB and plated on an LB-Lennox agar plate containing 100 µg/ml spectinomycin and 1 mM IPTG. After overnight growth, suppressors that arose were patched on both LB-Lennox agar plates supplemented with 100 µg/ml spectinomycin and LB-Lennox agar plates supplemented with 100 µg/ml spectinomycin, 1.0 mM IPTG, and 40 µg/ml X-Gal and grown at 37°C overnight. Only blue colonies were selected for further analysis; this screen eliminated mutants unable to derepress P_{hy} in the presence of IPTG. In addition, each P_{hy} -*yodL* or P_{hy} -*yisK* construct was transformed into a wildtype background to ensure that the construct remained fully functional with respect to preventing cell growth on LB-Lennox agar plates supplemented with the relevant antibiotic and 1 mM IPTG.

Whole-genome sequencing and analysis

Genomic DNA was isolated from six YodL-resistant suppressors obtained from independent cultures as well as the parent strain (BYD048) by inoculating a single colony in 6 ml LB-Lennox media and growing at 37°C for 4 hr in a roller drum. Cells were collected by spinning at 21,130 x g for 2 min at room temperature, resuspending the pellets in lysis buffer [20 mM Tris-HCl pH 7.5, 50 mM EDTA pH 8, 100 mM NaCl, and 2 mg/ml lysozyme] and incubating at 37°C for 30 min. Sarkosyl was added to a final concentration of 1% (w/v). Protein was removed by extracting with 600 µl phenol, centrifuging at 21,130 x g for 5 min at room temperature, and transferring the top (aqueous layer) to a new microcentrifuge tube. This was followed by an extraction with 600 µl phenol-saturated chloroform and centrifugation at 21,130 x g for 5 min at room temperature. After transferring the aqueous layer to a new microcentrifuge tube, a final extraction was performed with 100% chloroform, followed by centrifugation at 21,130 x

g for 5 min at room temperature. The aqueous layer was transferred to a new microcentrifuge tube, being careful to avoid the interphase material. To precipitate the genomic DNA, a 1/10th volume of 3.0 M Na-acetate and 1 ml of 100% ethanol was added, and the tube was inverted multiple times. The sample was centrifuged at 21,130 x g for 1 min at room temperature in a microcentrifuge. The pellet was washed with 150 μ l 70% ethanol and resuspended in 500 μ l TE [10 mM Tris pH 7.5, 1 mM EDTA, pH 8.0]. To eliminate potential RNA contamination, RNase was added to a final concentration of 200 μ g/ml and the sample was incubated at 55°C for 1 hr. To remove the RNase, the genomic DNA was re-purified by phenol-chloroform extraction and ethanol precipitation as described above. The final pellet was resuspended in 100 μ l TE. Bar-coded libraries were prepared from each genomic DNA sample using a TruSeq DNA kit according to manufacture specifications (Illumina), and the samples were subjected to Illumina-based whole-genome sequencing using a MiSeq 250 paired-end run (Illumina). CLC Genomics Workbench (Qiagen) was used to map the sequence reads against the *Bs168* reference genome and to identify single nucleotide polymorphisms, insertions, and deletions. Mutations associated with the P_{hy} integration constructs and those in which less than 40% of the reads differed from the reference genome were excluded as candidate changes responsible for suppression in our initial analysis (Table 2.6). The remaining suppressors mutations were identified by PCR amplifying *mreB* (using primer set OAS044 and OAS045) and *mbl* (using primer set OAS046 and OAS047), and sequencing with the same primers. To determine if the candidate suppressors alleles identified were sufficient to confer resistance to the original selective pressure, each was linked to a kanamycin resistance cassette and moved by transformation into a clean genetic background.

Results

YodL and YisK affect cell width

To identify novel factors involved in cellular morphogenesis, we created an ordered gene misexpression library comprising over 800 previously uncharacterized genes from *B. subtilis*. Each gene was placed under the control of an IPTG-inducible promoter (P_{hy}) and integrated in single copy (1X) at *amyE*, a non-essential locus in the *B. subtilis* chromosome. The library (called the BEIGEL for Bacillus Ectopic Inducible Gene Expression Library), was screened for misexpression phenotypes that perturbed growth on solid media, and also resulted in obvious defects in nucleoid morphology, changes in cell division frequency, and/or perturbations in overall cell shape in liquid cultures. Two strains, one harboring P_{hy} -*yodL* and one harboring P_{hy} -*yisK*, were unable to form colonies on plates containing inducer (Fig 2.1A) and also produced wide, irregular cells with slightly tapered poles following misexpression in LB liquid media (Fig 2.1B). Cell lysis and aberrant cell divisions were also observed. Introducing a second copy (2X) of each P_{hy} misexpression construct into the chromosome did not appreciably enhance cell widening at the 90 min post-induction timepoint, although cell lysis was more readily observed (Fig 2.1B). P_{hy} -*yisK* (2X) misexpression also led to a drop in optical density over time (Fig 2.2A), consistent with the cell lysis observed microscopically. We conclude that the activities of *yodL* and *yisK* target one or more processes integral to width control during cell elongation.

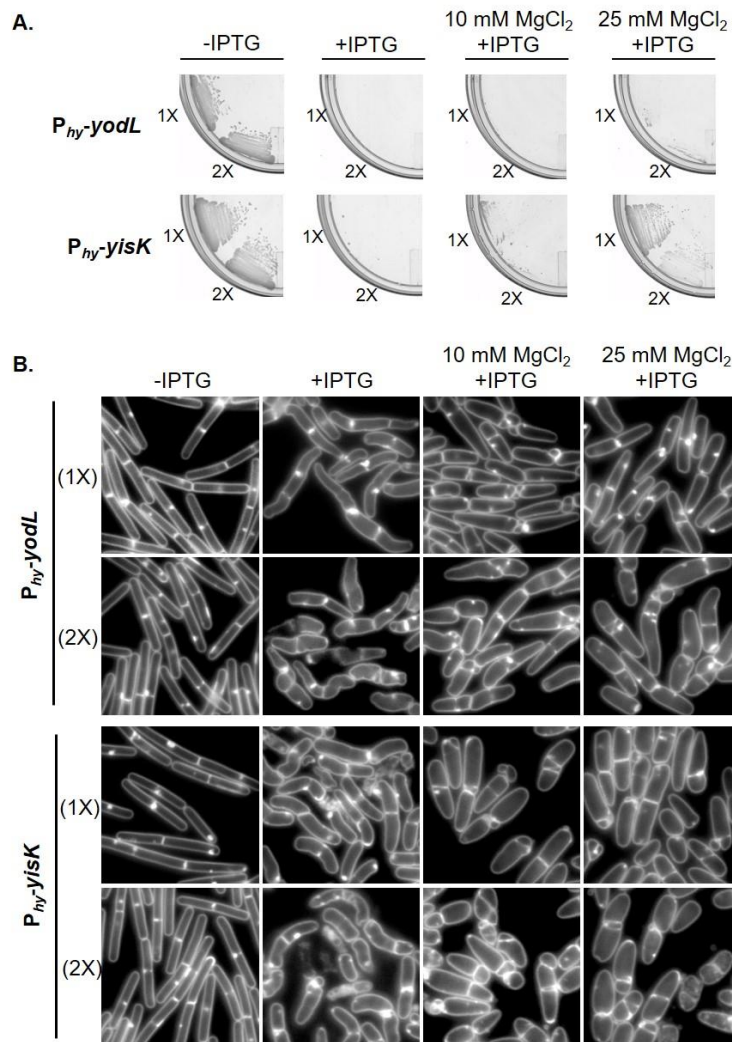


Fig. 2.1. Misexpression of YodL and YisK prevents cell growth on solid media and causes loss of cell shape in liquid media. (A) Cells harboring one (1X) or two (2X) copies of $P_{hy}\text{-yodL}$ (BAS040 and BAS191) or $P_{hy}\text{-yisK}$ (BAS041 and BYD074) were streaked on an LB plate supplemented with 100 $\mu\text{g/ml}$ spectinomycin and, when indicated, 1 mM IPTG or 1 mM IPTG and the denoted concentration of MgCl_2 . Plates were incubated for ~16 hrs at 37°C before image capture (top). (B) The strains described above were grown in LB-Lennox media at 37°C to mid-exponential and back-diluted to an OD_{600} of ~0.02. When indicated, 1 mM IPTG or 1 mM IPTG and the denoted concentration of MgCl_2 was added. Cells were grown for 1.5 hrs at 37°C before image capture. Membranes were stained with TMA-DPH. All images were scaled identically.

Growth curves in LB

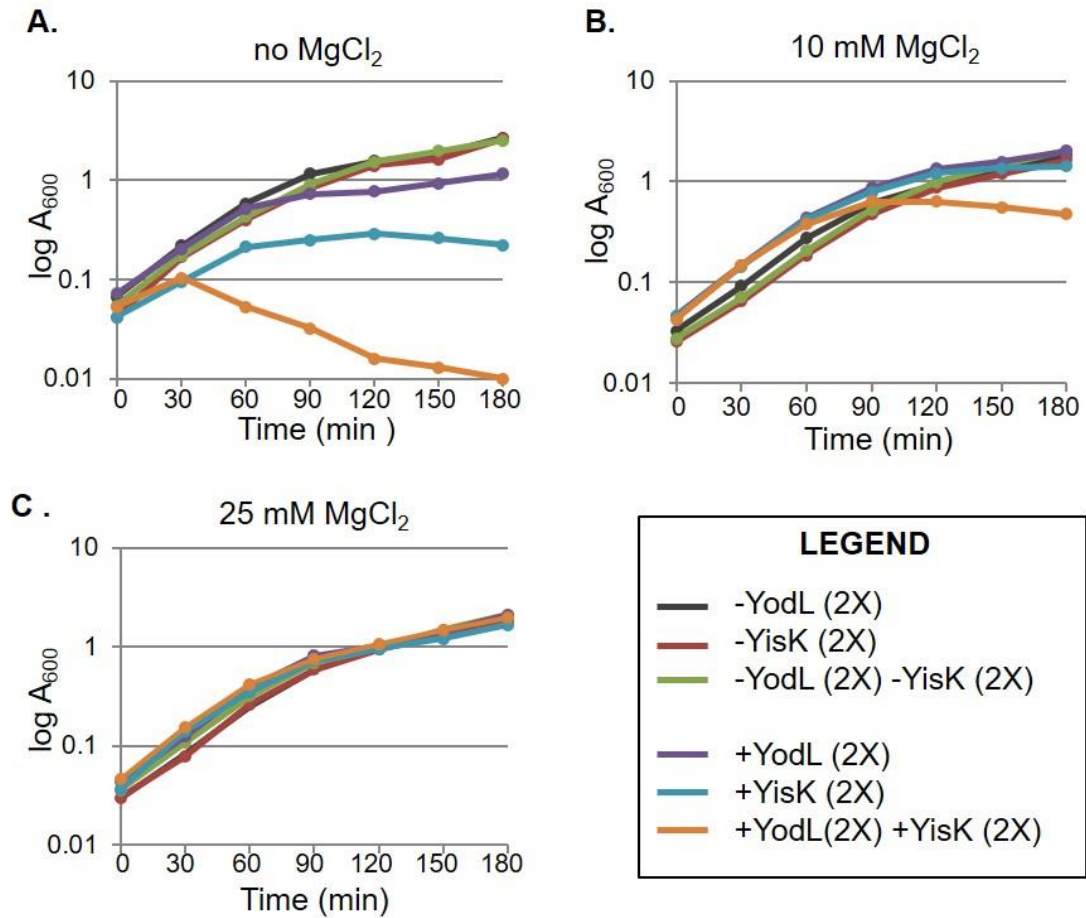


Fig. 2.2. Growth curves in LB following misexpression of YodL and/or YisK. $2X P_{hy}\text{-yodL}$ (BAS191), $2X P_{hy}\text{-yisK}$ (BYD074) and $2X P_{hy}\text{-yodL}$, $2X P_{hy}\text{-yisK}$ (BYD281) were grown in LB media at 37°C to mid-exponential diluted to an OD_{600} of <0.02 . At time 0, 1 mM IPTG or 1 mM IPTG and the indicated concentration of $MgCl_2$ was added.

The *yodL* and *yisK* misexpression phenotypes are similar to those observed when proteins involved in cell elongation are perturbed in *B. subtilis* (60, 61, 279). Since the addition of magnesium was previously reported to suppress the lethality and/or morphological phenotypes associated with depletion or deletion of some proteins important for cell elongation in *B. subtilis* (60-62, 257, 280), we assessed if the P_{hy} -*yodL* and P_{hy} -*yisK* misexpression phenotypes could be rescued by growing cells with media supplemented with two different concentrations of MgCl₂. The YodL-producing cells failed to grow on any LB media containing inducer, regardless of MgCl₂ concentration (Fig 2.1A). In contrast, LB supplemented with 25 mM MgCl₂ restored viability to the strain producing YisK (Fig 2.1A). Interestingly, even 25 mM MgCl₂ was not sufficient to suppress the cell-widening effect associated with YodL and YisK misexpression (Fig 2.1B), although these cells did not lyse (Fig 2.2C). Since PAB medium was often used in the prior studies showing MgCl₂ supplementation rescued cell shape (60-62, 257, 280), we also assayed for growth on PAB following YodL and YisK expression. PAB supplemented with 25 mM MgCl₂ rescued growth on plates (Fig 2.3A), but still did not rescue morphology in liquid culture (Fig 2.3B).

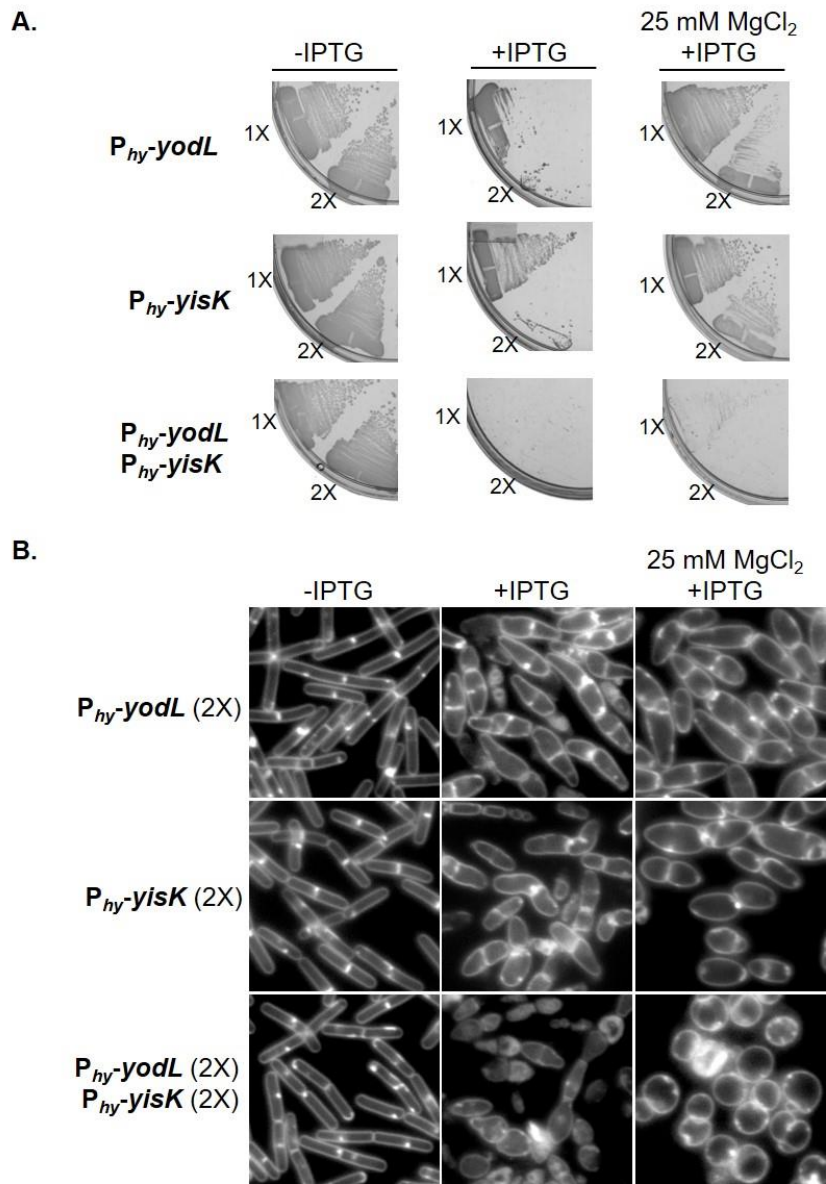


Fig. 2.3. Misexpression of YodL and YisK on PAB media. (A) Cells were streaked on PAB solid media supplemented with 100 μ g/ml spectinomycin and, when indicated, 1 mM IPTG and the denoted concentration of MgCl₂. Plates were incubated for ~16 hr at 37°C before image capture. (B) Cells were grown in PAB liquid media at 37°C to mid-exponential and back-diluted to an OD₆₀₀ of <0.02. When indicated, 1 mM IPTG and the denoted concentration of MgCl₂ was added. Cells were then grown for 1.5 hrs at 37°C before image capture. Membranes are stained with TMA-DPH (white). All images are shown at the same magnification.

yodL and *yisK* expression

To better understand the possible physiological functions of the *yodL* and *yisK* gene products, we analyzed the genes and their genetic contexts bioinformatically. *yodL* is predicted to encode a 12.5 kDa hypothetical protein which, based on amino acid similarity, is conserved in the *Bacillus* genus. In data from a global microarray study analyzing conditional gene expression in *B. subtilis*, *yodL* is expressed as a monocistronic mRNA, exhibiting peak expression ~2 hrs after entry into sporulation (281). *yodL* expression is most strongly correlated with expression of *racA* and *refZ* (*yttP*)(281), genes directly regulated by Spo0A (282). *yodL* was not previously identified as a member of the Spo0A regulon controlling early sporulation gene expression (282, 283), however a more recent study found that *yodL* expression during sporulation is reduced in a $\Delta spo0A$ mutant (284). Consistent with this observation, we identified a putative Spo0A box approximately ~75 bp upstream of the annotated *yodL* start codon (Fig 2.4A). *yisK* is predicted to encode a 33 kDa protein and is annotated as a putative catabolic enzyme based on its similarity to proteins involved in the degradation of aromatic amino acids (285). *yisK* was previously identified as a member of the SigH regulon, and possesses a SigH -35/-10 motif (Fig 2.4B)(283). Expression of *yisK* peaks ~2 hrs after entry into sporulation (270) and is most strongly correlated with expression of *kinA* (281), a gene regulated by both SigH (the stationary phase sigma factor)(283, 286-288) and Spo0A (282, 288). As with *yodL*, we identified a putative Spo0A box in the regulatory region upstream of the *yisK* start codon (Fig 2.4B).

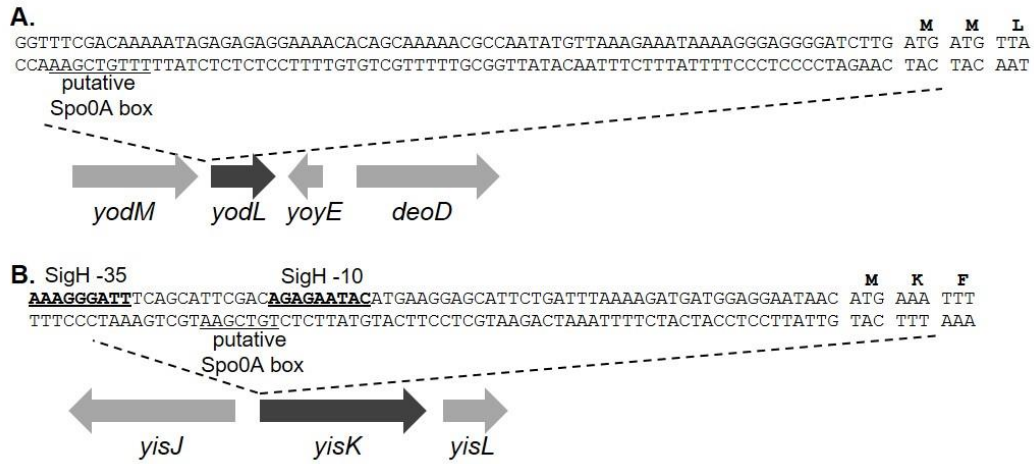


Fig. 2.4. DNA sequence upstream of *yodL* and *yisK*. (A) Putative Spo0A box (underlined) upstream of the *yodL* start codon. (B) SigH binding motifs (double underline) and putative Spo0A box (underlined) upstream of *yisK* start codon.

To independently test if *yodL* and *yisK* expression are consistent with Spo0A-dependent regulation, we fused the putative regulatory regions upstream of each gene to a *gfp* reporter gene, and integrated the fusions into the *amyE* locus. We then followed expression from the promoter fusions over a timecourse in CH liquid broth, a rich medium in which the cells first grow exponentially, transition to stationary phase, and finally gradually enter sporulation (Fig 2.5A-C). In this timecourse, GFP signal from *P_{yisK}-gfp* increased dramatically from time 0 (OD₆₀₀ ~0.6) to time 1 hr (OD₆₀₀ ~1.6) (Fig 2.5C), consistent with *yisK*'s prior characterization as a SigH-regulated gene (283). In contrast, GFP fluorescence from *P_{yodL}-gfp* became evident at a later timepoint (120 min) and was more heterogeneous (Fig 2.5C), consistent with expression patterns previously observed for other Spo0A-P regulated genes (289, 290).

To quantitate expression from the promoters, we generated *P_{yodL}-lacZ* and *P_{yisK}-lacZ* reporter strains and collected samples over a CH timecourse beginning with early exponential (OD₆₀₀ = 0.2). Expression from *P_{yodL}-lacZ* rose steadily beginning about 2 hrs after exit from exponential growth, and continued to rise at least until the final timepoint taken (Fig 2.5D). In contrast, expression from *P_{yisK}-lacZ* rose as cells transitioned from early to late exponential growth, reached peak levels shortly after exit from exponential growth, and remained steady for the remainder of the timepoints (Fig 2.5E). Wild-type expression from both *P_{yodL}-lacZ* and *P_{yisK}-lacZ* required both SigH and Spo0A, and was largely eliminated in the absence of both regulators (Fig 2.5D and 2.5E). We did not attempt to draw further conclusions from this data, since Spo0A and SigH each require the other for wildtype levels of expression (see discussion).

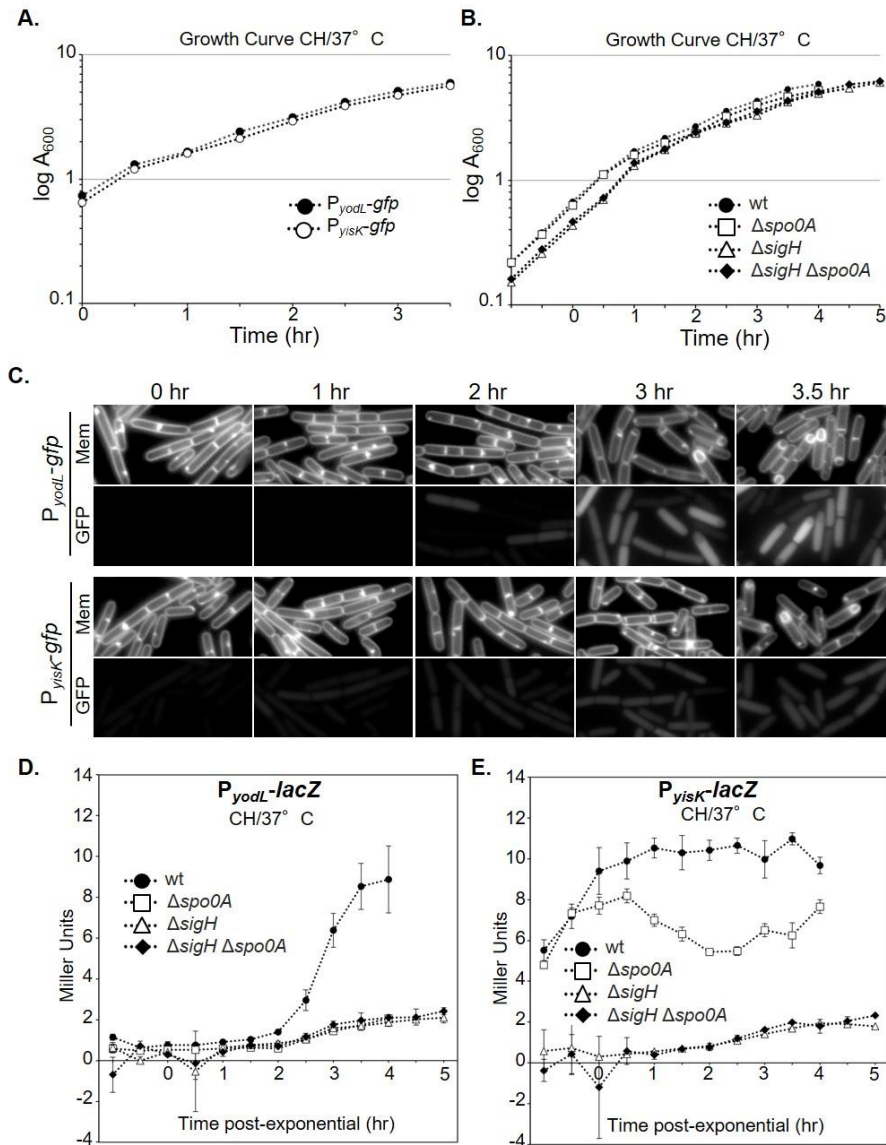


Fig. 2.5. Expression from *yodL* and *yisK* promoters during a CH timecourse. Expression from the putative *yodL* and *yisK* promoter regions was monitored in CH medium at 37°C over a timecourse. The OD₆₀₀ (A and B) and production of either GFP (C) or beta-galactosidase (D and E) was monitored at 30 min intervals. Membranes were stained with TMA-DPH. All GFP channel images were captured with 1 sec exposures and scaled identically to allow for direct comparison. In this media, time 0 represents the last exponential timepoint, not the initiation of sporulation.

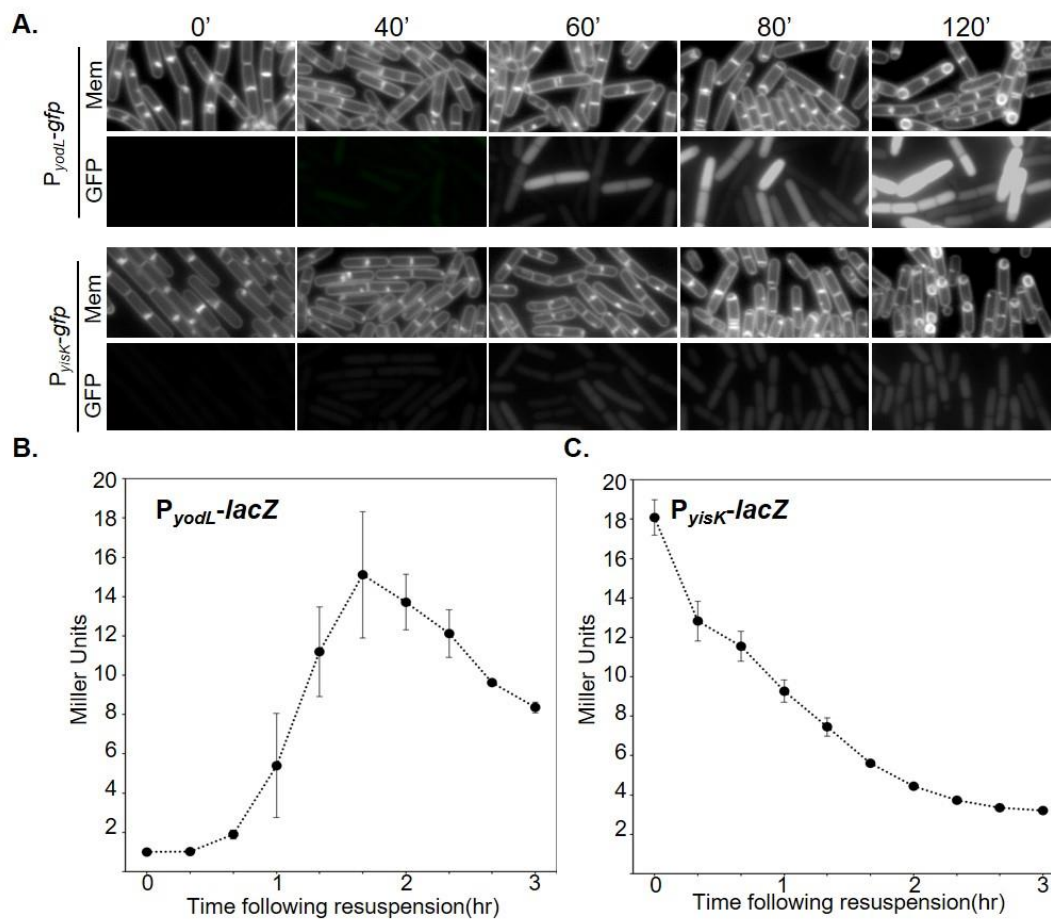


Fig. 2.6. Expression from *yodL* and *yisK* promoters following sporulation by resuspension. Expression from the putative *yodL* and *yisK* promoter regions was monitored in resuspension medium. The production of either GFP (A) or beta-galactosidase (B and C) was monitored at 20 min intervals. Membranes were stained with TMA-DPH. All GFP channel images were captured with 1 sec exposures and scaled identically to allow for direct comparison.

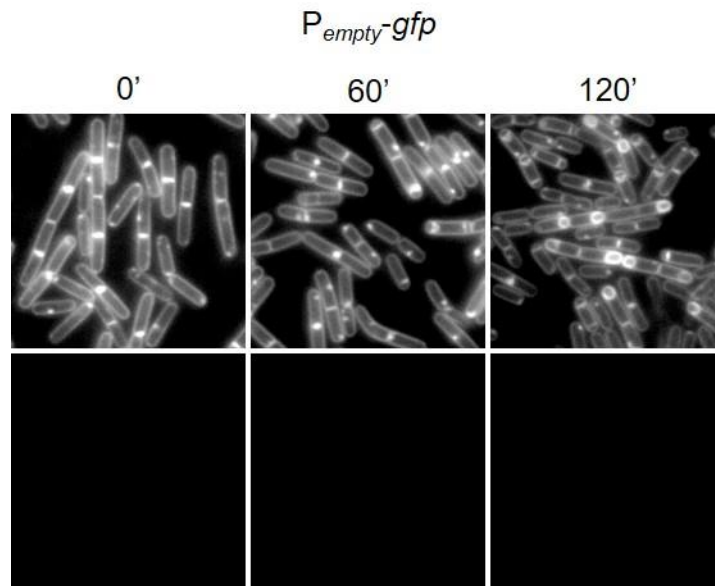


Fig. 2.7. A strain harboring a GFP reporter without a promoter during a sporulation timecourse. BAS205 ($P_{empty-gfp}$) was induced to sporulate via resuspension, and membranes are stained with TMA (white). Signal from GFP was scaled identically for all images and pseudocolored green. All images are shown at the same magnification.

We then followed expression from the promoter fusions over a time-course following the sporulation by resuspension method, which generates a more synchronous entry into sporulation (291). At time 0, neither the strain harboring P_{yodL} -*gfp*, nor the strain harboring P_{yisK} -*gfp* showed appreciable levels of fluorescence (Fig 2.6A), appearing similar to a negative control harboring *gfp* without a promoter (Fig 2.7). Between 0 and 40 min, both strains showed detectable increases in fluorescence. At 60 min, when the first polar division characteristic of sporulation begins to manifest, both strains were more strongly fluorescent (Fig 2.6A). GFP fluorescence from P_{yodL} was qualitatively more intense than fluorescence produced from P_{yisK} (all images were captured and scaled with identical parameters to allow for direct comparison). Moreover, the GFP signal continued to accumulate in the strain harboring P_{yodL} -*gfp* for at least two hrs (Fig 2.6A) and was heterogenous, consistent with activation by Spo0A. In contrast, the fluorescence signal produced from P_{yisK} -*gfp* was similar across the population and appeared similar at the 60 and 120 min timepoints (Fig 2.6A), consistent with SigH regulation.

To quantitate expression from the promoters during a sporulation by resuspension timecourse, we collected timepoints from strains harboring either the P_{yodL} -*lacZ* or P_{yisK} -*lacZ* reporter constructs and performed beta-galactosidase assays. Expression from P_{yodL} -*lacZ* rose rapidly between the 40 min and 100 min timepoints, and steadily declined thereafter (Fig 2.6B). The decline in signal was not observed for the GFP reporter, likely because the GFP is stable once synthesized (292). In contrast, expression from P_{yisK} -*lacZ* was highest at the time of resuspension (T0) and declined up until the final timepoint (Fig 2.6C).

Collectively, the patterns expression we observe for *yodL* are consistent with those observed for genes activated by high-threshold levels of Spo0A during sporulation,

including *racA*, *spoIIG*, and *spoIIA* (293). In contrast, *yisK*'s expression pattern is similar to that observed for *kinA* (281, 287, 294), with expression increasing in late exponential and stationary phase and early sporulation in a SigH-dependent manner (Fig 2.5), but decreasing during a sporulation by resuspension timecourse (Fig 2.6). We do not exclude the possibility that YodL and YisK might also function in other growth contexts.

A $\Delta yodL \Delta yisK$ mutant is defective in sporulation

Since *yodL* and *yisK* expression correlates with other early sporulation genes, we next investigated if the gene products influenced the production of heat-resistant spores. To determine the number of heat-resistant spores in a sporulation culture, we quantified the number of colony forming units (CFU) present in cultures before (total CFU) and after (heat-resistant CFU) a heat treatment that kills vegetative cells. These values were normalized to display the sporulation efficiency of the mutants relative to wildtype. Single mutants in which either *yodL* or *yisK* were deleted displayed only mild (97% and 94%, respectively) reductions in relative sporulation efficiency (Table 2.4). Although the single mutants always sporulated less efficiently than wildtype in each experimental replicate, the differences were not statistically significant with only six experimental replicates. In contrast, the $\Delta yodL \Delta yisK$ double mutant produced ~20% less heat-resistant spores than wildtype ($P < 0.0006$) (Table 2.4). No decrease in total CFU was observed for any of the mutants compared to wildtype, indicating that the reduction in heat-resistant spores in the $\Delta yodL \Delta yisK$ mutant was not due to reduced cell viability before heat treatment (Table 2.4). The gene downstream of *yisK*, *yisL*, is transcribed in the same direction as *yisK*. To determine if the reduction in sporulation we observed might be partially attributable to polar effects of the *yisK* deletion on *yisL* expression, we

introduced $P_{yisK-yisK}$ at an ectopic locus (*amyE*) in the $\Delta yodL \Delta yisK$ mutant and repeated the heat-kill assay. The ectopic copy of $P_{yisK-yisK}$ restored sporulation in the $\Delta yodL \Delta yisK$ to levels statistically indistinguishable from the $\Delta yodL$ single mutant (Table 2.4). These results lend support to the idea that YodL and YisK function during early sporulation and possess activities that, directly or indirectly, affect the production of viable spores. We do not exclude the possibility that YodL and YisK might also function outside the context of sporulation.

Given that *yisK* and *yodL* expression during vegetative growth leads to cell widening, we hypothesized that *yisK* and *yodL* mutants might produce thinner cells or spores during sporulation. However, no qualitative differences in cell or spore width were observed for the $\Delta yodL$, $\Delta yisK$, or $\Delta yodL \Delta yisK$ mutant populations compared to wildtype during a sporulation timecourse (Fig 2.8). We also observed no qualitative differences in the shapes of germinating cells (data not shown). Thus, although YodL and YisK contribute to the production of heat-resistant spores, they do not appear to be required to generate any of the major morphological changes required for spore production.

Table 2.4. Sporulation efficiency of *yodL* and *yisK* mutants. Sporulation efficiency is the number of spores/ml divided by the total cfu/ml $\times 100\%$. Relative sporulation efficiency is sporulation efficiency normalized to wildtype $\times 100\%$. The data shown is the average of three independent biological replicates. The difference in sporulation efficiency between wildtype and the $\Delta yodL \Delta yisK$ double mutant is statistically significant ($P < 0.0006$).

Strain	Strain #	Total cfu	Heat-resistant cfu	Sporulation efficiency	Relative sporulation efficiency
wildtype	<i>B. subtilis</i> 168	2.8×10^8 ($\pm 4.7 \times 10^7$)	1.9×10^8 ($\pm 4.5 \times 10^7$)	66.9% (± 5)	100%
$\Delta yodL$	BYD276	2.6×10^8 ($\pm 3.9 \times 10^7$)	1.7×10^8 ($\pm 2.8 \times 10^7$)	65.2% (± 7)	97%
$\Delta yisK$	BYD278	2.7×10^8 ($\pm 4.6 \times 10^7$)	2.4×10^8 ($\pm 2.7 \times 10^7$)	63.1% (± 6)	94%
$\Delta yodL \Delta yisK$	BYD279	3.1×10^8 ($\pm 6.5 \times 10^7$)	1.7×10^8 ($\pm 4.1 \times 10^7$)	54.1% (± 4)	81%
$\Delta yodL \Delta yisK$ <i>P_{yisK}-yisK</i>	BYD510	3.4×10^8 ($\pm 3.3 \times 10^7$)	2.3×10^8 ($\pm 4.1 \times 10^7$)	66.2% (± 7)	99%

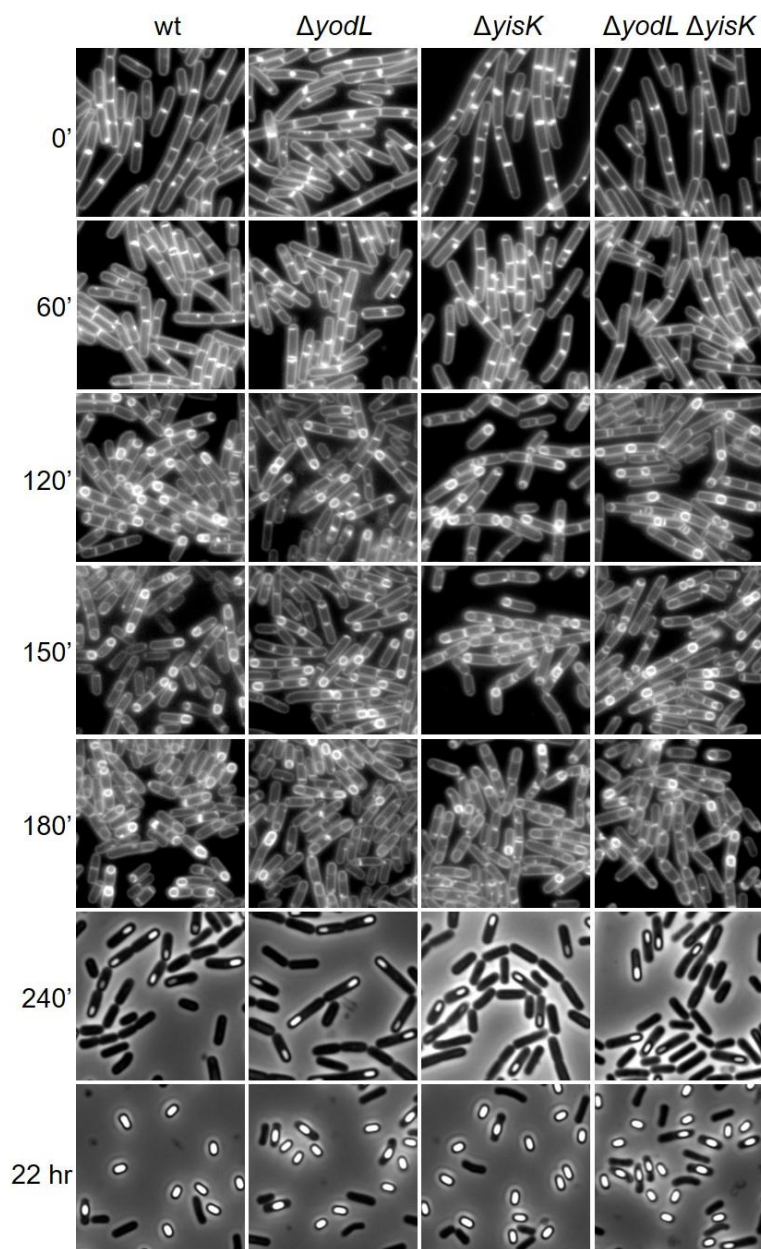


Fig. 2.8. Strains lacking *yodL* and/or *yisK* appear morphologically similar to wildtype during a sporulation timecourse. *B. subtilis* 168 (wt), BYD276 ($\Delta yodL$), BYD278 ($\Delta yisK$) and BYD279 ($\Delta yodL \Delta yisK$) were grown induced to sporulate via resuspension, and cells were grown for the indicated amount of time at 37°C before image capture. Membranes are stained with TMA-DPH (white). All images are shown at the same magnification.

MreB and Mbl are genetic targets of YodL and YisK activity

To identify genetic targets associated with YodL and YisK activity, we took advantage of the fact that misexpression of the proteins during vegetative growth prevents colony formation on plates and performed suppressor selection analysis. Strains harboring three copies of each misexpression cassette were utilized to reduce the chances of obtaining trivial suppressors in the misexpression cassette itself. In addition, $P_{hy-lacZ}$ was used as a reporter to eliminate suppressors unable to release LacI repression following addition of inducer. In total, we obtained 14 suppressors resistant to YodL expression and 13 suppressors resistant to YisK expression. Six of the suppressors resistant to YodL were subjected to whole-genome sequencing. The results of the sequencing are shown in Table A1.5. All of the suppressors possessed mutations in either *mreB* or *mbl*, genes previously shown to be important in regulating cell width (Table 2.5). Using targeted sequencing, we determined that the remaining suppressor strains resistant to YodL also harbored mutations in *mreB* or *mbl*. Since the phenotypes of YodL and YisK expression were similar, we also performed targeted sequencing of the *mreB* and *mbl* chromosomal regions in the YisK-resistant suppressors. All but one of the YisK-resistant suppressors possessed mutations in *mbl*; the remaining suppressor harbored a mutation in *mreB*.

Table 2.5. Whole-genome sequencing analysis of genomic DNA from six YodL-resistant suppressors. BYD048 (three copies of *P_{hy}-yodL*) was used for suppressor selection. Candidates were analyzed by whole-genome sequencing as described in the materials and methods.

Suppressors of YodL	GENE	COORDINATE	REFERENCE	SAMPLE	DISTRIBUTION	VARIANT
SYL#1	<i>lmrB</i>	289144	C	A	50% C, 50% A	G317C
	<i>yigA</i>	1284721	C	G	61% C, 39% G	G17R
	<i>mreB</i>	2860903	T	A	100% A	R282S
	<i>bioI</i>	3089273	G	T	50% G, 50% T	R381I
	<i>yycC-parB</i>	4205543	A	T	47% A, 53% T	intergenic
SYL#3	<i>mreB</i>	2861400	G	C	100% C	R117G
SYL#7	<i>mbl</i>	3747508	C	T	97% T	E250K
SYL#8	<i>mreB</i>	2861287	G	T	98% T	S154R
SYL#10	<i>mreB</i>	2861309	G	C	99% C	P147R
SYL#14	<i>mreB</i>	2860781	C	T	99% T	G323E
	<i>folC</i>	2866565	C	A	100% A	G14W

To determine if the point mutations we identified were sufficient to confer resistance to YodL or YisK misexpression, we generated the mutant alleles in clean genetic backgrounds and assayed for resistance to three copies (3X) of each misexpression construct (Table 2.6). In all cases but one, the engineered strains were resistant to the same selective pressure applied in the original selections (either 3X *yodL* or 3X *yisK*)(Table 2.6), indicating that the *mreB* or *mbl* mutations identified through sequencing were sufficient to confer resistance. When we attempted to engineer a strain harboring only MreB_{S154R}, all but one of the strains also possessed a second substitution, MreB_{R230C}. Although the remaining strain possessed only the MreB_{S154R} substitution in MreB, unlike the original suppressor identified by whole genome sequencing (Table 2.5), the MreB_{S154R} harboring strain was also sensitive to YodL expression. Based on these data, we suspect that the strain harboring MreB_{S154R} might be unstable, and possibly predisposed to the accumulation of second-site mutations.

The YodL-resistant strains generally possessed mutations resulting in amino acid substitutions with charge changes (Table 2.6). When mapped to the *T. maritima* MreB structure, 5/7 of the unique suppressor strains possessed amino acid substitutions in a region important for mediating the interaction between MreB and the bitopic membrane protein RodZ (MreB_{G143A}, MreB_{N145D}, MreB_{P147R}, MreB_{S154R}, and MreB_{R282S})(Table 2.6 and Fig 2.9) (78, 295); three of these substitutions occur in residues that make up the RodZ-MreB binding surface (MreB_{N140}, MreB_{P142}, and MreB_{R279} in *T. maritima*) (78).

Table 2.6. Analysis of suppressor strains resistant to YodL and/or YisK. The suppressor selections are described in detail in materials and methods. Candidate mutations were introduced into clean genetic backgrounds harboring three copies of P_{hy} -*yodL* or three copies of P_{hy} -*yisK*, and the resultant strains were assessed for resistance (R) or sensitivity (S) to either *yodL* or *yisK* expression as judged by ability to grow on LB plates supplemented with 1 mM IPTG and 100 μ g/ml spectinomycin. ¹Originally identified using whole-genome sequencing (Table S1). ²Residues previously implicated in the RodZ-MreB interaction (78). ³Residues previously implicated in resistance to A22 (296-298). The (*) indicates that two suppressors possessing the same nucleotide change were obtained in original selection. The underlined residues displayed specificity in resistance to YodL over YisK (top) or YisK over YodL (bottom).

Variants obtained following YodL misexpression			
<i>mreB</i>	MreB Variants	+YodL	+YisK
CGC→GGC	R117G ¹	R	R
GGA→GCA	G143A	R	R
AAT→GAT*	<u>N145D</u> ²	R	S
CCA→CGA*	<u>P147R</u> ^{1,2}	R	S
AGC→AGA	<u>S154R</u> ^{1,2}	--	--
AGC→AGA	S154R ¹	R	R
CGC→TGC	R230C		
AGA→AGT*	<u>R282S</u> ^{1,2}	R	S
GGG→GAG	G323E ¹	R	R
<i>mbl</i>	Mbl Variants	+YodL	+YisK
ACG→ATG	T158M	R	R
GAA→AAA*	E250K ¹	R	R
ACA→ATA	T317I	R	R
Variants obtained following YisK misexpression			
<i>mreB</i>	MreB Variants	+YisK	+YodL
CGC→TGC	R117G	R	R
<i>mbl</i>	Mbl Variants	+YisK	+YodL
ATG→ATA	M51I ³	R	R
CGC→TGC	<u>R63C</u> ³	R	S
GAC→AAC*	D153N ³	R	R
GGC→GAC	G156D ³	R	R
ACG→GCG*	T158A ³	R	R
GAG→GGG	E204G ³	R	R
GAA→AAA	E250K	R	R
TCT→ $\Delta\Delta\Delta$	<u>ΔS251</u>	R	S
CCT→CTT	<u>P309L</u> ³	R	S
GCC→ACC	A314T ³	R	R

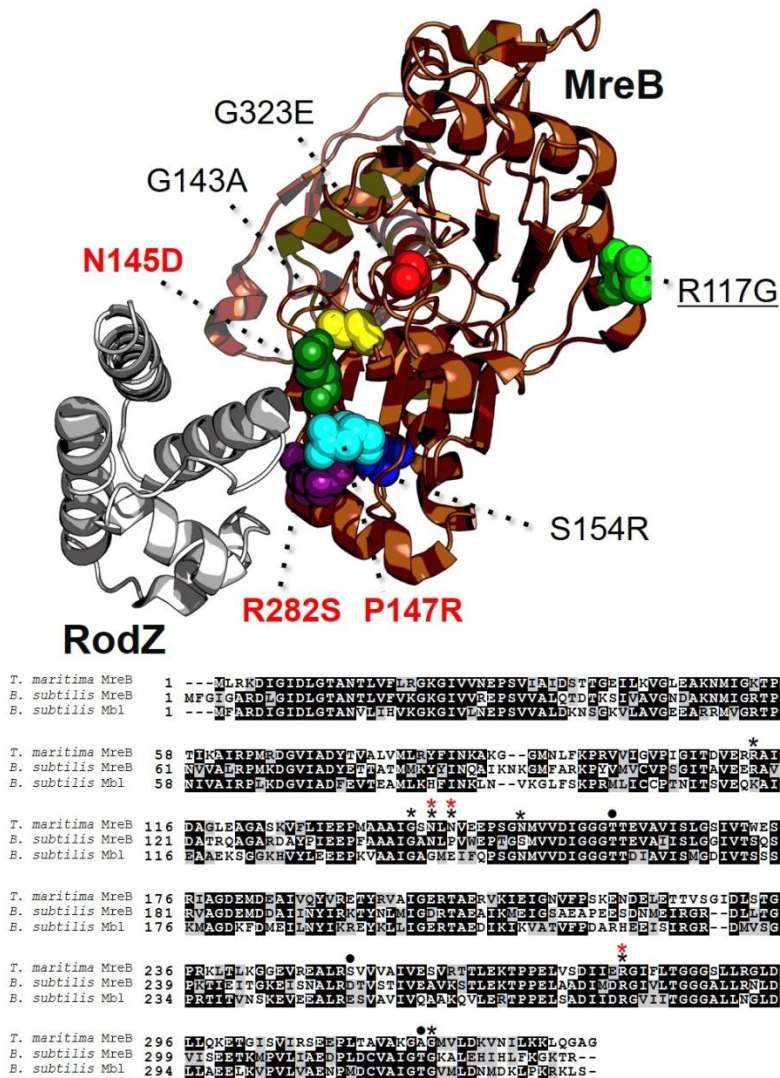


Fig. 2.9. Location of MreB residues conferring resistance to YodL. The co-crystal structure of RodZ-MreB (2WUS)(78) was extracted from the Protein Data Bank. MreB is labeled in brown and RodZ is labeled in grey. The identity and locations of the amino acid substitutions obtained from the YodL spontaneous suppressor selections are indicated on the structure, marked by a black asterisk above the relevant amino acid on the sequence alignment. Substitutions that confer resistance to YodL over YisK are shown in bold. Residues previously implicated in the MreB-RodZ interaction interface (78) are indicated by red asterisks. The filled circles indicate the location of the substitutions in Mbl conferring resistance to YodL misexpression. MreB_{R117G} (underlined) was identified in a suppressor selections conferring resistance to YodL as well as in suppressor selections conferring resistance to YisK.

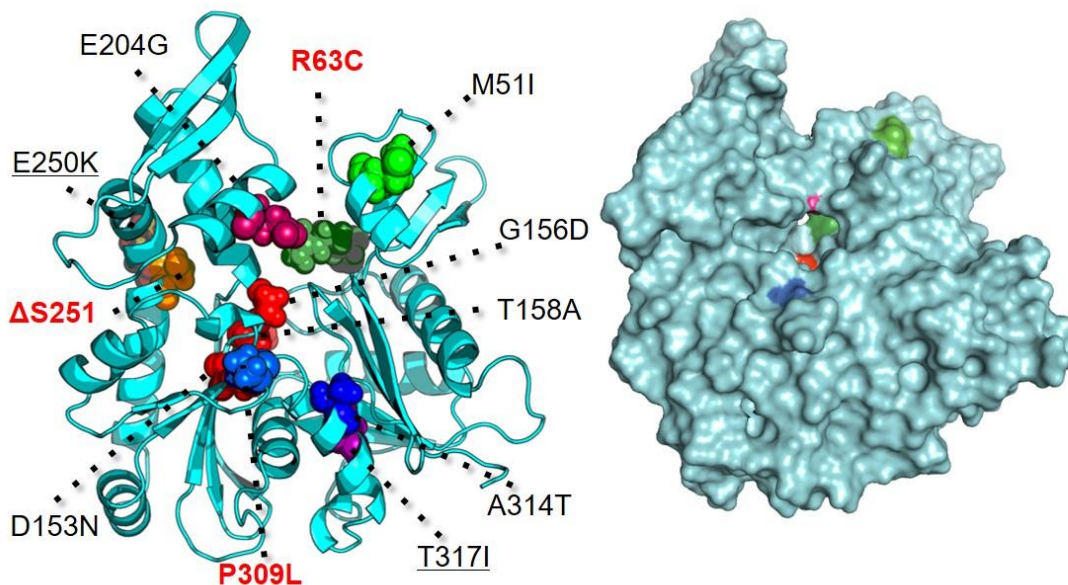
A majority of the YisK-resistant Mbl variants clustered in regions of Mbl that are predicted to make up the ATP-binding pocket (Table 2.6 and Fig 2.10). Moreover, seven of the substitutions occurred in amino acids previously associated with resistance to the MreB inhibitor A22 in *C. crescentus* and *Vibrio cholerae* (Fig 2.10) (253, 296, 298).

MreB_{R117G} and Mbl_{E250K} were independently isolated in both the YodL and YisK suppressor selections, raising the possibility that at least some of the other MreB and Mbl variants might exhibit cross-resistance to YodL and YisK misexpression. To test for cross-resistance, we generated the mutant alleles in clean genetic backgrounds, and then introduced 3X copies of P_{hy-yisK} into the YodL-resistant suppressors, and 3X copies P_{hy-yodL} into the YisK-resistant suppressors. We then assayed for the ability of the misexpression strains to grow on media in the presence of inducer. The results, summarized in Table 2.6, show that several of the variants exhibited resistance to both YodL and YisK. Three MreB variants, MreB_{N145D}, MreB_{P147R} and MreB_{R282S}, exhibited specificity in their resistance to YodL compared to YisK. Three Mbl variants, Mbl_{R63C}, Mbl_{ΔS251}, and Mbl_{P309L}, showed specificity in their resistance to YisK over YodL. These results suggest that the alleles exhibiting cross-resistance to both YisK and YodL are likely to be general, possibly conferring gain-of-function to either MreB or Mbl activity.

Fig. 2.10. Location of Mbl residues conferring resistance to YisK. The structure of *B. subtilis* Mbl, as predicted by I-TASSER (299), threaded to *T. maritima* MreB (1JCG)(78). The structure on the right is a surface prediction model. The identity and locations of the amino acid substitutions obtained from the YisK spontaneous suppressor selections are indicated on the structure, with substitutions conferring resistance to YisK over YodL in bold. The sequence alignment is of MreB from *T. maritima*, *B. subtilis* 168, *C. crescentus* NA1000, *E. coli* MG1655, and *V. cholera* N16961. The location of amino acid substitutions conferring YisK resistance are indicated by black asterisks. Residues also previously shown to confer resistance to A22 in *C. crescentus* NA1000 (253, 296) and *V. cholera* N16961 (298) are indicated by red and blue asterisks, respectively. The filled triangle corresponds to a residue shown by in vivo crosslinking to be important for the formation of antiparallel MreB protofilaments (300). The filled circle denotes the location of MreB_{R117G}, which was identified in spontaneous suppressor selections conferring resistance to both YodL and YisK. Mbl_{T317I} (underlined) was only identified in a spontaneous suppressor selection conferring resistance to YodL, although it exhibits cross-resistance to YisK (see Fig 2.5).

B. subtilis Mbl

Threaded to *T. maritima* MreB (PDB:1JCG)



<i>T. maritima</i> MreB	1	-----MURRDHGLDIDLTANTLVFLKGGKIVVNEPSVLRHDSSTG---EILKVGLEAK
<i>B. subtilis</i> MreB	1	---MFGEGARDLGLDIDLTANTLVFLKGGKIVVREPSVVAHQTDI---RSIVAVGNDAK
<i>B. subtilis</i> Mbl	1	-----MVARDTGLDIDLTANTLVFLKGGKIVLNEPSVVAIDKNSG---KIVAVGFEAR
<i>C. crescentus</i> MreB	1	MFSLSLFGVLSNDLDAIDLTANTLIVKGGKIVLNEPSVVAQRN--VGGRRVVAVGLAK
<i>E. coli</i> MreB	1	MKKKFRGMFSNDLSIDLTANTLIVKGGKIVLNEPSVVAQRDRAGSPKSVAVAGHDAK
<i>V. cholerae</i> MreB	1	MFKKLRGMFSNDLSIDLTANTLIVKGGKIVLDEPSVVAQRDRGRGKTVVAAGHAAK
		* * * * *
<i>T. maritima</i> MreB	50	NMEGRTPATLKAIREPMKDGVIADPTVALVMLRNFINKAKGG--MNLFRKRVLCGVPISGIT
<i>B. subtilis</i> MreB	53	NMEGRTPGNVVAIRPMKDGVIADMEPTATMVKYVINAQKNGKGFARKPVVVCVPSGIT
<i>B. subtilis</i> Mbl	50	RNVGRTPGNVVAIRPDKDGLVADFEVTEAMLKHFINKLVKQ--LFSKPRMLCEPNTIT
<i>C. crescentus</i> MreB	59	QMLGRTPGMEAIRPMKDGVIADFEVTEEMKPKIRKVVNRK--GFVN--PRVIVCVPSGAT
<i>E. coli</i> MreB	61	QMLGRTPGNVVAIRPMKDGVIADFEVTEKMLQHFTRQVHNS--FMRPSPRVLVCVPSGAT
<i>V. cholerae</i> MreB	61	QMLGRTPGNVVAIRPMKDGVIADFEVTEKMLQHFTRQVHNS--VLKPSPRVLCVPSGAT
		* * * * *
<i>T. maritima</i> MreB	108	DVERRAILDAGLQAGASNVLEEEPMAAAIQSNLNVPEPSGNMVVDIGGGTTEVAVISLG
<i>B. subtilis</i> MreB	113	AVERRAVIDATROAGARDAVLEIEEPPAAAIQGANLFWVEPTGSMVVDIGGGTTEVAVISLG
<i>B. subtilis</i> Mbl	108	SVEQKAIKEAIEKSGGKHVYVLEIEEPPKVAIIGAGMEIFQPSGNMVVDIGGGTTEVAVISLG
<i>C. crescentus</i> MreB	117	AVERRAINDSCLNAGARRVGLIDEPMAAAIGAGLPEHEPTGSMVVDIGGGTTEVAVISLS
<i>E. coli</i> MreB	120	QVERRAIRSRQAGARVYVLEIEPMAAIGAGLQVSEPTGSMVVDIGGGTTEVAVISLN
<i>V. cholerae</i> MreB	120	QVERRAIRSALQAGARVYVLEIEPMAAIGAGLRVSEPTGSMVVDIGGGTTEVAVISLN
		* * * * *
<i>T. maritima</i> MreB	168	SIVTWESIRIAGDEMDAIVQVRETVRVAIGERTAERKMEIGNVPEKNEDELTTVVS
<i>B. subtilis</i> MreB	173	GIVVSSSRVAGDEMDALINYRKYVNLVIGERTAERIKMEIGSAEAP--EESDNMIEIR
<i>B. subtilis</i> Mbl	168	DIVVSSSLKMAQDKFMEHDVYLRKRYRLIGERTAEDIRKVAIVTEH--DARHEIETIR
<i>C. crescentus</i> MreB	177	GIVVSSVVRVQDMDEALISYGRRHHLVIGETAERIKKEGTRPADGELSLDQVK
<i>E. coli</i> MreB	180	GIVVSSSVRIQGRDFDEALINYVRNIVGSLIGETAERIKHEIGSAMP--GDEVVEIEVR
<i>V. cholerae</i> MreB	180	GIVVSSSVRIQGRDFDEALINYVRNIVGSLIGETAERIKHEIGSAMP--GDEVVEIEVR
		* * * * *
<i>T. maritima</i> MreB	228	GLDLSVGLPRKLTIKGGQVREALRSVVVAIVESVRTTLEKTPPELVSDIERGIVLTGGG
<i>B. subtilis</i> MreB	231	GRDLTGLPFTIEITGFEISNLRDVTSTLWEAVRSTLEKTPPELADLMDRGIYLTGGG
<i>B. subtilis</i> Mbl	226	GRDVSGLPRTIIVNSKQVFEALRSVVAVLVGAMQVLEKTPPELADLMDRGIYLTGGG
<i>C. crescentus</i> MreB	237	GRDLMQGVPEVFTISEKQADAIAEPCQIVAEAVKVALEKTPPELADLMDRGIYLTGGG
<i>E. coli</i> MreB	238	GRNLAEQVPRGFTLNSNEILEALQELTGTIVSAVMVALEQCPPELADLMDRGIYLTGGG
<i>V. cholerae</i> MreB	238	GRNLAEQVPRGFTLNSNEILEALQELTGTIVSAVMVALEQCPPELADLMDRGIYLTGGG
		* * * * *
<i>T. maritima</i> MreB	288	SFLRGLDPLIQKQGTGFSVHRSFELPFAVAKQAPVVDKVNILLKIQGAG--
<i>B. subtilis</i> MreB	291	ALLRNLDKVISSEETGQFVLAEDRLDQVALCTGKALENHLPKKTR---
<i>B. subtilis</i> Mbl	286	ALLNGLDQILAEKQVVAEAPNDQVALCTGVVLDNMDKLPKPKLS---
<i>C. crescentus</i> MreB	297	ALLRGLDAEIRDHIGLIPVVAEDPLSCVALCGGKVALEHPKWKGVVBSLA
<i>E. coli</i> MreB	298	ALLRNLDRLMEETGIPVVAEDPLTCVARCGGKALEMIDMHGGDLSEEE-
<i>V. cholerae</i> MreB	298	ALLRDLDRLLMEETGIPVVAEDPLTCVARCGGKALEMIDMHGGDLSEEE-

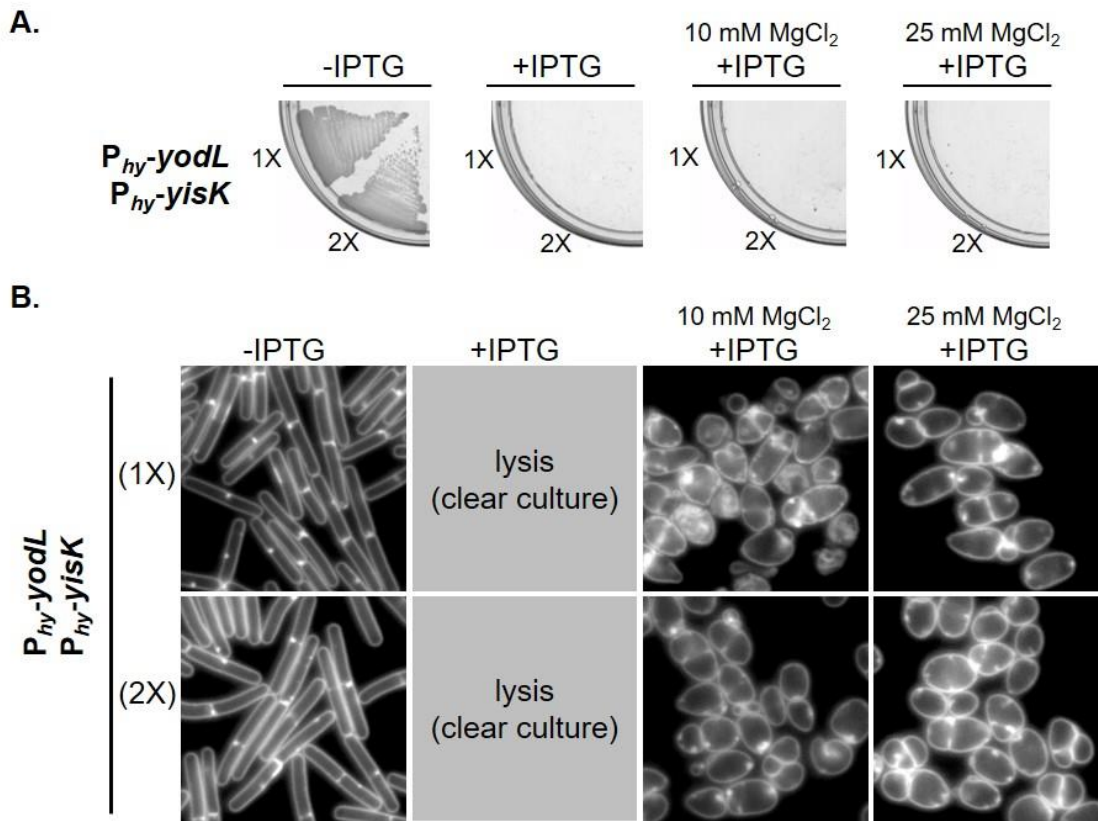


Fig. 2.11. YodL and YisK co-misexpression causes cell lysis. (A) BYD361 (*P_{hy}-yodL*, *P_{hy}-yisK*) and BYD281 (2X *P_{hy}-yodL*, 2X *P_{hy}-yisK*) were streaked on an LB plate with 100 μ g/ml spectinomycin and, when indicated 1 mM IPTG or 1 mM IPTG and the denoted concentration of MgCl₂. (B) Cells were grown in LB-Lennox media at 37°C to mid-exponential and back-diluted to an OD₆₀₀ of ~0.02. When indicated 1 mM IPTG or 1 mM IPTG and the denoted concentration of MgCl₂ were added. Cells were then grown for 1.5 hrs at 37°C before image capture. Membranes are stained with TMA-DPH. All images are shown at the same magnification.

YodL and YisK's cell-widening activities require MreB and Mbl, respectively

The phenotypic consequences of YodL and YisK misexpression are similar but not identical (Fig 2.1B), suggesting that YodL and YisK might have distinct targets. Consistent with this idea, YodL and YisK coexpression resulted in phenotypes distinct from misexpression of either YodL or YisK alone. More specifically, cells co-expressing YodL and YisK did not grow on plates, regardless of media or MgCl₂ concentration (Fig 2.3A and Fig 2.11A) and growth without lysis in liquid media required the presence of MgCl₂ (Fig 2.2, Fig 2.3B, and Fig 2.11B). Importantly, the co-expressing cells displayed a round morphology that strongly contrasted with strains expressing either YodL or YisK alone (Fig 2.3B and Fig 2.11B). The round morphology was unlikely due to higher expression of gene products (1X P_{hy-yodL} plus 1X P_{hy-yisK}), since cells harboring two copies (2X) of either P_{hy-yodL} or P_{hy-yisK} did not become round (Fig 2.1B and Fig 2.3B).

Based on the observation that YodL and YisK coexpression yields distinct phenotypes, and the fact that all of the YodL-specific suppressor mutations occurred in *mreB* (MreB_{N145D}, MreB_{P147R} and MreB_{R282S}), while all of the YisK-specific suppressor mutations occurred in *mbl* (Mbl_{R63C}, Mbl_{ΔS251}, and Mbl_{P309L}), we hypothesized that YodL targets MreB, whereas YisK targets Mbl. To test these hypotheses, we assessed if MreB and Mbl are specifically required for YodL and YisK function by taking advantage of the fact that *mreB* and *mbl* can be deleted in a Δ *ponA* background with only minor changes in cell shape (60, 61). The Δ *ponA* strain, which does not make PBP1, produces slightly longer and thinner cells than the parent strain, and requires MgCl₂ supplementation for normal growth (301, 302). We generated Δ *ponA* Δ *mreB* and Δ *ponA* Δ *mbl* strains and then introduced either two copies of P_{hy-yodL} or two copies of P_{hy-yisK} into each background. We reasoned that 2X expression would provide a more stringent

test for specificity than 1X expression, as off-target effects (if any), would be easier to detect. To assess the requirement of either *mreB* or *mbl* for YodL and YisK activity, cells were grown to exponential phase in LB media supplemented with 10 mM MgCl₂, back-diluted to a low optical density, and induced for 90 min before images were captured for microscopy. Uninduced controls all appeared as regular rods, although Δ *ponA* deletion strains were noticeably thinner than wildtype parents (Fig 2.12). The Δ *ponA* cells became wider following YodL expression, indicating that PBP1 is not required for YodL activity. We also observed that the poles of the Δ *ponA* mutant were less elongated and tapered than the wild-type control following YodL expression, suggesting that this particular effect of YodL expression is PBP1-dependent (Fig 2.12A). A Δ *ponA* Δ *mbl* mutant phenocopied the Δ *ponA* parent following YodL expression (Fig 2.12A), indicating that Mbl is not required for YodL's activity. In contrast, the Δ *ponA* Δ *mreB* strain did not show morphological changes following YodL expression, and instead appeared similar to the uninduced control. We conclude that YodL requires MreB for its cell-widening activity.

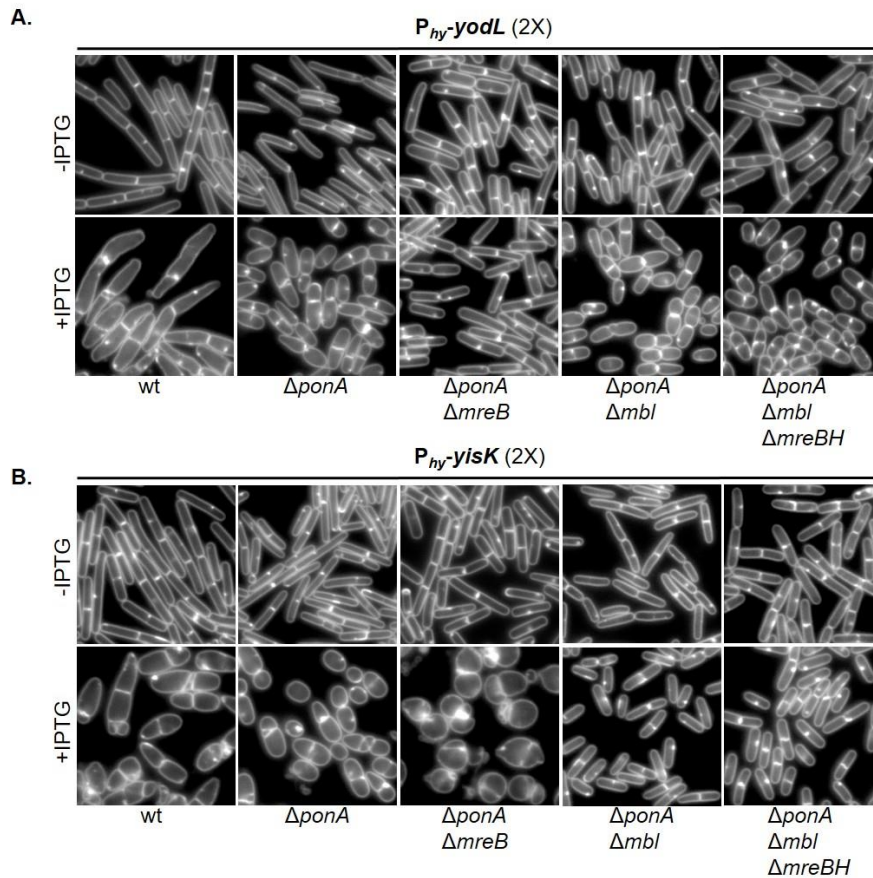


Fig. 2.12. YodL and YisK's cell-widening activities require MreB and Mbl, respectively. (A) Cells harboring 2X copies of $P_{hy-yodL}$ in a wildtype (BAS191), $\Delta ponA$ (BYD176), $\Delta ponA \Delta mreB$ (BYD263), $\Delta ponA \Delta mbl$ (BYD259) or $\Delta ponA \Delta mbl \Delta mreBH$ (BAS249) background were grown at 37°C in LB supplemented with 10 mM $MgCl_2$ to mid-exponential. To induce *yodL* expression, cells were back-diluted to an OD_{600} of ~0.02 in LB with 10 mM $MgCl_2$, and IPTG (1 mM) was added. Cells were grown for 1.5 hrs at 37°C before image capture. Membranes are stained with TMA-DPH. All images are shown at the same magnification. (B) Cells harboring 2X copies of $P_{hy-yisK}$ in a wildtype (BYD074), $\Delta ponA$ (BYD175), $\Delta ponA \Delta mreB$ (BYD262), $\Delta ponA \Delta mbl$ (BYD258) or $\Delta ponA \Delta mbl \Delta mreBH$ (BAS248) background were grown at 37°C in LB supplemented with 10 mM $MgCl_2$ to mid-exponential. To induce *yisK* expression, cells were back-diluted to an OD_{600} of ~0.02 in LB with 10 mM $MgCl_2$, and IPTG (1 mM) was added. Cells were grown for 1.5 hrs at 37°C before image capture. Membranes are stained with TMA-DPH. All images are shown at the same magnification.

We performed a similar series of experiments for YisK misexpression. The $\Delta ponA$ mutant was sensitive to YisK expression, indicating that PBP1 is not required for YisK-dependent cell-widening. Similarly, expression of YisK in a $\Delta ponA \Delta mreB$ mutant also resulted in loss of cell width control (Fig 2.12B), indicating that MreB is not required for YisK activity; however, unlike YisK expression in a wildtype or $\Delta ponA$ background, the cells became round (Fig 2.12B), more similar to the YodL and YisK co-expressing cells (Fig 2.3B and Fig 2.11). In contrast, a $\Delta ponA \Delta mbl$ mutant did not lose control over cell width following YisK expression (Fig 2.12B), indicating that YisK activity requires Mbl for its cell-widening activity. We conclude that YodL requires MreB, but not Mbl for its cell-widening activity, whereas YisK requires Mbl, but not MreB.

YisK possesses at least one additional target

Although YisK expression in a $\Delta ponA \Delta mbl$ mutant did not result in cell-widening, we observed that the induced cells appeared qualitatively shorter than the uninduced control, suggesting that YisK might possess a second activity (Fig 2.12B). Quantitation of cell lengths in a $\Delta ponA \Delta mbl$ mutant following YisK expression revealed that the YisK-induced cells were ~20% shorter than the uninduced cells (Fig 2.13A). In contrast, YodL expression did not result in a change in cell length in a $\Delta ponA \Delta mreB$ mutant (Fig 2.13B), suggesting the cell shortening effect is specific to YisK. We hypothesized that MreBH, the third and final *B. subtilis* MreB family member, might be YisK's additional target. We hypothesized that if MreBH is the additional target, then the cell shortening observed upon YisK expression in a $\Delta ponA \Delta mbl$ mutant strain should be lost in a $\Delta ponA \Delta mbl \Delta mreBH$ mutant background. However, we found that even when *mreBH* was additionally deleted, YisK expression still resulted in cell

shortening (Fig 2.13C). We conclude that YisK likely has at least one additional target that is not MreB or Mbl dependent, and that this additional target regulates some aspect of cell length.

Discussion

YodL and YisK's functional targets

Misexpression of YodL during vegetative growth results in cell-widening and lysis, and spontaneous suppressor mutations conferring resistance to YodL occur primarily in *mreB*. MreB is also required for YodL's cell-widening activity, whereas Mbl is not. By comparison, expression of YisK during vegetative growth also results in cell-widening and lysis, however, spontaneous suppressor mutations conferring resistance to YisK occur primarily in *mbl*. YisK's cell-widening activity requires Mbl, but not MreB. The simplest interpretation of these results is that YodL targets MreB function, while YisK targets Mbl function. Alternatively, YodL and YisK could target other factors that affect cell shape and simply require MreB and Mbl for their respective functions.

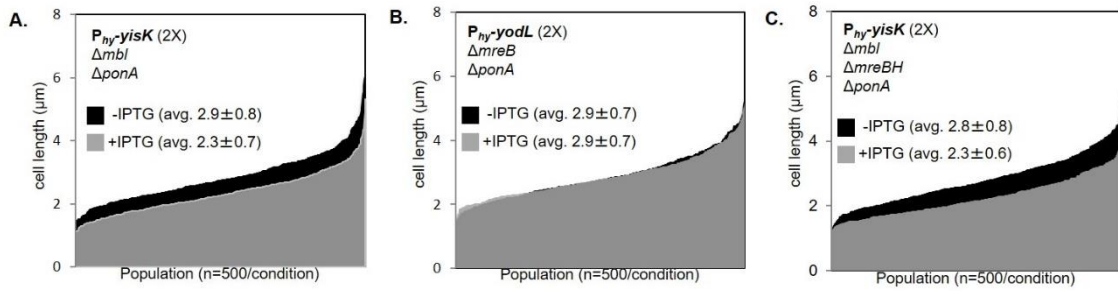


Fig. 2.13. YisK expression results in cell shortening. (A) Cells harboring 2X copies of $P_{hy}\text{-}yisK$ in a $\Delta\text{ponA } \Delta\text{mbl}$ background (BYD262) were grown at 37°C in LB supplemented with 10 mM MgCl_2 to mid-exponential. To induce $yisK$ expression, cells were back-diluted to an OD_{600} of ~ 0.02 in LB with 10 mM MgCl_2 and IPTG (1 mM) was added. Cells were grown for 1.5 hrs at 37°C before image capture. Membranes are stained with TMA-DPH. Cell lengths ($n=500/\text{condition}$) were measured before and after $yisK$ expression and rank-ordered from smallest to largest along the x-axis so the entire population could be visualized without binning. The uninduced population (black) is juxtaposed behind the induced population (semi-transparent, gray). The difference in average cell length before and after $P_{hy}\text{-}yisK$ induction were statistically significant ($P < 0.0001$). (B) Cells harboring 2X copies of $P_{hy}\text{-}yodL$ in a $\Delta\text{ponA } \Delta\text{mreB}$ background (BYD263) were grown, quantitated, and plotted as described above. The difference in average cell length before and after $P_{hy}\text{-}yodL$ induction were not statistically significant. (C) Cells harboring 2X copies of $P_{hy}\text{-}yisK$ in a $\Delta\text{ponA } \Delta\text{mbl } \Delta\text{mreBH}$ background (BAS248) were grown, quantitated, and plotted as described above. The difference in average cell length before and after $P_{hy}\text{-}yisK$ induction were statistically significant ($P < 0.0001$).

MreB variants specifically resistant to YodL activity, MreB_{N145D}, MreB_{P147R} and MreB_{R282S}, all result in charge change substitutions in residues previously shown to constitute the RodZ-MreB interaction surface (equivalent *T. maritima* residues are: MreB_{N140}, MreB_{N142} and MreB_{R279})(78). MreB_{G143A}, which exhibits cross-resistance to YisK, also maps near the RodZ-MreB interaction interface. The two remaining YodL-resistant MreB variants occur in (MreB_{R117G}) or near (MreB_{G323E}) residues previously associated with bypass of RodZ essentiality in *E. coli* (Fig 2.12)(77). A simple model explaining both the nature of the MreB variants we obtained in the suppressor selections, and YodL's MreB-dependent effect on cell shape, is that YodL acts by disrupting the interaction between RodZ and MreB. In this model, MreB's RodZ-independent activities would remain functional, and several observations are consistent with this idea. If YodL were to completely inactivate MreB function, then we would expect that expressing YodL in a $\Delta pona \Delta mbl \Delta mreBH$ background would generate round cells, similar to the phenotype observed when MreB is depleted in a $\Delta mbl \Delta mreBH$ mutant background (60), or when *mreB*, *mbl*, and *mreBH* are deleted in backgrounds with upregulated *sigI* expression (the triple mutant is otherwise lethal)(264). However, we observe that cells expressing YodL in a $\Delta pona \Delta mbl \Delta mreBH$ mutant instead form wide rods (Fig 2.6A). If YodL does specifically target MreB activity, then these results suggest that MreB likely retains at least some of its width-maintenance function. Morgenstein et al. recently found that the interaction between RodZ and MreB in *E. coli* is required for MreB rotation, but that MreB rotation was not required for rod shape or cell viability under standard laboratory conditions (80). This study is consistent with

prior findings indicating that RodZ is not absolutely required for maintenance of rod shape (77).

We hypothesize that the substitutions obtained in residues near the RodZ-MreB interface either enhance RodZ-MreB interaction, or decrease the ability of YodL to disrupt the RodZ-MreB interface. Although we did not identify YodL-resistant suppressor mutations in *rodZ*, it is possible that the requisite *rodZ* mutations are rare or lethal for the cell, thus we cannot rule out the possibility that YodL could target RodZ function. Similarly, although we found that MreB is required for YodL activity, we can envision a scenario in which a YodL-MreB interaction may be necessary to localize YodL to a cellular location where it can be effective against RodZ or some other cellular component. We think this possibility is less likely, as cells expressing YodL have a distinct phenotype from RodZ depletion in *B. subtilis*. More specifically, YodL expression results in cell widening and tapered poles (Fig 2.1B), whereas RodZ-depleted cells generate wide rods (260), similar to the phenotype we observed following YodL expression in a $\Delta ponA \Delta mbl \Delta mreBH$ mutant (Fig 2.6A). These results argue against the idea that YodL could work by inactivating RodZ function completely. Future work aimed at characterizing the nature of the YodL resistant suppressors and the effect of YodL on MreB function will shed light on the mechanism underlying YodL's observed activity.

Only three Mbl variants, Mbl_{R63C}, Mbl _{Δ S251}, and Mbl_{P309L}, showed specificity in resistance to YisK over YodL. Mbl_{R63C}, Mbl_{D153N}, Mbl_{G156D}, Mbl_{T158A}, Mbl_{E204G}, MreB_{P309L} and Mbl_{A314T} occur in residues that form Mbl's predicted ATP-binding pocket

(Fig 2.13), and substitutions in all seven of these residues have been previously implicated in A22 resistance (Fig 2.13)(253, 296, 298). We speculate that most, if not all of the substitutions in Mbl's ATP-binding pocket are gain-of-function with respect to Mbl polymerization, a hypothesis that can ultimately be tested in vitro. Similarly, we hypothesize that the Mbl_{M51I} substitution, located at the MreB head-tail polymerization interface (295), may overcome YisK activity by promoting Mbl polymerization. MreB_{E262} of *C. crescentus*, equivalent to *B. subtilis* Mbl_{E250} (Fig 2.13), is located at the interaction interface of antiparallel MreB protofilament bundles (300). If *B. subtilis* Mbl_{E250} is also present at this interface (this has not been tested to our knowledge), then Mbl_{E250K} could promote resistance to YodL and YisK by enhancing Mbl bundling. How might YisK exert its activity? One idea is that YisK disrupts Mbl bundling, possibly by competing for sites required for protofilament formation. An alternative possibility is that YisK somehow prevents Mbl from effectively binding or hydrolyzing ATP. It is also possible that Mbl is simply required for YisK to target one or more other factors involved in cell-width control.

In addition to Mbl-dependent cell widening, YisK expression resulted in cell shortening, an effect that only became apparent in a Δ *ponA* Δ *mbI* mutant background (Fig 2.6B and 2.7A). Given the similarities of MreB, Mbl, and MreBH to each other, we initially hypothesized that YisK-dependent effects on MreB and/or MreBH might be responsible for the decrease in cell length we observed; however, we found that *mreBH* was not required for cell shortening (Fig 2.6B and Fig 2.7C). Since YisK expression results in a dramatic loss of cell shape in Δ *mreB* mutant backgrounds (Fig 2.6A), we

were unable to confidently assess cell length changes to determine if there is a requirement for MreB in the cell-shortening phenotype. It is unlikely that YisK's additional activity affects MreB's role in maintaining cell width (at least not without Mbl), as YisK-expressing cells retain rod shape when *mbl* and *mreBH* are both deleted (Fig 2.6B). An exciting alternative possibility is that YisK activity affects another factor involved in cell length control. One attractive candidate is the cell wall hydrolase CwlO, a known modulator of cell length in *B. subtilis* (66) which recent genetic data also suggests depends at least in part on Mbl (69). Future experiments aimed at determining the identity and function of YisK's additional target should shed light on how cells regulate both cell length and cell width.

Identification of genes involved in cellular organization through a novel gene discovery pipeline

To systematically identify and characterize novel genes involved in cellular organization, we developed a gene discovery pipeline that combines known regulatory information (135), phenotypes obtained from misexpression screening, and suppressor selection analysis. The ability to identify genetic targets associated with the unknown genes provides a key parameter beyond phenotype from which to formulate testable hypotheses regarding each gene's possible function. The misexpression constructs we generated are inducible and present in single copy on the chromosome. We have found that to obtain phenotypes, our strategy works best when the unknown genes are expressed outside of their native regulatory context. Thus far, we have restricted our

gene function discovery pipeline to *B. subtilis*; however, the general approach should be broadly applicable to other organisms and diverse screening strategies.

In this work, we describe the use of the pipeline to identify and characterize two *B. subtilis* genes, *yodL* and *yisK*, that produce proteins capable of targeting activities intrinsic to cell width control. Although *yodL* and *yisK* were not previously recognized as members of the Spo0A regulon, both genes have putative Spo0A boxes and possess promoters that exhibit expression patterns consistent with other Spo0A-regulated genes (Fig 2.2-2.4). YisK is also a member of the SigH regulon (303), and our expression analysis is also consistent with expression of *yisK* during stationary phase (Fig 2.3). If the putative Spo0A box we identified is utilized in vivo, then we would predict based on our expression profiling that *yisK* is transcribed during exponential and early stationary phase via SigH, and then repressed as Spo0A-P accumulates during early sporulation. Such a pattern is similar to the regulation that has been proposed for *kinA* (35, 304). We also observe expression from P_{*yodL*} and P_{*yisK*} is reduced in the absence of Spo0A and SigH (Fig 2.3D-E). The specific contributions of these global regulators to *yodL* and *yisK* regulation cannot be determined by analyzing the expression profiles of the *sigH* and *spo0A* deletion strains alone, since *spo0A* depends on SigH for upregulation during the early stages of sporulation (286, 304). Moreover, since Spo0A inhibits expression of the *sigH* repressor AbrB (305-308), a *spo0A* mutant is also down for *sigH* expression.

A $\Delta yodL \Delta yisK$ double mutant reproducibly produces ~20% less heat-stable spores than wildtype, suggesting that the YodL and YisK have functions that affect spore development (either directly or indirectly). Most studies on sporulation genes are

biased toward factors that reduce sporulation efficiency by an order of magnitude or more in a standard heat-kill assay. However, even small differences in fitness (if reproducible) can contribute significantly to the ability of an organism to persist, especially in competitive environments (309). The 20% reduction in heat-resistant spores we observe in cells lacking YisK and YodL would likely result in a substantial fitness disadvantage to cells in the environment. We do not currently understand how YodL and YisK might function in spore development, but the identification of MreB and Mbl as genetic targets suggests the proteins likely regulate some aspect of PG synthesis. Future studies will be aimed at understanding the molecular and biochemical basis of YodL and YisK activity.

In this study, the morphological phenotypes associated with YodL and YisK occurred when the genes were expressed during vegetative growth. Consequently, it is formally possible (although we think unlikely), that the targeting of MreB and Mbl is simply a coincidence that is unrelated to the potential functions of the proteins during stationary phase or sporulation. Regardless of what YodL and YisK's physiological roles turn out to be, we have already been able to utilize misexpression of the proteins to obtain interesting variants of both MreB and Mbl that can now be used to generate testable predictions regarding how MreB and Mbl function in *B. subtilis*. Moreover, the apparent specificity with which YodL and YisK appear to target MreB and Mbl, respectively, make them potentially powerful tools to differentially target the activities of these two highly similar paralogs in vivo. Of course, more studies will be required to determine if YodL and YisK interact directly or indirectly to modulate MreB and Mbl

activity. In the meantime, it is exciting to speculate that many undiscovered modulators of MreB and MreB-like proteins exist, and that we have only just begun to scratch the surface regarding regulation of this important class of proteins. The identification and characterization of such modulators could go a long way toward addressing the significant gaps in our knowledge that exist regarding the regulation of PG synthesis in bacteria.

CHAPTER III
CHARACTERIZATION OF YisK, AN ENZYME IN THE
FUMARYLACETOACETATE HYDROLASE SUPERFAMILY

Introduction

The bacterial cell envelope is comprised in part by a meshwork of peptidoglycan (PG) that protects bacteria from osmotic lysis and helps maintain cell shape. PG is also the target of our most-utilized and highly tolerated antibiotics, so understanding the synthesis of this uniquely bacterial exopolymer is crucial to combating antibiotic resistance mechanisms.

PG synthesis is regulated by bacterial cytoskeletal proteins, namely FtsZ and MreB, which are hypothesized to guide the localization of enzymes involved in PG polymerization and crosslinking. Despite its conserved nature and critical function within the cell, regulation of MreB activity is poorly characterized. We have identified a putative enzyme, YisK, capable of perturbing the activity of an MreB family protein (Mbl) in the important Gram-positive model organism *Bacillus subtilis*.

YisK is a member of the Fumarylacetoacetate hydrolase (FAH) superfamily involved in aromatic amino acid catabolism. YisK-like proteins are found across all domains of life. In closely related *Bacillus* species, *yisK* is conserved by synteny with asparagine synthetase genes, which encode an enzyme that converts L-aspartate and L-glutamine to L-asparagine and L-glutamate. In more distantly related species, *yisK* has synteny with *rocD*, encoding an enzyme that mediates L-glutamate biosynthesis through

the glyoxylate pathway. The synteny is suggestive of a possible role for YisK in amino acid or dicarboxylate metabolism.

The goal of the present study was to characterize the function of YisK in *B. subtilis*, including to understand how its misexpression leads to loss of cell width control (310). We find that YisK perturbs Mbl localization, suggesting the cell widening is caused by disruption of the normal punctate-helical arrangement of Mbl within the cell. Moreover, YisK can interact directly with FtsE (this study, Chapter III), a component of an ABC transporter implicated in the Mbl-dependent regulation of cell length (66, 69). To gain further insight into YisK function, we obtained a ~ 2 Å crystal structure which revealed that YisK, like other members of the FAH superfamily, possesses a putative active site with residues critical for coordinating a required Mg^{2+} or Mn^{2+} . However, to our surprise, YisK's effect on Mbl is unlikely due to its enzymatic activity. We propose a model in which YisK utilizes interactions with Mbl to localize its to-be-determined activity to specific sites within the cell, possibly where its substrate is enriched or its product is utilized.

Materials and methods

General methods

All *B. subtilis* strains were derived from *B. subtilis* 168 unless specifically noted. *B. subtilis* strains utilized in this study are listed in Table 3.1. Plasmids are listed in Table 3.2. Oligonucleotide primers are listed in Table 3.3. The following concentrations of antibiotics were used for generating *B. subtilis* strains: 100 $\mu\text{g/ml}$ spectinomycin, 7.5 $\mu\text{g/ml}$ chloramphenicol, 0.8 mg/ml phleomycin, 10 $\mu\text{g/ml}$ tetracycline, and 10 $\mu\text{g/ml}$

kanamycin. To select for erythromycin resistance, plates were supplemented with 1 $\mu\text{g/ml}$ erythromycin (erm) and 25 $\mu\text{g/ml}$ lincomycin. *B. subtilis* transformations were carried out as described previously (271).

Cell growth

Cell growth and culturing was performed as described in Chapter II.

Microscopy

Microscopy (both phase contrast and fluorescence) was performed as described in Chapter II. GFP exposure time was 1 sec and all images were processed the same unless otherwise noted.

YisK rabbit polyclonal antibody production

Antibody production was carried out at the Texas A&M Comparative Medicine Program using YisK-His dialyzed in 50.0 mM Tris-HCl pH 7.5, 100 mM KCl, 2.0 mM DTT, 15% glycerol at a final concentration of 12.0 mg/mL. Briefly, an initial injection of 0.2 mL YisK-His (brought to 0.5 mL with Saline) with 0.5 mL Titermax Gold adjuvant was given to two white rabbits, followed in 6 weeks by three boosters, each separated by two weeks. At the end of the protocol, the animals were sacrificed and serum was collected from whole blood. The serum was frozen at -80°C in 10mL aliquots.

Table 3.1. Strains used in Chapter III.

Strain	Description	Reference
Parental		
<i>B. subtilis</i> 168	<i>Bacillus subtilis</i> laboratory strain 168 trpC2	BGSC (1A866)
<i>E. coli</i> DH5 α	F^- <i>endA1 glnV44 thi-1 recA1 relA1 gyrA96 deoR nupG Φ80dlacZΔM15 Δ(lacZYA-argF)U169, hsdR17($r_K^- m_K^+$), λ^-</i>	
<i>E. coli</i> BL21 (DE3)	F^- <i>ompT gal dcm lon hsdS_B($r_B^- m_B^-$) [malB⁺]_{K-12}(λ^S) λ(DE3 [<i>lacI lacUV5-T7p07 ind1 sam7 nin5</i>])</i>	
<i>E. coli</i> DHP1	F^- , <i>cya-99, araD139, galE15, galK16, rpsL1 (Strr), hsdR2, mcrA1, mcrB1;</i>	Tom Bernhardt
<i>B. subtilis</i> 168		
BAS175	<i>amyE::P_{xyl}-opt rbs-lytE-GFP (spec)</i> <i>yhdG::P_{hy}-opt rbs-yodL (phleo)</i> <i>yycR::P_{hy}-opt rbs-yodL (cat)</i>	This study
BAS177	<i>amyE::P_{xyl}-opt rbs-lytE-GFP (spec)</i> <i>yhdG::P_{hy}-opt rbs-yisK (phleo)</i> <i>yycR::P_{hy}-opt rbs-yisK (cat)</i>	This study
BAS220	<i>amyE::P_{xyl}-gfp-mreB (spec)</i> <i>yhdG::P_{hy}-opt rbs-yisK (phleo)</i> <i>yycR::P_{hy}-opt rbs-yisK (cat)</i>	This study
BAS316	<i>tet$\Omega$$\Delta$rodZ</i>	This study
BAS321	<i>tet$\Omega$$\Delta$rodZ</i> <i>amyE::P_{hy}-yodL (spec)</i> <i>yhdG::P_{hy}-yodL (phleo)</i>	This study
BAS334	<i>P_{yisK}-RBSyisK-Spo0Abox mutant</i>	This study
BYD181	<i>amyE::P_{xyl}-mbl-gfp (spec)</i> <i>yhdG::P_{hy}-opt rbs-yisK (phleo)</i>	This study
BYD182	<i>amyE::P_{xyl}-mbl-gfp (spec)</i> <i>yhdG::P_{hy}-opt rbs-yisK (phleo)</i> <i>yycR::P_{hy}-opt rbs-yisK (cat)</i>	This study
BYD278	Δ <i>yisK</i>	Chapter II
BYD468	<i>cwlO::cat</i> <i>amyE-P_{hy}-opt rbs-yisK (spec)</i> <i>yhdG-P_{hy}-opt rbs-yisK (phleo)</i>	This study
BYD476	<i>ftsEX::tet</i> <i>amyE-P_{hy}-opt rbs-yisK (spec)</i> <i>yhdG-P_{hy}-opt rbs-yisK (phleo)</i>	This study
BYD480	<i>kanΩmbl ΔponA ftsEX::tet</i> <i>amyE::P_{hy}-opt rbs-yisK (spec)</i> <i>yhdG::P_{hy}-opt rbs-yisK (phleo)</i>	This study

Table 3.1. Continued.

Strain	Description	Reference
BYD601	<i>yhdG:: P_{hy}-yisK E148A E150A D179A (phleo)</i>	This study
<i>E. coli</i> DH5α		
CAS54	<i>amyE::P_{xyl}-lytE-gfp (amp)</i>	This study
CAS72	<i>amyE::P_{xyl}-gfp-mreB (amp)</i>	This study
CYD784	<i>yisK-pET24b (kan)</i>	This study
CYD1191	<i>yhdG:: P_{hy}-yisK E148A E150A D179A (amp)</i>	This study
<i>E. coli</i> DHP1		
CYD394	<i>T25-rodZ (kan), mreB-T18 (amp)</i>	This study
CYD421	<i>T25-empty (kan), mreB-T18 (amp)</i>	This study
CYD422	<i>T25-rodZ (kan), empty-T18 (amp)</i>	This study
CYD439	<i>T25-rodZ (kan), mreB_{G143A}-T18 (amp)</i>	This study
CYD440	<i>T25-rodZ (kan), mreB_{R282S}-T18 (amp)</i>	This study
CYD441	<i>T25-rodZ (kan), mreB_{S154R}-T18 (amp)</i>	This study
CYD442	<i>T25-rodZ (kan), mreB_{P147R}-T18 (amp)</i>	This study
CYD443	<i>T25-rodZ (kan), mreB_{N145D}-T18 (amp)</i>	This study
CYD444	<i>T25-empty (kan), mreB_{G143A}-T18 (amp)</i>	This study
CYD445	<i>T25-empty (kan), mreB_{R282S}-T18 (amp)</i>	This study
CYD446	<i>T25-empty (kan), mreB_{S154R}-T18 (amp)</i>	This study
CYD447	<i>T25-empty (kan), mreB_{P147R}-T18 (amp)</i>	This study
CYD448	<i>T25-empty (kan), mreB_{N145D}-T18 (amp)</i>	This study
CYD599	<i>empty-T25 (kan), yisK-T18 (amp)</i>	This study
CYD600	<i>T25-empty (kan), yisK-T18 (amp)</i>	This study
CYD962	<i>ftsE-T25 (kan), yisK-T18 (amp)</i>	This study
CYD966	<i>yisK-T25 (kan), ftsX-T18 (amp)</i>	This study
CYD967	<i>yisK-T25 (kan), T18-ftsX (amp)</i>	This study
CYD968	<i>T25-yisK (kan), ftsX-T18 (amp)</i>	This study
CYD969	<i>T25-yisK (kan), T18-ftsX (amp)</i>	This study
CYD970	<i>ftsX-T25 (kan), yisK-T18 (amp)</i>	This study
CYD971	<i>ftsX-T25 (kan), T18-yisK (amp)</i>	This study
CYD972	<i>T25-ftsX (kan), yisK-T18 (amp)</i>	This study
CYD973	<i>T25-ftsX (kan), T18-yisK (amp)</i>	This study
CYD974	<i>yisK-T25 (kan), ftsEX-T18 (amp)</i>	This study
CYD982	<i>yisK-T25 (kan), empty-T18 (amp)</i>	This study
CYD984	<i>empty-T25 (kan), yisK-T18 (amp)</i>	This study
CYD985	<i>ftsE-T25 (kan), empty-T18 (amp)</i>	This study
CYD986	<i>empty-T25 (kan), ftsEX-T18 (amp)</i>	This study
CYD 1080	<i>yisK-T25 (kan), yisK-T18 (amp)</i>	This study

Table 3.1. Continued.

Strain	Description	Reference
CYD 1081	<i>yisK-T25 (kan), T18-yisK (amp)</i>	This study
CYD 1082	<i>T25-yisK (kan), yisK-T18(amp)</i>	This study
CYD 1083	<i>T25-yisK (kan), T18-yisK (amp)</i>	This study
CYD 1084	<i>yisK-T25 (kan), T18-empty (amp)</i>	This study
CYD 1085	<i>empty-T25 (kan), T18-yisK (amp)</i>	This study
CYD 1086	<i>T25-yisK (kan), T18-empty (amp)</i>	This study
CYD 1087	<i>T25-empty (kan), T18-yisK (amp)</i>	This study

Table 3.2. Plasmids used in Chapter III.

Plasmid	Description	Reference
pAS048	<i>amyE::P_{xyl}-gfp-mreB (amp)</i>	This study
pAS038	<i>amyE::P_{xyl}-lytE-gfp (amp)</i>	This study
pCH363	<i>empty-T18 (amp)</i>	Tom Bernhardt
pCH364	<i>T18-empty (amp)</i>	Tom Bernhardt
pKNT25	<i>empty-T25 (kan)</i>	Tom Bernhardt
pKT25	<i>T25-empty (kan)</i>	Tom Bernhardt
pMarA	<i>TnYLB-1 (kan), mariner-Himar1 (erm) (amp)</i>	
pYD104	<i>yisK-pET24b (kan)</i>	This study
pYD203	<i>T25-mreB (kan)</i>	This study
pYD204	<i>mreB-T25 (kan)</i>	This study
pYD205	<i>T18-mreB (amp)</i>	This study
pYD206	<i>mreB-T18 (amp)</i>	This study
pYD207	<i>rodZ-T18 (amp)</i>	This study
pYD208	<i>T18-rodZ (amp)</i>	This study
pYD209	<i>rodZ-T25 (kan)</i>	This study
pYD210	<i>T25-rodZ (kan)</i>	This study
pYD211	<i>mreB_{G143A}-T18 (amp)</i>	This study
pYD212	<i>mreB_{R282S}-T18 (amp)</i>	This study
pYD213	<i>mreB_{S154R}-T18 (amp)</i>	This study
pYD214	<i>mreB_{P147R}-T18 (amp)</i>	This study
pYD215	<i>mreB_{N145D}-T18 (amp)</i>	This study
pYD216	<i>yisK-T18 (amp)</i>	This study
pYD217	<i>T18-yisK (amp)</i>	This study
pYD218	<i>yisK-T25 (kan)</i>	This study
pYD219	<i>T25-yisK (kan)</i>	This study
pYD220	<i>ftsE-T25 (kan)</i>	This study
pYD221	<i>ftsX-T25 (kan)</i>	This study
pYD222	<i>T25-ftsX (kan)</i>	This study
pYD223	<i>ftsX-T18 (amp)</i>	This study
pYD224	<i>T18-ftsX (amp)</i>	This study
pYD225	<i>ftsEX-T18 (amp)</i>	This study
pYD1191	<i>yhdG:: P_{hy}-yisK E148A E150A D179A (amp)</i>	This study

Table 3.3. Oligonucleotides used in Chapter III.

Oligo	Sequence 5' to 3'
OAS247	CTTCGTATAGCATACATTATACGAACGGTATAATAAATATGAC AAGGGCCTTCT
OAS248	TCATCCGTCTGAAGCACAC
OAS251	TACCGTTCGTATAGCATACATTATACGAAGTTATCATACGGCA ATAGTTACCCTTAT
OAS252	TACCGTTCGTATAATGTATGCTATACGAAGTTATGGAGCTGTA ATATAAAAACCTTC
OAS253	TACCGTTCGTATAGCATACATTATACGAAGTTATGATTTTATG ACCGATGATGAAGA
OAS254	TACCGTTCGTATAATGTATGCTATACGAAGTTATAACTCTCTC CCAAAGTTGATC
OAS255	ATCGGAGAGCATTGGAAGAAA
OAS256	ATAACTTCGTATAATGTATGCTATACGAACGGTAATCATGAAA TCACCTAATCTTTTA
OAS257	ATAACTTCGTATAGCATACATTATACGAACGGTATAAAGTGA AAAAGCCGTTCCGT
OAS258	TTTAATGTCTCTGCAGTGCGA
OYD206	CATTGCATGCGTAACACACAGGAAACAGCTATGATGTTATCC GTGTTTAAAAAG
OYD207	GCATGGATCCGAACCGCTACCTGTCGTTTGTACAATCAGACG
OYD208	GCATGGATCCGGGCAGCGGTATGATGTTATCCGTGTTTAAAA AG
OYD209	GCATGAATTCTTATGTCGTTTGTACAATCAGACG
OYD210	CATTGCATGCGTAACACACAGGAAACAGCTATGTTTGAATT GGTGCTAGAG
OYD211	GCATGGATCCGAACCGCTACCTCTAGTTTTCCCTTTGAAAAGA TG
OYD212	GCATGGATCCGGGCAGCGGTATGTTTGAATTGGTGCTAGAG
OYD213	GCATGAATTCTTATCTAGTTTTCCCTTTGAAAAG
OYD245	AGAAGCGGCCGCTTATTCTG
OYD246	CTTCGTATAATGTATGCTATACGAACGGTACTCACTTTTATA TCCTCCCTTTTAC
OYD266	GCATGGATCCGTAACACACAGGAAACAGCTATGTCATTGGAT GATCTCCAAG
OYD267	GCATGAATTTCGAACCGCTACCAGATGACTTTTCTTCCTTTTAT TT
OYD268	GCATGGATCCGGGCAGCGGTATGTCATTGGATGATCTCCAAG
OYD269	GCATGAATTCTTAAGATGACTTTTCTTCCTTTTATT
OYD298	GCATGGATCCGTAACACACAGGAAACAGCTATGAAATTTGCG ACAGGGGAAC

Table 3.3. Continued.

Oligo	Sequence 5' to 3'
OYD299	GCATGAATTTCGAACCGCTACCGCCAATTTGGTTTGACAGCGTT
OYD300	GCATGGATCCGGGCAGCGGTATGAAATTTGCGACAGGGGAAC
OYD301	GCATGAATTCTTAGCCAATTTGGTTTGACAGCGTT
OYD475	GCATGGATCCGTAACACACAGGAAACAGCTATGATAGAGATG AAGGAAGTATAT
OYD476	GCATGAATTTCGAACCGCTACCATCATATGAACCATACTCCC
OYD479	GCATGGATCCGTAACACACAGGAAACAGCTATGATTAATAATT CTCGGGCGC
OYD480	GCATGAATTTCGAACCGCTACCTACTCGCAGAACTTGCGGA
OYD481	GCATGGATCCGGGCAGCGGTATGATTAATAATTCTCGGGCGC
OYD482	GCATGAATTCTTATACTCGCAGAACTTGCGGA

Western blot analysis

One mL or 200 μ L *B. subtilis* cells were pelleted at 8,000 rpm for 1 min on an Eppendorf Tabletop Centrifuge and resuspended to an OD₆₀₀ of 12.0 in *Bacillus* lysis buffer (20 mM Tris pH 7.5, 1 mM EDTA). For cultures grown in resuspension medium, the lysis buffer contained 10 mM EDTA. To the lysis buffer base, 10 mM MgCl₂ (not added to resuspension media lysis buffer), 1.0 mg/mL lysozyme, 1.0 μ L/mL protease inhibitor cocktail (Sigma), 10 μ g/mL DNaseI, 100 μ g/mL RNaseA was added. Samples were incubated for 10 min at 37°C. Twenty μ L of sample was then transferred to 20 μ L 2X SDS-PAGE loading buffer with β -mercaptoethanol (BME) and immediately boiled for 8 min, then placed on ice. Ten μ L of this was loaded on a (9 cm X 10 cm 16 lane) 4-20% Lonza Gold Precast Tris-Glycine SDS-PAGE gel and run for 10min at 80 V followed by 200 V until dye front at bottom edge of gel. Proteins were transferred to a PVDF membrane (Pall) at 100 V for one hr at room temperature in Towbin transfer buffer. The membranes were blocked for 1 hr with 1X PBS-0.05% (v/v) Tween20 containing 5% non-fat powdered milk. The membranes were then washed three times for 5 min each at room temperature with 1X PBS-0.05% (v/v) Tween20, then incubated overnight on an agitator at 4°C with rabbit α -YisK polyclonal primary antibody (serum) at a 1:10,000 dilution in 1X PBS-0.05% (v/v) Tween20 containing 5% non-fat powdered milk on an agitator. The following day (~16 hrs) the membranes were washed three times for 5 min with 1X PBS-0.05% (v/v) Tween20. The membranes were then incubated on an agitator with goat α -rabbit Horse Radish Peroxidase secondary antibody (Rockland) at a 1:10,000 dilution in 1X PBS-0.05% (v/v)

Tween20 containing 5% non-fat powdered milk for 1 hr at room temperature. The membrane was washed three times as described above and incubated with Pierce Supersignal West Femto Maximum Sensitivity Substrate according to manufacturers directions and captured image with an Amersham Imager 600 (GE).

Beta-galactosidase assay of transcriptional fusion

Beta-galactosidase assays were performed as described in Chapter II.

Protein expression and purification

pYD 104 yisK-pET24b (kan) was transformed into competent BL21 λ DE3 cells, plated on LB Lennox solid media supplemented with kanamycin (25 μ g/mL final), and incubated overnight at 37°C. Colonies were scraped off of the plate and resuspended in 3mL of Cinnibar media. This media was used to inoculate a 25mL Cinnibar culture at OD₆₀₀ = 0.1 in 250mL baffled flask with 0.1% glucose (w/v) shaken at 37°C until culture reached OD₆₀₀ of ~5. The culture was shifted to 16°C and then induced with 1.0mM IPTG overnight (~16 hrs). The cells were pelleted at 12,000 X g for 10 min at 4°C. The pellet was resuspended in 30 mL lysis buffer (50.0 mM Tris-HCl pH 8.0, 300 mM NaCl, 10.0 mM imidazole, 200 μ g/mL lysozyme, 10 μ g/mL DNase, 1 μ L per 35 OD*mL protease inhibitor cocktail) and lysed using a LM20 Microfluidizer (Microfluidics) at 20,000 psi. Cell debris was removed by centrifugation at 14,000 X g for 20 min at 4°C. The supernatant was collected and passed over a 1 mL bed volume NiNTA Sepharose resin (Qiagen), washed with 10 mL of wash buffer (50.0 mM Tris-

HCl pH 8.0, 300 mM NaCl, 25.0 mM imidazole). The protein was eluted with 2 x 0.5 mL of elution buffer (50.0 mM Tris-HCl pH 8.0, 300 mM NaCl) containing 100mM imidazole, followed by 3 x 0.5 mL of elution buffer containing 200 mM imidazole, followed by 3 x 0.5 mL of elution buffer containing 250 mM imidazole, followed by 4 x 0.5 mL of elution buffer containing 500 mM imidazole. Fractions 3-10 were pooled and then dialyzed against either 50.0 mM Tris-HCl pH 7.5, 100 mM KCl, 15% glycerol, 2.0 mM Dithiothreitol (DTT) for use in ATPase assays or 20.0 mM Hepes pH 7.5, 150 mM NaCl, 15% glycerol, 2.0 mM DTT for use in Thermal Shift Assays. Protein specifically purified for crystallization was dialyzed against 50.0 mM Tris-HCl pH 7.5, 1.0 mM DTT.

YisK crystallization

586 separate crystallization conditions were screened by 96 well plate method using a TPP LabTech Mosquito LCP machine. The highest quality initial conditions were obtained in 60% Tascimate (Hampton Research) pH 7.5, and 10% Tascimate (Hampton Research) pH 5.0, 20% poly(ethylene glycol) 2000 with divalent cations. Optimized conditions were 60% Tascimate, pH 7.0, 100mM MnCl₂ with crystallization by hanging drop method. YisK-His was 12 mg/mL concentration (by Bradford method) in 50.0 mM Tris pH 7.5, 1 mM DTT and set in a 1:1 ratio and 2:1 ratio with mother liquor (60% Tascimate pH 7.0, 100 mM MnCl₂). Total volume of drops was 2 µL and 3 µL respectively spotted on glass circular disk and suspended (sealed) on crystallization plate. Crystals that formed were sent to synchrotron for data collection.

Differential scanning fluorimetry

Differential Scanning Fluorimetry was performed as previously (311-313), with minor modifications. A master mix of 10.0 μ M YisK-His in 20.0 mM Hepes pH 7.5, 150 mM NaCl, 5.0 mM $MnCl_2$ was made with 5X Sypro Orange (Note: the 5000X Sypro Orange is added to the buffer of the master mix before YisK-His to avoid possible effects of the concentrated solvent that the Sypro Orange dissolved in). Thirty-nine microliters of this master mix was aliquoted into each well on a BioRad Hard-Shell PCR Plates, 96-well format, thin wall (HSP9601). To each well either 1 μ L of reaction buffer alone (20.0 mM Hepes pH 7.5, 150 mM NaCl) or 1 μ L of each compound being tested (stock concentrations of either 4.0 mM or 40.0 mM in reaction buffer) were added to give a final substrate/compound concentration either 100 μ M or 1000 μ M. Reactions were mixed by pipetting up and down after adding compound. The PCR plate was then sealed with BioRad Microseal 'B' seal (MSB1001), and centrifuged at 1000 x g for 3 min in a centrifuge equipped with a plate adaptor at RT (to remove bubbles). The plate was placed in a CFX96 Touch Real Time PCR machine running a custom thermal shift program. The specifications of the program were as follows: initial temperature, 25°C ramped to 95°C with a ramp time of 0.5°C/min. The FRET channel (X nm) was scanned at each temperature increase. The final data was analyzed using BioRad CFX Manager, and the derivative of the melting curve was used to determine the melting temperature of YisK in all assayed conditions.

Redundant factor screen

Transposon mutagenesis of a *ΔyodL ΔyisK* strain and subsequent redundant factor screening was performed as previously described (Duan and Herman, Appendix III, Dissertation).

B. subtilis metabolomics on ΔyisK and wild type

Strains 168WT and BYD 278 *ΔyisK* were streaked on LB Lennox solid medium and place at 37°C overnight (~16 hr). Cells from single colonies were used to inoculate 5 mL CH medium and cultures were placed in roller drum overnight at room temperature (~16 hr). When cells reached an OD₆₀₀ of between 0.4 and 0.7, the pre-culture was used to inoculate a 250 mL baffled flask containing 25 mL CH to a final OD₆₀₀ of 0.00625. Flasks were placed in a 37°C shaking waterbath rotating at 280 rpm until an OD₆₀₀ of ~4 (maximal expression of YisK by Western blot analysis). The volume of each culture was recorded and cells were immediately transferred to a 50 mL Falcon tube and quickly cooled by swirling tube in liquid N₂ for about 10 sec, being careful not to freeze the sample. The final temperature of the culture should be ~9°C. A reusable plastic filter system with 45 mm neck fitted with a 47 mm membrane (Pall Life Sciences 0.45 μm Metrical Membrane Filter), was attached to a 500 mL glass bottle with 45 mm neck, and entire setup was chilled for 10 min at -20°C. Two and a half mL of the OD₆₀₀ = 4 cells were applied to the filter and washed two times with 2.5 mL of 0.9% NaCl solution (filter sterilized) that was previously chilled at 4°C for 30min. The filter (and cells) was removed from the filtration device using sterile tweezers, and added to 5mL of ice-cold

1:3:1 chloroform : methanol : ddH₂O in a 50 mL conical tube. The entire tube, including the filter, was flash-frozen in liquid N₂ and stored at -80°C until further processing.

Sample processing

Samples were removed from the -80°C and placed on an ice water bath. Ten microliters of 1.0 mM 1,4 ¹³C₂ Succinate (Cambridge Isotope Labs) standard was pipetted into the solvent in which each filter was submerged. The conicals were shaken (2 sec) then vortexed manually (5 sec max setting), cooled for 5 sec on ice, and the process was repeated ten times. Each sample was then split into 5 separate brown-capped Precellys tubes (Precellys Lysing Kit Soil Grinding SK 38 Product number: KT03961-1-006.2) and shaken for 2 cycles at 30 sec each cycle at 6,800 rpm in the Precellys 24 bead mill homogenizer, chilling samples on ice for 2 min in between cycles. The contents of the tubes (lysed cells) were transferred to a new pre-chilled 1.5 mL microfuge tube and cell debris was removed by centrifuging the samples for 5 min at 21,130 x g in a 4°C tabletop microcentrifuge. The aqueous phases (top) were transferred to new pre-chilled 1.5 mL microfuge tubes using a 23 gauge needle attached to a 10 mL syringe, taking care to avoid the interface. The samples were then centrifuged for 2 min at 21,130 x g in a 4°C tabletop microcentrifuge to remove any residual cell debris. The supernatants for each sample (5 tubes total) were then transferred to a single pre-chilled 50 mL conical tube using a 23 gauge syringe. 0.5 mL of the sample was transferred to a 3 kDa molecular weight cutoff Amicon Ultra concentrator and the sample was centrifuged at 14,000 x g at 4°C for 30 min. This step removes protein and other

macromolecular contaminants which interfere with the sample's signal. The remaining (unfiltered) sample was frozen under Argon gas at -80°C . After 30 min centrifugation, approximately $300\mu\text{L}$ passes through the concentrator. This flowthrough is transferred to 9 mL of ice cold ddH₂O, flash frozen in liquid N₂, and then lyophilized overnight (~20 hr). The lyophilized sample is then resuspended in $120\mu\text{L}$ of 1:1 methanol : water (HPLC grade Ultrapure) by pipetting up and down, including along the side of the tube. The introduction of bubbles should be avoided. The resuspended material is centrifuged at 4°C at $3,220 \times g$ for 2 min to bring all liquid to the bottom of the tube, and then filtered through a nylon filter (MicroScience Microspin filter, Nylon, CINY02) by centrifuging at $10,000 \times g$ for 2 min at 4°C . The remaining sample (~ $100\mu\text{L}$) is transferred to an HPLC container fitted with a small volume insert and frozen at -80°C until the sample is run.

Sample run

Untargeted liquid chromatography high resolution accurate mass spectrometry (LC-HRAM) analysis was performed on a Q Exactive Plus orbitrap mass spectrometer (Thermo Scientific, Waltham, MA) coupled to a binary pump HPLC (UltiMate 3000, Thermo Scientific). For acquisition the Sheath, Aux and Sweep gasses were set at 50, 15 and 1 respectively. The spray voltage was set to 3.8 kV (Pos) or 2.8 kV (Neg) and the S-lens RF was set to 50. The source and capillary temperatures were maintained at 350°C and 350°C respectively. Full MS spectra were obtained at 70,000 resolution (200 m/z) with a scan range of 50-750 m/z . Full MS followed by ddMS2 scans were obtained at

35,000 resolution (MS1) and 17,500 resolution (MS2) with a 1.5 m/z isolation window and a stepped NCE (20, 40, 60). Samples were maintained at 4 °C before injection. The injection volume was 10 µL. Chromatographic separation was achieved on a Synergi Fusion 4 µm, 150 mm x 2 mm reverse phase column (Phenomenex, Torrance, CA) maintained at 25 °C using a solvent gradient method. Solvent A was water (0.1% formic acid). Solvent B was methanol (0.1% formic acid). The gradient method used was 0-5 min (10% B to 40% B), 5-7 min (40% B to 95% B), 7-9 min (95% B), 9-9.1 min (95% B to 10% B), 9.1-13 min (10% B). The flow rate was 0.4 mL min⁻¹. Sample acquisition was performed Xcalibur (Thermo Scientific). Data analysis was performed with Compound Discoverer 2.1 (Thermo Scientific).

YisK pull-down assay

Cell growth, protoplasting, and osmotic lysis.

Two 25 mL cultures of BYD 74 P_{hy}-YisK (2X) (see methods in Chapter II) and one 25 mL culture of BYD 278 Δ *yisK* were started at OD₆₀₀ = 0.00625 in LB-Lennox liquid media from exponentially growing 5 mL cultures. BYD 74 was induced at OD₆₀₀ ~0.2 for 20 min with 1.0 mM IPTG before pelleting at 3,000 x g for 10 min. Cell pellet was washed twice with 12.5 mL of 1X SMM (1.0 M sucrose, 40.0 mM maleic acid, 40.0 mM MgCl₂, pH 6.5) followed by resuspension in 2.5 mL of 1X SMM. Lysozyme was then added to the cells to 2 mg/mL final concentration, followed gentle agitation for ~10 min, after which time additional lysozyme was added to 4 mg/mL final concentration and the culture was gently agitated another 10 min to complete protoplasting. Protoplasts

were then pelleted at 3,000 x g in an Eppendorf tabletop centrifuge followed by discarding supernatant and flash freezing the cell pellet in liquid N₂. Protoplast pellet was osmotically lysed on ice by resuspending pellet in 0.75 mL cold buffer H (20.0 mM Hepes pH 8.0, 200 mM NaCl, 1 mM DTT, 1 mM MgCl₂, 1 mM CaCl₂) with DNaseI and RNaseA added to 10 µg/mL and 100 µg/mL final concentrations, respectively. Protoplasts were incubated on ice for 1 hr, vortexing every 15 min. Following incubation, pull-down was performed. The second BYD 74 culture was not induced, and was grown to OD₆₀₀ ~0.5 before protoplasting and osmotic lysis was performed as described above. BYD 278 was also grown to OD₆₀₀ ~0.5 and protoplasting and osmotic lysis was performed as described above.

Pull-down

Fifty µL aliquots of Dynabeads-Protein A resin slurry were added to Eppendorf tubes and washed with 1X PBS, as stated in manufacturers instructions (Invitrogen). Ten µL of α-YisK serum was added to Dynabeads-Protein A resin that was resuspended in 200µL of 1X PBS, and samples were incubated with rotation for 10 min at room temperature, after which samples were placed on magnet rack for 1 min and supernatant was removed. α-YisK bound Dynabeads-Protein A were washed three times by resuspending the resin in 200 µL of 1X PBS followed by mixing gently and placing samples back on the magnet rack, followed by removal of the supernatant. α-YisK bound resin was resuspended in 1 mL of lysed protoplasts, followed by incubation for 20 min with rotation at room temperature. Samples were placed on a magnet rack for 1

minute, followed by removal of the supernatant. Samples were then washed three times with 200 μ L of 1X PBS as previously stated. Sample bound resin were resuspended in 100 μ L 1X PBS and transferred to fresh Eppendorf tubes and placed on magnet rack for 1 min. The supernatant was removed, and proteins were eluted by adding 20 μ L of elution buffer (200 mM glycine pH 2.2), incubation for 2 min at room temperature followed by placing samples on magnet rack for 1 min and removing the supernatant, which contained eluted proteins. This supernatant was added to equal volume 2x SDS-PAGE buffer (see methods, Chapter III), followed by boiling the samples for 8 min and loading 10 μ L on a 4-20% Lonza Gold Tris-Glycine gel and running the gel as previously stated (see methods, Chapter III). Gel was stained with Sypro Ruby (Invitrogen) and imaged according to manufacturers instructions.

Results

Effect of YisK and YodL on Mbl and MreB localization

Mbl is required for YisK to perturb cell shape during misexpression, which raises the question: Does YisK affect Mbl localization? To address this question, I expressed YisK in a strain background harboring a chromosomal, xylose-inducible copy of Mbl-GFP. Before induction, Mbl-GFP expressed at non-saturating levels of xylose is observed as forming punctate foci distributed in a helical pattern along the lateral cell wall. In contrast, when YisK was expressed the punctate-helical pattern of Mbl-GFP was lost, and instead cytoplasmic and midcell Mbl-GFP localization was observed. In addition, cells became wider and lost their overall rod shape (Fig 3.1A). If Mbl-GFP was

induced with saturating levels of xylose, the Mbl-GFP signal was more distinct, and YisK expression no longer caused an obvious shape defect. However, the punctate-helical localization was not completely rescued (Fig 3.1B). These results suggest that YisK perturbs Mbl-GFP localization either directly or indirectly and that providing cells with extra copies of Mbl-GFP can partially suppress YisK activity. Consistent with this interpretation, addition of an additional YisK misexpression cassette in the chromosome abolished this partial rescue.

Although most of the YisK-resistant suppressor mutations we identified were found in *mbl*, we also identified *mreB* mutations that conferred resistance to YisK expression (Table 2.5). To determine if YisK specifically perturbed Mbl localization or if it might also affect MreB, I expressed YisK in a strain background harboring a chromosomal, xylose-inducible copy of MreB-GFP. Before induction, MreB-GFP expressed at non-saturating levels of xylose is observed as forming punctate foci distributed in a helical pattern along the lateral cell wall. In contrast, when YisK was expressed the punctate-helical pattern of MreB-GFP was lost, and instead cytoplasmic MreB-GFP localization was observed. Cells also became wider and lost their overall rod shape (Fig 3.1C). This result demonstrates that YisK changes MreB localization, even though MreB is not required for YisK activity (Fig 2.6). Since YisK non-specifically perturbed MreB function, this raised the question is YisK perturbing MreBH localization? Localization of the PG hydrolase LytE is dependent on MreBH (65), so we used LytE-GFP as a proxy to investigate perturbations in MreBH activity or localization. The expectation was that if MreBH activity or localization was perturbed, LytE-GFP

would no longer be properly localized. YisK misexpression results in a delocalization of LytE (Fig 3.2), which is evidence that the colocalized patches of MreB-like proteins are being disturbed upon YisK expression. LytE-GFP is also delocalized following expression of YodL (see Chapter II) (Fig 3.2). In order to determine if the delocalization of MreB and MreBH also required Mbl, we attempted to visualize MreB-GFP in the *mbl* knockout. However, even the strain lacking YisK was not healthy and showed aberrant shape, suggesting that MreB-GFP is not fully functional (data not shown).

Since localization of a protein can give insight into its function, I attempted to label YodL and YisK with fluorescent tags at either the N or C-terminus of the proteins. We tested the functionality of the fluorescently tagged proteins by determining if the fusions could still prevent growth on solid media following induction and/or induce cell widening when induced in liquid culture. Unfortunately, none of the tags were functional (data not shown).

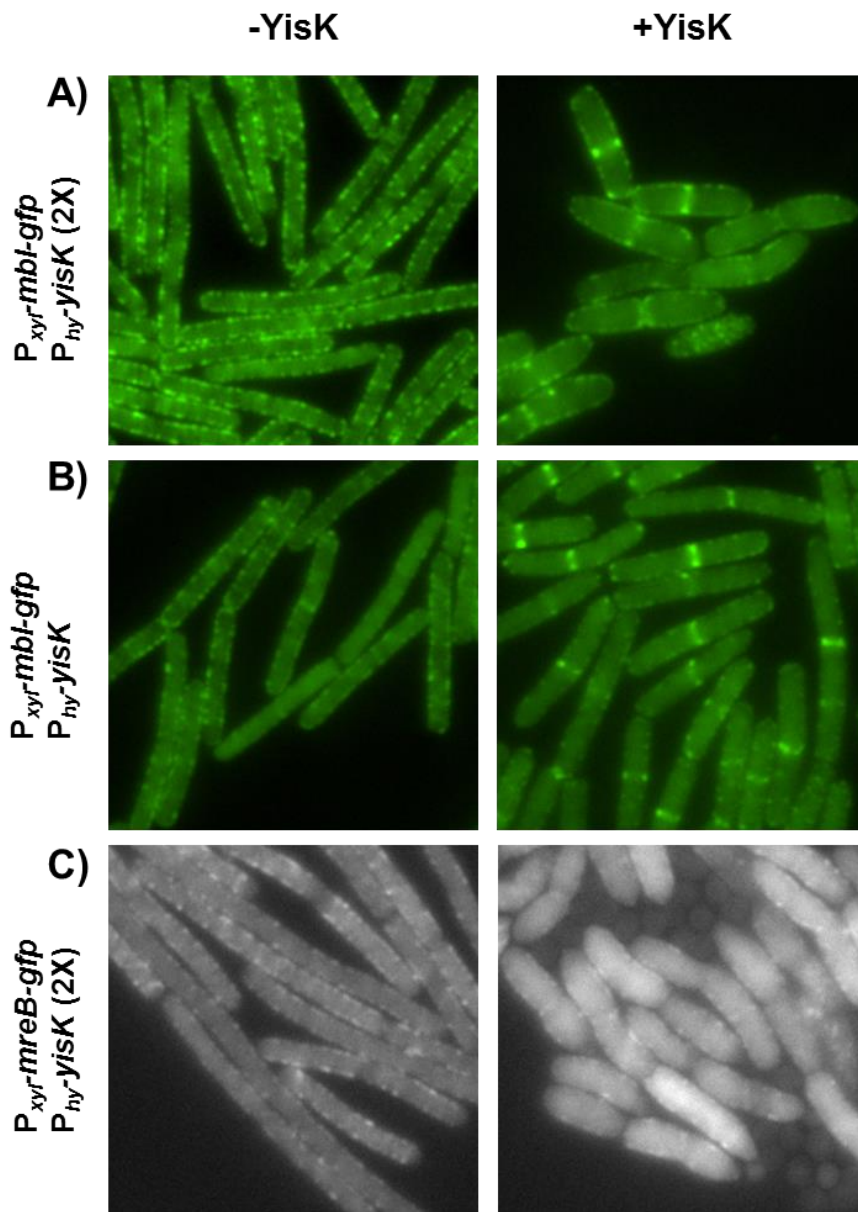


Figure 3.1. YisK perturbs Mbl-GFP localization and MreB-GFP localization during misexpression. A) Mbl-GFP was induced with 10 mM xylose for 60 min before 2X *yisK* was induced with 1 mM IPTG (during exponential growth) for 60 min. Images were taken on a 1% agarose pad. B) *mbl-gfp* induced with 33.3 mM xylose for 60 min before *yisK* induced with 1 mM IPTG (during exponential growth) for 60 min and images were taken on 1% Agarose pad. C) *mreB-gfp* was induced for 60 min with 5 mM xylose before 2X *yisK* induced with 1 mM IPTG (during exponential growth) for 60 min and images taken on 1% CH Agarose pad with open back.

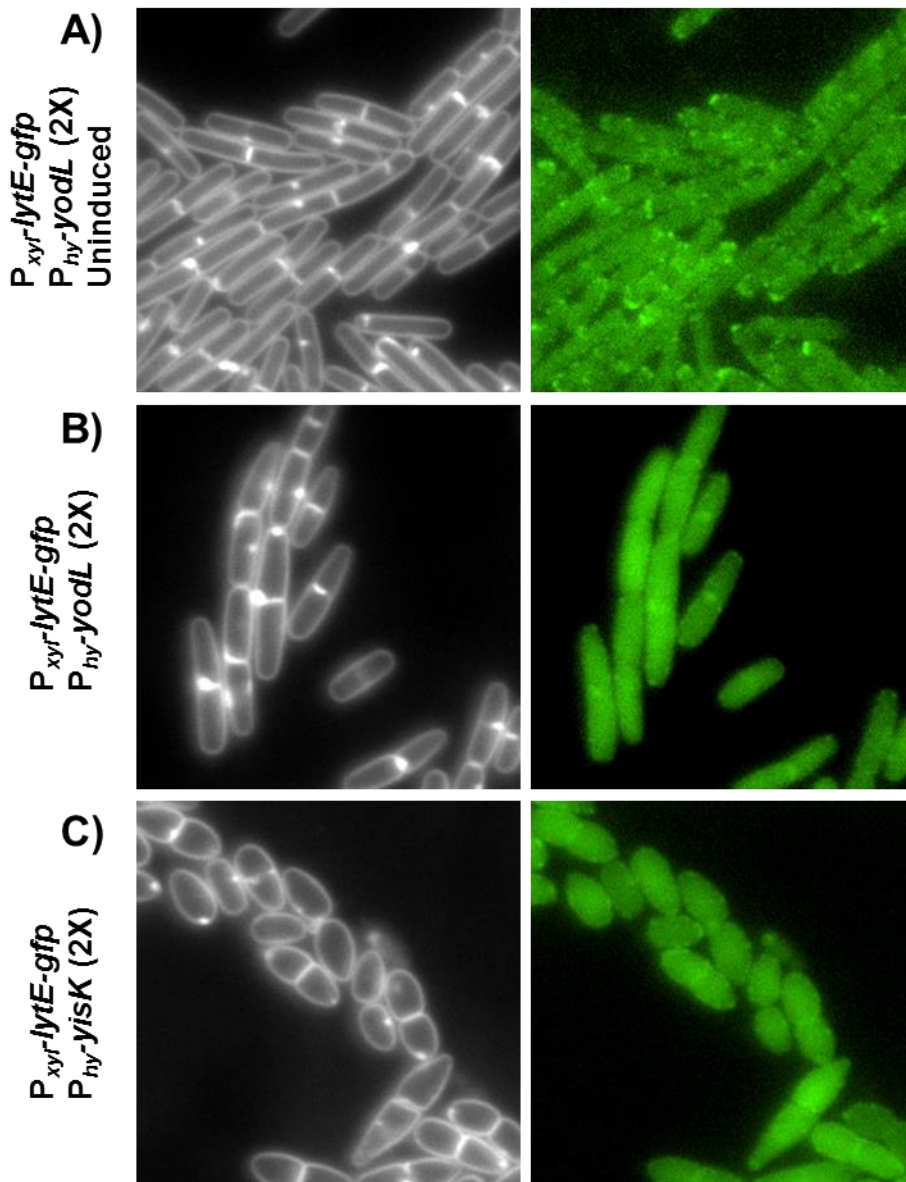


Figure 3.2. YisK and YodL perturb LytE-GFP localization. A) LytE-GFP expression was induced for with 10 mM xylose. B) LytE-GFP expression was induced for with 10 mM xylose, followed by 90 min YodL induction with 1 mM IPTG. C) LytE-GFP expression was induced for with 10 mM xylose, followed by 90 min induction of YisK with 1 mM IPTG. Membranes (white) were stained with TMA-DPH.

YisK expression profiling

Based on transcriptional profiling, *yisK* is a stationary phase protein (283) that also appears to be repressed by Spo0A early in sporulation (similar to the regulation of *kinA*) (Fig. 2.4, Chapter II). This expression pattern is consistent with our observation that YisK possesses a putative Spo0A box that overlaps with the -10 region of the SigH promoter (Fig 3.3A) (35). However, since transcription does not always correlate with protein abundance we investigated the levels of YisK protein present across different stages of growth (exponential, transition, stationary phase, and sporulation) using western blot analysis (Fig. 3.3). Samples were collected over a timecourse in CH medium, where cells can naturally transition through the growth phases mentioned above. Analysis of YisK during the CH timecourse showed peak expression during stationary phase (~ 180 min to 270 min), and protein levels tapering off as the cells underwent sporulation (~OD₆₀₀ 6.88) (Fig 3.3C). To estimate if YisK is present in high or low copy number in the cell, 10 ng of pure YisK-His was loaded alongside the samples. These results suggest that even at maximal levels, the copy number of YisK is less than 300 copies/cell (data not shown). This result is consistent with other data suggesting YisK is an enzyme (more below).

A strain harboring a mutant Spo0A box (0A box mutant) appeared to show a slight delay in YisK accumulation during the timecourse, as well as a slight delay in the steady state protein levels as cells sporulated (Fig 3.3C). These results were repeatable with independent biological replicates. However, the observation should be interpreted with caution, as the samples are not on the same membrane. It is possible that the levels

of YisK are higher in general throughout the experiment in the OA mutant, and that if the samples were on the same blot, the levels would be just as high (or higher) at the earlier timepoints. This possibility will be tested in the future.

Since the transitions between the growth stages are not sharply defined in CH, the samples were also collected under sporulation by resuspension conditions, where cells rapidly transition from exponential phase to stationary phase then sporulation more synchronously. Similar to the CH timecourse, YisK levels increased through the stages of the timecourse corresponding to stationary phase/early sporulation, with levels dropping as sporulation proceeded. In the OA box mutant, YisK appeared to accumulate over a similar timecourse, but reached higher levels that stayed higher longer (these samples were on the same membrane and thus can be directly compared). These results are consistent with the hypothesis that *yisK* expression is repressed by Spo0A-P as sporulation progresses.

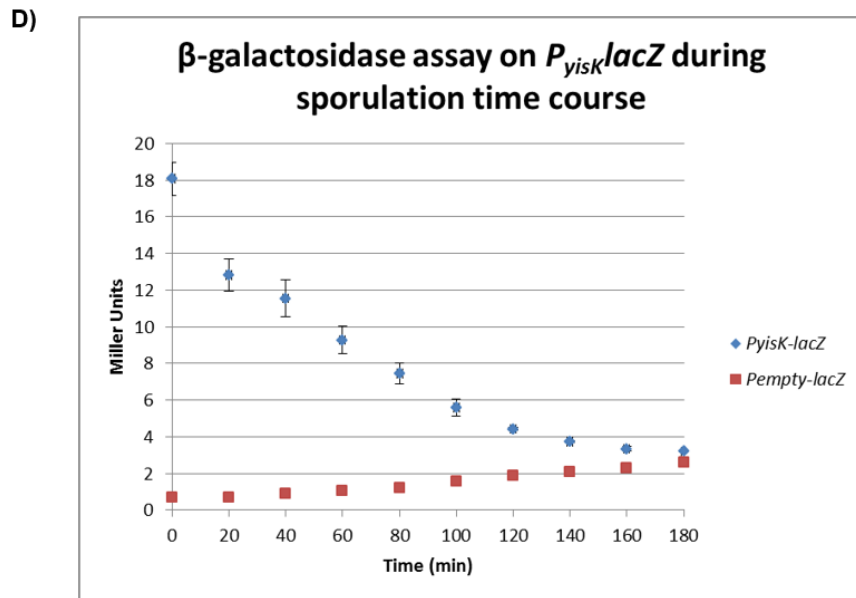
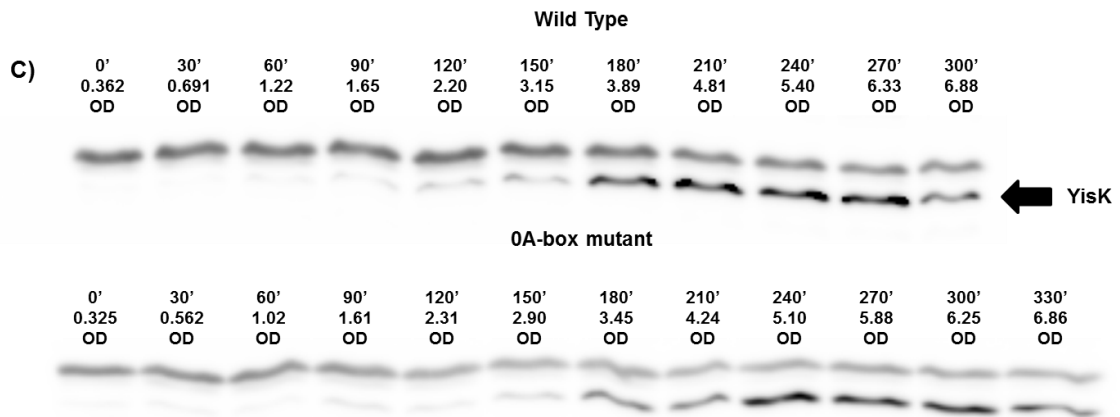


Figure 3.3. Continued.

YisK, in addition to causing Mbl-dependent cell widening, results in an Mbl-independent cell shortening phenotype, suggesting that YisK is capable of targeting one or more other factors involved in cell length control (Fig. 2.7, Chapter II). An obvious candidate is the ATP Binding Cassette (ABC) Transporter FtsEX. In this complex, FtsX is a membrane component, and FtsE is an associated cytoplasmic ATPase. In *B. subtilis*, FtsEX is required for function of the D,L-endopeptidase CwlO. CwlO is proposed to play a role in cleaving the PG crosslinking, allowing for the insertion of new PG during active growth (66, 69). FtsEX acts in the same genetic pathway as Mbl, and deletion mutants of *ftsE*, *ftsX*, or *cwlO* are shorter than wildtype (66). These observations led us to hypothesize that YisK might cause cell shortening by targeting the FtsEX complex. To test this hypothesis, we first tested if YisK interacted with FtsE (the cytoplasmic component of the transporter). A positive pairwise interaction between YisK and FtsE was observed that was absent in the negative controls (Fig 3.4)



Figure 3.4. Bacterial 2-hybrid of YisK and FtsE. Physical interaction results in production of beta-galactosidase and the subsequent blue color of the spot due to reaction of beta-galactosidase and X-Gal.

We next probed whether FtsEX was required for YisK-mediated effects on cell-shape. First, we tested if a $\Delta ftsEX$ mutant was still sensitive to YisK mediated cell widening and found that it was even more sensitive than wildtype to YisK activity (Fig 3.5A); similar results were obtained with a *cwI*O knockout (Fig 3.5B). These results suggest that YisK does not require FtsEX/CwI O to perturb Mbl function. The enhanced sensitivity of the *ftsEX* or *cwI*O knockout strains to YisK could suggest these backgrounds are more sensitive to perturbations in cell wall synthesis in general. Although we did not pursue this possibility further, it is consistent with current models suggesting FtsEX/CwI O function in PG synthesis (66, 69, 314). Alternatively, if YisK does disrupt any of the MreB-like proteins directly, it may be more free to do so in the absence of FtsEX.

To probe if YisK requires FtsEX for its cell shortening activity, we introduced the $\Delta ftsEX$ mutation into the $\Delta mbl \Delta ponA$ background. This background is resistant to YisK-dependent cell-widening, making cell length easier to quantitate. Before YisK induction, cells are already 20% shorter than wildtype due the $\Delta ftsEX$ deletion, consistent with prior observations that FtsEX function in cell length control (66). However, unlike the $\Delta mbl \Delta ponA$ only background (Fig 2.6, Chapter II), cells also lacking FtsEX did not become shortened following YisK misexpression (Table 3.4). In summary, our results suggest that YisK requires FtsEX, but not Mbl to cause cell shortening, and Mbl, but not FtsEX to cause cell widening (Fig 3.6).

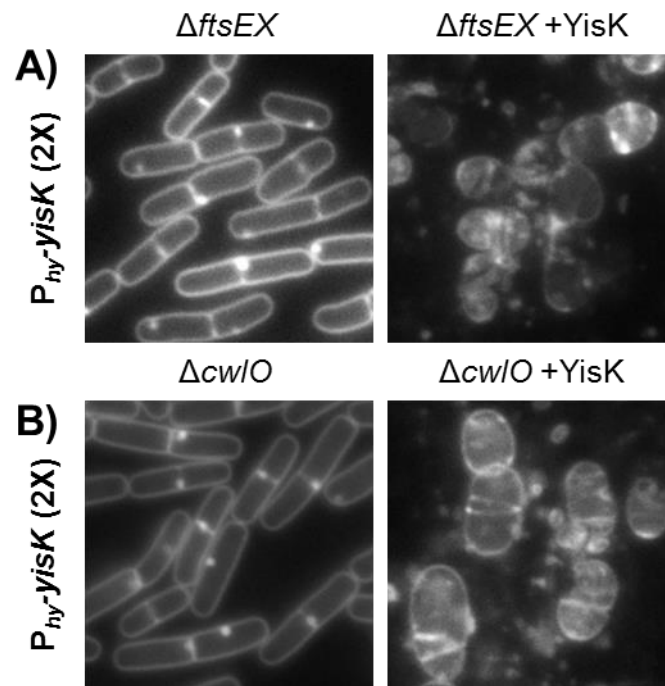


Figure 3.5. YisK does not require FtsEX or CwI0 for cell shape modifying activity. A) YisK was expressed for 90 min with 1.0 mM IPTG in the *ftsEX* knockout. B) YisK was expressed for 90 min with 1 mM IPTG in the *cwI0* knockout. Membranes were stained with TMA-DPH.

Table 3.4. *ftsEX* mutant resistant to YisK mediated cell shortening. YisK was misexpressed using 1.0 mM IPTG during exponential growth in liquid LB. Images were taken after 90 min and cell lengths (septum to septum) were quantitated for over 1000 cells from independent fields for each strain. The average cell length and standard deviation are shown.

Genotype (<i>ΔmbI ΔponA ΔftsEX</i> background)	Cell length (μm)
-YisK	2.4 (+/- 0.8)
+YisK	2.4 (+/- 0.8)

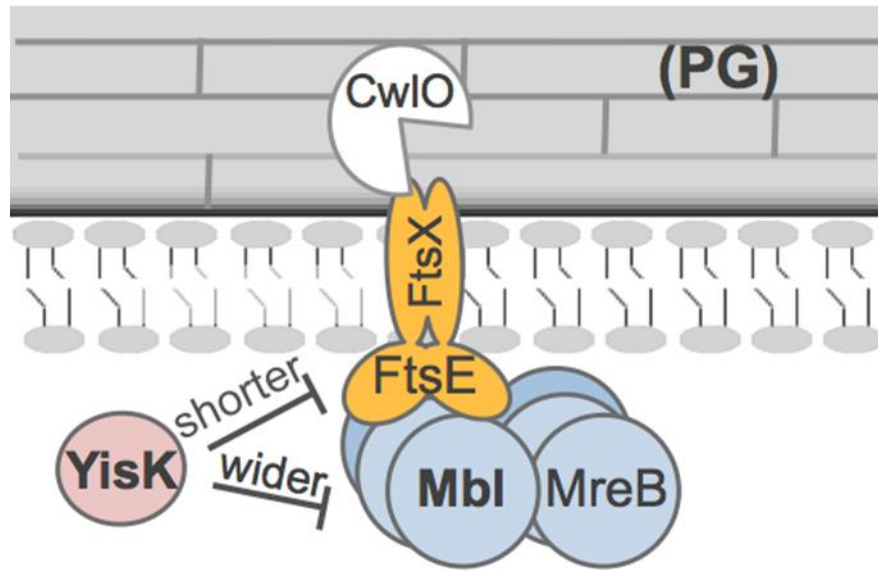


Figure 3.6. Model of interaction with components of the PG synthesis machinery. YisK mediates cell widening through an Mbl dependent process, and cell shortening through an FtsEX dependent process.

YodL-mediated cell widening does not require RodZ

MreB is required for YodL cell shape modifying activity during misexpression (Fig 2.6). Interestingly, most of the suppressors of YodL activity mapped to a region of MreB known to be important for RodZ binding (Fig 2.12, Table 2.6) (78, 79). This provoked the question, is YodL disturbing the MreB-RodZ interaction, and if so, is it interacting with MreB or RodZ? Although RodZ was previously thought to be essential in *E. coli* and *B. subtilis*, the essentiality in the former can be bypassed by mutations in *mreB* (77, 80) and our data suggest the apparent essentiality of the latter (260) can be attributed to polar effects on a downstream, essential gene, *pgsA*. We were able to successfully knock out *rodZ* by linking the deletion to an upstream resistance cassette as opposed to creating the deletion by introducing the cassette following the *rodZ* promoter.

With the $\Delta rodZ$ strain in hand, it was possible to test if RodZ was necessary for YodL's cell shape modifying activity. As shown in Figure 3.7, the $\Delta rodZ$ strain grows as a rod (albeit with some minicells – Duan and Herman, Appendix IV, Dissertation). Induction of *yodL* in the $\Delta rodZ$ mutant leads to rapid loss of cell shape and lysis, suggesting that RodZ is not required for YodL's affect on MreB. In fact, the cells were more highly sensitive to YodL misexpression, consistent with the idea that the *rodZ* knockout is more sensitive to perturbations in cell envelope synthesis. Since the YodL misexpression phenotype in wildtype (wide rods) (Fig. 2.1) does not phenocopy the $\Delta rodZ$ mutant, these results suggest that YodL is unlikely to act simply by disrupting the interaction between RodZ and MreB. Moreover, and consistent with the fact that we did

not identify and YodL-resistant suppressor mutations in *rodZ*, these results suggest YodL is unlikely to target RodZ directly.

We next sought to characterize the YodL-resistant MreB variants. Our genetic data suggest that YodL may perturb MreB function by interacting with the RodZ interaction interface (Fig. 2.12 and Fig. 2.6A, Chapter II). This interface appears to be important for the formation of stable MreB filaments, as RodZ targets this surface to increase the motion of MreB along the membrane (80). We can envision at least three ways the MreB variants might confer YodL resistance: 1) If RodZ and YodL compete for the same interaction surface of MreB, the variants could increase MreB's affinity for RodZ, allowing RodZ to outcompete YodL, 2) the variant may no longer effectively interact with YodL (and possibly RodZ) or 3) the variant could have increased capacity for MreB polymerization (general suppressor), making it more resistant to YodL's effects.

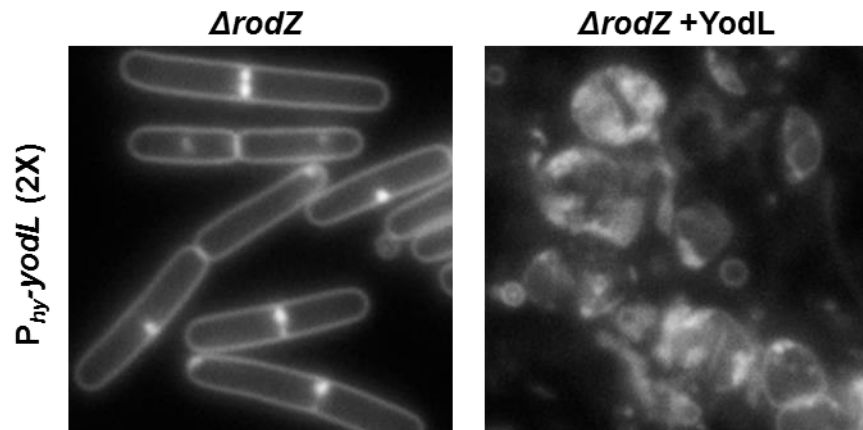


Figure 3.7. YodL misexpression in cells lacking RodZ. A $\Delta rodZ$ strain before and after 30 min YodL misexpression in liquid LB-Lennox medium supplemented with 10 mM $MgCl_2$ during exponential growth. YodL was induced with 1 mM IPTG. Membranes were stained with TMA-DPH.

To test the first possibility, we examined the variants with substitutions in residues previously implicated in interaction with RodZ to assess if they showed changes in RodZ-MreB interaction. We were able to detect a weak, but detectable interaction between MreB and RodZ using B2H (Fig. 3.8). Interestingly, this interaction was undetectable for several of the variants, consistent with model 2 (MreB_{G143A} and MreB_{P147R}), increased in one variant, consistent with model 1 (MreB_{R282S}), and similar to wild-type for another (MreB_{N145D}). These results suggest the resistance is unlikely to be simply explained by a single mechanism. Although we did not examine them by B2H, our prior analysis suggests that at least one variant, MreB_{R117G}, is likely to exhibit enhanced polymerization, consistent with model 3. Unfortunately, a direct interaction between YodL and MreB could not be detected by B2H (data not shown), so it was not possible to test if the MreB variants had reduced interaction with YodL. Moreover, it remains a possibility that YodL does not interact directly with MreB.

	RodZ _{wt}	negative controls	
MreB _{wt}			
MreB _{G143A}			
MreB _{R282S}			
MreB _{S154R}			
MreB _{P147R}			
MreB _{N145D}			

Figure 3.8. Bacterial 2-hybrid of MreB variants and RodZ. B2H between RodZ and MreB variants that conferred resistance to YisK activity. MreB or RodZ and each of the following MreB variants: MreB_{G143A}, MreB_{R282S}, MreB_{S154R}, MreB_{P147R} and MreB_{N145D} were assayed for interaction. Negative controls are either empty partner vector with MreB (center) or RodZ with the empty partner vector (right).

Biochemical characterization of YisK

To further characterize YisK function, the protein was overexpressed and purified with a C-terminal 6His tag (see Materials and Methods for more details). Briefly, strain harboring a T7-inducible YisK-6His construct was grown at 37°C in a medium that allowed high cell densities to be achieved. When the culture reached an OD₆₀₀ of ~10, the culture was placed at 16°C and 1.0 mM IPTG was added. After overnight growth, cell pellets were collected and frozen until further processing. The protein was purified using Ni-NTA chromatography and peak elution fractions were pooled and dialyzed in buffer containing glycerol for long-term storage. Analysis of the elution profile revealed a protein of the appropriate molecular weight (34 kDa) at >95% purity (Fig. 3.9), with a typical yield of 10 mg/25 ml of Cinnabar culture. The most abundant impurity, which ran at a slightly higher molecular weight than YisK-6His, was determined by LC-MS/MS to be OmpA from the *E. coli* overexpression host.

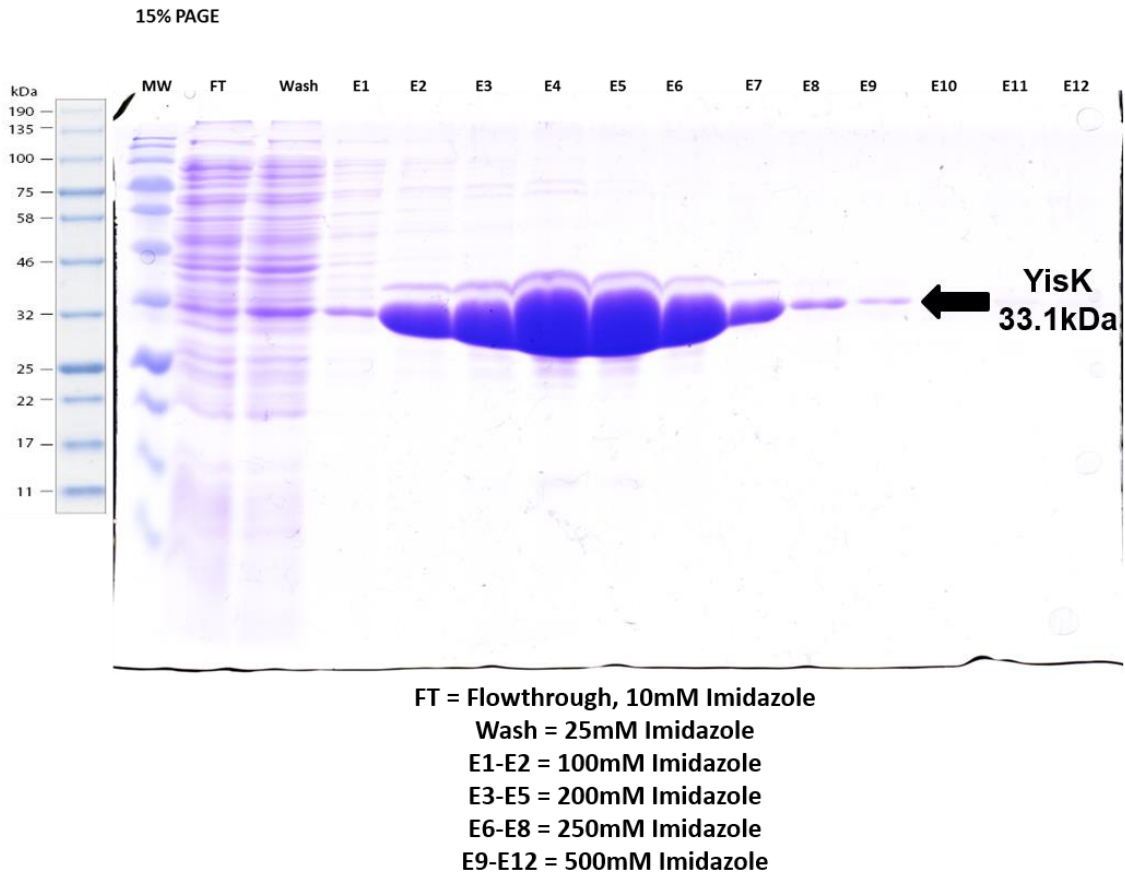


Figure 3.9. Purification of YisK-His using nickel affinity chromatography. Representative 15% Tris-Glycine SDS-PAGE Gel of YisK-His purification.

YisK crystallization

To optimize conditions for YisK crystallization, the glycerol was removed from the protein preparation and used to set 576 separate crystallization conditions by hanging drop method (see Methods). Further optimization of hits revealed one condition that produced robust, multi-faceted crystals (Fig. 3.10). This condition was pH 7.0, 100 mM MnCl₂ with 60% Tascimate. Tascimate is a complex mixture of dicarboxylic acids. The crystal structure was solved in collaboration with Dr. Inna Krieger and Dr. Jim Sacchettini. YisK crystallized as a dimer (Fig. 3.10), and consistent with this observation, we detected YisK self-interaction by B2H (Fig. 3.11). Although the resolution of the preliminary structure is around ~2 Å, the N and C terminal regions were disordered, and could not be resolved.

YisK is a member of the Fumarylacetoacetate Hydrolase (FAH) superfamily. Fumarylacetoacetate hydrolases are conserved across all domains of life, and they are involved in breaking Carbon-Carbon bonds (315-323). Typically, FAHs are involved in aromatic amino acid catabolism (315-319), although they have also been shown to participate in purine degradation (324, 325). The YisK crystal structure revealed a conserved triad of amino acids coordinating a Mn²⁺ or Mg²⁺ (Fig 3.12), a feature conserved in other members of the FAH superfamily. In addition, a small molecule that could not be resolved was present in the putative active site. This small molecule could have co-purified with YisK or been introduced during crystallization.

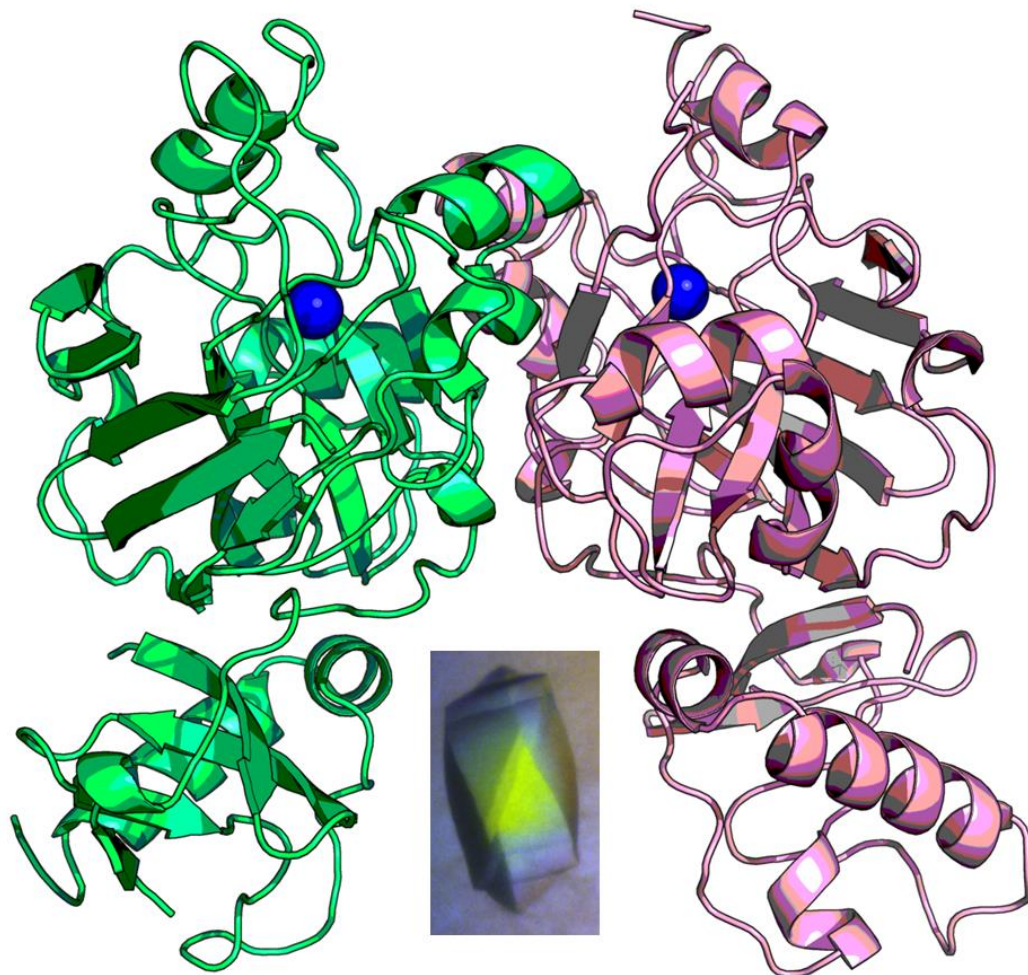


Figure 3.10. Preliminary crystal structure of YisK. The crystal structure of YisK was solved in collaboration with Dr. Inna Krieger and Dr. Jim Sacchettini using molecular replacement. Crystallization condition was 60% Tascimate, pH 7.0, 100 mM MnCl_2 . The structure shown has a 2.2 Å resolution. Cartoon depiction shown above using Pymol (326). Divalent cations are shown as blue spheres in putative active site. Image of protein crystal embedded at center of structure.



Figure 3.11. Bacterial 2-hybrid of YisK self-interaction. Negative controls are the center and right spots.

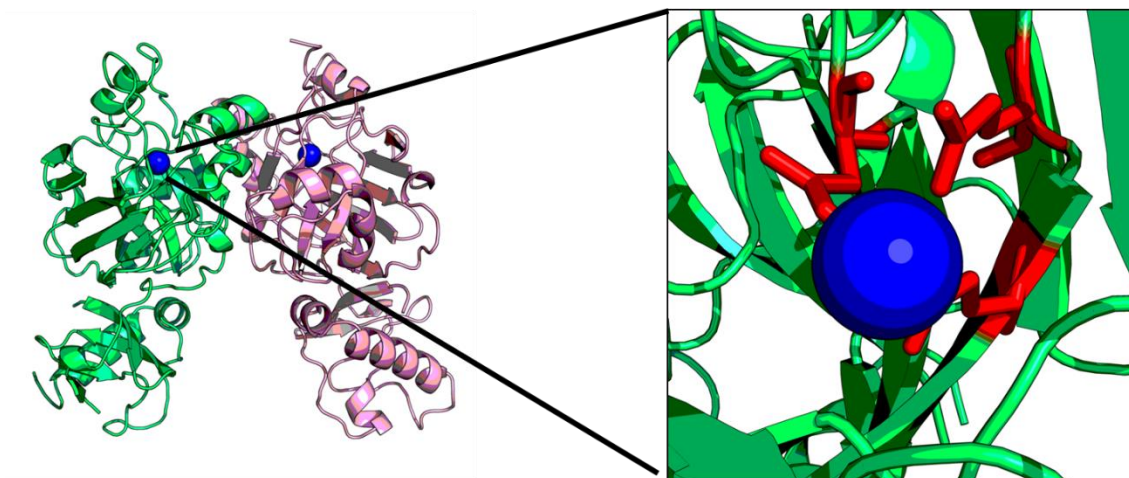


Figure 3.12. Illustration of YisK catalytic divalent cation within putative active site. A small molecule was bound in the putative active site of YisK, near the divalent cation.

Differential Scanning Fluorimetry (DSF) was used to screen the dicarboxylic acids present in the Tascimate for binding to YisK. This screen revealed one compound, L-tartrate, that stabilized YisK's melting temperature by 8°C (Fig 3.13), suggesting it was likely the compound bound in the crystal structure. Additional small molecules similar in structure to L-tartrate were screened to assess the importance of size and functional groups to binding. This included compounds such as D-ala-D-ala, which play a role in PG synthesis; in the literature L-tartrate was shown to be able to mimic D-ala-D-ala and bind bifunctional PBPs in the transpeptidase (TP) active site (327). A comprehensive list of the compounds screened by DSF is shown in Table 3.5. A summary of compounds that significantly enhanced YisK stability, as well those most structurally related that did not, is shown in Fig. 3.13.

This analysis revealed that dihydroxyfumarate (DHF) and L-tartrate had the most stabilizing affect on YisK (T_m shift of 8.5°C and 8.0°C, respectively, Fig 3.13). Closer examination of the DHF and L-tartrate structures suggest that YisK binds these compounds with a high degree of specificity. Fig 3.14 shows the structures of highly similar dicarboxylic acids that bound substantially less well to YisK, despite small changes in functional groups. For example, the only difference between L-tartrate and D-malate is that D-malate lacks a C3 hydroxyl group. The stereochemistry of the hydroxyl groups on the central carbons is also important, as meso-tartrate bound considerably less well than L-tartrate. DHF has a double bond between the C2 and C3 carbons, which would limit rotation around the double bond, maintaining the hydroxyl groups on C2 and C3 in a specific plane. Finally, the length of the molecule appears to

be important, as similar compounds of shorter or longer carbon chain lengths did not bind YisK well (Fig 3.13). These results suggest that YisK's substrate is likely to consist of four carbons, and be either close structural analogs or synonymous with L-tartrate or DHF. These results also suggest that YisK is unlikely to act as a fumarylacetoacetate hydrolase, as YisK does not bind fumarate at all.

YisK's enzymatic activity is not required for its effect on cell shape

YisK misexpression results in a profound impact on cell shape that is mediated, in part through disruption of Mbl and possibly MreB (Chapter II). Since YisK is likely an enzyme, the obvious question that emerged during this course of this study was whether or not YisK's enzymatic activity was responsible for the observed cell shape changes. To address this question, alanine substitutions were introduced in place of the acidic residues coordinating the divalent metal present in YisK's active site, creating YisK_{mu} (Fig. 3.15A). Surprisingly, when YisK_{mu} was expressed, cells appeared identical to the cells expressing wildtype YisK (Fig. 2.1 and Fig 3.15B), demonstrating that the catalytic activity of YisK is not essential for its shape modifying activity.

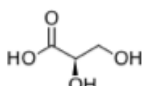
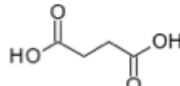
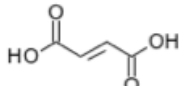
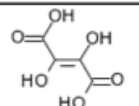
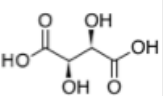
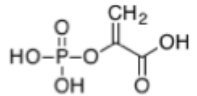
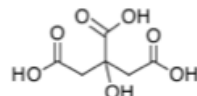
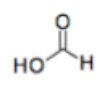
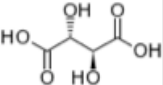
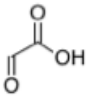
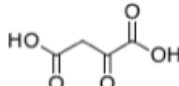
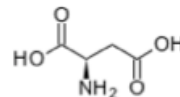
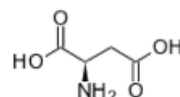
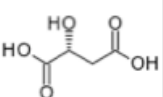
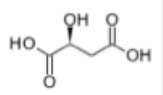
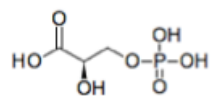
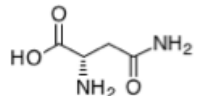
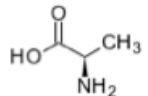
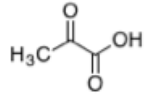
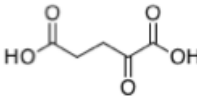
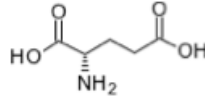
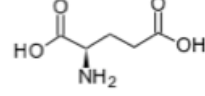
(T _m °C) Compound	Structure	Compounds producing a T _m 55- 57°C (not considered significant)		
(56) YisK only				
(64.5) DHF		D-glycerate	succinate	fumarate
(64) L-tartrate				
(59) meso-tartrate		phosphoenolpyruvate	citrate	formate
(58) glyoxylate				
(57.5) D-malate		oxaloacetate	L-aspartate	D-aspartate
(57.5) L-malate				
(57.5) pyruvate		3-phosphoglycerate	L-asparagine	D-alanine
				
		2-oxoglutarate	L-glutamate	D-glutamate

Figure 3.13. YisK Compound Screening using Differential Scanning Fluorimetry. 10.0 μ M YisK-His (see Methods) was mixed with 1000 μ M Substrate in 20.0 mM Hepes pH 7.5, 150 mM NaCl, 5.0 mM MnCl₂ with 5X Sypro Orange in a 96 well qPCR plate. Samples were heated from 25°C to 95°C, with a ramp time of 0.5°C per minute, scanning fluorescence intensity in the FRET channel. Melting temperature was determined using the derivative of the melting curve. The greater the melting temperature change upon substrate addition (compared to YisK alone), the more significant the binding.

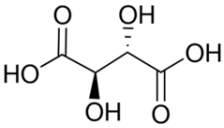
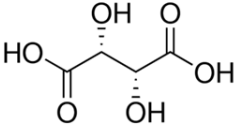
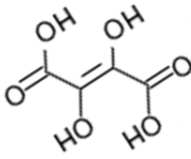
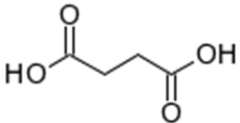
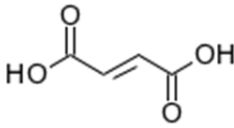
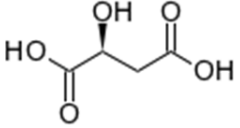
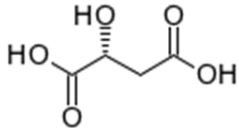
			
YisK only 56°C	meso-tartrate 59°C	L-tartrate 64.0°C	DHF 64.5°C
			
Succinate 55.5°C	Fumarate 55.5°C	L-malate 57.5°C	D-malate 57.5°C

Figure 3.14. Specificity of YisK binding. Dicarboxylic acids with similar structures were screened for binding to YisK using DSF. The melting temperature of YisK in the presence of these compounds is indicated.

Table 3.5. Summary of compounds screened by differential scanning fluorimetry for binding to YisK. 10 μ M YisK-His, 20.0 mM Hepes pH 7.5, 150 mM NaCl, 5.0 mM $MnCl_2$, and 5X Sypro Orange were used for all samples. All compounds were screened at 1000 μ M final concentration.

Compound	T_m (°C)
Protein Only	56
Ammonium Tartrate	65
L-(+)-Tartaric Acid	64.5
Glyoxylate	58
Pyruvate	57.5
Ammonium Citrate	57
Phosphoenolpyruvate	57
DL-Malic Acid	57
Fumarate	56.5
Oxaloacetate	56.5
Sodium Acetate	56
Glutamate	56
mDAP	56
Ammonium Chloride	56
Succinic Acid	55.5
Sodium Formate	55.5
ATP	57
ADP	56.5
AMPPNP	56.5
NAD ⁺	56
NADH	56
NADP ⁺	56
D-Glyceric Acid	56
D-Malic Acid	57.5
L-Malic Acid	57.5
D-Alanine	57
Cyclic D-alanine L-alanine	56.5
Ampicillin	57
Carbenicillin	55.5
D-Alanine-D-Alanine	56.5
L- Asparagine	56.5
L-Aspartate	56.5
α -ketoglutarate disodium salt	57.5
D-3-phosphoglycerate disodium salt	57
Mesotartrate	59
Dihydroxyfumarate	64.5

Table 3.5. Continued

Compound	T_m (°C)
D-Aspartate	56.5
D-Glutamate	56.5

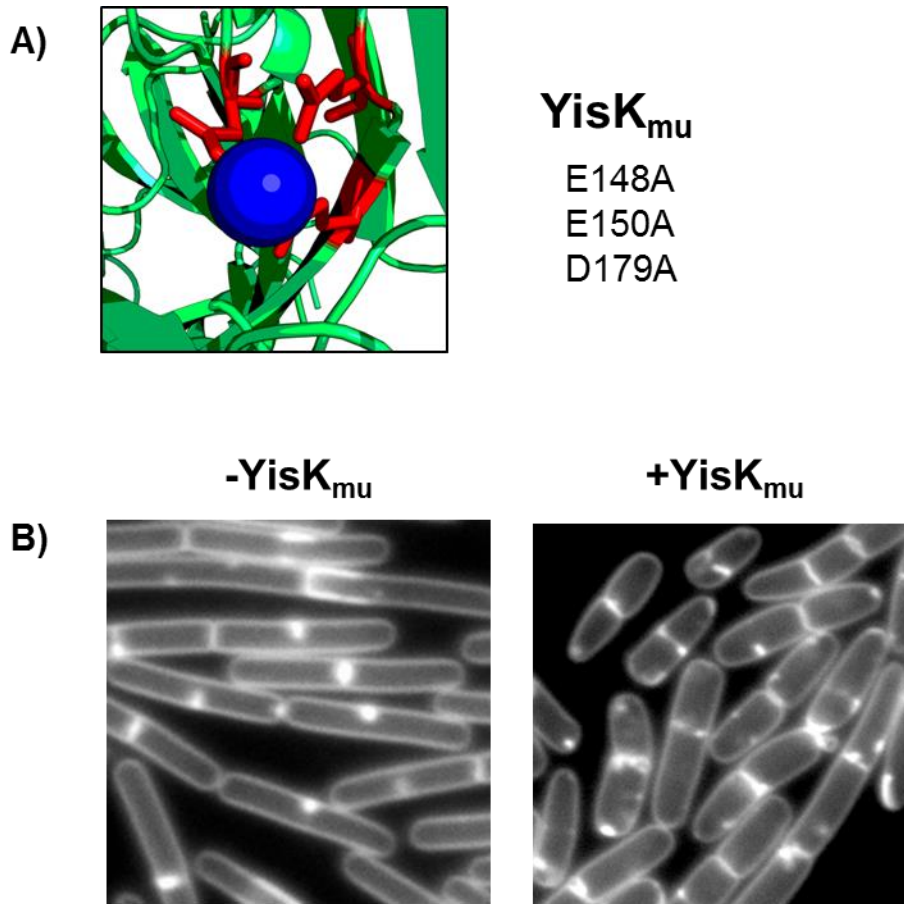


Figure 3.15. Images of cells expressing a YisK catalytic mutant. A) Residues in the putative active site of YisK that coordinates the divalent cation that is critical for catalysis. B) Before and after 90 min of misexpression of YisK_{mu} (single copy integrated in the chromosome) with 1.0 mM IPTG during exponential growth in liquid LB-Lennox.

Prompted by the separability of the catalytic function of YisK and its cell shape modifying activity, we designed substitutions in regions of YisK (based on the crystal structure) predicted to be important for YisK dimerization, as well as in one acidic residue outside the catalytic domain that was conserved in other YisK homologs across the genera. These variants were then classified based on their ability to self-interact or interact with FtsE by B2H, as well as their ability to prevent growth of *B. subtilis* following induction on plates (Fig 3.16). From these results we inferred that YisK self-interaction, YisK-FtsE interaction, and catalytic activity are not required for YisK to kill cells. Second, the E30 residue appears to be critical for YisK perturb cell growth (Fig 3.16) and shape (data not shown). While it is possible MreB_{E30A} is misfolded, this seems highly unlikely since the variant is fully able to support the YisK-YisK and YisK-FtsE B2H interactions.

	YisK-YisK interaction	YisK-FtsE interaction	Growth +YisK
WT	+++	+++	none
E148A E150A	-	+++	none
E148A E150A D179A	++	-	none
H189A	-	-	none
D199A	+	+++	none
T255A	-	+++	none
E30A	+++	+++	+++

Figure 3.16. Characterization of YisK variants. Substitutions in regions of YisK that hypothesized to be important for YisK catalysis (red), self-interaction (blue) or perturbation of cell shape (green). (+) positive interaction, (-) no interaction. The number of (+) symbols signifies the magnitude of the interaction or phenotype. YisK-YisK interaction and YisK-FtsE interaction were tested using B2H. Growth +YisK corresponds to growth observed after overnight growth at 37°C on an LB plate supplemented with spectinomycin and 1.0 mM IPTG plate.

Investigation of YisK's role in sporulation

Initially thought that YisK may play a role in sporulation (see Chapter II), but did not see any obvious indication of YisK's role aside from a minor sporulation defect. We also observed no obvious differences in timing or morphology of spore germination in a $\Delta yisK$ mutant (Fig. 3.17). We hypothesized that YisK's role in sporulation might be masked by the presence of a redundant factor. To screen for possible redundant factors, a genomic library of sporulation proficient mutants was isolated and introduced into $\Delta yisK\Delta yodL$ strain harboring a reporter for a late sporulation gene, $P_{cotD}-lacZ$. When cells sporulate, the promoter is activated, driving *lacZ* transcription and synthesis of beta-galactosidase. The beta-galactosidase activity can be monitored on solid sporulation medium plates (DSM) that have been supplemented with X-Gal (see Duan and Herman, Dissertation). White colonies, indicating delayed or inhibited sporulation, were identified through visual screening, and the associated transposon was moved into a clean $P_{cotD}-lacZ$ background that was either wildtype or $\Delta yisK\Delta yodL$. Only strains that exhibited a sporulation defect when combined with $\Delta yisK\Delta yodL$, but no delay in wild-type were selected for further analysis. The locations of the transposon insertions, which were determined using inverse PCR and sequencing, are summarized in Table 3.6.

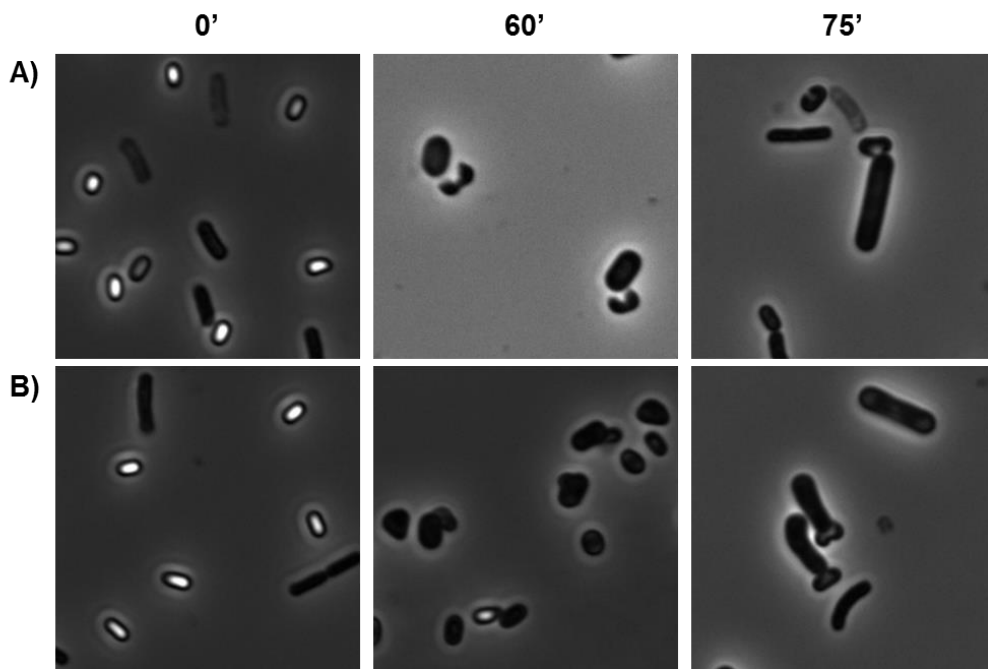


Figure 3.17. Phase-contrast microscopy of spore germination. *B. subtilis* 168 spores (A) or $\Delta yisK$ spores (B) were resuspended in LB and phase contrast images were taken at the indicated timepoints.

Table 3.6. Redundant factor screen for YisK during sporulation conditions. All transposons were mapped to *B. subtilis* genome and locations are noted.

Strain (RFL #)	Transposon insertion site
6	after the 23 rd bp in <i>engD</i>
20	after the 101 th bp in <i>veg</i>
30 & 81	4 bp upstream of <i>ssrA</i>
49, 62 & 89	60 bp upstream of <i>rpsU</i>
59	genes encoding 16S rRNA
61	90 bp upstream of <i>dnaD</i>
64 & 84	genes encoding 23S rRNA
90	32 bp upstream of <i>pgk</i>

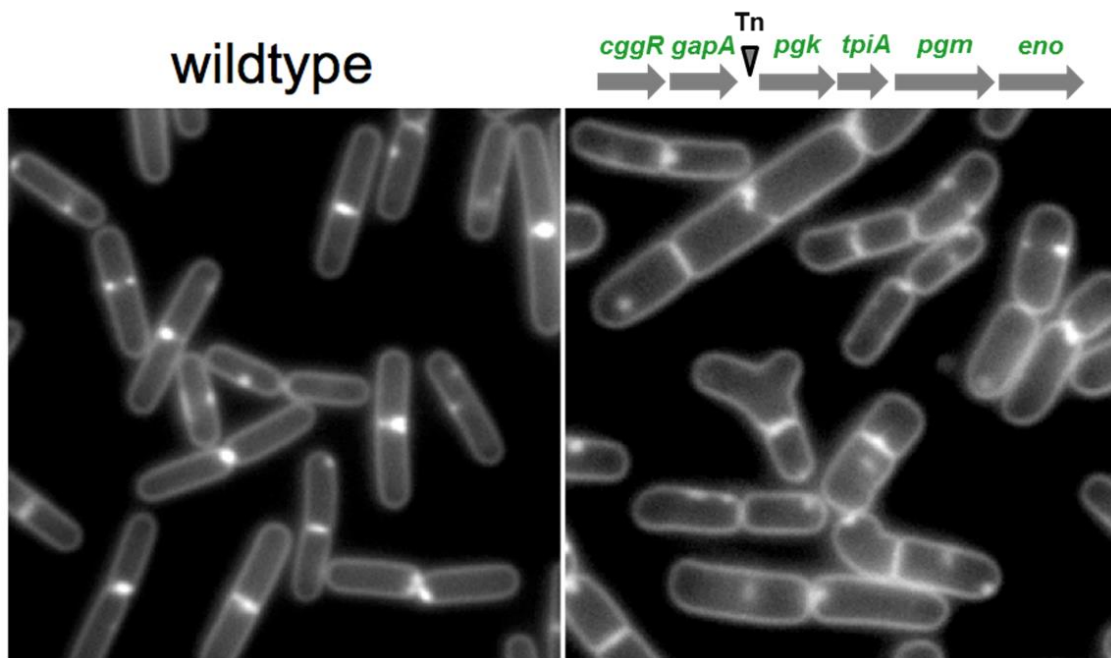


Figure 3.18. Phenotype of the Tn insertion between *gapA* and *pgk*. Cells were grown to exponential phase in CH medium at 37°C. Membranes were stained with TMA-DPH.

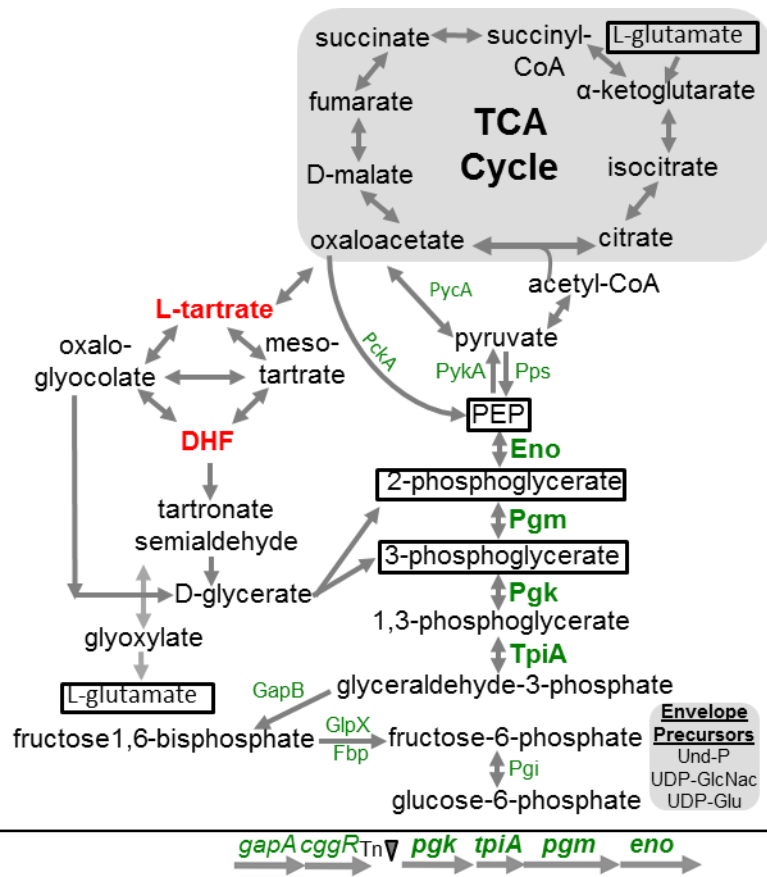


Figure 3.19. Overview of relevant metabolic pathways. Metabolites within the glyoxylate pathway can feed into central carbon metabolism via D-glycerate or L-tartrate

One of the mutants of particular interest because of its relationship to carbon metabolism possessed a transposon insertion in the intergenic region between *gapA* (glyceraldehyde-3-phosphate dehydrogenase) and *pgk* (phosphoglycerate kinase) within the *gapA* operon (Fig 3.18). The *gapA* operon encodes enzymes for the bottom half of glycolysis as well as CggR, a transcription factor that represses the operon in the absence of glucose (140). Previously, the five glycolysis genes downstream of *cggR* were described to be essential (140), although a recent paper shows that only *gapA*, *pgm*, and *eno* are essential (16).

We have not tested the expression levels of the genes downstream of the transposon. However, cells harboring this transposon exhibit cell shape defects when even in an otherwise wildtype background (Fig 3.18). This observation would be consistent with the insertion disrupting the pools of PG precursors and cell wall homeostasis (Fig 3.19). Our compound screening data suggests YisK is capable of binding compounds present in the glyoxylate pathway (Fig 3.19, red text), yet YisK bears neither amino acid homology, nor structural similarity to characterized tartrate/malate dehydrogenases, enzymes that catalyze the conversion of L-tartrate to oxalloglycolate and meso-tartrate to D-glycerate (328). Therefore, we think L-tartrate is unlikely to be YisK's physiological substrate. Instead, we hypothesize YisK catalyzes the conversion of DHF to tartronate semialdehyde via decarboxylation. No gene product has ever been associated with DHF decarboxylation (158), so if the hypothesis is correct, YisK will be the first enzyme of its kind ever characterized. Our initial attempts to assay

for this activity failed, as the substrate for the reaction (DHF) was found to spontaneously decarboxylate at room temperature in aqueous solution.

Interestingly, the L-tartrate catabolism pathway redundantly produces the gluconeogenic metabolites 2-phosphoglycerate and 3-phosphoglycerate important metabolites in cell wall precursor synthesis (Fig. 3.19). Thus, one hypothesis to explain the sporulation defect we observed is that during sporulation, the demand for these metabolites from alternative pathways is increased. Future experiments will be aimed at assessing if the redundancy can be attributed to either a $\Delta yodL$ or a $\Delta yisK$ deficiency, as well investigating the molecular basis for the other redundant factors identified.

Untargeted metabolic profiling of the $\Delta yisK$ compared to wild-type

There are many challenges to associating uncharacterized gene products with cellular functions, particularly when they lack obvious knockout phenotypes. The tractability problem is just one of many. While we were able to associate a phenotype with YisK misexpression, these data only suggest that YisK has the capacity to interact with components of the cell elongation machinery. While we think this observation is significant (see discussion) it does not illuminate what type of enzymatic activity YisK might possess. Similarly, while the DSF screening revealed potential substrates for YisK, there is no guarantee that that they are actually the physiologically relevant substrates. Therefore, in addition to our genetic and biochemical approaches, we sought to explore the effects of a *yisK* deletion on the *B. subtilis* metabolome using an untargeted approach. For this study, samples were prepared from both wild-type and

ΔyisK mutant (see material and methods). The sample preparation required extensive optimization to identify conditions to quickly and efficiently harvest total cellular metabolites relatively free of protein contaminants. Two different metabolite extraction methods were attempted; bead breaking coupled with solvent extraction and solvent only extraction; according to the literature, the extraction efficiencies with these methods are were equivalent (329, 330). However, it was clear from microscopy that the solvent-only method left cells intact, raising the concern that the metabolites might not be fully released (Fig. 3.20).

Moreover, in our hands, the bead breaking method consistently yielded a lower signal to noise ratio than the solvent extracted sample, suggesting this method resulted in contaminants that suppressed metabolite ionization. Since it was suspected that this suppressing contaminant was protein, the extraction solvent was switched from 60% ethanol to using 1:3:1 chloroform:methanol:water, a condition which should denature protein. While this adjustment improved the signal, ultimately the best signal was obtained by additionally passing the solvent extracted samples through a 3 kDa MWCO protein concentrator before lyophilization and resuspension for Mass Spectrometry. This modification increased the signal intensity by at least an order of magnitude (Fig 3.21), Dr. Klemashevich optimized the LC/MS/MS parameters for signal strength as well as for compound resolution (Fig 3.22).

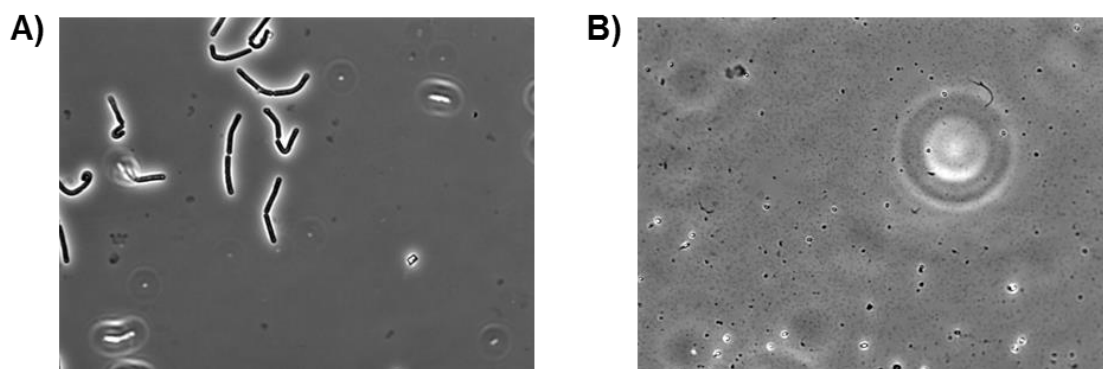


Figure 3.20. Phase-contrast microscopy of samples. A) following solvent only extraction and B) following bead-beating and by solvent extraction.

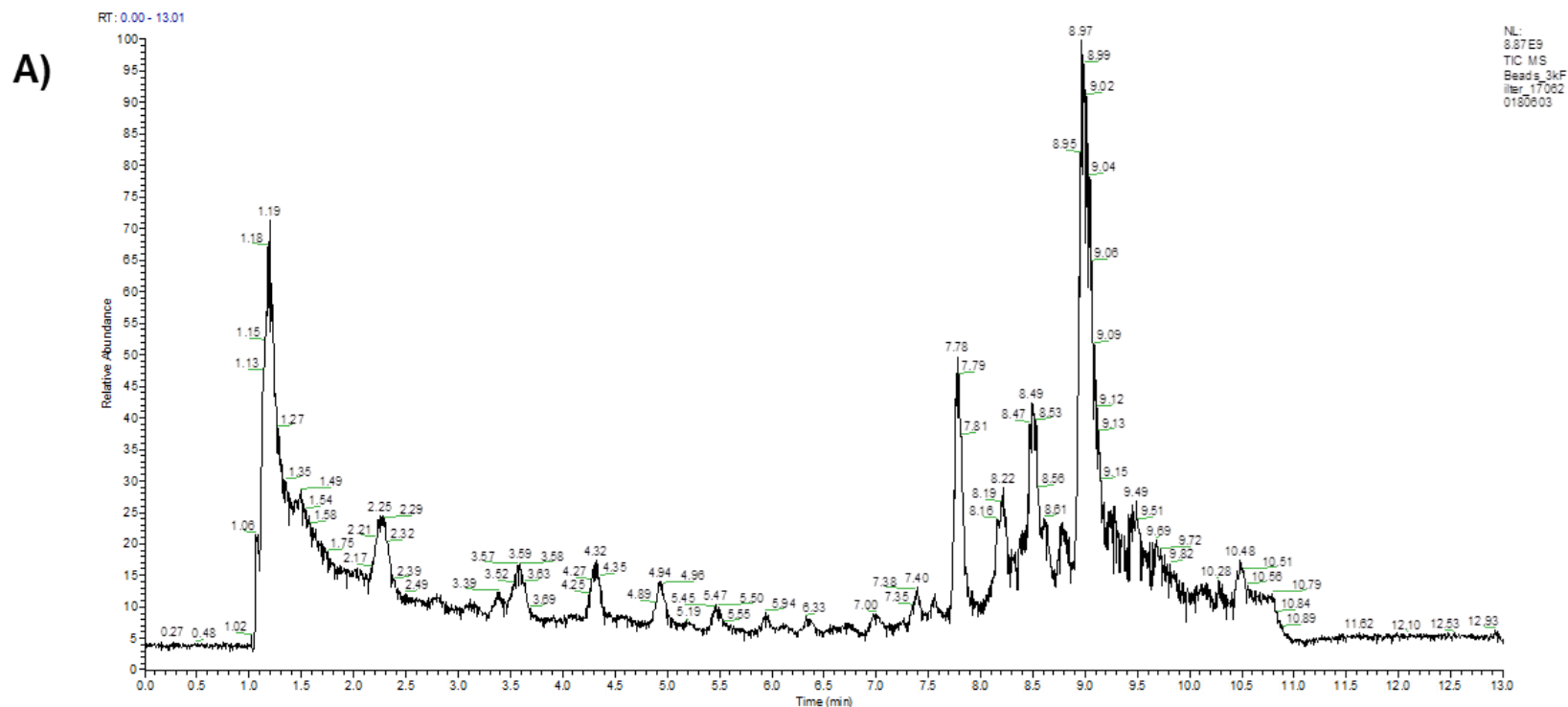


Figure 3.21. Total ion concentration of LC/MS/MS of metabolite extractions using optimized LC method and bead breaking lysis. A) Extract passed through a 3 kDa MWCO protein concentrator prior to lyophilization and resuspension B) Extract lyophilized and resuspended without protein removal. Elution time is on the x-axis and relative ion abundance is on the y-axis.

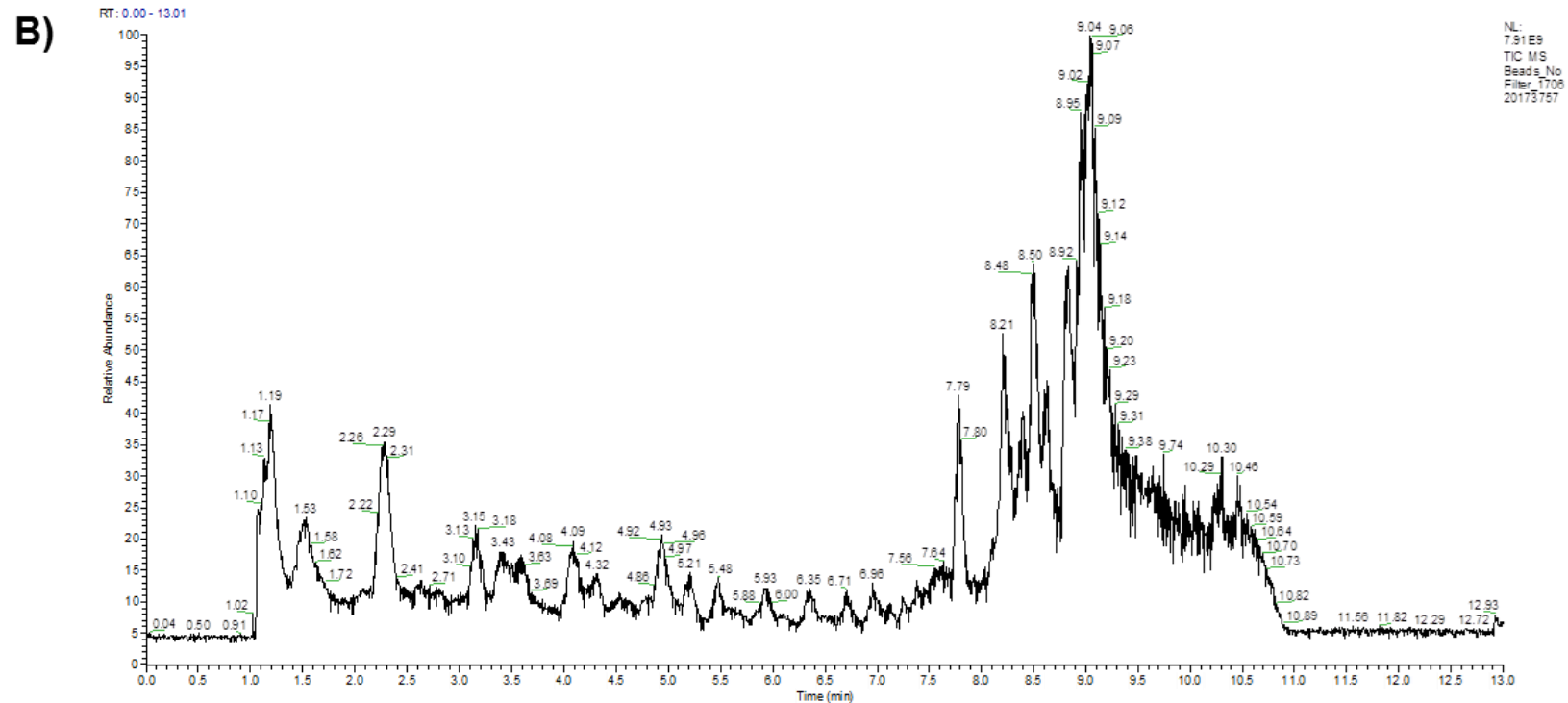
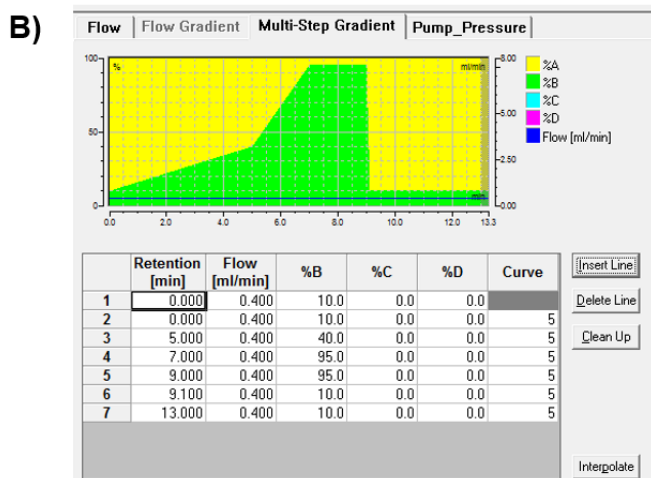


Figure 3.21. Continued.

A)

	CD ID's	Compounds	Features	Chem Spider Hits	Time	Cost per Sample
New LC	150	5033	20004	5835	13 min	\$8.75
Old LC	86	3654	10532	4422	60 min	\$35

Short Method



Long Method

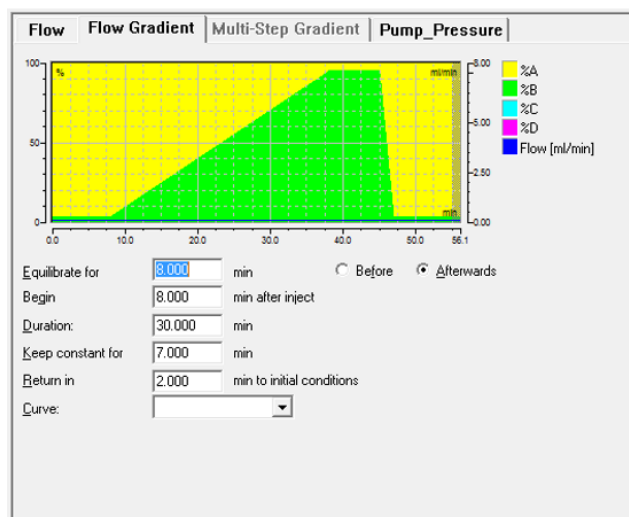


Figure 3.22. Optimized LC/MS/MS parameters. A) Overall summary of cost and effectiveness of LC/MS/MS. B) Summary plots of LC method used; short method refers to the New LC and long method refers to the Old LC in panel A, respectively. CD ID's are Compound Discoverer ID's, and so absolute confirmed compounds compared to an accepted standard in MZ Cloud Database.

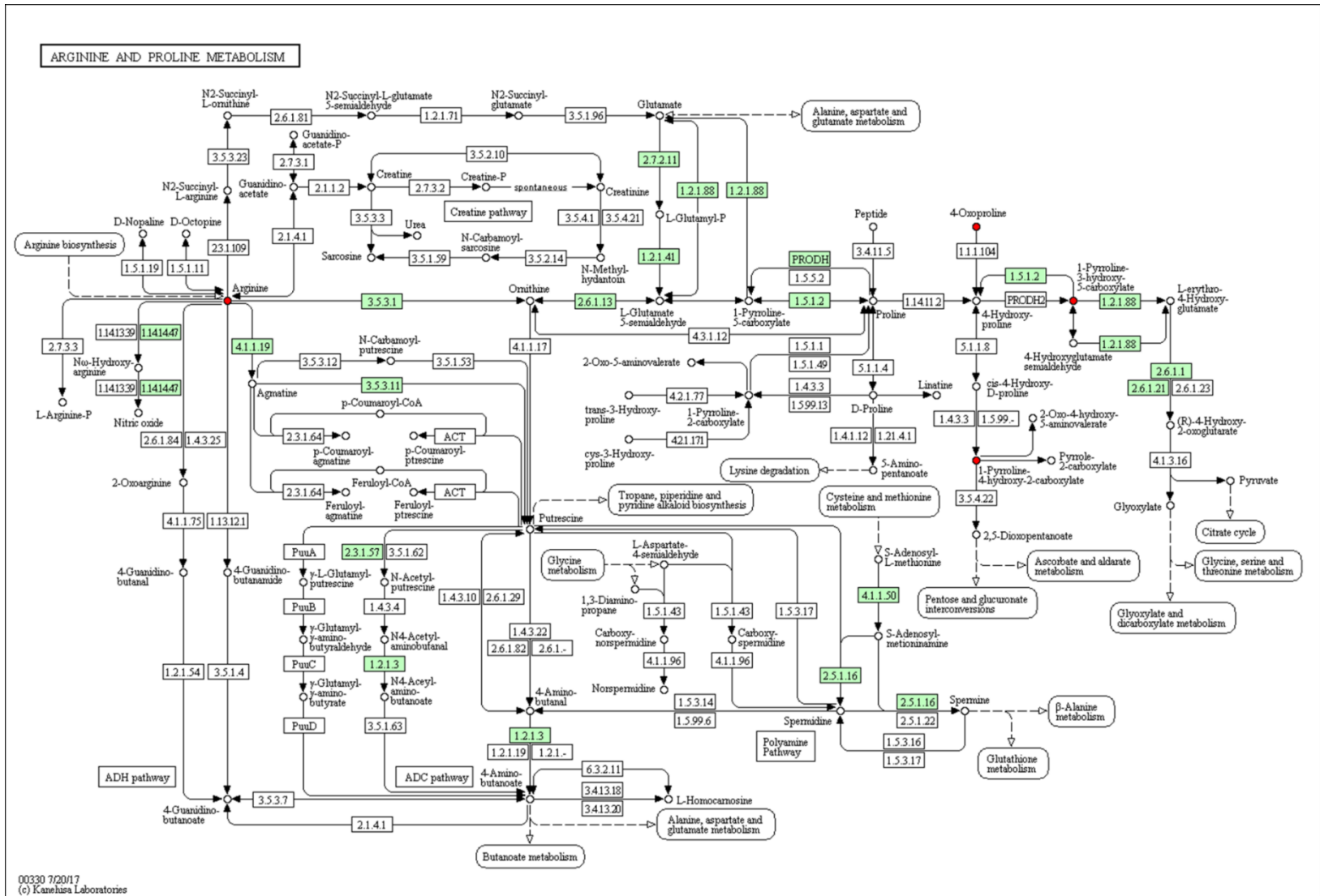
Whole organism untargeted metabolomic profiling was performed on three biological and experimental replicates of wildtype and the $\Delta yisK$ mutant grown to stationary phase in CH media ($OD_{600} = 4$, peak YisK expression in CH medium according to western blot analysis). Samples were run using LC/MS/MS parameters in both positive and negative ionization modes. Differential analysis was performed using Compound Discoverer (version 2.0), and metabolites that were depleted or enriched by at least two-fold in the *yisK* knockout compared to the wild-type control were identified. All compounds positively identified using MZ Cloud are shown in Table 3.7. All putative compounds identified through ChemSpider are shown in Table A1.1 (included as a separate file, see Appendix I). Since ChemSpider results are identified only by MS spectrum, not MS and MS² spectrum against a positive standard (like MZ Cloud), the hits in Table A1.1 are considered more tentative. ChemSpider and MZ Cloud results were subsequently mapped against KEGG pathways using the KEGG Mapper Search and Color Pathways Tool (158) with *Bacillus subtilis* strain 168 reference pathways.

Pathways with multiple metabolites that are perturbed in the *yisK* knockout are shown in Fig 3.23-3.25, with metabolites that were decreased in *yisK* knockout indicated in red and compounds increased in the *yisK* knockout indicated in green. None of the metabolites identified resided in the dicarboxylate/glyoxylate pathways. This was not entirely surprising because the liquid chromatography methods available in the IMAC cannot be performed with ion-pairing. As a result, many hydrophilic or charged molecules cannot be resolved.

Table 3.7. MZ cloud summary of identified compounds. Compounds that changed more than two-fold in relative abundance in the $\Delta yisK$ mutant compared to wild-type are shown along with their ChemSpider and KEGG ID.

KEGG ID	Name	Bg Color	Foreground Color	Scan Mode	ChemSpider ID	MZ Cloud ID
C01877	4-Oxoproline	red	black	negative	366185	1268
C06593	Caprolactam	red	black	positive	7480	2867
Not Found	N,N-Diethylethanamine	red	black	positive	10617374	2816
Not Found	Tetraglyme	red	black	positive	13835433	3460
C11118	N-Methyl-2-pyrrolidone	red	black	positive	12814	2810
Not Found	δ -Valerolactam	red	black	positive	12144	2988
Not Found	2-Ethyl-2-oxazoline	red	black	positive	59786	3282
Not Found	2,2,6,6-Tetramethyl-4-piperidinol	red	black	positive	68000	2886
C02206	2,2,6,6-Tetramethyl-1-piperidinol (TEMPO)	red	black	positive	478474	1418
Not Found	Atenolol acid	red	black	positive	56653	991
C05011	4-Hydroxytamoxifen	red	black	positive	4447687	3126
C07101	2,4,5-Trichlorophenol	green	black	negative	7001	2763
C00153	Nicotinamide	green	black	positive	911	517

Figure 3.23 Metabolites decreased more than two-fold in the $\Delta yisK$ mutant compared to wild-type in the Arginine and Proline metabolism pathway. Red circles denote a decrease of at least two-fold, while green circles denote an increase of at least two fold. Both MZ cloud and ChemSpider results were plotted.



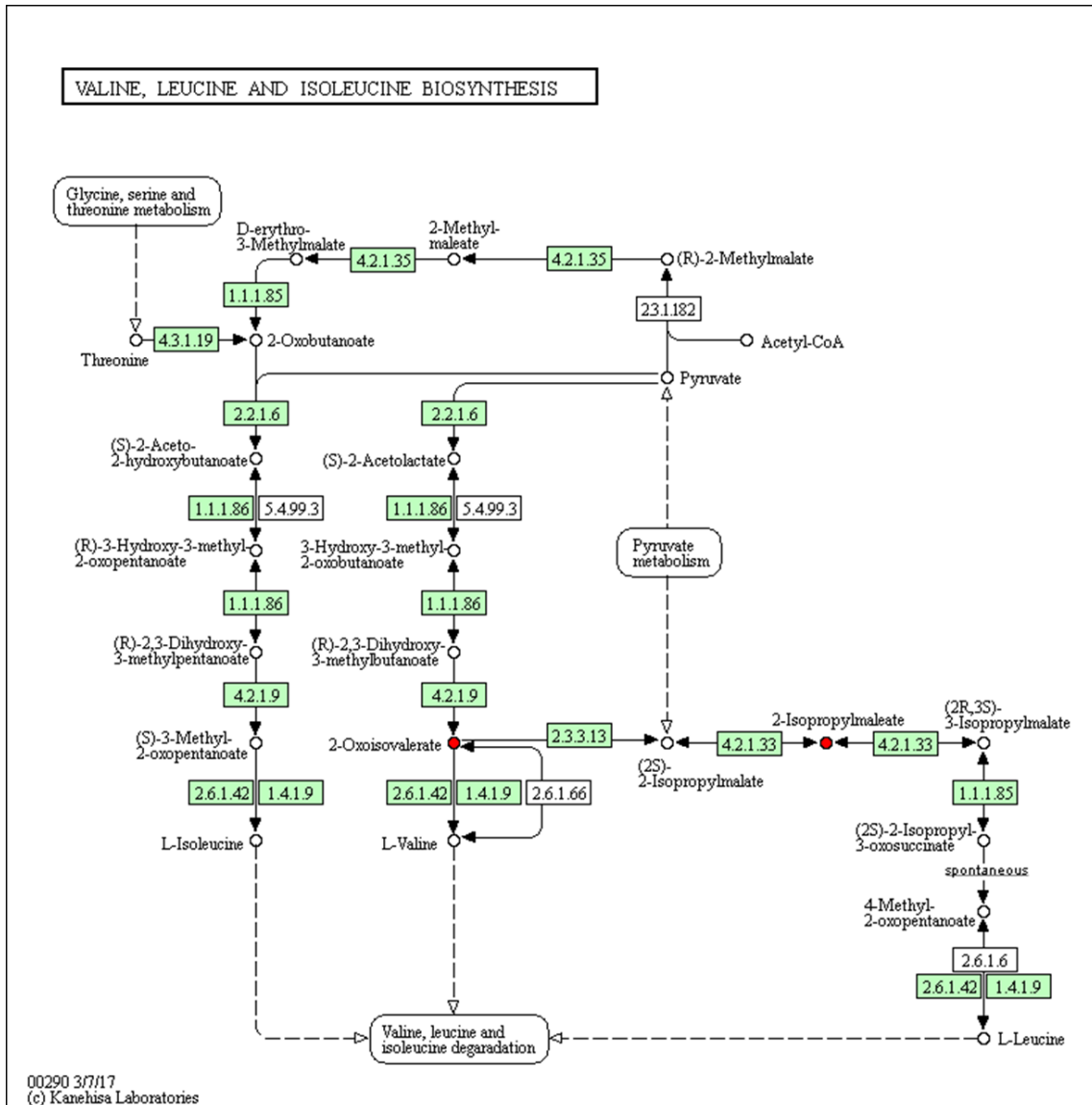


Figure 3.24. Metabolites decreased more than two-fold in the $\Delta yisK$ mutant compared to wild-type in Valine, Leucine, and Isoleucine biosynthesis pathway. Red circles denote a decrease of at least two-fold, while green circles denote an increase of at least two-fold. Both MZ cloud and ChemSpider results were plotted.

Figure 3.25. Metabolites decreased more than two-fold in the $\Delta yisK$ mutant compared to wild-type in the Nicotinate and Nicotinamide metabolism pathway. Red circles denote a decrease of at least two-fold, while green circles denote an increase of at least two-fold. Both MZ cloud and ChemSpider results were plotted.

Regardless, we did identify several compounds that were differentially affected in the $\Delta yisK$ mutant compared to wild-type. 4-Oxoproline, 1-Pyrroline-3-hydroxy-5-carboxylate, 1-Pyrroline-4-hydroxy-2-carboxylate are all reduced by at least 2 fold in the *yisK* knockout compared to wildtype. These metabolites reside within the Arginine and Proline Metabolism pathway (Fig 3.23) and can feed into the glyoxylate pathway. In fact, 4-Oxoproline and 1-Pyrroline-3-hydroxy-5-carboxylate are only five reactions and 3 reactions away from glyoxylate, respectively. In addition, Arginine itself is reduced in the *yisK* knockout (Fig 3.23), whereas Nicotinamide is significantly increased (Fig 3.25). 2-Oxoisovalerate and 2-Isopropylmaleate, metabolites in the Valine biosynthesis pathway (where pyruvate from central carbon metabolism feeds into Valine), were both reduced by at least two fold in the *yisK* knockout compared to wildtype (Fig 3.24). These preliminary data suggest that YisK alters the flow of carbon through several amino acid synthesis nodes. They also highlight the need for alternative methodologies to detect, in particular, polar metabolites. In the future, samples will be run on a column that is more amenable to the profiling of more polar compounds.

Native immunoprecipitation of YisK-associated proteins

To identify *in vivo* YisK interaction partners, co-immunoprecipitations (pull-down assays) were performed. Although the pull-down assays successfully pulled down YisK, they did not pull down any other proteins (Fig 3.26). I am currently pursuing *in vivo* crosslinking followed by pull-down in order to capture transient interactions of YisK with other proteins in the cell.

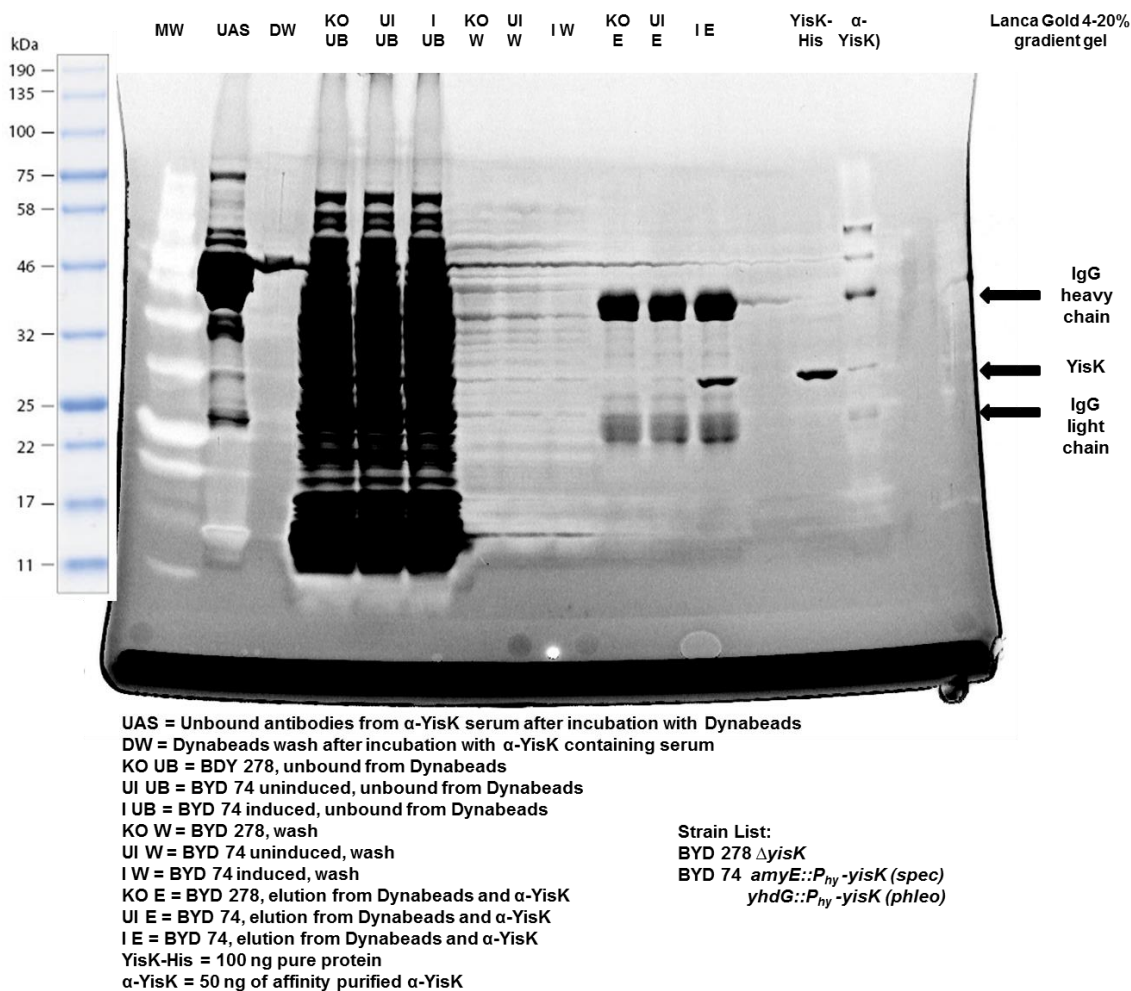


Figure 3.26. YisK pull-down assay using α -YisK and dynabeads protein A. Pull-down was performed as described (see methods). BYD 278 $\Delta yisK$ and BYD 74 *P_{hy}-yisK* (2X) (see methods in Chapter II). BYD 74 was induced for 20 min with 1.0 mM IPTG before subjected to protoplasting followed by osmotic lysis and pull-down. BYD 74 UI (uninduced) and BYD 278 were grown to same OD₆₀₀ (~0.5) before protoplasting followed by osmotic lysis and pull-down. Gel stained with Sypro Ruby, with relevant bands indicated by arrows. Contrast of image enhanced to make bands clearer.

Discussion

YisK perturbs the proper localization of Mbl-GFP during misexpression, which is consistent with the loss of rod shape observed (Fig 3.1). The loss of Mbl's punctate-helical localization is accompanied by a strong relocalization of Mbl-GFP to midcell. In *B. subtilis*, MreB was recently shown to require the presence of Lipid I for localization to the membrane (331). If Mbl also requires Lipid I for localization, this result might suggest that YisK misexpression leads to an enrichment of Lipid I at midcell. Our Mbl suppressor data suggests YisK misexpression disrupts Mbl protofilament bundles (Chapter II), and recent evidence shows that a functional sandwich fusion to natively expressed YisK localizes to punctate regions around the membrane (Tingfeng Guo and Jennifer Herman, unpublished data). Based on these additional data, we hypothesize that YisK localization is restricted in the cell, and that disruption of Mbl along the cell length frees Mbl to relocalize to Lipid I present at midcell.

Although YisK specifically requires Mbl (but not MreB) for its cell shape modifying activity, we were surprised to observe that misexpression of YisK also results in loss of the punctate-helical localization of MreB-GFP (Fig. 3.1) and of LytE-GFP (a proxy for MreBH) (Fig 3.2). Since cells are not round, this result suggests that either there is still some Mbl/MreB present at the membrane, or that the midcell-localized Mbl is capable of supporting an overall rod shape. If this hypothesis is correct, then it would suggest that cells growing following YisK expression are incorporating new cell envelope material through polarized growth, a possibility that can be tested using PG labeling techniques (57).

YisK is a stationary phase protein, and our data suggests *yisK* is repressed during sporulation by a Spo0A box that overlaps the -10 region of its SigH promoter (Fig 3.3). Our data also suggest that YisK is an enzyme, so this result suggests that whatever the enzymatic activity of YisK is during stationary phase, it may be detrimental if it is not downregulated during sporulation.

We also observe that YisK interacts by B2H with FtsE, the cytoplasmic component of the ABC transporter FtsEX via Bacterial 2-hybrid (Fig 3.4). While YisK-mediated cell widening does not require FtsEX (actually cells become round and lyse) (Fig 3.5), YisK mediated cell shortening does (Fig 3.6). It is not clear whether this is a general sensitivity of the the *ftsEX* or *cwlO* knockouts to perturbations in cell envelope synthesis or if it is specific to YisK activity, but this can be investigated by examining if the *ftsEX* is also more sensitive to misexpression of YodL.

MreB was shown to be required for YodL cell shape modifying activity, and some of the specific suppressors of YodL activity resided on an interface of MreB known to be important for interaction with the cell shape protein RodZ (78). We found that *rodZ* from *B. subtilis* could be deleted without a loss of rod shape, and further showed that *rodZ* was not essential for the cell shape modifying activity of YodL (Fig 3.7). This allowed us to probe the mechanism of the suppressors in MreB conferring resistance to YodL activity. Suppressors in MreB could confer resistance by increasing the affinity of MreB for RodZ, thereby outcompeting YodL for the same interface. Additionally, suppressors in MreB could also function by abrogating interaction with YodL. Finally, non-specific suppressors of MreB which could also suppress YodL

activity could do so by a general mechanism, such as enhancing MreB's ability to polymerize or form protofilament bundles.

These data raise the question as to what is YodL's role in the cell. We identified *yodL* as a previously uncharacterized sporulation gene (Chapter II). Since RodZ couples MreB to the cell synthesis machinery and YodL shares the same/overlapping interaction interface on MreB with RodZ, it seems plausible that MreB interaction with YodL would exclude MreB interaction with RodZ. Therefore, native expression of YodL during sporulation should uncouple MreB from cell envelope synthesis. This is logical from an evolutionary standpoint, as under limited resources the cell would need to transition from lateral cell wall synthesis to polar septal synthesis and eventually spore formation. This begs the question: what is the role of MreB during sporulation (Duan and Herman, Dissertation)?

The role of MreB-like proteins during sporulation in *B. subtilis* has not been elucidated, although distinct roles for MreB-like proteins during sporulation has been shown for other organisms (58). In *B. subtilis*, Mbl has a SigE promoter (sporulation promoter), suggesting a distinct role for Mbl during sporulation. This data supports YisK being repressed during sporulation, as perhaps this ensures that YisK does not perturb Mbl function during this stage of developmental growth.

The YisK crystal structure was solved at $\sim 2\text{\AA}$ resolution, although the N and C terminal regions which reside towards the bottom of the structure (Fig 3.10) are poorly resolved. Initial attempts at making N or C terminal fluorescent fusions as well as His tagging YisK resulted in a loss of its ability to cause a loss of cell shape upon

misexpression, suggesting this region of the protein is important for YisK's ability to interact with and/or perturb Mbl. Consistent with this possibility, the YisK_{E30A} variant's substitution occurs in a conserved acidic amino acid in this region of the protein.

YisK is a member of the fumarylacetoacetate hydrolase (FAH) superfamily; however, our data suggest that YisK is not involved in aromatic amino acid metabolism, and is instead most likely involved in metabolism of dicarboxylic acids. Perhaps the most critical finding of this study was that YisK_{mu} (E148A, E150A, and E179) no longer supports coordination of the divalent cation critical for catalysis in FAHs, but misexpression of YisK_{mu} still resulted in loss of cell shape (Fig. 3.15). This suggested that the enzymatic activity of YisK was not related to its cell shape modifying activity. Given that YisK copy number is probably pretty low (<300 at maximal expression), the cell-shape modifying activity during misexpression is probably an artifact of overexpression of a protein that interacts with Mbl. Based on the crystal structure and genetic data (Fig. 3.16) the current model is that YisK interacts with Mbl with its N and C terminal region as well as uses interactions with FtsEX to localize to a region of the cell where its substrate is present and/or its product is needed, during a stage in the cell cycle (stationary) where the metabolic pathway that YisK plays a role in will be needed (Fig. 3.27).

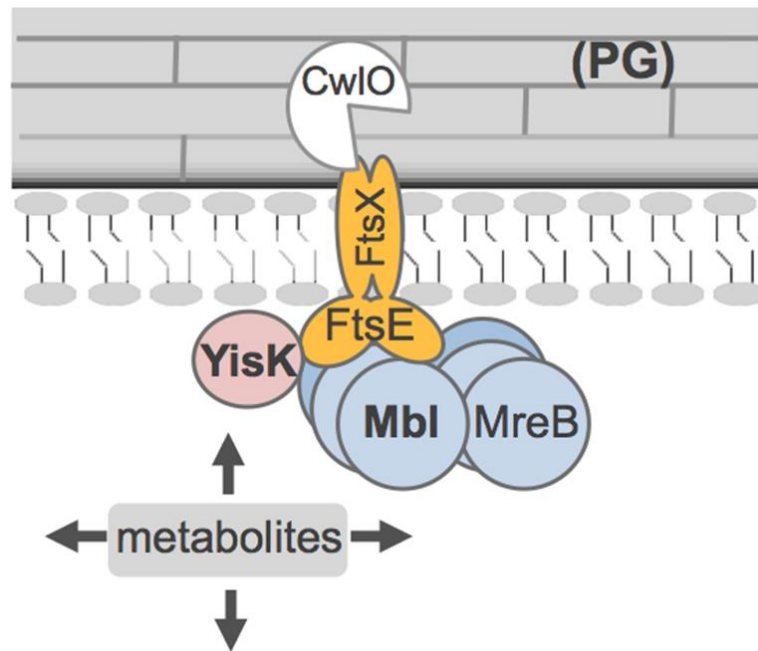


Figure 3.27. Current model of YisK *in vivo* function. YisK uses Mbl and FtsEX to localize to a region of the cell where its substrates may be present and/or the product of its reaction may be required.

Based on the data, it appeared that YisK played a role in dicarboxylic acid metabolism (Fig. 3.21). However, we were unable to obtain interaction partners with YisK using pull-downs of cytosolic proteins from cell lysates. This negative result could be due to either transient interactions of YisK with the cell envelope synthesis machinery, or interactions with membrane bound proteins (or even small molecules such as Lipid II). To address the former possibility, *in vivo* crosslinking followed by pull-down will be performed; the latter possibility will be tested by a membrane solubilization followed by pulldown. The metabolomics data was able to link the proline metabolic pathway that was closely related to (only a few enzymatic steps away from) the glyoxylate pathway, but did not result in direct evidence of YisK playing a role in dicarboxylic acid metabolism. It is possibly that L-tartrate or dihydroxyfumarate (DHF) are actually mimicking the true substrate, and that they should be treated as a pharmacophore or backbone structure that would be the core of the true substrate. It has previously been shown that L-tartrate acts as a mimic of D-ala-D-ala, and so it is not farfetched to hypothesize that it may not be the true substrate (327). Proline has never been tested for binding to YisK, but will be tested in the future. Subsequent metabolomics experiments using a *yisK* knockout will be performed, focusing on hydrophilic compounds including those involved in central carbon metabolism, in an effort to identify YisK's native metabolic pathway. In addition to whatever information is obtained concerning YisK function, the overall approach used for characterization of YisK can be applied for elucidation of other enzymes of unknown function(s).

CHAPTER IV
CHARACTERIZATION AND MANIPULATION OF PBSX, A DEFECTIVE
PROPHAGE IN *B. subtilis*

Introduction

PBSX is a defective prophage-like element in *B. subtilis* 168 that specifically targets and kills *B. subtilis* W23. PBSX-like prophages are conserved in *B. subtilis* strains as well as some strains of *B. pumilis* and *B. licheniformis* (214, 215); these phagocin kill related species of *B. subtilis* while leaving their respective strain unaffected. PBSX induction results in amplification of phage DNA (209, 217, 332), the packaging of ~13 kb (209) of random chromosomal DNA from the host (195, 211), and subsequent lysis of the host; however, there has been evidence to suggest that the packaging of chromosomal DNA is not completely random, and that some feature of the DNA (whether sequence specific or structure specific) is guiding the packaging (209). PBSX is thought to kill in the same manner as pyocins, by dissipating the membrane potential (333). Since PBSX packages chromosomal DNA and also kills its target upon adsorption, it is not useful as a transducing phage.

A thermosensitive mutant (*xhi-1479*) that induces PBSX when the temperature is shifted from 37°C to 48°C was originally isolated in 1976 (224), although it was not until the early 1990's that the phage repressor, *xre*, was identified, along with the mutations that confer temperature sensitivity (*xre G4S A19V L78V*); however, it was

never identified which of the point mutations within *xre* were required for temperature sensitivity (219, 220).

Although PBSX was the focus of significant research, most of the work is between thirty and fifty years old, and while the data strongly supports the authors' conclusion(s), the tools available at the time do not rule out other possible interpretations, and some of the data is conflicting (195, 211, 217). In the following chapter, we use modern molecular biology techniques such as single-cell assays, Gibson Assembly (334), and next generation sequencing, alongside the robustness of *B. subtilis* genetics, to characterize PBSX. Furthermore, we approach PBSX as a modular system for phagocin production, and have successfully switched its specificity to target its resident strain, *B. subtilis* 168.

Materials and methods

General methods

All *B. subtilis* strains were derived from *B. subtilis* 168 unless specifically noted. *B. subtilis* strains utilized in this study are listed in Table 4.1. Plasmids are listed in Table 4.2. Oligonucleotide primers are listed in Table 4.3. The following concentrations of antibiotics were used for generating *B. subtilis* strains: 100 µg/ml spectinomycin, 7.5 µg/ml chloramphenicol, 0.8 mg/ml phleomycin, 10 µg/ml tetracycline, and 10 µg/ml kanamycin. To select for erythromycin resistance, plates were supplemented with 1 µg/ml erythromycin (*erm*) and 25 µg/ml lincomycin. *B. subtilis* transformations were carried out as described previously (271).

Table 4.1. Strains used in Chapter IV.

Strain	Description	Reference
Parental		
<i>B. subtilis</i> 168	<i>Bacillus subtilis</i> strain 168 <i>trpC2</i>	BGSC (1A866)
<i>B. subtilis</i> W23	<i>Bacillus subtilis</i> subsp. <i>spizizenii</i>	BGSC (2A9)
<i>E. coli</i> DH5 α	<i>F</i> <i>endA1 glnV44 thi-1 recA1 relA1 gyrA96 deoR nupG Φ80dlacZΔM15 Δ(lacZYA-argF)U169, hsdR17(<i>r_K⁻ m_K⁺</i>), λ-</i>	
<i>E. coli</i> TG1	<i>glnV44 thi-1 Δ(lac-proAB) Δ(mcrB-hsdSM)5, (<i>r_K⁻ m_K⁻</i>) F' [traD36 proAB⁺ lacI^q lacZΔM15]</i>	
<i>B. subtilis</i> 168		
BAS259	<i>xre G4S A19V L78V</i>	This study
BAS260	<i>xre G4S A19V</i>	This study
BAS342	<i>xre G4S A19V xhlB::kan</i>	This study
BAS350	<i>xre G4S A19V PBSX--Z hybridΩkan</i>	This study
BAS362	<i>xre G4S A19V xhlA::kan</i>	This study
BAS363	<i>xre G4S A19V xhlAB::kan</i>	This study
<i>E. coli</i> DH5α		
CAS85	<i>pminiMAD xre A19V (amp)</i>	This study
CAS89	<i>pminiMAD xre G4S A19V L78V (amp)</i>	This study
CAS91	<i>pminiMAD xre G4S A19V (amp)</i>	This study
CAS104	<i>pminiMAD xre G4S (amp)</i>	This study
<i>E. coli</i> TG1		
CAS86	<i>pminiMAD xre A19V (amp)</i>	This study
CAS90	<i>pminiMAD xre G4S A19V L78V (amp)</i>	This study
CAS92	<i>pminiMAD xre G4S A19V (amp)</i>	This study
CAS105	<i>pminiMAD xre G4S (amp)</i>	This study

Table 4.2. Plasmids used in Chapter IV.

Plasmid	Description	Reference
pminiMAD	<i>pminiMAD</i>	Dan Kearns
pAS061	<i>pminiMAD xre A19V (amp)</i>	This study
pAS065	<i>pminiMAD xre G4S A19V (amp)</i>	This study
pAS064	<i>pminiMAD xre G4S A19V L78V (amp)</i>	This study
pAS076	<i>pminiMAD xre G4S (amp)</i>	This study

Table 4.3. Oligonucleotides used in Chapter IV.

Oligo	Sequence 5' to 3'
OAS196	TCTGAGACTCTTCAATCTGCTGCCTATCATACTATGACCTC
OAS197	GAGGTCATAGTATGATAGGCAGCAGATTGAAGAGTCTCAGA
OAS198	CTGCATATCGCGGTATGCAACCTGCAGGTCCGGATCTGAGA
OAS199	TCTCAGATCCGGACCTGCAGGTTGCATACCGCGATATGCAG
OAS249	TACCGTTCGTATAGCATAACATTATACGAAGTTATGGATCCCAG CGAACCATTTG
OAS250	TACCGTTCGTATAATGTATGCTATACGAAGTTATGTGACAAA TTCCTCGTAGG
OAS286	AAGAATTGTACAGGAAAAGCT
OAS287	CTTCGTATAATGTATGCTATACGAACGGTAAAAAATCCCCCTT TAATGCTGC
OAS288	CTTCGTATAGCATAACATTATACGAACGGTAGGAGAGATGAAA ATGGTAAACAT
OAS289	CAATACGGAAAAGTGGTTCTCA
OAS297	ATGGCATTAAAAGCACAAAACACG
OAS298	TATTTGTTTACGCCTGAACTGTC
OAS299	GACAGTTCAGGCGTAAACAAATA
OAS300	CTTCGTATAATGTATGCTATACGAACGGTAAACGGCTGATTGA CGAGTATAAA
OAS301	CTTCGTATAGCATAACATTATACGAACGGTAGATCGCAGCGCA ATTAAGCTG
OAS302	TTGCCACTTCATCTCCGTAGA
OAS310	ATGCAGACACAACACTAGTGGAAG
OAS311	ATAACTTCGTATAATGTATGCTATACGAACGGTACTCTCACTC CTCCTTCACATG
OAS312	ATAACTTCGTATAGCATAACATTATACGAACGGTAAGGGGGAT TTTTATGAACACGT
OAS313	CGAAGGTCAAAGAAAAAATGTCC
OAS314	ATAACTTCGTATAGCATAACATTATACGAACGGTAGGAGAGAT GAAAATGGTAAACAT
OJH265	TTTGGATCCGCTCCAGCCATCTTCTGAC
OJH266	TGATACGATTTCTTCCTGTGTCCTTTTC
OJH267	AAAAGGACACAGGAAGAAATCGTATCA
OJH268	AAAAGCTTTTTAACACGTGGCACAGCTCA

Media

TY Broth is (per Liter) 10g tryptone, 5g yeast extract, 5g NaCl. This is autoclaved liquid setting for 20 min, followed by addition of 0.2μM filter sterilized MgSO₄ to 10mM and MnSO₄ to 100μM.

TY bottom agar is TY Broth + 1.5% (w/v) Bacto agar

TY top agar is TY Broth + 0.5% (w/v) Bacto agar

Loop in-loop out strain construction of unmarked temperature sensitive xre mutants

A single point mutant was generated in *xre* to make *A19V* by using overlap PCR. oJH 265 and oJH 266 as well as oJH 267 and oJH 268 were used to amplify fragments of *xre* from *B. subtilis* 168 genomic DNA while generating the *A19V* mutation (in the primers). Overlap PCR was performed using 0.5 μL each of the previously constructed fragments as template with oJH 265 and oJH 268, generating the full *xre A19V* construct. The construct was cloned into pminiMAD vector using BamHI/HindIII cut sites, making pAS061 *xre A19V* (erm)(amp), followed by transformation of *B. subtilis* 168 by single crossover homologous recombination and plating on LB-Lennox solid media supplemented with 1 μg/ml erythromycin with 25 μg/ml lincomycin (MLS) and incubated at room temperature for more than 24 hrs. Six colony isolates were then selected and Loop in-Loop out protocol (18) was used to generate the markerless point mutant in 168WT. *xre A19V* could not be made (see Results). The *G4S* mutation was generated in the *xre A19V* background by using pAS061 *xre A19V* as template for PCR with oJH 265 and oAS 196 as well as oAS 197 and oJH 268. Overlap PCR was

performed using 0.5 μ L of each previously constructed fragment as template with oJH 265 and oJH 268, generating the full *xre G4S A19V* construct. The construct was cloned into pminiMAD vector using BamHI/HindIII cut sites, making pAS065 *xre G4S A19V* (erm)(amp), followed by transformation of *B. subtilis* 168 by single crossover homologous recombination and plating on LB Lennox solid media supplemented with 1 μ g/ml erythromycin with 25 μ g/ml lincomycin (MLS) and incubated at room temperature for more than 24 hrs. Six colony isolates were then selected and Loop in-Loop out protocol (18) was used to generate markerless point mutant BAS 260 *xre G4S A19V*. The *L78V* mutation was generated in the *xre G4S A19V* background by using pAS065 *xre G4S A19V* as template for PCR with oJH 265 and oAS 198 as well as oAS 199 and oJH 268. Overlap PCR was performed using 0.5 μ L of each previously constructed fragment as template with oJH 265 and oJH268, generating the full *xre G4S A19V L78V* construct. The construct was cloned into pminiMAD vector using BamHI/HindIII cut sites, making pAS064 *xre G4S A19V L78V* (erm)(amp), followed by transformation of *B. subtilis* 168 by single crossover homologous recombination and plating on LB Lennox solid media supplemented with 1 μ g/ml erythromycin with 25 μ g/ml lincomycin (MLS) and incubated at room temperature for more than 24 hrs. Six colony isolates were then selected and Loop in-Loop out protocol (18) was used to generate markerless point mutant BAS 259 *xre G4S A19V L78V*. The *xre G4S* only point mutant was constructed by amplifying fragments of *xre* from *B. subtilis* 168 genomic using oJH 265 and oAS 196 as well as oAS 197 and oJH268. Overlap PCR was performed using 0.5 μ L of each previously constructed fragment as template with oJH

265 and oJH 268, generating the full *xre G4S* construct. The construct was cloned into pminiMAD vector using BamHI/HindIII cut sites, making pAS076 *xre G4S* (erm)(amp), followed by transformation of *B. subtilis* 168 by single crossover homologous recombination and plating on LB Lennox solid media supplemented with 1 µg/ml erythromycin with 25 µg/ml lincomycin (MLS) and incubated at room temperature for more than 24 hrs. Six colony isolates were then selected and Loop in-Loop out protocol (18) was used, although *xre G4S* is extremely temperature sensitive and not stable, and so strains could not be generated.

Lysis curves

An exponentially growing 5 mL culture of *B. subtilis* strains in TY broth was used to inoculate a 25 mL TY culture in a 250 mL baffled flask shaking at 280 rpm at 37°C in a New Brunswick C76 Shaker Bath at OD₆₀₀ = 0.00625. The culture was grown until between OD₆₀₀ of 0.1-0.25 (stated in figure) before shifting flask to a 48°C water bath that was shaking at 280rpm. OD₆₀₀ readings were taken at specified time intervals.

Lysate preparation

Cell debris was removed from lysates by centrifuging at 12,000 x g for 20 min at 4°C and passing the supernatant through 0.2 µm cellulose acetate filter (VWR). The lysates were stored at 4°C.

Killing units assay (spotting plates).

TY bottom agar plates were poured fresh and let dry. 200 μ L of a 5 mL BAS 338 *B. subtilis* W23 culture grown in TY broth to stationary phase (~5 hrs at 37°C) was added to 3 mL of TY top agar whose temperature was below 55°C, vortexed quickly, and poured (overlay) on the TY bottom agar plates and let dry. Prepared lysates were serial diluted in 10-fold increments in fresh TY broth and 10 μ L of each dilution was spotted on W23 overlaid plates and let air dry before they were placed in the incubator at 37°C overnight.

Adsorption assay

Five mL cultures of *B. subtilis* 168 or *B. subtilis* W23 were grown until OD₆₀₀ ~0.4 and 1 mL of each was pelleted at 8,000 x g in a tabletop centrifuge for 1 min. Supernatant was removed for each pellet and discarded, and pellets were resuspended in 250 μ L of PBSX lysate. Resuspended pellets were incubated at room temperature for 30 min, followed by centrifugation at 8,000 x g in tabletop centrifuge for 1 min. 100 μ L of each supernatant was subsequently serial diluted in 10-fold increments in fresh TY broth and 10 μ L of each dilution was spotted on W23 overlaid plates and let air dry before they were placed in the incubator at 37°C overnight (as previously stated).

Microscopy

Microscopy was performed as described in Chapter II. For fluorescent microscopy, exposure time for GFP channel was 1 sec, CFP channel was 1 sec, and

TxRed channel was 400 ms unless otherwise stated. All images were adjusted equivalently unless otherwise stated. All microscopy mounts for images presented in Chapter IV were done on 1% agarose pads.

Alexa Fluor 488 Maleimide labeled PBSX

PBSX was poly(ethylene glycol) (PEG) precipitated from a BAS 260 lysate by adding 7.5 mL of 3X PEG 8000 (30% poly(ethylene glycol) 8000, 3.0 M NaCl) to 15 mL of lysate, mixing by pipetting up and down and inverting the tube, and incubating overnight at 4°C (~16 hrs). PBSX was pelleted by centrifuging at 12,000 x g for 20 min at 4°C. The PBSX pellet was washed once with 10 mL of 1X PBS followed by another round of centrifugation at 12,000 x g for 20 min at 4°C. Afterwards, the PBSX pellet was let resuspend in this 10 mL 1X PBS overnight at 4°C (~16 hrs). The resuspended phage sample (~10 mL) was mixed with 4 mL of 1X PBS and added to an Amicon 100 kDa concentrator (concentrator was first rinsed with 3 mL PBS followed by centrifugation at 6,000 x g for 5 min) and centrifuged at 6,000 x g for 5 min at 4°C. An additional 9 mL of cold 1X PBS was added to the sample and centrifugation was repeated. This process was repeated three times, followed by concentrating the sample to 1mL by centrifuging at 12,000 x g for 20 min at 4°C. The sample was then fluorescently labeled by incubating with Alexa Fluor 488 C₅ Maleimide (Invitrogen) at a final dye concentration of 5 µg/mL for 5 min at room temperature. The labeled phage was immediately dialyzed at a 1/400 ratio for three buffer exchanges at 2 hr increments at

4°C. The labeled PBSX was stored in the dark at 4°C, and the viability was confirmed by spotting the Alexa Fluor 488-labeled PBSX on W23.

Gibson assembly to generate the PBSX-PBSZ hybrid phage in B. subtilis strain 168

oAS 297 and oAS 298 were used with *B. subtilis* W23 genomic DNA template to amplify PBSZ *gene 27* with 7500 bp downstream (Piece 1). oAS 299 and oAS 300 were used with W23 genomic DNA template to amplify from 7500bp downstream of *gene 27* to 15,000bp downstream of *gene 27* (Piece 2). A kanamycin resistance cassette was amplified from pWX114a using oAS 249 and oAS 250. oAS 301 and oAS 302 were used on *B. subtilis* 168 genomic to amplify the region immediately downstream of *xlyA* (Piece 4). Piece 1 had a 30bp overlap with Piece 2, which had a 30bp overlap with the kanamycin cassette. Piece 4 had a 30bp overlap with the kanamycin resistance cassette. All of the amplified fragments with respective 30bp overhangs (Piece 1, 2, 4, and kanamycin cassette) were ligated together in a 20 µL isothermal single step Gibson Assembly reaction (334), and the entire reaction was used to transform BAS 260 *xre G4S A19V* by double crossover homologous recombination, and the cells were plated on TY solid media supplemented with 10 µg/mL kanamycin and incubated overnight at 37°C (~16 hrs).

Gibson assembly to generate xhIA, xhIB, and xhIAB knockouts

BAS 362 xre G4S A19V xhIA::kan

oAS 310 and oAS 311 were used with *B. subtilis* 168 genomic DNA template to amplify the upstream region of *xhIA* (Piece 1). A kanamycin cassette was amplified as previously stated (Methods, Chapter IV). oAS 312 and oAS 313 were used with *B. subtilis* 168 genomic DNA template to amplify the downstream region of *xhIA* (Piece 3). All of the amplified fragments with respective 30bp overhangs (Piece 1, 3, and kanamycin cassette) were ligated together in a 20 μ L isothermal single step Gibson Assembly reaction (334) and the entire reaction was used to transform BAS 260 *xre G4S A19V* by double crossover homologous recombination, and the cells were plated on TY solid media supplemented with 10 μ g/mL kanamycin and incubated overnight at 37°C (~16 hrs).

BAS 342 xre G4S A19V xhIB::kan

oAS 286 and oAS 287 were used with *B. subtilis* 168 genomic DNA template to amplify the region upstream of *xhIB* (Piece 1). A kanamycin cassette was amplified as previously stated (Methods, Chapter IV). oAS 288 and oAS 289 were used with *B. subtilis* 168 genomic DNA template to amplify the region downstream of *xhIB* (Piece 3). All of the amplified fragments with respective 30bp overhangs (Piece 1, 3, and kanamycin cassette) were ligated together in a 20 μ L isothermal single step Gibson Assembly reaction (334) and the entire reaction was used to transform BAS 260 *xre G4S A19V* by double crossover homologous recombination, and the cells were plated on TY

solid media supplemented with 10 µg/mL kanamycin and incubated overnight at 37°C (~16 hrs).

BAS 363 xre G4S A19V xhlAB::kan

Piece 1 and the kanamycin resistance cassette were amplified as previously stated (Methods, Chapter IV, BAS 362 strain construction). oAS 314 and oAS 313 were used with *B. subtilis* 168 genomic DNA template to amplify the region downstream of *xhlB* (Piece 3). All of the amplified fragments with respective 30bp overhangs (Piece 1, 3, and kanamycin cassette) were ligated together in a 20 µL isothermal single step Gibson Assembly reaction (334) and the entire reaction was used to transform *BAS 260 xre G4S A19V* by double crossover homologous recombination, and the cells were plated on TY solid media supplemented with 10 µg/mL kanamycin and incubated overnight at 37°C (~16 hrs).

Results

PBSX can be induced via temperature shift of an *xre G4S A19V L78V* mutant from 37°C to 48°C (219). Although it was speculated that the mutation conferring temperature sensitivity was A19V (as it resided within the predicted helix-turn-helix motif), it was never experimentally determined. *B. subtilis* 168 containing *xre G4S*, *xre A19V*, *xre G4S A19V*, and *xre G4S A19V L78V* at the native locus (unmarked) were constructed (or attempted to be constructed) and subjected to temperature shifts to assay for thermostability. *xre G4S A19V* and *xre G4S A19V L78V* both conferred

thermosensitivity to *B. subtilis* strain 168 and resulted in the production of functional PBSX (Fig 4.1A). There did not appear to be any difference in the lysis dynamics or killing efficiency comparing the *xre G4S A19V* and *xre G4S A19V L78V* (Fig 4.1B). Electron microscopy was used to confirm the presence of fully assembled phagocin particles (Fig 4.1C). Although an *xre A19V* was attempted to be made, it could not be constructed, suggesting that the *xre A19V* mutant encodes a nonfunctional Xre. In the context of phage induction, a nonfunctional phage repressor results in initiation of the lytic cycle of the prophage, and subsequent cell death; therefore, any nonfunctional Xre variant will be unable to be isolated. Furthermore, when making the *xre G4S* mutant, the only transformants obtained were those grown at room temperature on a TY plate (non-permissive even at 37°C) and were difficult to propagate; *xre G4S* merodiploid transformants were constructed that would only grow at room temperature as well. These strains barely grew in liquid TY media, and when the strains were sent for sequencing, the sequencing results showed they were wild-type *xre*. This indicates that the *xre G4S* mutant encodes a highly temperature sensitive Xre that exhibits a dominant negative phenotype (shown in merodiploid strain), and that the strains that grew in liquid media were revertants.

PBSX specifically targets *B. subtilis* W23 while PBSZ specifically targets *B. subtilis strain* 168 (168WT). This resistance is caused by the inability of PBSX to adsorb to 168WT as shown through an adsorption assay, as well as fluorescently labelled PBSX single cell adsorption assay (Fig 4.2). PBSX clearly adsorbs to W23 in both batch adsorption and single cell adsorption assays (Fig 4.2).

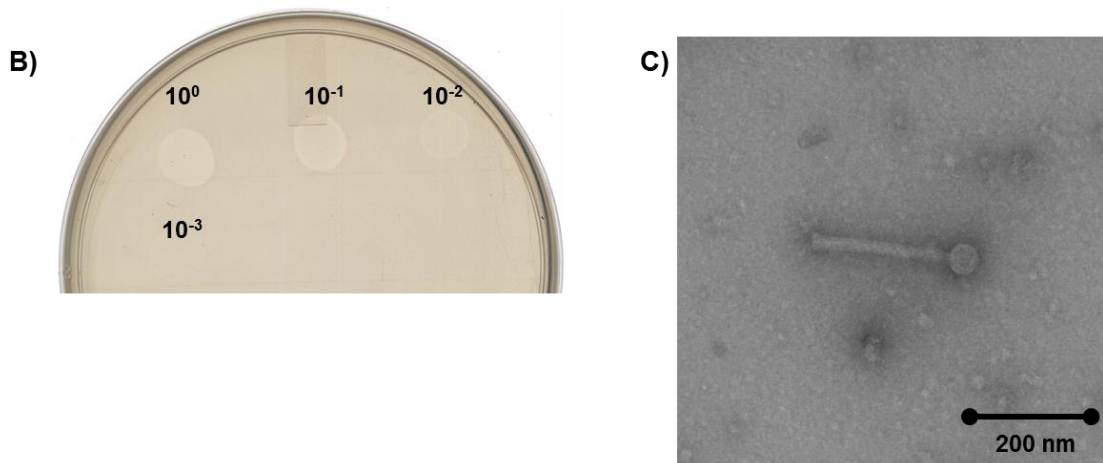
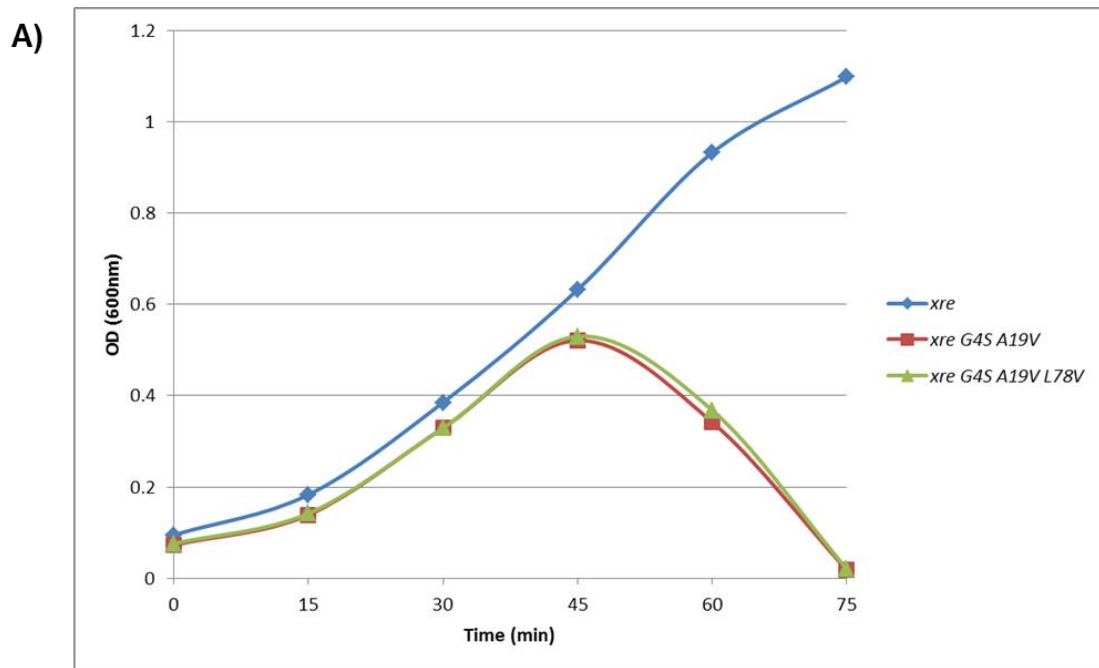


Figure 4.1. PBSX is successfully induced and assembled from thermosensitive *xre*. A) Lysis curve of 168WT, BAS 259 *xre G4S A19V L78V*, and BAS 260 *xre G4S A19V*. Time zero denotes temperature shift from 37°C to 48°C at OD₆₀₀ ~ 0.100. Time is denoted in minutes along the X-axis and OD₆₀₀ is denoted along the Y-axis. B) Spotting 10 μL of BAS 259 *xre G4S A19V L78V* lysate (serially diluted) on a lawn of W23 and incubation at 37°C overnight. C) BAS 259 *xre G4S A19V L78V* lysate concentrated via ultracentrifugation and stained with Uranyl Acetate and visualized at 25,000 x magnification using Jeol 1200 Transmission Electron Microscope.

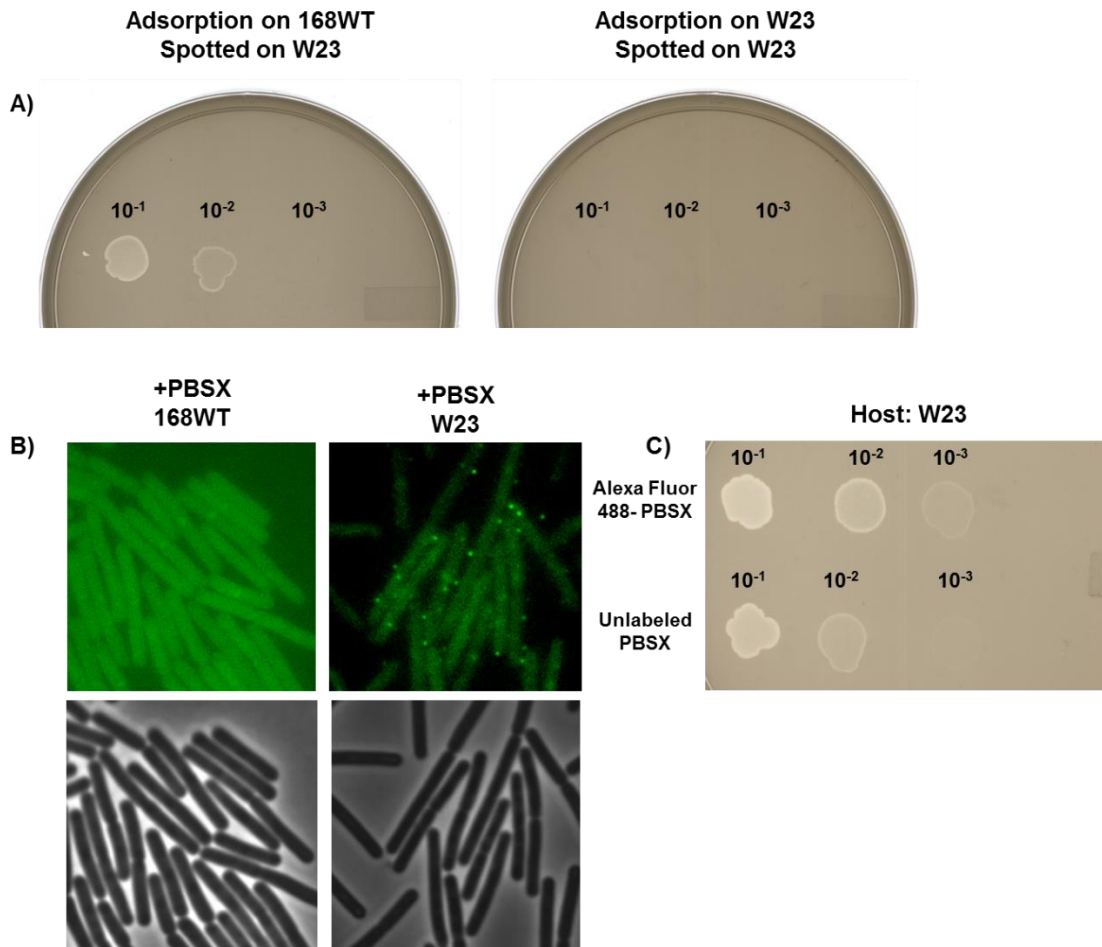


Figure 4.2. PBSX adsorbs to *B. subtilis* W23 but not *B. subtilis* strain 168WT. A) PBSX was adsorbed for 30 min on strain denoted, culture was pelleted, and supernatant was serially diluted and spotted on sensitive strain. TY plate was incubated overnight at 37°C. B) Single cell adsorption assay using Alexa Fluor 488 labeled PBSX adsorbed for 10 min with either 168WT or W23. GFP channel on top two panels and image contrast adjusted to allow punctate foci (phagocin) to appear clearer. PBSX+168WT control image contrast adjusted maximally to look for the presence of any phagocin. Bottom two panels are phase contrast images of the cells. C) Unlabeled and Alexa Fluor 488 labeled PBSX spotted on W23.

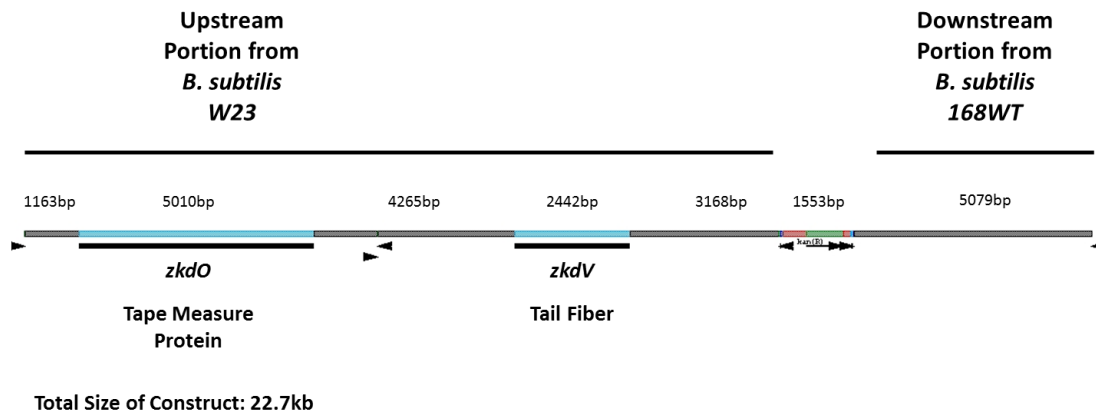


Figure 4.3. Genetic construct of hybrid PBSX-PBSZ phagocin. The tape measure and tail fiber genes from PBSZ were linked to a kanamycin cassette using Gibson Assembly and the subsequent linear DNA piece was transformed into *B. subtilis* 168 through homologous recombination

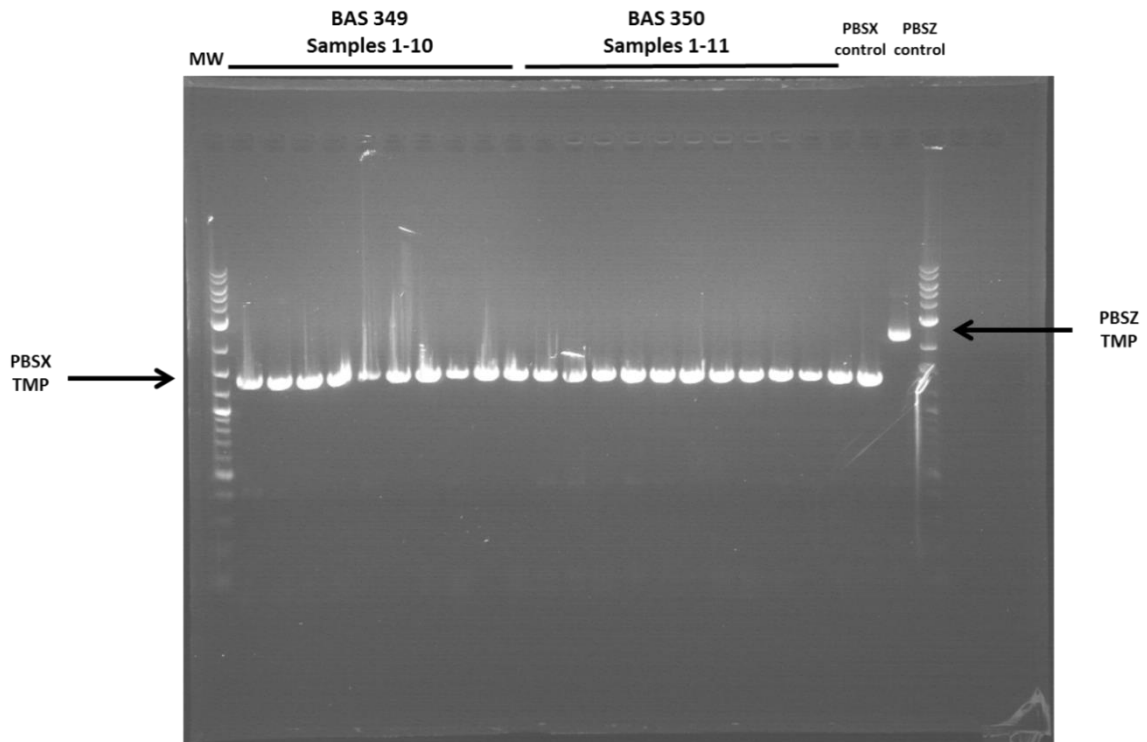


Figure 4.4. DNA gel confirmation of tape measure proteins. Lane 2 to lane 11 are for BAS 349 hybrid PBSZ and lane 12 to lane 22 are for BAS 350 *xre G4S A19V* hybrid PBSZ strain.

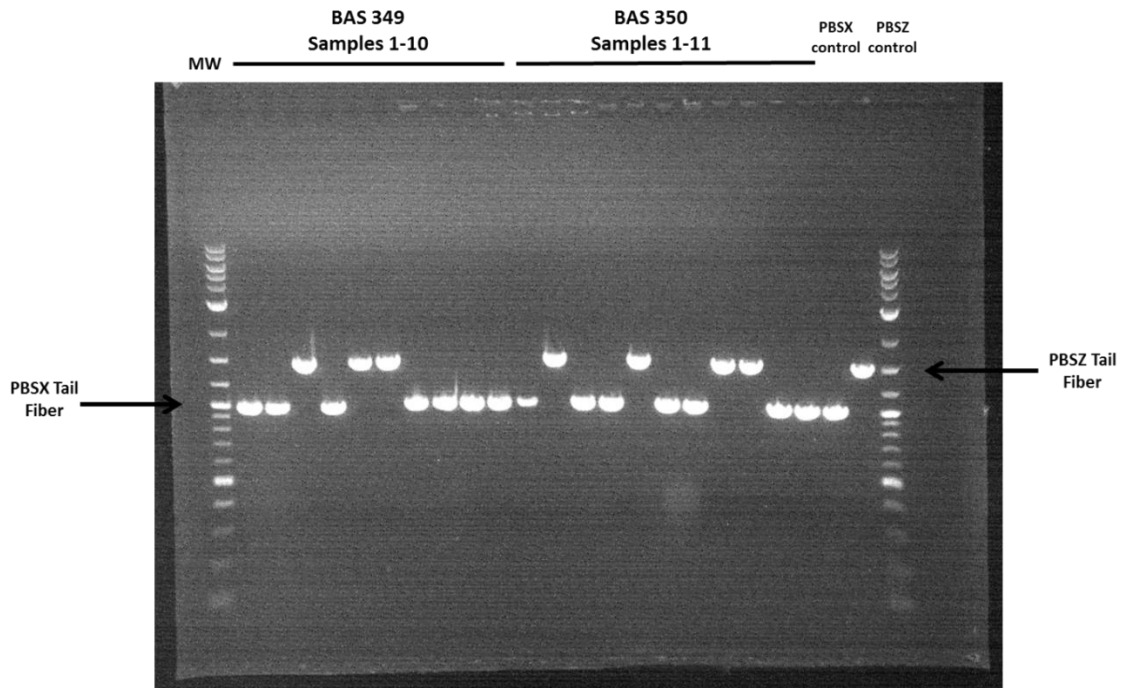


Figure 4.5. DNA gel confirmation of tail fiber proteins. Lane 2 to lane 11 are for BAS 349 hybrid PBSZ and lane 12 to lane 22 are for BAS 350 *xre G4S A19V* hybrid PBSZ strain.

When comparing PBSX and PBSZ, the two phagocin are almost identical, with the exception of the tape measure protein and the tail fiber protein. The tape measure protein and the tail fiber protein are both larger in PBSZ than those in PBSX, and the differing regions reside in the C-terminal region of the tape measure protein and the C-terminal region of the tail fiber protein. This begged the question: what was the determinant of specificity, and furthermore, were these two phagocin modular? To determine the minimum requirement for specificity, a single enzymatic assembly construct fusing the tape measure and tail fiber proteins of PBSZ to PBSX within the *B. subtilis* 168 genome (Fig 4.3) was generated and subsequently transformed into *B. subtilis* 168. We were unable to generate a temperature sensitive PBSZ or work within *B. subtilis* W23, as it was not naturally competent, and all methods to transform *B. subtilis* W23 proved ineffective (unpublished, Sperber, Theodore and Young) (335-338). Transformants were plated on kanamycin, isolated, and then grown up in liquid culture for induction by Mitomycin C (BAS 349 hybrid PBSZ) or temperature shift (BAS 350 *xre G4S A19V* hybrid PBSZ). Lysates were then spotted for host sensitivity on 168WT and W23. Concurrently, genomics of all strains were made (see Chapter II Methods) and subsequently the Tape Measure protein and the Tail Fiber protein were amplified by PCR and run on a 1% Agarose gel to look for a hybrid phagocin construct (21 strains were constructed and screened). (Fig 4.4-4.5). All transformants of BAS 349 and BAS 350 failed to have crossover of the PBSZ Tape Measure protein (Fig 4.3 and Fig 4.4), although 8/21 had successful crossover of the PBSZ Tail Fiber protein (Fig 4.3 and Fig 4.5). When the lysates of all 21 isolates were spotted on either 168WT or W23, only

lysates of strains which possessed the PBSZ Tail Fiber would kill 168WT and subsequently no longer kill W23 (Fig. 4.6). This data demonstrates that the Tail Fiber of PBSZ is sufficient to confer a switch of host for PBSX.

The ability switch specificity of the phagocin PBSX within *B. subtilis* 168 in a system that allowed thermoinducibility of the phagocin brought about a need to produce more phagocin per induced bacterial cell. Increasing phage per cell during phage infection (burst size) can be achieved by knocking out the holin gene, which allows increased accumulation of phage as the cell continues to produce phage after a time when typically, the holin would trigger cell lysis (through the other lysis proteins). In *B. subtilis*, *xlyA* is the endolysin (N-acetylmuramoyl-L-alanine amidase), *xhlB* is the holin, and *xhIA* is a membrane associated protein; *xhIA* and *xhlB* are both required for host lysis, and PBSX encodes a second endolysin outside of the lysis cassette (*xlyB*) (339, 340). It is not clear what the role of *xhIA* is during host lysis, as it does not appear to act as an antiholin, rather it seems to act in concert with *xhlB* to facilitate host lysis (340). The lysis genes *xhIA*, *xhlB*, and both *xhIAB* were systematically knocked out without leaving any antibiotic resistance marker (see Methods) in the temperature sensitive *xre* background and lysis curves were performed. Consistent with previous literature (340), $\Delta xhlB$ delays lysis by around 20min and lysis itself is less concerted (Fig 4.7), $\Delta xhIA$ prevents cell lysis but also causes growth to plateau around transition ($OD_{600} \sim 0.8$), and $\Delta xhIAB$ allows further cell growth into stationary phase and prevents cell lysis (Fig 4.7). Unlysed cells were subsequently lysed (see Methods) and all strains were serially diluted and spotted on *B. subtilis* W23 to assay for killing units. If the lysis gene knockouts

allow additional accumulation of phage (similar to holin knockouts in Gram-negative), then the killing units will increase. Unfortunately, we did not have an increase in killing units in BAS 362 or BAS 363 (Fig 4.8) over killing units in wild type (BAS 260); however, this could have been an issue with cell lysis of the *xhIA* or *xhIAB* knockouts, and so variations on the lysis method will be performed to ensure accurate assaying of killing activity. Currently, a Western blot based approach using an antibody that is specific for the major capsid protein is being utilized to quantify the number of phagocin in both the wild type and the *xhIA* and *xhIAB* knockouts (BAS 362 and BAS 363, respectively).

During traditional phage infection, the membrane potential of the cell is transiently dissipated as the phage DNA is ejected into the cell; this process is followed by the subsequent plugging of the hole, repolarization of the host cell, and the progression of the phage infection cycle, either lytic or lysogenic. Failure of the host cell to reestablish the membrane potential results in cell death. It is thought that PBSX (and other phagocins) kill their host by mechanically puncturing and depolarizing the membrane, while not subsequently closing the hole, similar to pyocins (333).

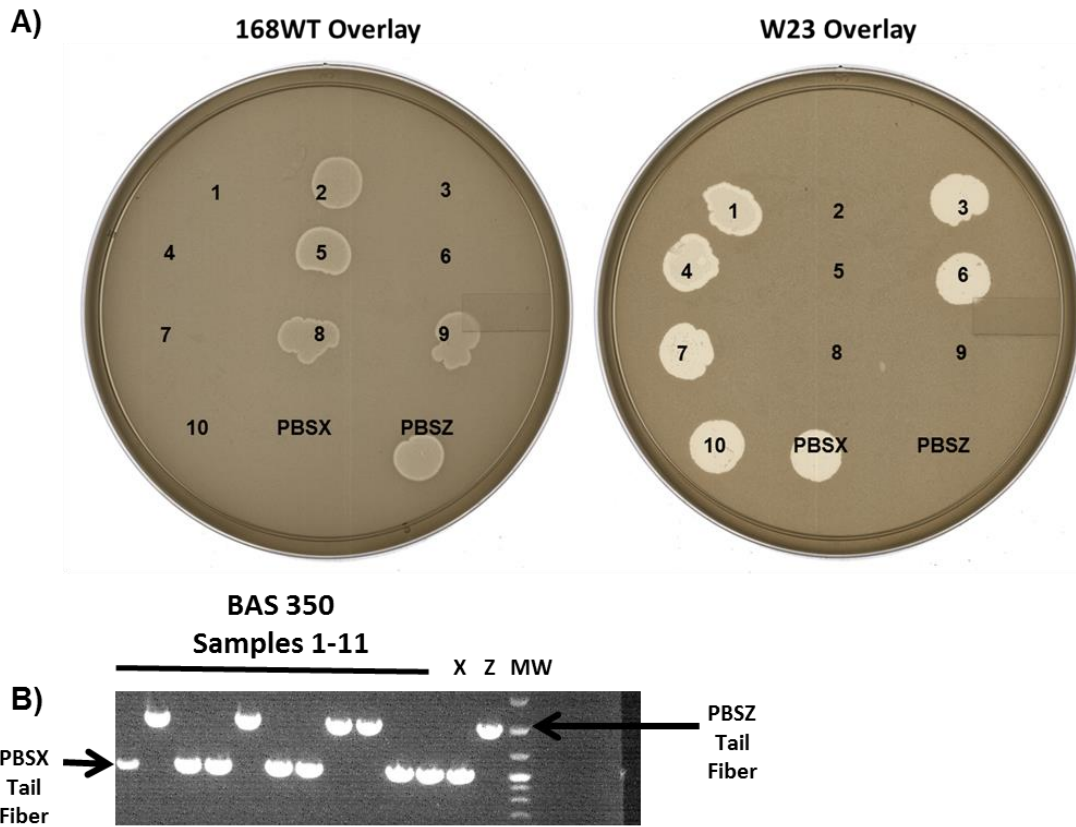


Figure 4.6. The tail fiber of PBSZ is sufficient to switch host specificity from *B. subtilis* W23 to *B. subtilis* 168. A) Spotting 10 μ L of BAS 350 *xre G4S A19V* hybrid PBSZ (strains 1-11) on 168WT or W23 as a host. B) DNA gel confirmation of which tail fiber genes were integrated into the different BAS 350 strains. Note that all strains that contained a PBSZ tail fiber gene produced lysates that no longer killed W23 but instead killed 168WT.

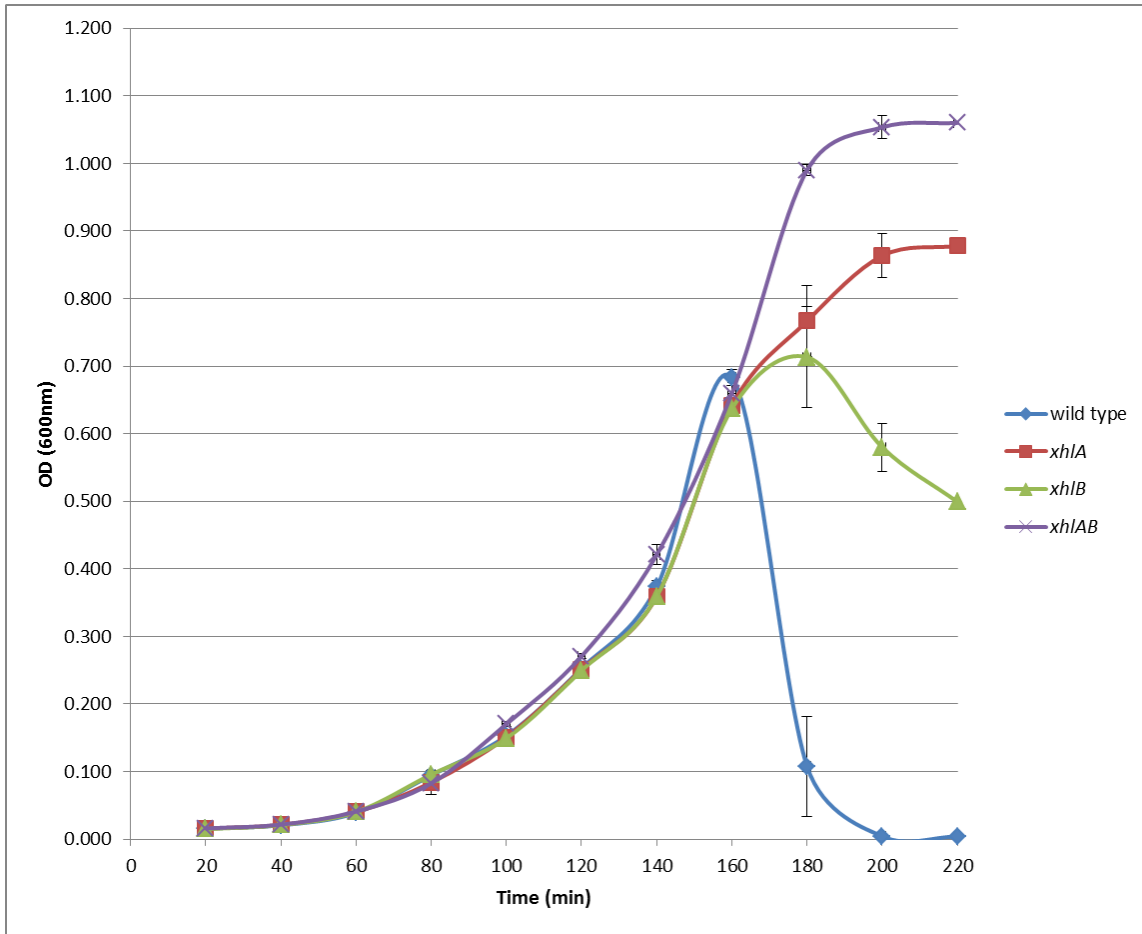


Figure 4.7. Lysis curve of PBSX lysis gene knockouts. Knockouts of the lysis genes *xhlA* and *xhlB* were assayed for defect in cell lysis dynamics. Wild-type is BAS 260 *xre G4S A19V*; all other knockouts were constructed in this temperature sensitive background. PBSX induced by shifting from 37°C to 48°C at around 120 min OD₆₀₀ ~0.220.

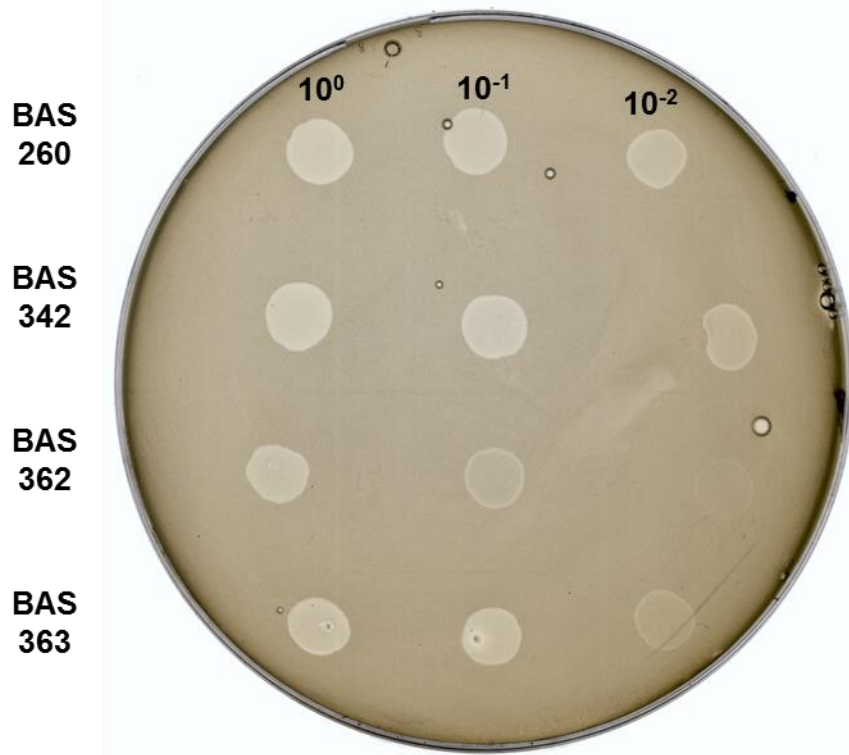


Figure 4.8. Lysate spotting of WT, *xhIA*, *xhIB*, and *xhIAB* knockouts. 10 μ L of PBSX lysates were serial diluted in TY and spotted on *B. subtilis* W23. Killing zones are clear spots on the plate. BAS 260 *xre G4S A19V*, BAS 342 *xre G4S A19V xhIB::kan*, BAS 362 *xre G4S A19V xhIA::kan*, BAS 363 *xre G4S A19V xhIAB::kan*.

To visualize membrane depolarization at the single cell level, we used Alexa Fluor 488 labeled PBSX and stained the host with the Nernstian voltage indicator dye Thioflavin T (ThT) (341, 342). Thioflavin T is a fluorescent cationic dye that is retained in the cell when a membrane potential is present (341). Due to crossover between the GFP and CFP channels, the individual fluorescent phages could not be visualized (Fig 4.9); however, cells that were phase dark (dead) had lost their Thioflavin T signal (Fig 4.9A). However, it does not appear that ThT is only reporting on membrane potential. Dinitrophenol (DNP) permeabilizes the cell to H^+ ions, causing a loss of $\Delta\Psi$ and ΔpH , and the cells treated with DNP still retained ThT (Fig 4.9B). Furthermore, when cells were treated with the K^+ ionophore valinomycin alongside a potassium clamp (causes a loss of $\Delta\Psi$), overall ThT became less retained, but it was not significantly different than the solvent only control. Controls in the Prindle et al. 2015 paper used valinomycin and CCCP. I could not reproduce his valinomycin result and my DNP did not behave similarly to his CCCP control. Although it appears that ThT can report on phage depolarization of the membrane, the lack of response of ThT to characterized membrane potential disrupting compounds prevents the further use of this dye until it is better characterized, despite its use in the literature (341, 342). Other voltage sensitive dyes that are better characterized are DiSC₃(5) and DiBAC₄(3) (343), and may prove useful in further experiments.

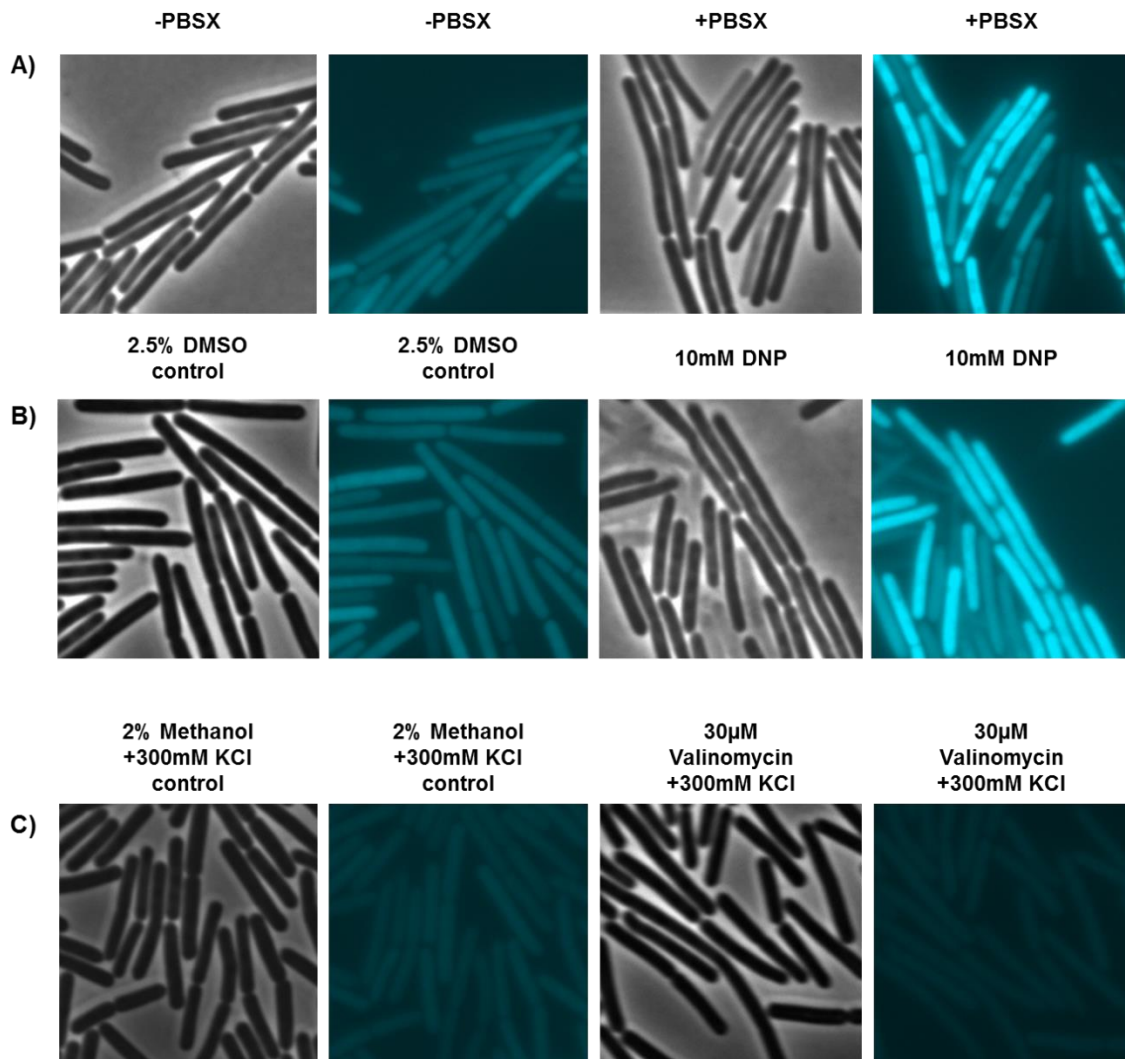


Figure 4.9. Single cell membrane potential assay using Alexa Fluor 488 labeled PBSX and Thioflavin T (ThT) stained *B. subtilis* W23. A) Mid exponential culture of *B. subtilis* W23 was incubated with 10 μ L of Alexa Fluor 488 Labeled PBSX for 5 min at room temperature before pelleting and resuspending in PBS (control incubated with 10 μ L of 1X PBS). Cells were labeled with 10 μ M ThT for at least an hour (in TY culture) before time point to give time for dye to accumulate. B) Exponentially growing cells were treated with 10 mM DNP for 20 min and stained with 10 μ M ThT as previously stated. Phase contrast and CFP channel images taken. Solvent only control image on the far left. C) Exponentially growing cells were treated with 30 μ M Valinomycin with a 300 mM KCl clamp for 40 min and stained with 10 μ M ThT as previously stated. Phase contrast and CFP channel images taken. Solvent only control with 300 mM KCl clamp on far left.

At the same time, a complementary approach was taken to visualize dissipation of membrane potential by PBSX at the single cell level (Fig 4.10). 5-Cyano-2,3-ditolyl tetrazolium chloride (CTC) is a live-dead stain that functions by being reduced into an insoluble red fluorescent formazan product by actively respiring cells (via electron transport chain). This dye allowed the use of respiration as a proxy for membrane potential, as cells cannot continue respiration in the absence of membrane potential. Cells treated with Alexa Fluor 488 labeled PBSX prior to staining with CTC had marked reduction in CTC staining; notably, cells showing a phage adsorbed had little to no CTC staining. PBSX untreated cells stained that were processed in the same manner as the PBSX treated cells showed strong CTC signal across the entire field of view. There are numerous cells in the PBSX treated sample that do not show phage adsorbed to the surface but lack CTC signal. An explanation for this observation is that phage had already adsorbed and disrupted the membrane potential but fell off during the pelleting and resuspension process. If this is the situation, it would suggest that after the initial phage adsorption to the cell and depolarization of the membrane, that the cell cannot subsequently regenerate its membrane potential even if the phage is somehow removed from the surface.

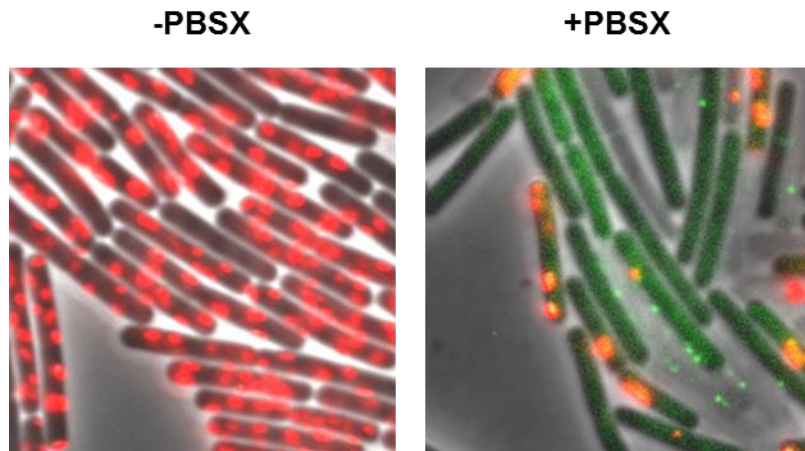


Figure 4.10. PBSX single cell adsorption assay with redox dye CTC. Exponentially growing *B. subtilis* W23 was incubated with 2 μ L of Alexa Fluor 488 labeled PBSX for 10 min before spinning down and resuspending in 1X PBS with 4 mM CTC and incubating for 5 min before imaging on 1% agarose pad. GFP channel (1 sec exp) and TxRed channel (400 ms exp) used for imaging.

Table 4.4. PBSX-Z requires glucosylated teichoic acids and minor teichoic acids for killing activity. R denotes resistance to killing and S denotes sensitivity to killing (or infection).

Mutant (<i>Bs168</i> parent)	PBSZ	PBSX-Z	SPP1
<i>ugtP::erm</i>	?	S	S
<i>ggaA::erm</i>	R	R	S
<i>ggaB::erm</i>	R	R	S
<i>gtaB::erm</i>	R	R	S
<i>yueB::erm</i>	S	S	R

Discussion:

In this work, PBSX was characterized using single cell assays and modern genetics approaches that further elucidate the nature of the lysogenic repressor *xre* as well as the lysis genes *xhlA* and *xhlB*. Although previous literature suggested that A19V was the point mutation (within the helix-turn-helix motif) that would confer temperature sensitivity to Xre, at least two point mutations (G4S and A19V) are required to confer the temperature sensitivity. Furthermore, having all three point mutations (G4S, A19V, and L78V) does not result in any difference in lysis dynamics upon thermal induction of PBSX (Fig 4.1A). An *xre* A19V mutant was unobtainable; after screening over 148 transformants, no transformant was temperature sensitive (unable to grow at 48°C due to PBSX induction), and all isolates sent for sequencing were wild type *xre*. *xre* G4S appeared to be an extremely temperature sensitive allele, with the merodiploid isolate (plasmid integrated by single crossover) growing only at room temperature while the mutant (presumably) barely grew at room temperature. Neither of these isolates were stable; they were difficult to culture in liquid media, and reverted to wild-type (sequenced *xre*). The thermoinducible *xre* strains (BAS 259 *xre* G4S A19V L78V and BAS 260 *xre* G4S A19V) produced fully assembled PBSX that targeted and killed *B. subtilis* W23. It has not yet been determined whether or not *xre* G4S A19V is thermolabile or if it undergoes a conformational change at the higher temperatures preventing interaction with its cognate binding sites.

Generating the temperature sensitive *xre* mutant allows for a thermoinducible PBSX; this allows for specific induction of only PBSX in *B. subtilis* strain 168, rather

than using Mitomycin C or Carbadox to SOS induce the phagocin (this would also induce SP β). From a phage therapeutics standpoint, the ability to thermoinduce PBSX avoids the added cost of expensive reagents such as Mitomycin C. From a clinical application standpoint, purifying a single phage from a lysate rather than a cocktail of phage (if SOS response was used to induce) makes the method of production easier to pass through stringent guidelines for treatment of patients. Since *xre* was shown to have sequence homology to other phage repressors (219), the current work could be used to generate temperature sensitive alleles of phage repressors in other systems, thereby eliminating the need to use SOS induction of lysogenic phages and the drawbacks that coincide with this technique.

It was already known that PBSX kills *B. subtilis* W23 and PBSZ kills *B. subtilis* 168 (219). Using a plate based adsorption assay (Fig 4.2A) as well as an Alexa Fluor 488 labeled PBSX single cell adsorption assay (Fig 4.2B), it was shown that PBSX specifically adsorbs to *B. subtilis* W23 but not *B. subtilis strain* 168. While some phage are suggested to have a preference for the cell poles during infection (344), PBSX did not appear to show a preference for the cell poles or the lateral cell wall (Fig 4.2B).

The ability to switch specificity of PBSX from targeting *B. subtilis* W23 to targeting *B. subtilis* 168 (Fig 4.6) suggests some level of modularity within the PBSX-like phagocins in *Bacillus* (215). Whether this modularity in host range can be extended to organisms outside of the *Bacillus* genera is the focus of additional studies. Ideally, further experiments will identify which portion of the tail fiber is necessary and sufficient to confer specificity for the host. If specificity can be altered to more distant

organisms, one could target specific pathogens, even in the human gut, while leaving beneficial bacteria unaffected. Furthermore, the BAS 363 *xre G4S A19V xhlAB::kan* strain would be a powerful system for commercial or clinical production of large quantities of the PBSX (variant), as it is thermoinducible and lysis inhibited (Fig 4.7), thereby avoiding use of SOS response inducing chemicals like Mitomycin C, and should generate more phagocin per volume of cell culture than wild-type.

The use of Thioflavin T (ThT) as a voltage sensitive membrane stain has only recently appeared in the literature (341, 342), and has not been extensively characterized. Phase dark cells in the PBSX treated culture lacked strong fluorescence, and some cells that appeared alive in phase contrast appeared to lack fluorescence (Fig 4.9A); presumably, these cells were killed by phagocin, although the experiment will have to be repeated with phagocin labeled with a compatible fluorophore to be used with ThT. An alternative explanation of the results is that the cells which had PBSX adsorbed to them were actually brighter, as the “hole” in the membrane generated by PBSX would allow increased flow of the dye into the cell. Using a compatibly labeled fluorescent PBSX will address this question. Use of characterized compounds that disrupt the membrane potential were inconclusive (Fig 4.9B and 4.9C), once again highlighting that ThT is not well characterized as a bacterial membrane potential dye. *B. subtilis* W23 cells incubated with fluorescent PBSX had lost their metabolic activity after only five minutes of incubation with the phagocin, suggesting that not only is the adsorption of PBSX rapid but the killing is almost instant (Fig 4.10). Further experiments using fluorescently

labelled phages (like SPO1) will be performed to interrogate lack of perturbation of the metabolic state of the cell upon phage adsorption.

CHAPTER V

SUMMARY AND FUTURE DIRECTIONS

Summary of Chapters II and III

Screening a *B. subtilis* misexpression library allowed for the identification of two previously uncharacterized genes, *yodL* and *yisK*, that are involved in cell morphogenesis. *yodL* and *yisK* would not have been identified through screening knockout/knockdown libraries or through homology modeling; the knockout phenotypes are mild (see Chapter II), and while *yisK* shares homology with fumarylacetoacetate hydrolases (see Chapter III), these enzymes have not been linked to cell morphogenesis at this time. Furthermore, *yodL* is novel, and does not show homology to any genes of known function. Using a suppressor analysis followed by a genetic approach allowed for the discovery that YodL activity requires *mreB* and that YisK activity requires *mbl* for their shape modifying activity, specifically. This is interesting considering MreB and Mbl are highly similar, and their overlapping and distinct roles in cell envelope synthesis are still being investigated (60, 61, 65, 68).

This is the first time that suppressor mutants were able to be obtained in the MreB-like proteins in a Gram-positive bacterium. Small molecule inhibitors such as A22 do not affect Gram-positives (254, 255), and so it has been difficult for the scientific community to tease apart the unique functions of each MreB-like protein in *B. subtilis*. Much of the current information differentiating the unique roles of the different MreB-like proteins in *B. subtilis* has been through interrogating their differential regulation (60,

61, 65, 68), although certain specific functions such as regulation of the autolysin CwlO by Mbl and LytE by MreBH (and genetically to MreB) have been determined (66, 69).

Using the line of evidence that Mbl regulates FtsEX and CwlO activity and that YisK appeared to target Mbl, YisK was identified as interacting with FtsE, facilitating its cell shortening activity. This would suggest a localization of YisK at the membrane, alongside FtsEX and Mbl, although analysis of YisK's primary amino acid sequence as well as the crystal structure of YisK suggests a cytoplasmic localized protein. Preliminary results with a functional YisK-GFP sandwich protein under the native promoter shows a punctate-helical localization along the lateral cell wall, reminiscent of Mbl localization (Guo and Herman, unpublished). This result is exciting, as the localization of YisK alludes to a possible mechanism of affecting cell shape during misexpression conditions.

In the process of solving the crystal structure, a compound binding YisK in the putative active site was revealed. Through differential scanning fluorimetry analysis (311-313), it was shown that the compound in the structure was most likely L-tartrate, and that YisK binds dicarboxylic acids with a high degree of specificity, as even changes in chirality (i.e. mesotartrate or dihydroxyfumarate) can have significant effects on the ability of YisK to bind a compound (Fig 3.14). It is likely that the true substrate for YisK *in vivo* is a compound highly similar to L-tartrate or dihydroxyfumarate.

In mutating residues which coordinate the divalent cation that is critical for catalysis in characterized FAHs, it was observed that the ability of YisK to perturb cell shape is distinct and separable from its activity as an enzyme. Along these lines, a

mutational analysis of YisK was performed, where YisK was assayed for self-interaction, FtsE interaction, and loss of cell shape activity (when misexpressed). YisK E30A was capable of self-interaction and FtsE interaction, but could no longer kill on a plate or result in a loss of cell shape when misexpressed (Fig 3.16). This variant needs to be purified in order to assay for binding L-tartrate (to confirm its active site is still folded correctly), but this variant also shows a separability of the shape modifying activity of YisK with its role as an enzyme. These data inform our current model, that YisK uses Mbl and FtsE to localize to a region of the cell where its substrate is present and/or its product is needed (Fig 3.28). Enzymes involved in carbon metabolism interacting with the PG synthesis machinery is not uncommon (156, 157, 160), and could serve the important function of substrate channeling, especially in instances where the substrate or product of a reaction is unstable. Furthermore, localization of YisK at/near the PG synthesis machinery could play a role in regulating the metabolic flux through different pathways by competing for shared precursors. One may speculate that expression of *yisK* during stationary phase, when cell density is high and nutrients are limited, could be a mechanism of *B. subtilis* retooling its PG synthesis machinery to utilize other pathways for generation of the required precursors.

Summary of Chapter IV

Mutations within the PBSX repressor (Xre) that confer temperature sensitivity to Xre were determined to be G4S and A19V. *xre G4S* was extremely temperature sensitive and therefore was not stable, and *xre A19V* was probably nonfunctional, as mutants were

unobtainable. Xre G4S A19V was stable at 37°C and showed thermal sensitivity at 48°C, while showing no difference in lysis dynamics or measurable killing units of PBSX when compared to Xre G4S A19V L78V (Fig 4.1). It was successfully shown using bulk culture and single-cell assays that PBSX specifically adsorbs to *B. subtilis* W23 and not *B. subtilis* 168. Furthermore, single-cell adsorption assays suggest that there is not a preference for phage adsorption at the cell pole over the lateral cell wall.

It was determined that the tail fiber of PBSZ was sufficient to confer selectivity to a host, as a hybrid PBSX-Z where the tail fiber of PBSZ replaces that of PBSX can kill *B. subtilis* 168 and loses the ability to kill *B. subtilis* W23. There was no detectable difference in killing on a plate assay using *B. subtilis* 168 as a host between PBSX-Z and PBSZ; therefore, there is not enough evidence yet to speculate why the tape measure protein in PBSZ is different from the tape measure protein of PBSX, and what that means for its selectivity of host as well as its killing activity.

In an effort to increase PBSX production, the lysis genes *xhIA*, *xhIB*, and both *xhIAB* were knocked out and the subsequent strains were assayed for lysis by performing a growth curve after inducing PBSX. In good agreement with the literature, *xhIA* is essential for lysis, although *xhIB* is the annotated holin for PBSX (340). It is not entirely clear what the role of *xhIA* and *xhIB* are in Gram-positive lysis in *B. subtilis*, and this is a topic for further investigation. Unfortunately, the *xhIA*, and *xhIAB* knockout strains did not appear to produce additional PBSX (Fig 4.8), although this could be a technical problem with lysing the (*xhIA*, *xhIAB*) cells, or representative of a lack of sensitivity for determining killing units with the plate assay. To overcome these two obstacles, an

immunoblot will be used to assay wild-type PBSX lysates, *xhIA*, and *xhIAB* lysates for the number of PBSX produced.

PBSX is thought to kill by disrupting the membrane potential, similar to pyocins (333). The voltage sensitive dye ThT (341, 342) was used in an effort to develop a single-cell assay demonstrating that PBSX kills by depolarizing the cell, and that only a single PBSX is required to kill the cell. Unfortunately, ThT did not perform reliably as a membrane potential indicator dye, as the positive controls with DNP still showed ThT staining (Fig 4.9B), even in the absence of membrane potential. The absence of membrane potential was confirmed in this DNP treated sample, as the OD₆₀₀ did not change after the addition of DNP to the cell culture. Furthermore, use of valinomycin alongside a potassium clamp (300 mM K⁺) did result in a loss of ThT signal, but no differently than the potassium clamp with solvent only control (Fig 4.9C). Therefore, better characterized membrane potential dyes should be used (343) and this experiment repeated, as ThT is not behaving as reported in the literature (341, 342). Use of the dye CTC, which acts as an indicator of cellular metabolism, showed that PBSX treatment of *B. subtilis* W23 halts metabolic function within 10 min of treatment with PBSX, and the fluorescently labeled PBSX can be seen as punctate loci on the bacterial cell surface. Dissipation of membrane potential can cause depletion of ATP levels (345), delocalization of cytoskeletal and cell division proteins (345), and abrogation of cellular metabolism, which supports the idea that PBSX kills *B. subtilis* W23 by mechanically puncturing the membrane and dissipating the membrane potential.

Overall, a novel modular system was developed for production of PBSX that shows potential to be adapted for commercial or clinical production of phagocin that targets a bacterial species of interest, provided functional tail fiber fusions or other factors essential for swapping specificity to the target of interest are successful. Production of PBSX within *B. subtilis* (a Gram-positive) eliminates the need for purifying away endotoxin from the lysate if it were used in a clinical setting (346), and since PBSX does not replicate, it is dosable.

Future directions for YisK

The major questions remaining to be answered regarding YisK are: 1) what protein(s) is YisK's localization at the membrane dependent on? 2) What are YisK's physical interaction partners? 3) What is the true substrate for YisK, and what overall role does YisK play in *B. subtilis* metabolism? 4) Is YisK activity or localization regulated by phosphorylation or other post-translational modifications?

Current approaches include identifying factors that are responsible for YisK's localization at the membrane. A genetic approach is being applied, systematically looking at YisK localization under native conditions in an *ftsEX* mutant, *mbI* mutant, and *mbI* variants that conferred resistance to YisK misexpression activity. YisK-GFP sandwich proteins of some of the YisK variants (YisK E30A) are being generated in order to continue characterization of the variants.

Although initial pull-down assays were unsuccessful, *in vivo* crosslinking followed by pull-down of YisK will be performed in an effort to capture transient

interactions that may have been lost during the lysis and subsequent pull-down procedure. Successfully identified interaction partners will be confirmed via biochemical and genetic approaches, and co-crystal structure(s) will be obtained.

Metabolomics and differential pathway analysis of 168WT and $\Delta yisK$ will be performed to ascertain the *in vivo* substrate of YisK, as well as the metabolic pathway that YisK plays a role in. Based on this data, thermal shifts will be performed to confirm which compounds bind YisK, as well as enzymatic assays for YisK activity. Further enzymatic characterization including K_m , K_d , k_{cat} , and the catalytic mechanism of YisK will be performed by our collaborators (Raushel group). Interrogation of YisK's enzymatic activity holds the promise of elucidating subcellular localization of carbon metabolism at sites of active growth as a general feature of enzymes involved in carbon metabolism.

Post-translational modification of a protein can alter its localization and/or its activity and/or its interaction partners (175). Other enzymes involved in central carbon metabolism, particularly YvcK, have been shown to be phosphorylated, and that the modification plays a crucial role in its native function. Although YvcK's localization and enzymatic activity appear unaffected by its phosphorylation state, its ability to compensate for a loss of MreB in directing proper localization of PBP1 relies on it being phosphorylated (123). This data suggests phosphorylation playing a role in YvcK's interaction partners. Along those lines, a phosphorylated protein dye coupled with SDS-PAGE or α -Phosphate probe coupled with Western blot will be used to assay for modification of YisK across its expression conditions. If YisK is modified post-

translationally, further investigation will be conducted as to what role the modification has on YisK activity under native expression conditions. Mass spectrometry can also be used to look for post-translational modification of YisK across various expression conditions.

Characterization of YodL is still a significant endeavor, as initial efforts were largely focused on YisK after the initial experiments and data was collected (see Chapter II). Biochemical characterization of YodL was not possible, because expression and purification of the protein proved problematic. Expression of YodL was toxic to the cells, affecting FtsZ function and preventing proper division in *E. coli* (Duan and Herman, Dissertation). When YodL was tagged with a removable His-Sumo tag, expression was successful, but subsequent cleaving of the tag caused YodL to become insoluble. Expression of YodL will be performed again in an *E. coli* suppressor strain that is resistant to YodL activity. Purification techniques will be based on previously purified proteins that are also small and highly basic, such as histones in eukaryotes (YodL is 12 kDa with a PI = 9.59). After successful purification, YodL interaction partners will be identified via pull-down assays, and YodL will be crystallized by itself and with any/all of its interaction partners. One may speculate based on the current data that YodL directly interacts with MreB.

PBSX future directions

A modular production system for PBSX was developed based on the literature (219, 220, 340), and factors involved in host specificity for PBSX were characterized.

Although the specificity of PBSX was altered from targeting *B. subtilis* W23 to targeting *B. subtilis* 168 by switching the tail fibers, targeting more evolutionarily distant bacteria may prove challenging. Instead swapping in the entire tail fiber from phages that target another host, one may have to splice the desired tail fiber with the PBSX tail fiber (at various locations) to allow for proper folding of the tail fiber as well as connection to the PBSX baseplate. Proper folding of the tail fiber may also require specific phage chaperones, which may complicate the process of switching host specificity. The end goal is the ability to use PBSX to target human pathogens, especially those in the gut, where a high degree of specificity would prevent damage to the human gut microbiome during clinical treatment.

In characterizing the point mutations in *xre* that confer temperature sensitivity to the PBSX repressor, it was inadvertently determined that a point mutation (G4S) confers extreme temperature sensitivity to the repressor (i.e. unstable even at room temperature). This raises the possibility of finding temperature sensitive alleles of *xre* that are stable at room temperature but unstable at 37°C. By identifying one of these alleles and using it in a strain that produces a PBSX that targets a particular pathogen, one could have a robust treatment method in a clinical setting. For example, one would sporulate the *B. subtilis* 168 containing PBSX (modified to target particular pathogen) at low temperatures. These spores would then be applied to the subject (topically or ingested), and would germinate at 37°C in favorable conditions or upon interaction with bacterial PG fragments triggering germination (130). At this temperature and point in the *B. subtilis* life cycle, PBSX is induced at the site where the treatment is required.

REFERENCES

1. Nakano MM, Zuber P. 1998. Anaerobic growth of a "strict aerobe" (*Bacillus subtilis*). Annual review of microbiology 52:165-190.
2. Aguilar C, Vlamakis H, Losick R, Kolter R. 2007. Thinking about *Bacillus subtilis* as a multicellular organism. Current opinion in microbiology 10:638-643.
3. Zeigler DR, Pragai Z, Rodriguez S, Chevreux B, Muffler A *et al.* 2008. The origins of 168, W23, and other *Bacillus subtilis* legacy strains. J Bacteriol 190:6983-6995.
4. Burkholder PR, Giles NH, Jr. 1947. Induced biochemical mutations in *Bacillus subtilis*. American journal of botany 34:345-348.
5. Albertini AM, Galizzi A. 1999. The sequence of the trp operon of *Bacillus subtilis* 168 (*trpC2*) revisited. Microbiology 145 (Pt 12):3319-3320.
6. Cahn FH, Fox MS. 1968. Fractionation of transformable bacteria from ocompetent cultures of *Bacillus subtilis* on renografin gradients. J Bacteriol 95:867-875.
7. Hadden C, Nester EW. 1968. Purification of competent cells in the *Bacillus subtilis* transformation system. J Bacteriol 95:876-885.
8. Konkol MA, Blair KM, Kearns DB. 2013. Plasmid-encoded ComI inhibits competence in the ancestral 3610 strain of *Bacillus subtilis*. J Bacteriol 195:4085-4093.
9. Dubnau D, Cirigliano C. 1972. Fate of transforming DNA following uptake by competent *Bacillus subtilis*. IV. The endwise attachment and uptake of transforming DNA. Journal of molecular biology 64:31-46.
10. Hahn J, Maier B, Haijema BJ, Sheetz M, Dubnau D. 2005. Transformation proteins and DNA uptake localize to the cell poles in *Bacillus subtilis*. Cell 122:59-71.
11. Bodmer WF. 1966. Integration of deoxyribonuclease-treated DNA in *Bacillus subtilis* transformation. The Journal of general physiology 49:233-258.
12. Mejean V, Claverys JP. 1988. Polarity of DNA entry in transformation of *Streptococcus pneumoniae*. Molecular & general genetics : MGG 213:444-448.

13. Mejean V, Claverys JP. 1993. DNA processing during entry in transformation of *Streptococcus pneumoniae*. The Journal of biological chemistry 268:5594-5599.
14. Burton B, Dubnau D. 2010. Membrane-associated DNA transport machines. Cold Spring Harbor perspectives in biology 2:a000406.
15. Maier B, Chen I, Dubnau D, Sheetz MP. 2004. DNA transport into *Bacillus subtilis* requires proton motive force to generate large molecular forces. Nature structural & molecular biology 11:643-649.
16. Koo BM, Kritikos G, Farelli JD, Todor H, Tong K *et al.* 2017. Construction and analysis of two genome-scale deletion libraries for *Bacillus subtilis*. Cell systems 4:291-305 e297.
17. Wagner JK, Marquis KA, Rudner DZ. 2009. SirA enforces diploidy by inhibiting the replication initiator DnaA during spore formation in *Bacillus subtilis*. Molecular microbiology 73:963-974.
18. Duan Y, Huey JD, Herman JK. 2016. The DnaA inhibitor SirA acts in the same pathway as Soj (ParA) to facilitate *oriC* segregation during *Bacillus subtilis* sporulation. Molecular microbiology 102:530-544.
19. Ben-Yehuda S, Fujita M, Liu XS, Gorbatyuk B, Skoko D *et al.* 2005. Defining a centromere-like element in *Bacillus subtilis* by identifying the binding sites for the chromosome-anchoring protein RacA. Molecular cell 17:773-782.
20. Lenarcic R, Halbedel S, Visser L, Shaw M, Wu LJ *et al.* 2009. Localisation of DivIVA by targeting to negatively curved membranes. The EMBO journal 28:2272-2282.
21. Ramamurthi KS, Losick R. 2009. Negative membrane curvature as a cue for subcellular localization of a bacterial protein. Proc Natl Acad Sci U S A 106:13541-13545.
22. Oliva MA, Halbedel S, Freund SM, Dutow P, Leonard TA *et al.* 2010. Features critical for membrane binding revealed by DivIVA crystal structure. The EMBO journal 29:1988-2001.
23. Ben-Yehuda S, Rudner DZ, Losick R. 2003. RacA, a bacterial protein that anchors chromosomes to the cell poles. Science 299:532-536.
24. Wu LJ, Errington J. 2003. RacA and the Soj-Spo0J system combine to effect polar chromosome segregation in sporulating *Bacillus subtilis*. Molecular microbiology 49:1463-1475.

25. Ben-Yehuda S, Losick R. 2002. Asymmetric cell division in *B. subtilis* involves a spiral-like intermediate of the cytokinetic protein FtsZ. *Cell* 109:257-266.
26. Levin PA, Losick R. 1996. Transcription factor Spo0A switches the localization of the cell division protein FtsZ from a medial to a bipolar pattern in *Bacillus subtilis*. *Genes & development* 10:478-488.
27. Pogliano J, Osborne N, Sharp MD, Abanes-De Mello A, Perez A *et al.* 1999. A vital stain for studying membrane dynamics in bacteria: a novel mechanism controlling septation during *Bacillus subtilis* sporulation. *Molecular microbiology* 31:1149-1159.
28. Eichenberger P, Fawcett P, Losick R. 2001. A three-protein inhibitor of polar septation during sporulation in *Bacillus subtilis*. *Molecular microbiology* 42:1147-1162.
29. Miller AK, Brown EE, Mercado BT, Herman JK. 2016. A DNA-binding protein defines the precise region of chromosome capture during *Bacillus* sporulation. *Molecular microbiology* 99:111-122.
30. Piggot PJ, Hilbert DW. 2004. Sporulation of *Bacillus subtilis*. *Current opinion in microbiology* 7:579-586.
31. Tocheva EI, Lopez-Garrido J, Hughes HV, Fredlund J, Kuru E *et al.* 2013. Peptidoglycan transformations during *Bacillus subtilis* sporulation. *Molecular microbiology* 88:673-686.
32. Setlow B, Atluri S, Kitchel R, Koziol-Dube K, Setlow P. 2006. Role of dipicolinic acid in resistance and stability of spores of *Bacillus subtilis* with or without DNA-protective alpha/beta-type small acid-soluble proteins. *J Bacteriol* 188:3740-3747.
33. Hilbert DW, Piggot PJ. 2004. Compartmentalization of gene expression during *Bacillus subtilis* spore formation. *Microbiology and molecular biology reviews* : MMBR 68:234-262.
34. Molle V, Fujita M, Jensen ST, Eichenberger P, Gonzalez-Pastor JE *et al.* 2003. The Spo0A regulon of *Bacillus subtilis*. *Molecular microbiology* 50:1683-1701.
35. Fujita M, Gonzalez-Pastor JE, Losick R. 2005. High- and low-threshold genes in the Spo0A regulon of *Bacillus subtilis*. *J Bacteriol* 187:1357-1368.

36. Narula J, Fujita M, Igoshin OA. 2016. Functional requirements of cellular differentiation: lessons from *Bacillus subtilis*. *Current opinion in microbiology* 34:38-46.
37. Meeske AJ, Riley EP, Robins WP, Uehara T, Mekalanos JJ *et al.* 2016. SEDS proteins are a widespread family of bacterial cell wall polymerases. *Nature* 537:634-638.
38. Kieser KJ, Baranowski C, Chao MC, Long JE, Sasseti CM *et al.* 2015. Peptidoglycan synthesis in *Mycobacterium tuberculosis* is organized into networks with varying drug susceptibility. *Proc Natl Acad Sci U S A* 112:13087-13092.
39. Typas A, Banzhaf M, Gross CA, Vollmer W. 2011. From the regulation of peptidoglycan synthesis to bacterial growth and morphology. *Nature reviews. Microbiology* 10:123-136.
40. Slovak PM, Wadhams GH, Armitage JP. 2005. Localization of MreB in *Rhodobacter sphaeroides* under conditions causing changes in cell shape and membrane structure. *J Bacteriol* 187:54-64.
41. Fenton AK, Gerdes K. 2013. Direct interaction of FtsZ and MreB is required for septum synthesis and cell division in *Escherichia coli*. *The EMBO journal* 32:1953-1965.
42. Szwedziak P, Lowe J. 2013. Do the divisome and elongasome share a common evolutionary past? *Current opinion in microbiology* 16:745-751.
43. van der Ploeg R, Verheul J, Vischer NO, Alexeeva S, Hoogendoorn E *et al.* 2013. Colocalization and interaction between elongasome and divisome during a preparative cell division phase in *Escherichia coli*. *Molecular microbiology* 87:1074-1087.
44. Liechti G, Kuru E, Packiam M, Hsu YP, Tekkam S *et al.* 2016. Pathogenic *Chlamydia* lack a classical sacculus but synthesize a narrow, mid-cell peptidoglycan ring, regulated by MreB, for cell division. *PLoS pathogens* 12:e1005590.
45. Ouellette SP, Karimova G, Subtil A, Ladant D. 2012. *Chlamydia* co-opts the rod shape-determining proteins MreB and Pbp2 for cell division. *Molecular microbiology* 85:164-178.

46. Pilhofer M, Aistleitner K, Biboy J, Gray J, Kuru E *et al.* 2013. Discovery of chlamydial peptidoglycan reveals bacteria with murein sacculi but without FtsZ. *Nature communications* 4:2856.
47. Osawa M, Erickson HP. 2013. Liposome division by a simple bacterial division machinery. *Proc Natl Acad Sci U S A* 110:11000-11004.
48. Bisson-Filho AW, Hsu YP, Squyres GR, Kuru E, Wu F *et al.* 2017. Treadmilling by FtsZ filaments drives peptidoglycan synthesis and bacterial cell division. *Science* 355:739-743.
49. Bernhardt TG, de Boer PA. 2005. SlmA, a nucleoid-associated, FtsZ binding protein required for blocking septal ring assembly over chromosomes in *E. coli*. *Molecular cell* 18:555-564.
50. Cho H, McManus HR, Dove SL, Bernhardt TG. 2011. Nucleoid occlusion factor SlmA is a DNA-activated FtsZ polymerization antagonist. *Proc Natl Acad Sci U S A* 108:3773-3778.
51. Cho H, Bernhardt TG. 2013. Identification of the SlmA active site responsible for blocking bacterial cytokinetic ring assembly over the chromosome. *PLoS genetics* 9:e1003304.
52. Wu LJ, Errington J. 2004. Coordination of cell division and chromosome segregation by a nucleoid occlusion protein in *Bacillus subtilis*. *Cell* 117:915-925.
53. Wu LJ, Ishikawa S, Kawai Y, Oshima T, Ogasawara N *et al.* 2009. Noc protein binds to specific DNA sequences to coordinate cell division with chromosome segregation. *The EMBO journal* 28:1940-1952.
54. Adams DW, Wu LJ, Errington J. 2015. Nucleoid occlusion protein Noc recruits DNA to the bacterial cell membrane. *The EMBO journal* 34:491-501.
55. Bork P, Sander C, Valencia A. 1992. An ATPase domain common to prokaryotic cell cycle proteins, sugar kinases, actin, and hsp70 heat shock proteins. *Proc Natl Acad Sci U S A* 89:7290-7294.
56. Jones LJ, Carballido-Lopez R, Errington J. 2001. Control of cell shape in bacteria: helical, actin-like filaments in *Bacillus subtilis*. *Cell* 104:913-922.
57. Kuru E, Hughes HV, Brown PJ, Hall E, Tekkam S *et al.* 2012. In Situ probing of newly synthesized peptidoglycan in live bacteria with fluorescent D-amino acids. *Angewandte Chemie (International ed. in English)* 51:12519-12523.

58. Heichlinger A, Ammelburg M, Kleinschnitz EM, Latus A, Maldener I *et al.* 2011. The MreB-like protein Mbl of *Streptomyces coelicolor* A3(2) depends on MreB for proper localization and contributes to spore wall synthesis. *J Bacteriol* 193:1533-1542.
59. Lee JC, Stewart GC. 2003. Essential nature of the *mreC* determinant of *Bacillus subtilis*. *J Bacteriol* 185:4490-4498.
60. Kawai Y, Asai K, Errington J. 2009. Partial functional redundancy of MreB isoforms, MreB, Mbl and MreBH, in cell morphogenesis of *Bacillus subtilis*. *Molecular microbiology* 73:719-731.
61. Kawai Y, Daniel RA, Errington J. 2009. Regulation of cell wall morphogenesis in *Bacillus subtilis* by recruitment of PBP1 to the MreB helix. *Molecular microbiology* 71:1131-1144.
62. Formstone A, Errington J. 2005. A magnesium-dependent *mreB* null mutant: implications for the role of *mreB* in *Bacillus subtilis*. *Molecular microbiology* 55:1646-1657.
63. Daniel RA, Errington J. 2003. Control of Cell Morphogenesis in Bacteria. *Cell* 113:767-776.
64. Kawai Y, Mercier R, Errington J. 2014. Bacterial cell morphogenesis does not require a preexisting template structure. *Current biology : CB* 24:863-867.
65. Carballido-Lopez R, Formstone A, Li Y, Ehrlich SD, Noirot P *et al.* 2006. Actin homolog MreBH governs cell morphogenesis by localization of the cell wall hydrolase LytE. *Developmental cell* 11:399-409.
66. Meisner J, Montero Llopis P, Sham LT, Garner E, Bernhardt TG *et al.* 2013. FtsEX is required for CwlO peptidoglycan hydrolase activity during cell wall elongation in *Bacillus subtilis*. *Molecular microbiology* 89:1069-1083.
67. Schirner K, Errington J. 2009. The cell wall regulator $\{\sigma\}$ I specifically suppresses the lethal phenotype of *mbl* mutants in *Bacillus subtilis*. *J Bacteriol* 191:1404-1413.
68. Mirouze N, Ferret C, Yao Z, Chastanet A, Carballido-Lopez R. 2015. MreB-dependent inhibition of cell elongation during the escape from competence in *Bacillus subtilis*. *PLoS genetics* 11:e1005299.

69. Dominguez-Cuevas P, Porcelli I, Daniel RA, Errington J. 2013. Differentiated roles for MreB-actin isologues and autolytic enzymes in *Bacillus subtilis* morphogenesis. *Molecular microbiology* 89:1084-1098.
70. Salzberg LI, Powell L, Hokamp K, Botella E, Noone D *et al.* 2013. The WalRK (YycFG) and sigma(I) RsgI regulators cooperate to control CwlO and LytE expression in exponentially growing and stressed *Bacillus subtilis* cells. *Molecular microbiology* 87:180-195.
71. Huang WZ, Wang JJ, Chen HJ, Chen JT, Shaw GC. 2013. The heat-inducible essential response regulator WalR positively regulates transcription of *sigI*, *mreBH* and *lytE* in *Bacillus subtilis* under heat stress. *Research in microbiology* 164:998-1008.
72. Garner EC, Bernard R, Wang W, Zhuang X, Rudner DZ *et al.* 2011. Coupled, circumferential motions of the cell wall synthesis machinery and MreB filaments in *B. subtilis*. *Science* 333:222-225.
73. Dominguez-Escobar J, Chastanet A, Crevenna AH, Fromion V, Wedlich-Soldner R *et al.* 2011. Processive movement of MreB-associated cell wall biosynthetic complexes in bacteria. *Science* 333:225-228.
74. van Teeffelen S, Wang S, Furchtgott L, Huang KC, Wingreen NS *et al.* 2011. The bacterial actin MreB rotates, and rotation depends on cell-wall assembly. *Proc Natl Acad Sci U S A* 108:15822-15827.
75. Salje J, van den Ent F, de Boer P, Lowe J. 2011. Direct membrane binding by bacterial actin MreB. *Molecular cell* 43:478-487.
76. Ursell TS, Nguyen J, Monds RD, Colavin A, Billings G *et al.* 2014. Rod-like bacterial shape is maintained by feedback between cell curvature and cytoskeletal localization. *Proc Natl Acad Sci U S A* 111:E1025-1034.
77. Shiomi D, Toyoda A, Aizu T, Ejima F, Fujiyama A *et al.* 2013. Mutations in cell elongation genes *mreB*, *mrdA* and *mrdB* suppress the shape defect of RodZ-deficient cells. *Molecular microbiology* 87:1029-1044.
78. van den Ent F, Johnson CM, Persons L, de Boer P, Lowe J. 2010. Bacterial actin MreB assembles in complex with cell shape protein RodZ. *The EMBO journal* 29:1081-1090.
79. Bendezu FO, Hale CA, Bernhardt TG, de Boer PA. 2009. RodZ (YfgA) is required for proper assembly of the MreB actin cytoskeleton and cell shape in *E. coli*. *The EMBO journal* 28:193-204.

80. Morgenstein RM, Bratton BP, Nguyen JP, Ouzounov N, Shaevitz JW *et al.* 2015. RodZ links MreB to cell wall synthesis to mediate MreB rotation and robust morphogenesis. *Proc Natl Acad Sci U S A* 112(40):12510-12515.
81. Mayer JA, Amann KJ. 2009. Assembly properties of the *Bacillus subtilis* actin, MreB. *Cell motility and the cytoskeleton* 66:109-118.
82. Bean GJ, Amann KJ. 2008. Polymerization properties of the *Thermotoga maritima* actin MreB: roles of temperature, nucleotides, and ions. *Biochemistry* 47:826-835.
83. van den Ent F, Izore T, Bharat TA, Johnson CM, Lowe J. 2014. Bacterial actin MreB forms antiparallel double filaments. *eLife* 3:e02634.
84. Galkin VE, Orlova A, Egelman EH. 2012. Are ParM filaments polar or bipolar? *Journal of molecular biology* 423:482-485.
85. Baba T, Ara T, Hasegawa M, Takai Y, Okumura Y *et al.* 2006. Construction of *Escherichia coli* K-12 in-frame, single-gene knockout mutants: the Keio collection. *Molecular systems biology* 2:2006 0008.
86. Peters JM, Colavin A, Shi H, Czarny TL, Larson MH *et al.* 2016. A comprehensive, CRISPR-based functional analysis of essential genes in bacteria. *Cell* 165:1493-1506.
87. Gitai Z, Dye N, Shapiro L. 2004. An actin-like gene can determine cell polarity in bacteria. *Proc Natl Acad Sci U S A* 101:8643-8648.
88. Typas A, Sourjik V. 2015. Bacterial protein networks: properties and functions. *Nature reviews. Microbiology* 13:559-572.
89. Muller S, Strack SN, Hoefler BC, Straight PD, Kearns DB *et al.* 2014. Bacillaene and sporulation protect *Bacillus subtilis* from predation by *Myxococcus xanthus*. *Applied and environmental microbiology* 80:5603-5610.
90. McLoon AL, Guttenplan SB, Kearns DB, Kolter R, Losick R. 2011. Tracing the domestication of a biofilm-forming bacterium. *J Bacteriol* 193:2027-2034.
91. Bernhardt TG, de Boer PA. 2004. Screening for synthetic lethal mutants in *Escherichia coli* and identification of EnvC (YibP) as a periplasmic septal ring factor with murein hydrolase activity. *Molecular microbiology* 52:1255-1269.

92. Surdova K, Gamba P, Claessen D, Siersma T, Jonker MJ et al. 2013. The conserved DNA-binding protein WhiA is involved in cell division in *Bacillus subtilis*. *J Bacteriol* 195:5450-5460.
93. Burby PE, Nye TM, Schroeder JW, Simmons LA. 2017. Implementation and data analysis of Tn-seq, whole-genome resequencing, and single-molecule real-time sequencing for bacterial genetics. *J Bacteriol* 199(1). pii: e00560-16.
94. Riley M, Abe T, Arnaud MB, Berlyn MK, Blattner FR et al. 2006. *Escherichia coli* K-12: a cooperatively developed annotation snapshot--2005. *Nucleic acids research* 34:1-9.
95. Levin BJ, Huang YY, Peck SC, Wei Y, Martinez-Del Campo A et al. 2017. A prominent glyceryl radical enzyme in human gut microbiomes metabolizes trans-4-hydroxy-L-proline. *Science* 355.
96. Nicholson JK, Holmes E, Kinross J, Burcelin R, Gibson G et al. 2012. Host-gut microbiota metabolic interactions. *Science* 336:1262-1267.
97. Sekirov I, Russell SL, Antunes LC, Finlay BB. 2010. Gut microbiota in health and disease. *Physiological reviews* 90:859-904.
98. Smith PM, Howitt MR, Panikov N, Michaud M, Gallini CA et al. 2013. The microbial metabolites, short-chain fatty acids, regulate colonic Treg cell homeostasis. *Science* 341:569-573.
99. Williams EA, Coxhead JM, Mathers JC. 2003. Anti-cancer effects of butyrate: use of micro-array technology to investigate mechanisms. *The Proceedings of the Nutrition Society* 62:107-115.
100. Wang Z, Klipfell E, Bennett BJ, Koeth R, Levison BS et al. 2011. Gut flora metabolism of phosphatidylcholine promotes cardiovascular disease. *Nature* 472:57-63.
101. Franzosa EA, Hsu T, Sirota-Madi A, Shafquat A, Abu-Ali G et al. 2015. Sequencing and beyond: integrating molecular 'omics' for microbial community profiling. *Nature reviews. Microbiology* 13:360-372.
102. Furusawa Y, Obata Y, Fukuda S, Endo TA, Nakato G et al. 2013. Commensal microbe-derived butyrate induces the differentiation of colonic regulatory T cells. *Nature* 504:446-450.

103. Haiser HJ, Gootenberg DB, Chatman K, Sirasani G, Balskus EP *et al.* 2013. Predicting and manipulating cardiac drug inactivation by the human gut bacterium *Eggerthella lenta*. *Science* 341:295-298.
104. Human Microbiome Project Consortium. 2012. Structure, function and diversity of the healthy human microbiome. *Nature* 486:207-214.
105. Joice R, Yasuda K, Shafquat A, Morgan XC, Huttenhower C. 2014. Determining microbial products and identifying molecular targets in the human microbiome. *Cell metabolism* 20:731-741.
106. Schnoes AM, Brown SD, Dodevski I, Babbitt PC. 2009. Annotation error in public databases: misannotation of molecular function in enzyme superfamilies. *PLoS computational biology* 5:e1000605.
107. Jacobson MP, Kalyanaraman C, Zhao S, Tian B. 2014. Leveraging structure for enzyme function prediction: methods, opportunities, and challenges. *Trends in biochemical sciences* 39:363-371.
108. Bastard K, Smith AA, Vergne-Vaxelaire C, Perret A, Zapparucha A *et al.* 2014. Revealing the hidden functional diversity of an enzyme family. *Nature chemical biology* 10:42-49.
109. Lespinet O, Labedan B. 2005. Orphan enzymes? *Science* 307:42.
110. Mackie A, Keseler IM, Nolan L, Karp PD, Paulsen IT. 2013. Dead end metabolites--defining the known unknowns of the *E. coli* metabolic network. *PLoS one* 8:e75210.
111. Pierucci O. 1978. Dimensions of *Escherichia coli* at various growth rates: model for envelope growth. *J Bacteriol* 135:559-574.
112. Sargent MG. 1975. Control of cell length in *Bacillus subtilis*. *J Bacteriol* 123:7-19.
113. Schaechter M, Maaloe O, Kjeldgaard NO. 1958. Dependency on medium and temperature of cell size and chemical composition during balanced growth of *Salmonella typhimurium*. *Journal of general microbiology* 19:592-606.
114. Sharpe ME, Hauser PM, Sharpe RG, Errington J. 1998. *Bacillus subtilis* cell cycle as studied by fluorescence microscopy: constancy of cell length at initiation of DNA replication and evidence for active nucleoid partitioning. *J Bacteriol* 180:547-555.

115. Shehata TE, Marr AG. 1971. Effect of nutrient concentration on the growth of *Escherichia coli*. *J Bacteriol* 107:210-216.
116. Campos M, Surovtsev IV, Kato S, Paintdakhi A, Beltran B *et al.* 2014. A constant size extension drives bacterial cell size homeostasis. *Cell* 159:1433-1446.
117. Taheri-Araghi S, Bradde S, Sauls JT, Hill NS, Levin PA *et al.* 2015. Cell-size control and homeostasis in bacteria. *Current biology* : CB 25:385-391.
118. Deforet M, van Ditmarsch D, Xavier JB. 2015. Cell-size homeostasis and the incremental rule in a bacterial pathogen. *Biophysical journal* 109:521-528.
119. Tanouchi Y, Pai A, Park H, Huang S, Stamatov R *et al.* 2015. A noisy linear map underlies oscillations in cell size and gene expression in bacteria. *Nature* 523:357-360.
120. Harris LK, Theriot JA. 2016. Relative rates of surface and volume synthesis set bacterial cell size. *Cell* 165:1479-1492.
121. Gorke B, Foulquier E, Galinier A. 2005. YvcK of *Bacillus subtilis* is required for a normal cell shape and for growth on Krebs cycle intermediates and substrates of the pentose phosphate pathway. *Microbiology* 151:3777-3791.
122. Foulquier E, Pompeo F, Bernadac A, Espinosa L, Galinier A. 2011. The YvcK protein is required for morphogenesis via localization of PBP1 under gluconeogenic growth conditions in *Bacillus subtilis*. *Molecular microbiology* 80:309-318.
123. Foulquier E, Pompeo F, Freton C, Cordier B, Grangeasse C *et al.* 2014. PrkC-mediated phosphorylation of overexpressed YvcK protein regulates PBP1 protein localization in *Bacillus subtilis mreB* mutant cells. *The Journal of biological chemistry* 289:23662-23669.
124. Foulquier E, Galinier A. 2017. YvcK, a protein required for cell wall integrity and optimal carbon source utilization, binds uridine diphosphate-sugars. *Scientific reports* 7:4139.
125. Sperber AM, Herman JK. 2017. Metabolism shapes the cell. *J Bacteriol* 199(11). pii: e00039-17.
126. Chaudhuri RR, Allen AG, Owen PJ, Shalom G, Stone K *et al.* 2009. Comprehensive identification of essential *Staphylococcus aureus* genes using transposon-mediated differential hybridisation (TMDH). *BMC genomics* 10:291.

127. Fleurie A, Manuse S, Zhao C, Campo N, Cluzel C *et al.* 2014. Interplay of the serine/threonine-kinase StkP and the paralogs DivIVA and GpsB in *pneumococcal* cell elongation and division. *PLoS genetics* 10:e1004275.
128. Fiuza M, Canova MJ, Zanella-Cleon I, Becchi M, Cozzone AJ *et al.* 2008. From the characterization of the four serine/threonine protein kinases (PknA/B/G/L) of *Corynebacterium glutamicum* toward the role of PknA and PknB in cell division. *The Journal of biological chemistry* 283:18099-18112.
129. Molle V, Kremer L. 2010. Division and cell envelope regulation by Ser/Thr phosphorylation: *Mycobacterium* shows the way. *Molecular microbiology* 75:1064-1077.
130. Shah IM, Laaberki MH, Popham DL, Dworkin J. 2008. A eukaryotic-like Ser/Thr kinase signals bacteria to exit dormancy in response to peptidoglycan fragments. *Cell* 135:486-496.
131. Yeats C, Finn RD, Bateman A. 2002. The PASTA domain: a beta-lactam-binding domain. *Trends in biochemical sciences* 27:438.
132. Hardt P, Engels I, Rausch M, Gajdiss M, Ulm H *et al.* 2017. The cell wall precursor lipid II acts as a molecular signal for the Ser/Thr kinase PknB of *Staphylococcus aureus*. *International journal of medical microbiology : IJMM* 307:1-10.
133. Elbaz M, Ben-Yehuda S. 2010. The metabolic enzyme ManA reveals a link between cell wall integrity and chromosome morphology. *PLoS genetics* 6:e1001119.
134. Cleasby A, Wonacott A, Skarzynski T, Hubbard RE, Davies GJ *et al.* 1996. The x-ray crystal structure of phosphomannose isomerase from *Candida albicans* at 1.7 angstrom resolution. *Nature structural biology* 3:470-479.
135. Nicolas P, Mader U, Dervyn E, Rochat T, Leduc A *et al.* 2012. Condition-dependent transcriptome reveals high-level regulatory architecture in *Bacillus subtilis*. *Science* 335:1103-1106.
136. Hansen T, Wendorff D, Schonheit P. 2004. Bifunctional phosphoglucose/phosphomannose isomerases from the Archaea *Aeropyrum pernix* and *Thermoplasma acidophilum* constitute a novel enzyme family within the phosphoglucose isomerase superfamily. *The Journal of biological chemistry* 279:2262-2272.

137. Yeom SJ, Ji JH, Kim NH, Park CS, Oh DK. 2009. Substrate specificity of a mannose-6-phosphate isomerase from *Bacillus subtilis* and its application in the production of L-ribose. *Applied and environmental microbiology* 75:4705-4710.
138. Young FE, Arias L. 1967. Biosynthesis of the N-acyl-galactosamine in cell walls of *Bacillus subtilis*. *J Bacteriol* 94:1783-1784.
139. Zaritsky A, Woldringh CL, Einav M, Alexeeva S. 2006. Use of thymine limitation and thymine starvation to study bacterial physiology and cytology. *J Bacteriol* 188:1667-1679.
140. Commichau FM, Rothe FM, Herzberg C, Wagner E, Hellwig D *et al.* 2009. Novel activities of glycolytic enzymes in *Bacillus subtilis*: interactions with essential proteins involved in mRNA processing. *Molecular & cellular proteomics : MCP* 8:1350-1360.
141. Commichau FM, Gunka K, Landmann JJ, Stulke J. 2008. Glutamate metabolism in *Bacillus subtilis*: gene expression and enzyme activities evolved to avoid futile cycles and to allow rapid responses to perturbations of the system. *J Bacteriol* 190:3557-3564.
142. Commichau FM, Herzberg C, Tripal P, Valerius O, Stulke J. 2007. A regulatory protein-protein interaction governs glutamate biosynthesis in *Bacillus subtilis*: the glutamate dehydrogenase RocG moonlights in controlling the transcription factor GltC. *Molecular microbiology* 65:642-654.
143. Commichau FM, Stulke J. 2008. Trigger enzymes: bifunctional proteins active in metabolism and in controlling gene expression. *Molecular microbiology* 67:692-702.
144. Morita T, Kawamoto H, Mizota T, Inada T, Aiba H. 2004. Enolase in the RNA degradosome plays a crucial role in the rapid decay of glucose transporter mRNA in the response to phosphosugar stress in *Escherichia coli*. *Molecular microbiology* 54:1063-1075.
145. Huang X, Holden HM, Raushel FM. 2001. Channeling of substrates and intermediates in enzyme-catalyzed reactions. *Annu Rev Biochem* 70:149-180.
146. Bulutoglu B, Garcia KE, Wu F, Minter SD, Banta S. 2016. Direct evidence for metabolon formation and substrate channeling in recombinant TCA cycle enzymes. *ACS Chem Biol* 11:2847-2853.

147. Hollinshead WD, Rodriguez S, Martin HG, Wang G, Baidoo EE *et al.* 2016. Examining *Escherichia coli* glycolytic pathways, catabolite repression, and metabolite channeling using Δ *pfk* mutants. *Biotechnol Biofuels* 9:212.
148. Butland G, Peregrin-Alvarez JM, Li J, Yang W, Yang X *et al.* 2005. Interaction network containing conserved and essential protein complexes in *Escherichia coli*. *Nature* 433:531-537.
149. Marchadier E, Carballido-Lopez R, Brinster S, Fabret C, Mervelet P *et al.* 2011. An expanded protein-protein interaction network in *Bacillus subtilis* reveals a group of hubs: Exploration by an integrative approach. *Proteomics* 11:2981-2991.
150. Yamamoto H, Kurosawa S, Sekiguchi J. 2003. Localization of the vegetative cell wall hydrolases LytC, LytE, and LytF on the *Bacillus subtilis* cell surface and stability of these enzymes to cell wall-bound or extracellular proteases. *J Bacteriol* 185:6666-6677.
151. Meyer FM, Gerwig J, Hammer E, Herzberg C, Commichau FM *et al.* 2011. Physical interactions between tricarboxylic acid cycle enzymes in *Bacillus subtilis*: evidence for a metabolon. *Metab Eng* 13:18-27.
152. Islam MM, Wallin R, Wynn RM, Conway M, Fujii H *et al.* 2007. A novel branched-chain amino acid metabolon. Protein-protein interactions in a supramolecular complex. *The Journal of biological chemistry* 282:11893-11903.
153. An S, Kumar R, Sheets ED, Benkovic SJ. 2008. Reversible compartmentalization of de novo purine biosynthetic complexes in living cells. *Science* 320:103-106.
154. Chien AC, Hill NS, Levin PA. 2012. Cell size control in bacteria. *Current biology* : CB 22:R340-349.
155. Monahan LG, Harry EJ. 2016. You are what you eat: metabolic control of bacterial division. *Trends in microbiology* 24:181-189.
156. Weart RB, Lee AH, Chien AC, Haeusser DP, Hill NS *et al.* 2007. A metabolic sensor governing cell size in bacteria. *Cell* 130:335-347.
157. Chien AC, Zareh SK, Wang YM, Levin PA. 2012. Changes in the oligomerization potential of the division inhibitor UgtP co-ordinate *Bacillus subtilis* cell size with nutrient availability. *Molecular microbiology* 86:594-610.

158. Kanehisa M, Sato Y, Kawashima M, Furumichi M, Tanabe M. 2016. KEGG as a reference resource for gene and protein annotation. *Nucleic acids research* 44:D457-D462.
159. Hill NS, Buske PJ, Shi Y, Levin PA. 2013. A moonlighting enzyme links *Escherichia coli* cell size with central metabolism. *PLoS genetics* 9:e1003663.
160. Beaufay F, Coppine J, Mayard A, Laloux G, De Bolle X *et al.* 2015. A NAD-dependent glutamate dehydrogenase coordinates metabolism with cell division in *Caulobacter crescentus*. *The EMBO journal* 34:1786-1800.
161. Radhakrishnan SK, Pritchard S, Viollier PH. 2010. Coupling prokaryotic cell fate and division control with a bifunctional and oscillating oxidoreductase homolog. *Developmental cell* 18:90-101.
162. Monahan LG, Hajduk IV, Blaber SP, Charles IG, Harry EJ. 2014. Coordinating bacterial cell division with nutrient availability: a role for glycolysis. *MBio* 5:e00935-00914.
163. Levin PA, Margolis PS, Setlow P, Losick R, Sun D. 1992. Identification of *Bacillus subtilis* genes for septum placement and shape determination. *J Bacteriol* 174:6717-6728.
164. Levin PA, Shim JJ, Grossman AD. 1998. Effect of *minCD* on FtsZ ring position and polar septation in *Bacillus subtilis*. *J Bacteriol* 180:6048-6051.
165. Levin PA, Schwartz RL, Grossman AD. 2001. Polymer stability plays an important role in the positional regulation of FtsZ. *J Bacteriol* 183:5449-5452.
166. Jorgenson MA, Young KD. 2016. Interrupting biosynthesis of O Antigen or the lipopolysaccharide core produces morphological defects in *Escherichia coli* by sequestering undecaprenyl phosphate. *J Bacteriol* 198:3070-3079.
167. Jorgenson MA, Kannan S, Laubacher ME, Young KD. 2016. Dead-end intermediates in the enterobacterial common antigen pathway induce morphological defects in *Escherichia coli* by competing for undecaprenyl phosphate. *Molecular microbiology* 100:1-14.
168. Danese PN, Oliver GR, Barr K, Bowman GD, Rick PD *et al.* 1998. Accumulation of the enterobacterial common antigen lipid II biosynthetic intermediate stimulates *degP* transcription in *Escherichia coli*. *J Bacteriol* 180:5875-5884.

169. D'Elia MA, Millar KE, Beveridge TJ, Brown ED. 2006. Wall teichoic acid polymers are dispensable for cell viability in *Bacillus subtilis*. *J Bacteriol* 188:8313-8316.
170. D'Elia MA, Pereira MP, Chung YS, Zhao W, Chau A *et al.* 2006. Lesions in teichoic acid biosynthesis in *Staphylococcus aureus* lead to a lethal gain of function in the otherwise dispensable pathway. *J Bacteriol* 188:4183-4189.
171. Brown S, Santa Maria JP, Jr., Walker S. 2013. Wall teichoic acids of gram-positive bacteria. *Annual review of microbiology* 67:313-336.
172. Mitsui N, Murasawa H, Sekiguchi J. 2011. Disruption of the cell wall lytic enzyme CwLO affects the amount and molecular size of poly-gamma-glutamic acid produced by *Bacillus subtilis* (natto). *The Journal of general and applied microbiology* 57:35-43.
173. Zhao L, Ye J, Fu J, Chen GQ. 2017. Engineering peptidoglycan degradation related genes of *Bacillus subtilis* for better fermentation processes. *Bioresource technology*.
174. Cooper S, Helmstetter CE. 1968. Chromosome replication and the division cycle of *Escherichia coli* B/r. *Journal of molecular biology* 31:519-540.
175. Pisithkul T, Patel NM, Amador-Noguez D. 2015. Post-translational modifications as key regulators of bacterial metabolic fluxes. *Current opinion in microbiology* 24:29-37.
176. Nam TW, Park YH, Jeong HJ, Ryu S, Seok YJ. 2005. Glucose repression of the *Escherichia coli* *sdhCDAB* operon, revisited: regulation by the CRP*cAMP complex. *Nucleic acids research* 33:6712-6722.
177. Sievert C, Nieves LM, Panyon LA, Loeffler T, Morris C *et al.* 2017. Experimental evolution reveals an effective avenue to release catabolite repression via mutations in XylR. *Proc Natl Acad Sci U S A* 114:7349-7354.
178. Fujita Y. 2009. Carbon catabolite control of the metabolic network in *Bacillus subtilis*. *Bioscience, biotechnology, and biochemistry* 73:245-259.
179. Bruckner R, Titgemeyer F. 2002. Carbon catabolite repression in bacteria: choice of the carbon source and autoregulatory limitation of sugar utilization. *FEMS microbiology letters* 209:141-148.

180. Twort FW. 2011. An investigation on the nature of ultra-microscopic viruses by Twort FW, L.R.C.P. Lond., M.R.C.S. (From the Laboratories of the Brown Institution, London). *Bacteriophage* 1:127-129.
181. D'Herelle F. 2007. On an invisible microbe antagonistic toward dysenteric bacilli: brief note by Mr. F. D'Herelle, presented by Mr. Roux. 1917. *Research in microbiology* 158:553-554.
182. Salmond GP, Fineran PC. 2015. A century of the phage: past, present and future. *Nature reviews. Microbiology* 13:777-786.
183. Summers WC. 2001. Bacteriophage therapy. *Annual review of microbiology* 55:437-451.
184. Summers WC. 2012. The strange history of phage therapy. *Bacteriophage* 2:130-133.
185. Young R. 2014. Bacteriophage Genomics. *In* Kutty GF (ed.), BICH 689. Texas A&M University.
186. Zeng L, Skinner SO, Zong C, Sippy J, Feiss M et al. 2010. Decision making at a subcellular level determines the outcome of bacteriophage infection. *Cell* 141:682-691.
187. Zeng L, Golding I. 2011. Following cell-fate in *E. coli* after infection by phage lambda. *Journal of visualized experiments : JoVE*:e3363.
188. Shao Q, Trinh JT, McIntosh CS, Christenson B, Balazsi G *et al.* 2017. Lysis-lysogeny coexistence: prophage integration during lytic development. *MicrobiologyOpen* 6(1): e00395.
189. Trinh JT, Szekely T, Shao Q, Balazsi G, Zeng L. 2017. Cell fate decisions emerge as phages cooperate or compete inside their host. *Nature communications* 8:14341.
190. Kourilsky P, Knapp A. 1974. Lysogenization by bacteriophage lambda. III. Multiplicity dependent phenomena occurring upon infection by lambda. *Biochimie* 56:1517-1523.
191. Oppenheim AB, Kobiler O, Stavans J, Court DL, Adhya S. 2005. Switches in bacteriophage lambda development. *Annual review of genetics* 39:409-429.
192. St-Pierre F, Endy D. 2008. Determination of cell fate selection during phage lambda infection. *Proc Natl Acad Sci U S A* 105:20705-20710.

193. Giladi H, Goldenberg D, Koby S, Oppenheim AB. 1995. Enhanced activity of the bacteriophage lambda PL promoter at low temperature. *Proc Natl Acad Sci U S A* 92:2184-2188.
194. Obuchowski M, Shotland Y, Koby S, Giladi H, Gabig M *et al.* 1997. Stability of CII is a key element in the cold stress response of bacteriophage lambda infection. *J Bacteriol* 179:5987-5991.
195. Okamoto K, Mudd JA, Mangan J, Huang WM, Subbaiah TV *et al.* 1968. Properties of the defective phage of *Bacillus subtilis*. *Journal of molecular biology* 34:413-428.
196. Plunkett G, 3rd, Rose DJ, Durfee TJ, Blattner FR. 1999. Sequence of Shiga toxin 2 phage 933W from *Escherichia coli* O157:H7: Shiga toxin as a phage late-gene product. *J Bacteriol* 181:1767-1778.
197. Young R. 2013. Phage lysis: do we have the hole story yet? *Current opinion in microbiology* 16:790-797.
198. Dewey JS, Savva CG, White RL, Vitha S, Holzenburg A *et al.* 2010. Micron-scale holes terminate the phage infection cycle. *Proc Natl Acad Sci U S A* 107:2219-2223.
199. Savva CG, Dewey JS, Moussa SH, To KH, Holzenburg A *et al.* 2014. Stable micron-scale holes are a general feature of canonical holins. *Molecular microbiology* 91:57-65.
200. Young R. 2014. Phage lysis: three steps, three choices, one outcome. *Journal of microbiology* 52:243-258.
201. Pang T, Savva CG, Fleming KG, Struck DK, Young R. 2009. Structure of the lethal phage pinhole. *Proc Natl Acad Sci U S A* 106:18966-18971.
202. Xu M, Struck DK, Deaton J, Wang IN, Young R. 2004. A signal-arrest-release sequence mediates export and control of the phage P1 endolysin. *Proc Natl Acad Sci U S A* 101:6415-6420.
203. Xu M, Arulandu A, Struck DK, Swanson S, Sacchettini JC *et al.* 2005. Disulfide isomerization after membrane release of its SAR domain activates P1 lysozyme. *Science* 307:113-117.
204. Sun Q, Kutty GF, Arockiasamy A, Xu M, Young R *et al.* 2009. Regulation of a muralytic enzyme by dynamic membrane topology. *Nature structural & molecular biology* 16:1192-1194.

205. Rajaure M, Berry J, Kongari R, Cahill J, Young R. 2015. Membrane fusion during phage lysis. *Proc Natl Acad Sci U S A* 112:5497-5502.
206. Cahill J, Rajaure M, O'Leary C, Sloan J, Marrufo A *et al.* 2017. Genetic analysis of the Lambda spanins Rz and Rz1: identification of functional domains. *G3 (Bethesda, Md.)* 7:741-753.
207. Loessner MJ. 2005. Bacteriophage endolysins--current state of research and applications. *Current opinion in microbiology* 8:480-487.
208. Krogh S, O'Reilly M, Nolan N, Devine KM. 1996. The phage-like element PBSX and part of the skin element, which are resident at different locations on the *Bacillus subtilis* chromosome, are highly homologous. *Microbiology* 142 (Pt 8):2031-2040.
209. Anderson LM, Bott KF. 1985. DNA packaging by the *Bacillus subtilis* defective bacteriophage PBSX. *Journal of virology* 54:773-780.
210. Haas M, Yoshikawa H. 1969. Defective bacteriophage PBSH in *Bacillus subtilis*. I. Induction, purification, and physical properties of the bacteriophage and its deoxyribonucleic acid. *Journal of virology* 3:233-247.
211. Haas M, Yoshikawa H. 1969. Defective bacteriophage PBSH in *Bacillus subtilis*. II. Intracellular development of the induced prophage. *Journal of virology* 3:248-260.
212. Okamoto K, Mudd JA, Marmur J. 1968. Conversion of *Bacillus subtilis* DNA to phage DNA following mitomycin C induction. *Journal of molecular biology* 34:429-437.
213. Wood HE, Dawson MT, Devine KM, McConnell DJ. 1990. Characterization of PBSX, a defective prophage of *Bacillus subtilis*. *J Bacteriol* 172:2667-2674.
214. Steensma HY, Robertson LA. 1978. Lysogeny in *Bacillus*. *FEMS Microbiology Letters* 3:313-317.
215. Steensma HY, Robertson LA, van Elsas JD. 1978. The occurrence and taxonomic value of PBS X-like defective phages in the genus *Bacillus*. *Antonie van Leeuwenhoek* 44:353-366.
216. Reuss DR, Thurmer A, Daniel R, Quax WJ, Stulke J. 2016. Complete genome sequence of *Bacillus subtilis* subsp. *subtilis* Strain 6. *Genome announcements* 4.

217. Thurm P, Garro AJ. 1975. Bacteriophage-specific protein synthesis during induction of the defective *Bacillus subtilis* bacteriophage PBSX. *Journal of virology* 16:179-183.
218. Steensma HY, Sondermeijer PJ. 1977. A counting method for determining the burst size of defective phages from *Bacillus subtilis*. *Antonie van Leeuwenhoek* 43:305-316.
219. Wood HE, Devine KM, McConnell DJ. 1990. Characterisation of a repressor gene (*xre*) and a temperature-sensitive allele from the *Bacillus subtilis* prophage, PBSX. *Gene* 96:83-88.
220. McDonnell GE, McConnell DJ. 1994. Overproduction, isolation, and DNA-binding characteristics of Xre, the repressor protein from the *Bacillus subtilis* defective prophage PBSX. *J Bacteriol* 176:5831-5834.
221. Ptashne M. 1986. A genetic switch: Gene control and phage. lambda. Palo Alto, CA (US); Blackwell Scientific Publications; None.
222. Van Kaer L, Van Montagu M, Dhaese P. 1987. Transcriptional control in the EcoRI-F immunity region of *Bacillus subtilis* phage phi 105. Identification and unusual structure of the operator. *Journal of molecular biology* 197:55-67.
223. McDonnell GE, Wood H, Devine KM, McConnell DJ. 1994. Genetic control of bacterial suicide: regulation of the induction of PBSX in *Bacillus subtilis*. *J Bacteriol* 176:5820-5830.
224. Buxton RS. 1976. Prophage mutation causing heat inducibility of defective *Bacillus subtilis* bacteriophage PBSX. *Journal of virology* 20:22-28.
225. Shields DC, Sharp PM. 1987. Synonymous codon usage in *Bacillus subtilis* reflects both translational selection and mutational biases. *Nucleic acids research* 15:8023-8040.
226. Sharp PM, Cowe E, Higgins DG, Shields DC, Wolfe KH *et al.* 1988. Codon usage patterns in *Escherichia coli*, *Bacillus subtilis*, *Saccharomyces cerevisiae*, *Schizosaccharomyces pombe*, *Drosophila melanogaster* and *Homo sapiens*; a review of the considerable within-species diversity. *Nucleic acids research* 16:8207-8211.
227. Schirmer T, Keller TA, Wang YF, Rosenbusch JP. 1995. Structural basis for sugar translocation through maltoporin channels at 3.1 Å resolution. *Science* 267:512-514.

228. Ferguson AD, Hofmann E, Coulton JW, Diederichs K, Welte W. 1998. Siderophore-mediated iron transport: crystal structure of FhuA with bound lipopolysaccharide. *Science* 282:2215-2220.
229. Locher KP, Rees B, Koebnik R, Mitschler A, Moulinier L *et al.* 1998. Transmembrane signaling across the ligand-gated FhuA receptor: crystal structures of free and ferrichrome-bound states reveal allosteric changes. *Cell* 95:771-778.
230. Elliott J, Arber W. 1978. *E. coli* K-12 pel mutants, which block phage lambda DNA injection, coincide with *ptsM*, which determines a component of a sugar transport system. *Molecular & general genetics* : MGG 161:1-8.
231. Erni B, Zanolari B, Kocher HP. 1987. The mannose permease of *Escherichia coli* consists of three different proteins. Amino acid sequence and function in sugar transport, sugar phosphorylation, and penetration of phage lambda DNA. *The Journal of biological chemistry* 262:5238-5247.
232. Martin-Verstraete I, Michel V, Charbit A. 1996. The levanase operon of *Bacillus subtilis* expressed in *Escherichia coli* can substitute for the mannose permease in mannose uptake and bacteriophage lambda infection. *J Bacteriol* 178:7112-7119.
233. Luria SE, Delbruck M. 1943. Mutations of bacteria from virus sensitivity to virus resistance. *Genetics* 28:491-511.
234. Braun V. 2009. FhuA (TonA), the career of a protein. *J Bacteriol* 191:3431-3436.
235. Liu J, Chen CY, Shiomi D, Niki H, Margolin W. 2011. Visualization of bacteriophage P1 infection by cryo-electron tomography of tiny *Escherichia coli*. *Virology* 417:304-311.
236. Sandulache R, Prehm P, Kamp D. 1984. Cell wall receptor for bacteriophage Mu G(+). *J Bacteriol* 160:299-303.
237. Sao-Jose C, Baptista C, Santos MA. 2004. *Bacillus subtilis* operon encoding a membrane receptor for bacteriophage SPP1. *J Bacteriol* 186:8337-8346.
238. Sao-Jose C, Lhuillier S, Lurz R, Melki R, Lepault J *et al.* 2006. The ectodomain of the viral receptor YueB forms a fiber that triggers ejection of bacteriophage SPP1 DNA. *The Journal of biological chemistry* 281:11464-11470.
239. Vinga I, Baptista C, Auzat I, Petipas I, Lurz R *et al.* 2012. Role of bacteriophage SPP1 tail spike protein gp21 on host cell receptor binding and trigger of phage DNA ejection. *Molecular microbiology* 83:289-303.

240. Baptista C, Santos MA, Sao-Jose C. 2008. Phage SPP1 reversible adsorption to *Bacillus subtilis* cell wall teichoic acids accelerates virus recognition of membrane receptor YueB. *J Bacteriol* 190:4989-4996.
241. Karamata D, Pooley HM, Monod M. 1987. Expression of heterologous genes for wall teichoic acid in *Bacillus subtilis* 168. *Molecular & general genetics : MGG* 207:73-81.
242. Yasbin RE, Maino VC, Young FE. 1976. Bacteriophage resistance in *Bacillus subtilis* 168, W23, and interstrain transformants. *J Bacteriol* 125:1120-1126.
243. Yasbin RE, Ledbetter M. 1978. Isolation of a *Bacillus subtilis* 168 derivative sensitive to defective bacteriophage PBSX. *Journal of virology* 25:703-704.
244. Glaser L, Ionesco H, Schaeffer P. 1966. Teichoic acids as components of a specific phage receptor in *Bacillus subtilis*. *Biochimica et biophysica acta* 124:415-417.
245. Young KD. 2010. Bacterial shape: two-dimensional questions and possibilities. *Annual review of microbiology* 64:223-240.
246. Silhavy TJ, Kahne D, Walker S. 2010. The bacterial cell envelope. *Cold Spring Harbor perspectives in biology* 2:a000414.
247. Holtje JV. 1998. Growth of the stress-bearing and shape-maintaining murein sacculus of *Escherichia coli*. *Microbiology and molecular biology reviews : MMBR* 62:181-203.
248. Young KD. 2007. Bacterial morphology: why have different shapes? *Current opinion in microbiology* 10:596-600.
249. Young KD. 2006. The selective value of bacterial shape. *Microbiology and molecular biology reviews : MMBR* 70:660-703.
250. Randich AM, Brun YV. 2015. Molecular mechanisms for the evolution of bacterial morphologies and growth modes. *Frontiers in microbiology* 6:580.
251. Figge RM, Divakaruni AV, Gober JW. 2004. MreB, the cell shape-determining bacterial actin homologue, co-ordinates cell wall morphogenesis in *Caulobacter crescentus*. *Molecular microbiology* 51:1321-1332.
252. Colavin A, Hsin J, Huang KC. 2014. Effects of polymerization and nucleotide identity on the conformational dynamics of the bacterial actin homolog MreB. *Proc Natl Acad Sci U S A* 111:3585-3590.

253. Gitai Z, Dye NA, Reisenauer A, Wachi M, Shapiro L. 2005. MreB actin-mediated segregation of a specific region of a bacterial chromosome. *Cell* 120:329-341.
254. Iwai N, Nagai K, Wachi M. 2002. Novel S-benzylisothiourea compound that induces spherical cells in *Escherichia coli* probably by acting on a rod-shape-determining protein(s) other than penicillin-binding protein 2. *Bioscience, biotechnology, and biochemistry* 66:2658-2662.
255. Bean GJ, Flickinger ST, Westler WM, McCully ME, Sept D *et al.* 2009. A22 disrupts the bacterial actin cytoskeleton by directly binding and inducing a low-affinity state in MreB. *Biochemistry* 48:4852-4857.
256. Takacs CN, Poggio S, Charbon G, Pucheault M, Vollmer W *et al.* 2010. MreB drives de novo rod morphogenesis in *Caulobacter crescentus* via remodeling of the cell wall. *J Bacteriol* 192:1671-1684.
257. Kruse T, Bork-Jensen J, Gerdes K. 2005. The morphogenetic MreBCD proteins of *Escherichia coli* form an essential membrane-bound complex. *Molecular microbiology* 55:78-89.
258. Bendezu FO, de Boer PA. 2008. Conditional lethality, division defects, membrane involution, and endocytosis in mre and mrd shape mutants of *Escherichia coli*. *J Bacteriol* 190:1792-1811.
259. Varma A, Young KD. 2009. In *Escherichia coli*, MreB and FtsZ direct the synthesis of lateral cell wall via independent pathways that require PBP 2. *J Bacteriol* 191:3526-3533.
260. Muchova K, Chromikova Z, Barak I. 2013. Control of *Bacillus subtilis* cell shape by RodZ. *Environmental microbiology* 15:3259-3271.
261. Alyahya SA, Alexander R, Costa T, Henriques AO, Emonet T *et al.* 2009. RodZ, a component of the bacterial core morphogenic apparatus. *Proc Natl Acad Sci U S A* 106:1239-1244.
262. Niba ET, Li G, Aoki K, Kitakawa M. 2010. Characterization of *rodZ* mutants: RodZ is not absolutely required for the cell shape and motility. *FEMS microbiology letters* 309:35-42.
263. Cabeen MT, Jacobs-Wagner C. 2010. The bacterial cytoskeleton. *Annual review of genetics* 44:365-392.

264. Schirner K, Errington J. 2009. The cell wall regulator σ^I specifically suppresses the lethal phenotype of *mbl* mutants in *Bacillus subtilis*. *J Bacteriol* 191:1404-1413.
265. Defeu Soufo HJ, Graumann PL. 2006. Dynamic localization and interaction with other *Bacillus subtilis* actin-like proteins are important for the function of MreB. *Molecular microbiology* 62:1340-1356.
266. Tseng CL, Shaw GC. 2008. Genetic evidence for the actin homolog gene *mreBH* and the bacitracin resistance gene *bcrC* as targets of the alternative sigma factor SigI of *Bacillus subtilis*. *J Bacteriol* 190:1561-1567.
267. Masuda H, Tan Q, Awano N, Wu KP, Inouye M. 2012. YeeU enhances the bundling of cytoskeletal polymers of MreB and FtsZ, antagonizing the CbtA (YeeV) toxicity in *Escherichia coli*. *Molecular microbiology* 84:979-989.
268. Tan Q, Awano N, Inouye M. 2011. YeeV is an *Escherichia coli* toxin that inhibits cell division by targeting the cytoskeleton proteins, FtsZ and MreB. *Molecular microbiology* 79:109-118.
269. Masuda H, Tan Q, Awano N, Yamaguchi Y, Inouye M. 2012. A novel membrane-bound toxin for cell division, CptA (YgfX), inhibits polymerization of cytoskeleton proteins, FtsZ and MreB, in *Escherichia coli*. *FEMS microbiology letters* 328:174-181.
270. Yakhnina AA, Gitai Z. 2012. The small protein MbiA interacts with MreB and modulates cell shape in *Caulobacter crescentus*. *Molecular microbiology* 85:1090-1104.
271. Ababneh QO, Herman JK. 2015. CodY regulates SigD levels and activity by binding to three sites in the *fla/che* operon. *J Bacteriol* 197:2999-3006.
272. Harwood CR, Cutting SM. 1990. *Molecular biological methods for Bacillus*. Wiley, New York, NY.
273. Branda SS, González-Pastor JE, Ben-Yehuda S, Losick R, Kolter R. 2001. Fruiting body formation by *Bacillus subtilis*. *Proc Natl Acad Sci U S A* 98:11621-11626.
274. Youngman PJ, Perkins JB, Losick R. 1983. Genetic transposition and insertional mutagenesis in *Bacillus subtilis* with *Streptococcus faecalis* transposon Tn917. *Proc Natl Acad Sci U S A* 80:2305-2309.

275. Wagner JK, Marquis KA, Rudner DZ. 2009. SirA enforces diploidy by inhibiting the replication initiator DnaA during spore formation in *Bacillus subtilis*. *Molecular microbiology* 73:963-974.
276. Rasband W. 1997-2015. ImageJ. U.S. National Institutes of Health, Bethesda, Maryland.
277. Schaeffer P, Millet J, Aubert JP. 1965. Catabolic repression of bacterial sporulation. *Proc Natl Acad Sci U S A* 54:704-711.
278. Ababneh QO, Herman JK. 2015. RelA inhibits *Bacillus subtilis* motility and chaining. *J Bacteriol* 197:128-137.
279. Abhayawardhane Y, Stewart GC. 1995. *Bacillus subtilis* possesses a second determinant with extensive sequence similarity to the *Escherichia coli mreB* morphogene. *J Bacteriol* 177:765-773.
280. Leaver M, Errington J. 2005. Roles for MreC and MreD proteins in helical growth of the cylindrical cell wall in *Bacillus subtilis*. *Molecular microbiology* 57:1196-1209.
281. Nicolas P, Mäder U, Dervyn E, Rochat T, Leduc A *et al.* 2012. Condition-dependent transcriptome reveals high-level regulatory architecture in *Bacillus subtilis*. *Science* 335:1103-1106.
282. Molle V, Fujita M, Jensen ST, Eichenberger P, González-Pastor JE *et al.* 2003. The Spo0A regulon of *Bacillus subtilis*. *Molecular microbiology* 50:1683-1701.
283. Britton RA, Eichenberger P, Gonzalez-Pastor JE, Fawcett P, Monson R *et al.* 2002. Genome-wide analysis of the stationary-phase sigma factor (Sigma-H) regulon of *Bacillus subtilis*. *J Bacteriol* 184:4881-4890.
284. Arrieta-Ortiz ML, Hafemeister C, Bate AR, Chu T, Greenfield A *et al.* 2015. An experimentally supported model of the *Bacillus subtilis* global transcriptional regulatory network. *Molecular systems biology* 11(11):839.
285. Caspi R, Altman T, Billington R, Dreher K, Foerster H *et al.* 2014. The MetaCyc database of metabolic pathways and enzymes and the BioCyc collection of Pathway/Genome Databases. *Nucleic acids research* 42:D459-471.
286. Predich M, Nair G, Smith I. 1992. *Bacillus subtilis* early sporulation genes *kinA*, *spo0F*, and *spo0A* are transcribed by the RNA polymerase containing sigma H. *J Bacteriol* 174:2771-2778.

287. Antoniewski C, Savelli B, Stragier P. 1990. The *spoIIIJ* gene, which regulates early developmental steps in *Bacillus subtilis*, belongs to a class of environmentally responsive genes. *J Bacteriol* 172:86-93.
288. Fujita M, Sadaie Y. 1998. Promoter selectivity of the *Bacillus subtilis* RNA polymerase σ A and σ H holoenzymes. *Journal of Biochemistry* 124:89-97.
289. Chastanet A, Vitkup D, Yuan GC, Norman TM, Liu JS *et al.* 2010. Broadly heterogeneous activation of the master regulator for sporulation in *Bacillus subtilis*. *Proc Natl Acad Sci U S A* 107:8486-8491.
290. de Jong IG, Veening J-W, Kuipers OP. 2010. Heterochronic phosphorelay gene expression as a source of heterogeneity in *Bacillus subtilis* spore formation. *J Bacteriol* 192:2053-2067.
291. Sterlini JM, Mandelstam J. 1969. Commitment to sporulation in *Bacillus subtilis* and its relationship to development of actinomycin resistance. *The Biochemical journal* 113:29-37.
292. Pan Q, Losick R. 2003. Unique degradation signal for ClpCP in *Bacillus subtilis*. *J Bacteriol* 185:5275-5278.
293. Fujita M, González-Pastor JE, Losick R. 2005. High- and low-threshold genes in the Spo0A Regulon of *Bacillus subtilis*. *J Bacteriol* 187:1357-1368.
294. Jiang M, Shao W, Perego M, Hoch JA. 2000. Multiple histidine kinases regulate entry into stationary phase and sporulation in *Bacillus subtilis*. *Molecular microbiology* 38:535-542.
295. van den Ent F, Amos LA, Lowe J. 2001. Prokaryotic origin of the actin cytoskeleton. *Nature* 413:39-44.
296. Dye NA, Pincus Z, Fisher IC, Shapiro L, Theriot JA. 2011. Mutations in the nucleotide binding pocket of MreB can alter cell curvature and polar morphology in *Caulobacter*. *Molecular microbiology* 81:368-394.
297. Gitai Z, Dye N, Shapiro L. 2004. An actin-like gene can determine cell polarity in bacteria. *Proc Natl Acad Sci U S A* 101:8643-8648.
298. Srivastava P, Demarre G, Karpova TS, McNally J, Chatteraj DK. 2007. Changes in nucleoid morphology and origin localization upon inhibition or alteration of the actin homolog, MreB, of *Vibrio cholerae*. *J Bacteriol* 189:7450-7463.

299. Yang J, Yan R, Roy A, Xu D, Poisson J *et al.* 2015. The I-TASSER suite: protein structure and function prediction. *Nature methods* 12:7-8.
300. van den Ent F, Izore T, Bharat TA, Johnson CM, Lowe J. 2014. Bacterial actin MreB forms antiparallel double filaments. *eLife* 3:e02634.
301. Murray T, Popham DL, Setlow P. 1998. *Bacillus subtilis* cells lacking penicillin-binding protein 1 require increased levels of divalent cations for growth. *J Bacteriol* 180:4555-4563.
302. Popham DL, Setlow P. 1996. Phenotypes of *Bacillus subtilis* mutants lacking multiple class A high-molecular-weight penicillin-binding proteins. *J Bacteriol* 178:2079-2085.
303. Britton RA, Eichenberger P, Gonzalez-Pastor JE, Fawcett P, Monson R *et al.* 2002. Genome-wide analysis of the stationary-phase sigma factor (sigma-H) regulon of *Bacillus subtilis*. *J Bacteriol* 184:4881-4890.
304. Fujita M, Sadaie Y. 1998. Feedback loops involving Spo0A and AbrB in in vitro transcription of the genes involved in the initiation of sporulation in *Bacillus subtilis*. *Journal of biochemistry* 124:98-104.
305. Dubnau EJ, Cabane K, Smith I. 1987. Regulation of spo0H, an early sporulation gene in bacilli. *J Bacteriol* 169:1182-1191.
306. Weir J, Predich M, Dubnau E, Nair G, Smith I. 1991. Regulation of *spo0H*, a gene coding for the *Bacillus subtilis* sigma H factor. *J Bacteriol* 173:521-529.
307. Perego M, Spiegelman GB, Hoch JA. 1988. Structure of the gene for the transition state regulator, *abrB*: regulator synthesis is controlled by the *spo0A* sporulation gene in *Bacillus subtilis*. *Molecular microbiology* 2:689-699.
308. Strauch M, Webb V, Spiegelman G, Hoch JA. 1990. The SpoOA protein of *Bacillus subtilis* is a repressor of the *abrB* gene. *Proc Natl Acad Sci U S A* 87:1801-1805.
309. Wisner MJ, Lenski RE. 2015. A comparison of methods to measure fitness in *Escherichia coli*. *PloS one* 10:e0126210.
310. Duan Y, Sperber AM, Herman JK. 2016. YodL and YisK possess shape-modifying activities that are suppressed by mutations in *Bacillus subtilis mreB* and *mbl*. *J Bacteriol* 198:2074-2088.

311. Niesen FH, Berglund H, Vedadi M. 2007. The use of differential scanning fluorimetry to detect ligand interactions that promote protein stability. *Nature protocols* 2:2212-2221.
312. Layton CJ, Hellinga HW. 2010. Thermodynamic analysis of ligand-induced changes in protein thermal unfolding applied to high-throughput determination of ligand affinities with extrinsic fluorescent dyes. *Biochemistry* 49:10831-10841.
313. Layton CJ, Hellinga HW. 2011. Quantitation of protein-protein interactions by thermal stability shift analysis. *Protein science : a publication of the Protein Society* 20:1439-1450.
314. Noone D. 2014. A highly unstable transcript makes CwlO D,L-endopeptidase expression responsive to growth conditions in *Bacillus subtilis*. *J Bacteriol* 196(2):237-47
315. Bateman RL, Bhanumoorthy P, Witte JF, McClard RW, Grompe M *et al.* 2001. Mechanistic inferences from the crystal structure of fumarylacetoacetate hydrolase with a bound phosphorus-based inhibitor. *The Journal of biological chemistry* 276:15284-15291.
316. Bateman RL, Ashworth J, Witte JF, Baker LJ, Bhanumoorthy P *et al.* 2007. Slow-onset inhibition of fumarylacetoacetate hydrolase by phosphinate mimics of the tetrahedral intermediate: kinetics, crystal structure and pharmacokinetics. *The Biochemical journal* 402:251-260.
317. Manjasetty BA, Niesen FH, Delbruck H, Gotz F, Sievert V *et al.* 2004. X-ray structure of fumarylacetoacetate hydrolase family member *Homo sapiens* FLJ36880. *Biological chemistry* 385:935-942.
318. Grogan G. 2005. Emergent mechanistic diversity of enzyme-catalysed beta-diketone cleavage. *The Biochemical journal* 388:721-730.
319. Timm DE, Mueller HA, Bhanumoorthy P, Harp JM, Bunick GJ. 1999. Crystal structure and mechanism of a carbon-carbon bond hydrolase. *Structure (London, England : 1993)* 7:1023-1033.
320. Hopper DJ, Chapman PJ, Dagley S. 1971. The enzymic degradation of alkyl-substituted gentisates, maleates and malates. *The Biochemical journal* 122:29-40.
321. Bayly RC, Chapman PJ, Dagley S, Di Berardino D. 1980. Purification and some properties of maleylpyruvate hydrolase and fumarylpyruvate hydrolase from *Pseudomonas alcaligenes*. *J Bacteriol* 143:70-77.

322. Poh CL, Bayly RC. 1980. Evidence for isofunctional enzymes used in m-cresol and 2,5-xyleneol degradation via the gentisate pathway in *Pseudomonas alcaligenes*. J Bacteriol 143:59-69.
323. Zhou NY, Fuenmayor SL, Williams PA. 2001. *nag* genes of *Ralstonia* (formerly *Pseudomonas*) sp. strain U2 encoding enzymes for gentisate catabolism. J Bacteriol 183:700-708.
324. Werner AK, Romeis T, Witte CP. 2010. Ureide catabolism in *Arabidopsis thaliana* and *Escherichia coli*. Nature chemical biology 6:19-21.
325. Percudani R, Carnevali D, Puggioni V. 2013. Ureidoglycolate hydrolase, amidohydrolase, lyase: how errors in biological databases are incorporated in scientific papers and vice versa. Database : the journal of biological databases and curation 2013:bat071.
326. Schrodinger, LLC. 2010. The PyMOL Molecular Graphics System, Version 1.3r1.
327. Jeong JH, Kim YS, Rojviriyaya C, Ha SC, Kang BS *et al.* 2013. Crystal structures of bifunctional penicillin-binding protein 4 from *Listeria monocytogenes*. Antimicrobial agents and chemotherapy 57:3507-3512.
328. Tipton PA, Peisach J. 1990. Characterization of the multiple catalytic activities of tartrate dehydrogenase. Biochemistry 29:1749-1756.
329. Meyer H, Liebeke M, Lalk M. 2010. A protocol for the investigation of the intracellular *Staphylococcus aureus* metabolome. Analytical biochemistry 401:250-259.
330. Meyer H, Weidmann H, Lalk M. 2013. Methodological approaches to help unravel the intracellular metabolome of *Bacillus subtilis*. Microbial cell factories 12:69.
331. Schirner K, Eun YJ, Dion M, Luo Y, Helmann JD *et al.* 2015. Lipid-linked cell wall precursors regulate membrane association of bacterial actin MreB. Nature chemical biology 11:38-45.
332. Anderson LM, Ruley HE, Bott KF. 1982. Isolation of an autonomously replicating DNA fragment from the region of defective bacteriophage PBSX of *Bacillus subtilis*. J Bacteriol 150:1280-1286.
333. Brackmann M, Nazarov S, Wang J, Basler M. 2017. Using force to punch holes: mechanics of contractile nanomachines. Trends in cell biology 27:623-632.

334. Gibson DG. 2011. Enzymatic assembly of overlapping DNA fragments. *Methods in enzymology* 498:349-361.
335. Hauser PM, Karamata D. 1994. A rapid and simple method for *Bacillus subtilis* transformation on solid media. *Microbiology* 140 (Pt 7):1613-1617.
336. Yang MM, Zhang WW, Bai XT, Li HX, Cen PL. 2010. Electroporation is a feasible method to introduce circularized or linearized DNA into *B. subtilis* chromosome. *Molecular biology reports* 37:2207-2213.
337. Cao G, Zhang X, Zhong L, Lu Z. 2011. A modified electro-transformation method for *Bacillus subtilis* and its application in the production of antimicrobial lipopeptides. *Biotechnology letters* 33:1047-1051.
338. Meddeb-Mouelhi F, Dulcey C, Beauregard M. 2012. High transformation efficiency of *Bacillus subtilis* with integrative DNA using glycine betaine as osmoprotectant. *Analytical biochemistry* 424:127-129.
339. Longchamp PF, Mauel C, Karamata D. 1994. Lytic enzymes associated with defective prophages of *Bacillus subtilis*: sequencing and characterization of the region comprising the N-acetylmuramoyl-L-alanine amidase gene of prophage PBSX. *Microbiology* 140 (Pt 8):1855-1867.
340. Krogh S, Jorgensen ST, Devine KM. 1998. Lysis genes of the *Bacillus subtilis* defective prophage PBSX. *J Bacteriol* 180:2110-2117.
341. Prindle A, Liu J, Asally M, Ly S, Garcia-Ojalvo J *et al.* 2015. Ion channels enable electrical communication in bacterial communities. *Nature* 527:59-63.
342. Humphries J, Xiong L, Liu J, Prindle A, Yuan F *et al.* 2017. Species-independent attraction to biofilms through electrical signaling. *Cell* 168:200-209 e212.
343. Te Winkel JD, Gray DA, Seistrup KH, Hamoen LW, Strahl H. 2016. Analysis of antimicrobial-triggered membrane depolarization using voltage sensitive dyes. *Frontiers in cell and developmental biology* 4:29.
344. Edgar R, Rokney A, Feeney M, Semsey S, Kessel M *et al.* 2008. Bacteriophage infection is targeted to cellular poles. *Molecular microbiology* 68:1107-1116.
345. Strahl H, Hamoen LW. 2010. Membrane potential is important for bacterial cell division. *Proc Natl Acad Sci U S A* 107:12281-12286.

346. Cao X, Zhu B, Zhang X, Dong H. 2016. Polymyxin B immobilized on cross-linked cellulose microspheres for endotoxin adsorption. *Carbohydrate polymers* 136:12-18.

APPENDIX

ChemSpider summary of compounds decreased more than two-fold in the $\Delta yisK$ mutant compared to wild-type (Table A1.1) discussed in Chapter III is included as a separate file.

Table A1.1. ChemSpider summary of compounds decreased more than two-fold in the $\Delta yisK$ mutant compared to wild-type. Compound discoverer differential analysis results comparing *yisK* knockout metabolome to wild-type metabolome during stationary growth. Compounds in this table are identified by only their MS spectrum, and not by their MS² spectrum, and thus represent tentative hits. Bg Color is Background Color; red is decrease of at least two-fold of metabolite in the $\Delta yisK$ mutant compared to wild-type while green is an increase of at least two-fold compared to wild-type.